



12-2003

The effects of wing inertia variations on spin recovery characteristics of single-engine general-aviation aircraft

Jeffrey Duane Daly

Recommended Citation

Daly, Jeffrey Duane, "The effects of wing inertia variations on spin recovery characteristics of single-engine general-aviation aircraft. " Master's Thesis, University of Tennessee, 2003.
https://trace.tennessee.edu/utk_gradthes/5211

This Thesis is brought to you for free and open access by the Graduate School at Trace: Tennessee Research and Creative Exchange. It has been accepted for inclusion in Masters Theses by an authorized administrator of Trace: Tennessee Research and Creative Exchange. For more information, please contact trace@utk.edu.

To the Graduate Council:

I am submitting herewith a thesis written by Jeffrey Duane Daly entitled "The effects of wing inertia variations on spin recovery characteristics of single-engine general-aviation aircraft." I have examined the final electronic copy of this thesis for form and content and recommend that it be accepted in partial fulfillment of the requirements for the degree of Master of Science, with a major in Aerospace Engineering.

Ralph Kimberlin, Major Professor

We have read this thesis and recommend its acceptance:

Accepted for the Council:
Carolyn R. Hodges

Vice Provost and Dean of the Graduate School

(Original signatures are on file with official student records.)

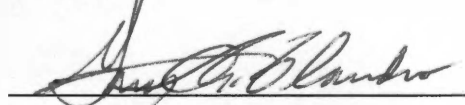
To the Graduate Council:

I am submitting herewith a thesis written by Jeffrey Duane Daly entitled "The Effects of Wing Inertia Variations on Spin Recovery Characteristics of Single-Engine General-Aviation Aircraft." I have examined the final paper copy of this thesis for form and content and recommend that it be accepted in partial fulfillment of the requirements for the degree of Master of Science, with a major in Aerospace Engineering.



Ralph D. Kimberlin, Major Professor

We have read this thesis
and recommend its acceptance:



G. A. Flandro



F. G. Collins

Accepted for the Council:



Vice Provost and Dean of Graduate
Studies

**THE EFFECTS OF WING INERTIA VARIATIONS
ON SPIN RECOVERY CHARACTERISTICS OF
SINGLE-ENGINE GENERAL-AVIATION AIRCRAFT**

A Thesis Presented for the
Master of Science
Degree
The University of Tennessee, Knoxville

Jeffrey Duane Daly
December 2003

Thesis
2003
.D25

Copyright © 2003 by Jeffrey Duane Daly.

All rights reserved.

ACKNOWLEDGEMENTS

I deeply acknowledge the love and dedicated support provided by my family. I expressly thank my wife, Sarah, for her untiring encouragement, patience, tolerance, and help given to me at accomplishing my Master of Science degree. I could not have done this without her and without the love of my daughter, Hannah.

I am grateful to the Canadian Forces for affording me this opportunity. The staff and students at UTSI were immensely helpful in my post graduate success. I am especially thankful to Dr. R. Kimberlin, my advisor, for his great ideas, unquestionable knowledge, and for inspiring me to undertake a thesis study very close to my heart. I thank Dr. G. Flandro for his advice and generosity, and Dr. A. Vakili for his guidance. I am indebted to Mr. Michael Rigsby for his direct assistance and dogged dedication towards my thesis test program and to Mr. Mike Leigh for his uncanny and brilliant instrumentation talents. Special mention goes to Mr. Chris Armstrong and Mr. Gary Payne for their manufacturing genius and speedy service. Mr. Jim Goodman's support was also invaluable.

"Per Ardua Ad Astra"

ABSTRACT

An experimental study of the effects of variations in rolling moments of inertia on spin recovery was conducted for single-engine general-aviation aircraft. The test method selected was flight test of a Froude number $1/6^{\text{th}}$ dynamically scaled radio-controlled model, typical of a general-aviation aircraft. A model of a Piper PA-28-180 Cherokee of 1970's vintage was constructed, instrumented with a flight data recorder and hobby-type sensors, and fitted with a spin recovery parachute system. Ground video recordings supplemented the on-board instrumentation to provide data to analyze spin and recovery behaviour. To replicate increased rolling moments of inertia for the full-scale airplane, the experimental approach was based on changes in rolling moments of inertia created by variations of fuel capacity in the wing of the full-scale airplane. A total of 11 flights and 38 spins were carried out over an IYMP range from -56×10^{-4} to 8×10^{-4} . Angle of attack, spin rate about the spin axis, and turns to recovery were essential to analyze the spin behaviour. Premature recoveries prevented the stock and increased inertia spins from developing their potential energy level resulting in lower than expected angle of attack and spin rate. Generally, however, angle of attack and spin rate increased as the rolling moment of inertia was increased, but turns to recovery never exceeded $1\frac{3}{4}$ turns using the standard spin technique. Ailerons-against spin maneuvers caused turns to recovery to rapidly increase due to higher spin rates, with higher rolling moments of inertia worsening the recovery to the point of being unrecoverable. This occurred only for left spins with right spins being more benign. Spin rate and angle of attack were determined to be the key elements deciding whether or not a spin would be more severe from increasing the rolling moment of inertia. Increased rolling moments of inertia may not always cause spin recovery to degrade due to other predominant forces and moments. However, given enough spin turns, suitable additional wing inertia, and the right control deflections, there will be a point where the spin will become unrecoverable. It was found that an increase of 20 gallons of fuel load in the wing at mid-span (IYMP of 8×10^{-4}) caused unrecoverable spins in only the ailerons-against left spin. The Piper PA-28-180 Cherokee and other similar general-aviation airplanes should exhibit worsening spin recovery characteristics as fuel capacity in the wing is increased to the point where at approximately 20 additional gallons of fuel may trigger unrecoverable spins. Overall, this and previous

research from the 1940's to the 1970's concluded that increasing wing mass degrades spin recovery given the right circumstances. It was also found that hobby-type piezo-electric rate gyros are suitable for spin testing in radio-controlled models, however, they must be calibrated over their complete dynamic range to ensure the gain setting is correct and they must be corrected for temperature changes by pre-flight data or other means.

Recommendations go to the general-aviation community. Pilots must avoid applying ailerons against the spin (either purposely or inadvertently) during entry or recovery for this Piper PA-28-180 Cherokee design, as recovery may never occur. Precautions must also be exercised when spin testing or certifying a general-aviation airplane that has fuel in the wings, or has been modified with additional fuel capacity in the wings, as unrecoverable spins may result.

TABLE OF CONTENTS

<u>CHAPTER</u>	<u>PAGE</u>
I. INTRODUCTION.....	1
II. BACKGROUND AND THEORETICAL CONSIDERATIONS	3
Literature Review	3
Theoretical Considerations	8
III. EXPERIMENTAL APPROACH	23
Experimental Objectives.....	23
Experimental Set-up and Method	23
IV. RESULTS AND ANALYSIS	39
Test Flight Data	39
Spin Behaviour	42
Data Analysis.....	43
Overall Effect of Moment of Inertia Changes on Spin Recovery	55
Correlation of Model Results to the Full-Scale Airplane	57
V. CONCLUSIONS AND RECOMMENDATIONS	59
Conclusions	59
Recommendations	61
LIST OF REFERENCES	63
APPENDICES	69
APPENDIX A: The Test Model	71
APPENDIX B: Instrumentation	87
APPENDIX C: Spin Recovery Parachute System	107
APPENDIX D: Mass Properties and Moments of Inertia Measurements.....	117
APPENDIX E: Flight Test Plan	125
APPENDIX F: Flight Data.....	135
APPENDIX G: Model Spin Parameters from Flight Tests	173
APPENDIX H: Level Flight Data	181
VITA.....	185

LIST OF TABLES

<u>TABLE</u>	<u>PAGE</u>
Table 2-1. Spin Mode Terminology [4].....	10
Table 2-2. Spin Recovery Guidelines [4].	10
Table 2-3. Gyroscopic Precessional Effects.	13
Table 3-1. Model Mass Properties at Forward CG Setting (24.8% MAC).	29
Table 3-2. IYMP and Weight Properties for the Full-Scale Airplane.	30
Table 3-3. Aircraft Spin Configurations (L = left, R = right).....	31
Table 4-1. Number of Spin Events versus Aircraft Configuration.....	39
Table 4-2. Level Flight Instrumentation Parameters.	44
Table 4-3. Left Spin Aerodynamic Elements – Ailerons-Against the Spin.....	55
Table A-1. Full-Scale Airplane and Model Specifications.....	79
Table A-2. Control Surface Throws, Tolerances and Settings [38].....	80
Table B-1. Tattletale Flight Data Acquisition Unit Specifications.....	95
Table B-2. Rate Gyro Specifications.....	96
Table B-3. AOA and AOS Sensor Specifications.	96
Table B-4. Pulse Width Modulation Converter Specifications.	97
Table B-5. Rate Table Specifications	97
Table D-1. Postal Scale Specifications.....	121
Table D-2. Moment of Inertia Results.....	122
Table D-3. Moment of Inertia Error Analysis at the Forward CG Setting.	122
Table E-1. Test Matrix.....	131
Table G-1. Flight Data. Forward Center of Gravity. Left Spins.....	175
Table G-2. Flight Data. Forward Center of Gravity. Right Spins.	176
Table G-3. Flight Data. Mid Center of Gravity. Left Spins.	177
Table G-4. Flight Data. Mid Center of Gravity. Right Spins.	178
Table G-5. Flight Data. Aft Center of Gravity. Left Spins.....	179
Table G-6. Flight Data. Aft Center of Gravity. Right Spins.....	180

LIST OF FIGURES

<u>FIGURE</u>	<u>PAGE</u>
Figure 2-1. Balance of Aerodynamic and Inertia Pitching Moments in a Spin [16].	9
Figure 2-2. Body Axes and Rotation Rate Conventions [39].	14
Figure 2-3. Effect of Reynolds Number on Lift [2].	21
Figure 3-1. Author with Test Model Prior to Taxi.	25
Figure 3-2. Effect of Parachute Line Length [30].	28
Figure 3-3. Average Angle of Attack Flow Corrections for Spinning Aircraft with Vane Type Sensors Mounted on Wingtip Booms [29].	35
Figure 3-4. Average Angle of Sideslip Flow Corrections for Spinning Aircraft with Vane Type Sensors Mounted on Wingtip Booms [29].	36
Figure 4-1. Effects of CG Position and Inertia States on Spin AOA.	48
Figure 4-2. Angle of Attack Averaged Between Left and Right Spins.	50
Figure 4-3. Effects of CG Position and Inertia States on Spin Rate.	52
Figure 4-4. Effects of CG Position and Inertia States on Turns for Recovery.	54
Figure A-1. Model of the 1/6 th Scale Piper PA-28-180 Cherokee with Radio Transmitter.	81
Figure A-2. Photo of Model's Access Door.	81
Figure A-3. Semi-Span Wing Planform Layout.	82
Figure A-4. Sample Compufoil Template of a NACA 652-415 Airfoil.	83
Figure A-5. Bottom View of Wing.	84
Figure A-6. Bottom View of Fuselage with Wing Removed.	84
Figure A-7. Setup and Downloading FDR Data.	85
Figure A-8. Author (right) with Thesis Advisor (left), Model and Recovery Vehicle.	85
Figure B-1. Tattletale Flight Data Acquisition Unit.	98
Figure B-2. Close-up of Tattletale Acquisition Unit.	98
Figure B-3. Tattletale FDR Installation.	99
Figure B-4. View of the Rudder (left) and Aileron (right) Position Sensors.	99
Figure B-5. Gyro Installation on Left Fuselage Side.	100
Figure B-6. Sideslip Sensor at Left Wingtip.	100

<u>FIGURE</u>	<u>PAGE</u>
Figure B-7. Angle of Attack Sensor at Right Wingtip.....	101
Figure B-8. Sample of Calibration Raw Data from FDR.....	101
Figure B-9. Elevator Position Calibration Curve.....	102
Figure B-10. Aileron Position Calibration Curve.	102
Figure B-11. Rudder Position Calibration Curve.....	103
Figure B-12. Gyro Calibration Operation.	103
Figure B-13. Roll Rate Calibration Curve.	104
Figure B-14. Pitch Rate Calibration Curve.....	104
Figure B-15. Yaw Rate Calibration Curve.....	105
Figure B-16. Angle of Sideslip Calibration.	105
Figure B-17. Angle of Attack Calibration Curve.....	106
Figure B-18. Angle of Sideslip Calibration Curve.....	106
Figure C-1. Side View of Spin Recovery Parachute Assembly.....	111
Figure C-2. Bottom View of Spin Recovery Parachute Boom and Mount.....	111
Figure C-3. Spin Recovery Parachute Mount – Bottom View.....	112
Figure C-4. Spin Recovery Mount – Side View	112
Figure C-5. Spin Recovery Mount – Top View.....	113
Figure C-6. Spin Recovery Parachute Servo and Pushrod.....	113
Figure C-7. Spin Parachute Mounted.....	114
Figure C-8. Spin Parachute.	114
Figure C-9. Spin Recovery Parachute and Risers.	115
Figure C-10. Spin Recovery Parachute Attachments.....	115
Figure D-1. Torsional Bifilar Swinging Method to Determine Inertial Properties [8].	123
Figure D-2. Moment of Inertia about the X Axis.....	123
Figure D-3. Moment of Inertia about the Y Axis.....	124
Figure D-4. Moment of Inertia about the Z Axis.....	124
Figure F-1. Spin #A1U.....	137
Figure F-2. Spin # A2U.....	138
Figure F-3. Spin # A3D.....	139

FIGURE**PAGE**

Figure F-4. Spin # A4D.	140
Figure F-5. Spin # B1U.	141
Figure F-6. Spin # B2U.	142
Figure F-7. Spin # B3D.	143
Figure F-8. Spin # B4D.	144
Figure F-9. Spin # C1U.	145
Figure F-10. Spin # C2U.	146
Figure F-11. Spin # C4D.	147
Figure F-12. Spin # D1U.	148
Figure F-13. Spin # D2U.	149
Figure F-14. Spin # D3D.	150
Figure F-15. Spin # D4D.	151
Figure F-16. Spin # E1U.	152
Figure F-17. Spin # E2U.	153
Figure F-18. Spin # E3D.	154
Figure F-19. Spin # E4D.	155
Figure F-20. Spin # F1U.	156
Figure F-21. Spin # F2U.	157
Figure F-22. Spin # F3D.	158
Figure F-23. Spin # F4D.	159
Figure F-24. Spin # G1U.	160
Figure F-25. Spin # G2U.	161
Figure F-26. Spin # H1U.	162
Figure F-27. Spin # H2U.	163
Figure F-28. Spin # H3D.	164
Figure F-29. Spin # H4D.	165
Figure F-30. Spin # J1U.	166
Figure F-31. Spin # J2U.	167
Figure F-32. Spin # J5A.	168

<u>FIGURE</u>	<u>PAGE</u>
Figure F-33. Spin # K1U.....	169
Figure F-34. Spin # K2U.....	170
Figure F-35. Spin # B1UA.....	171
Figure F-36. Spin # B2UA.....	172
Figure H-1. Level Flight Data.....	183

LIST OF SYMBOLS

AGL	Above Ground Level
AOA	Angle of Attack
AOS	Angle of Sideslip
b	Wing Span (ft)
C_D	Coefficient of Drag
CG	Center of Gravity
C_L	Coefficient of Lift
D	Distance between the bifilar string supports (feet)
DC	Direct Current
FDR	Flight Data Recorder
Fr	Froude Number
g	Acceleration of Gravity
I	Moment of Inertia about a Body Axis
I_x	Rolling Moment of Inertia about the x Body Axis (slug ft ²)
I_y	Pitching Moment of Inertia about the y Body Axis (slug ft ²)
I_z	Yawing Moment of Inertia about the z Body Axis (slug ft ²)
IYMP	Inertia Yawing-Moment Parameter = $\frac{I_x - I_y}{mb^2}$ (dimensionless)
l	Linear Geometric Dimension
L	Length of bifilar string supports (feet)
lbf	Pounds Force
m	Mass of Airplane (slugs)
MAC	Mean Aerodynamic Chord
mah	milli-amp-hour
M_0I	Moment of Inertia
MSL	Mean Sea Level
NACA	National Advisory Committee For Aeronautics
NASA	National Aeronautics and Space Administration
P	Engine Power

p	Roll Rate (deg/s), positive right roll
PC	Personal Computer
PCM	Pulse Code Modulation
PN	Part Number
pot	potentiometer
q	Pitch Rate (deg/s), positive up pitch
r	Radius of Spin Axis (ft)
r	Yaw Rate (deg/s), positive right yaw
Re	Reynolds Number
RPRV	Remotely Piloted Research Vehicle
S	Area of a Flight Surface
S/N	Serial Number
t	Time
V	Spin Descent Velocity
VDC	Volts Direct Current
W	Gross Weight (lbf)
x, y, z	Body Axes
α	Angle of Attack (deg), positive up pitch
α_t	True Angle of Attack at the Center of Gravity
β	Angle of Sideslip (deg), positive right sideslip
Γ	Dihedral Angle
δ_a	Aileron Deflection (deg), positive right roll
δ_e	Elevator Deflection (deg), positive up pitch
δ_r	Rudder Deflection (deg), positive right yaw
θ_T	Wing Twist
μ	Free Stream Coefficient of Viscosity for Air
ρ	Free Stream Air Density
τ	Period of Oscillation (seconds)
ω	Angular Velocity
Ω	Spin Rate

CHAPTER I

INTRODUCTION

Aircraft spin accidents have plagued aviation since the invention of the airplane. In the early 1900's, the stall/spin problem was such a mystery that stall/spin accidents significantly slowed the progress of aviation. No research was conducted in this area until 1919, when the National Advisory Committee For Aeronautics (NACA) first carried out flight tests to better understand stability and control of aircraft [1]. However, the onset of World War II essentially required all of NACA's resources to be devoted to military applications, including the creation of NASA Langley's vertical spin tunnels in 1927 and 1941. Prior to the 1970's, general-aviation research by NACA and the British had been irregular to nonexistent with only periodic surges in research to improve general-aviation stall/spin safety. In 1970, it was realized that stall-related accidents accounted for the largest portion of fatalities and injuries in general aviation flying, despite the improvements made over the post war years. General-aviation stall/spin research was once again thrust ahead primarily by NACA's successor, the National Aeronautics and Space Administration (NASA), producing over 100 technical papers in this area [2].

Chambers et al [2] points out that the NASA program had pioneered the use of low cost radio-controlled models for the prediction of stall/spin characteristics. This technique was controversial, meeting with mixed reactions from the aviation industry, and never receiving widespread acceptance. This was partially due to difficulty in flying the dynamically scaled models and accuracy problems related to Reynolds number effects. Reynolds number effects were, however, more predominant with NASA's smaller 1/12th scale spin tunnel models. NASA's use of radio-controlled models for spin testing research was successful many times from 1975 to 1992 [3, 4, 5, 6, 7]. NASA's partnership with industry also resulted in successful spin tests using radio-controlled models [8, 9]. Instrumentation methods were limited at the time with *Kershner* [10] developing some miniature sensor devices for radio-controlled spin test models.

Aircraft spin research for the general-aviation community has been scarce since the 1980's. Although much has been accomplished and theories developed, there is still much to explore that can benefit aviation safety. With the increasing desire for general-aviation

aircraft with greater fuel capacity, there arises new concerns for spin recovery. *Kimberlin* [11] points out that some general aviation aircraft have exhibited worse spin recovery characteristics from increased rolling moments of inertia due to additional fuel in the wings. This adverse effect was greater than previously thought and warrants specific research into the spin recovery nature from variations in rolling moments of inertia.

This study is an experimental investigation into the effects of rolling moment of inertia variations upon spin recovery. The test method selected is a 1/6th dynamically scaled radio-controlled model, typical of a general-aviation aircraft. It is to be appropriately instrumented with modern flight data sensors and equipment, and the aircraft fitted with a spin recovery parachute system. It is proposed that by varying the rolling moments of inertia of the model, effects will be apparent upon spin recovery so that findings can be correlated to the full-scale general-aviation aircraft.

After a presentation of the background information associated with this research in Chapter II, the experimental approach is discussed in Chapter III and results analyzed in Chapter IV. Finally, conclusions and recommendations are presented in Chapter V.

CHAPTER II

BACKGROUND AND THEORETICAL CONSIDERATIONS

Literature Review

General

A thorough review of existing work in the field of aircraft spin dynamics revealed a wide scope of efforts to better understand its complicated nature. In-depth literature searches were fine tuned to isolate the work previously carried out in the two fields of inertia effects on spin characteristics and the method of using radio-controlled model airplanes for spin studies. Overall, it was found that NACA and NASA contributed to 95% of the previous research applicable to this thesis study.

Effects of Rolling Moments of Inertia Variations on Spin Recovery

Classic work by *Neihouse* [12] in 1942 found that variations of mass distribution along the wings required different spin recovery techniques. As the wing mass was increased, the effectiveness of the rudder as a spin recovery device decreased, whereas the elevator increased. This was important information for during World War II when in many instances fuel, guns, bombs and engines were put on the wings requiring use of down elevator as the primary spin recovery device. In 1946, *Neihouse et al* [13] further refined his earlier work to determine tail-sizing requirements to make spin recoveries satisfactory. This was followed by *Neihouse* [14] again in 1948, analyzing the data from testing that took place in 1938 [*Seidman and Neihouse*, 15] to determine the effects of variations in moments of inertia on spin recovery characteristics of a single-engine low-wing monoplane. The experimental approach was to gradually increase all axis moments of inertia by a constant percentage but maintain the same weight. In general, it was found that increasing the moments of inertia (about all axes at the same time) led to flatter spins, slower angular and vertical velocities, and slower recoveries. These were important findings for the day, but no specific effects were apparent from just the rolling moments of inertia changes, and no aerodynamic explanations were given.

It was also in the early 1940's when the inertia yawing moment parameter

($IYMP = \frac{I_x - I_y}{mb^2}$) was introduced, which is still in use today. The IYMP is used to describe the relative distribution of the mass of the airplane between the wing and fuselage. It's also a dimensionless parameter relating the rolling and pitching moments of inertia such that it is independent of the size and weight of the airplane. When the weight of the airplane is distributed mainly along the wing, the moment of inertia in roll is greater than that in pitch, and the IYMP value is positive. This situation is referred to as wing-heavy loading. Conversely, when the weight is distributed mainly along the fuselage, IYMP becomes negative and is referred to as fuselage-heavy loading. *Bowman* [16] states that almost all light general-aviation aircraft fall into zero loading category where the moments of inertia in roll and pitch are about equal. It is, however, as mentioned earlier, the aim of this thesis study to investigate the effects of positive IYMP wing-heavy loadings upon spin recovery.

British tests by *Kerr* [17] in 1953 conceived another important non-dimensional parameter: the ratio of pitching to rolling moments of inertia (I_y/I_x). It was found that recovery standards improved as the I_y/I_x inertia ratio increased. Although, not explained in any more detail, one would assume that increased rolling moments of inertia, with other inertia moments constant, would have an adverse effect on spin recovery. This parameter apparently was not used in the aircraft community, but rather the IYMP parameter was favoured.

Bowman [16] made an excellent summary of all NASA (and NACA) research related to general-aviation aircraft spin and recovery characteristics up until 1971. He pointed out that most of the applicable research was performed before and during World War II and not performed on general-aviation airplanes, but many of the airplanes and spin tunnel models tested during that period were similar to current general-aviation airplanes with regard to factors that are important in spinning. He stated that three factors were found to be of almost overriding importance in spinning. These factors were the relative distribution of mass between the wing and the fuselage, the density of the airplane relative to the air, and the tail design. Also noted was that most results were only based on spin-tunnel tests of free-spinning dynamically scaled models with some correlation to full-scale spin tests. *Bowman* made an analysis of the mass effects by adding external wing tanks to a general-aviation airplane. His comments, however, were restricted stating that as weight was increased along

the wings, the elevator became the primary recovery control (as *Neihouse* [12] discovered in 1942). Therefore, no new research or theories had been conceived to detail effects of mass variations upon spin recovery since *Neihouse* in the 1940's.

It wasn't until 1979 when more headway was made with general-aviation spin testing that considered moment of inertia variations. Based on a general-aviation spin program that *Bowman and Burk* [18] initiated in 1976, *Stough and Patton* [19] presented in 1979 the results for the first full-scale airplane in the NASA stall/spin program. *Stough and Patton* also pointed out that stall/spin was the cause in 30 percent of all fatal general-aviation accidents, yet aircraft designers did not have a reliable means of determining stall/spin characteristics prior to prototype flight tests. To determine the effects of varying mass distribution on spin and spin recovery characteristics, tests were conducted at inertia yawing-moment parameters (IYMP) values from -50×10^{-4} (slightly fuselage heavy loaded, $I_x < I_y$) to $+50 \times 10^{-4}$ (slightly wing heavy loaded, $I_x > I_y$) while maintaining a constant center of gravity and relatively constant gross weight. Generally, it was found that adding mass to the wings did not appreciably change the spin mode, but recovery was slower from the spin. For all the configurations tested (including increased IYMP), the airplane consistently recovered from one-turn spins within one additional turn by application of normal recovery controls. After a closer look at the data from *Stough and Patton* [19], the following observations are made by the thesis author: increasing the IYMP caused no change or slightly decreased spin AOA (by up to 6%), slightly slowed spin rate (by up to 6%), and required one extra turn at most to recovery using normal recovery controls.

In summary, spin characteristics related to changes in moments of inertia were confined to limited tests carried out by *Neihouse* in the 1940's and *Stough and Patton* in the late 1970's. No more recent evidence was found indicating specific research into the effects of wing moments of inertia variations upon spin recovery.

Radio-Controlled Model Technology Used For Spin Testing

Radio-controlled model tests commenced in 1975 by *Burk and Wilson* [8] in conjunction with Piper Aircraft Corporation to develop the technique and evaluate stall/spin characteristics of general-aviation aircraft. It offered an effective, low-cost, low-risk method for exploratory research on the spin characteristics of a particular airplane in the development

phase. Although no useful spin data were contained in the report, the research opened a new technology for spin testing that this thesis study closely examined and utilized.

Concurrently in 1975, *Layton* [3] undertook a remotely piloted research vehicle (RPRV) program with a $3/8^{\text{th}}$ dynamically scaled model of an F-15 airplane to determine the usefulness of the RPRV technique in high-risk flight testing, including spin testing. The result was good agreement between the model and the full-scale aircraft, and the RPRV was concluded to be a practical method for obtaining flight research data.

Bowman et al [4] mentioned that due to the long history of research on military designs (driven by national priorities), model test methods and interpretation procedures have resulted in a relatively high level of confidence in extrapolation of model results to full-scale conditions. So, to rectify the 30-year long void in spin research for general-aviation airplanes, *Bowman et al* conducted specific tests in 1978 to verify the correlation of model and airplane spin characteristics for a low-wing general-aviation airplane. Correlation of a $1/5^{\text{th}}$ dynamically scaled radio-controlled model with a full-scale airplane at a IYMP of -50×10^{-4} revealed the following: the radio-controlled model exhibited all the spin modes obtained on the airplane; the steep spin modes of the radio-controlled model were up to 20° steeper than that of the airplane; model spin rate varied from slightly faster to slightly slower; and model recovery results generally predicted recoveries that were faster than the results obtained on the airplane, however, in cases where the angle of attack and spin rate matched that of the airplane, recoveries were essentially the same. Reynolds numbers were 300,000 for the model and 2,500,000 for full-scale tests.

DiCarlo and Johnson [5] followed suit in 1979 and employed a $1/5^{\text{th}}$ dynamically scaled radio-controlled model along with the full-scale airplane to explore the effects of wing leading-edge modifications on the stalling and spinning characteristics of a low-wing general-aviation aircraft. They found that the model had excellent correlation to the full-scale airplane, despite model tests data based on low Reynolds number.

In 1981, *McCormick* [6] more deeply analyzed NASA's reports at [4, 5, 19] and made some important observations regarding the radio-controlled spin model. It was observed that the model and full-scale airplane gave consistent correlation results, not being too affected by Reynolds number effects.

Finally, *Yip et al* [7] utilized a 1/4 dynamically scaled radio-controlled model of a spin-resistant trainer configuration to determine the stall departure and spin resistance characteristics provided by an outboard wing leading edge droop modification. The model flight results were generally in good agreement with previously obtained wind-tunnel data.

In summary, the use of radio-controlled models to evaluate stall/spin characteristics appears to be useful and provides a reasonable prediction of full-scale behaviour. Nevertheless, Reynolds number effects must be carefully considered for the particular application.

Motivation for Investigation into Wing Inertia Effects on Spin Recovery

The historical spin research applicable to general-aviation airplanes has been erratic with only partial knowledge gained concerning the effects of moments of inertia variations upon spin recovery. It is desired to continue to focus in the area of inertia effects on spin recovery to provide aircraft designers with more general knowledge of the potential consequences and certification difficulties when increasing the rolling moment of inertia. *Kimberlin* [11] pointed out personal experiences of general-aviation aircraft that were believed to possess good spin recovery characteristics, but in fact did not, most likely due to increased fuel capacity in the wings. Therefore, the experimental approach to be pursued will be based on changes in rolling moments of inertia created by variations of fuel capacity in the wing. This approach will enable a realistic appreciation of any potential adverse effects on spin recovery.

The thesis author's 20+ year experience at building and flying radio-controlled model airplanes supports the idea of employing radio-controlled models for this thesis study. In addition, a fuselage of a 1/6th scale model of a representative general-aviation aircraft was available for spin testing. It was provided by the author's advisor, Dr. R.D. Kimberlin, at the University of Tennessee Space Institute. The fuselage availability would provide a head start to the construction phase of the project. Suitable airport facilities were also available to permit such radio-controlled spin tests.

To accomplish this task, much work was required to be completed in eight months. This included the model's dynamically scaled design and construction of the remaining parts (wing, tail section, landing gear, engine system, fuel system), creation of suitable

instrumentation and in-flight data recording system, creation of a spin recovery parachute system, moments of inertia measurements, shakedown flight testing, and finally spin testing.

In view of the above, it is the goal of this thesis study to investigate the general effects of rolling moment variations upon spin recovery using a dynamically scaled radio-controlled airplane, adequately instrumented with modern off-the-shelf hobby systems, as much as possible. In addition to the general results obtained, more specific results will be applicable to the full-scale representative aircraft. Spin performance of Unmanned Air Vehicles (UAVs) may also directly benefit from the results.

Theoretical Considerations

Applicable Spin Theory Considerations

The intent of this section is to raise some important theoretical elements that were the basis for discussion later in Chapter IV of this paper. References [4, 11, 20, 21, 22, 23, 24, 25] provided excellent aircraft spin theory. *Kimberlin* [11] defines an aircraft spin as:

“A spin is an out-of-control maneuver at angles of attack beyond the stall during which the airplane rotates about its center of gravity and an axis perpendicular to the earth while descending vertically at high rates of descent.”

There is no simple formula that will predict how an airplane will spin and recover. In complex flows such as aircraft spin dynamics, the six equations of motion that govern the flow are time varying, involve non-linear inertial cross couplings and intense flow separation at high angles of attack. Solutions to these equations are not available with current methods, although some predictions have been made for the perfectly constrained steady spin, but have not replaced the need for actual flight tests.

There are many factors that influence the characteristics of a spin. Autorotative lift and drag forces from the wing, mass distribution, center of gravity position, fore and aft fuselage shape and size, tail size, airfoil thickness, airplane gyroscopic and precessional effects, flight control inputs, and propeller precession all effect the dynamics between inertial and aerodynamic forces/moments in a spin. Their relative strengths determine the severity of a spin and its recovery, as well as causing any oscillatory behaviour. In all cases, however, it is always the overall aerodynamic forces versus the inertial forces that determine spin

characteristics and recovery ability. As an example, Figure 2-1 shows the aerodynamic and inertial moments about the pitch axis.

Neihouse et al [20] summarized the results of NACA's efforts to determine the most effective control manipulation for spin recovery, establishing the so-called "NACA Recovery Procedure" for general-aviation type aircraft. That procedure consisted of moving the rudder quickly against the spin, followed by forward stick about $\frac{1}{2}$ turn later while maintaining neutral ailerons. This procedure came to vary depending upon the mass distribution of the aircraft. For example, wing loaded aircraft were found to require down elevator as the primary recovery control. *Bowman et al* [4] established the NASA terminology and guidelines normally used in describing various types of developed spin modes and turns for recovery for full-scale aircraft. Tables 2-1 and 2-2 detail the criteria for the spin modes and turns for recovery, respectively. *Neihouse et al* [20] mentioned an important effect on spin recovery. Essentially, changes can be made to mass and aerodynamic properties with little or no effect on spin recovery, but, there may be a certain point ("a cliff") when just the slightest change can have a dramatic effect on the results. This thesis study expects such a response of the model as the rolling moment of inertia is increased.

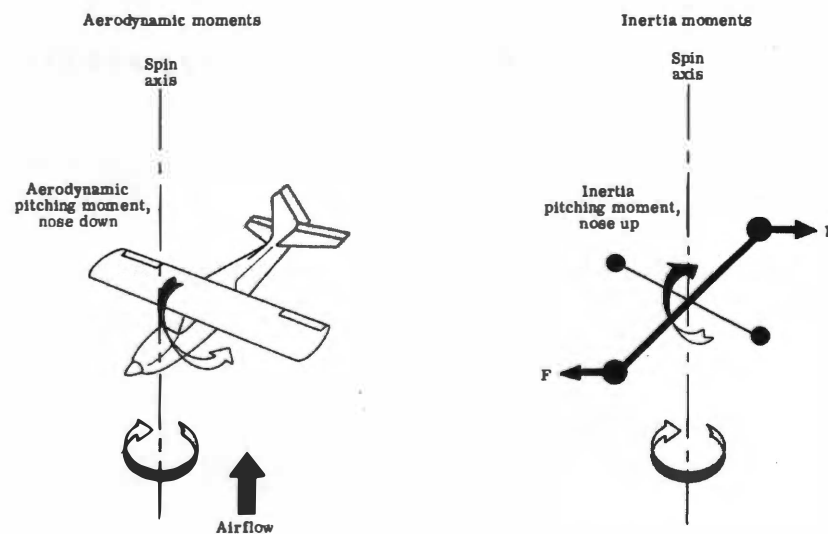


Figure 2-1. Balance of Aerodynamic and Inertia Pitching Moments in a Spin [16].

Table 2-1. Spin Mode Terminology [4].

Spin Mode	Angle of Attack Range (degrees)
Flat	65 to 90
Moderately Flat	45 to 65
Moderately Steep	30 to 45
Steep	20 to 30

Table 2-2. Spin Recovery Guidelines [4].

Description of Recovery	Turns for Recovery
Fast	0 to 1.5
Slow	1.5 to 3
Very Slow	Greater than 3
Recovery Controls Ineffective	No Recovery

Increasing the moments of inertia about any axis normally makes the airplane more spin resistant. But, once the spin is entered, it may become more difficult to stop. Changes in moments of inertia also directly affect gyroscopic precessional effects, described later in the following paragraphs.

Normal steep spins usually incorporate roll, pitch and yaw. As centrifugal force develops during rotation, the nose of the airplane tends to rise. The amount that it rises depends on the CG position, mass distribution, and speed of rotation. When a spin becomes abnormal and starts to flatten (say from increased centrifugal forces as spin rate increases), the rolling portion of the rotation dissipates and converts into yaw. Also, the radius of rotation about the spin axis begins to shorten because the force vectors are more aligned vertically along the spin axis, and the descent rate usually slows for the fully developed flat spin. At very high angles of attack during a flat spin, autorotation may even be stimulated

more from the fuselage than the wing. By using ailerons-against the spin, the inside wing creates more drag and normally increases the rotational speed, thereby increasing the centrifugal forces causing the nose to raise even more. Any lift on the inside wing and reduced lift on the outside wing will tend to level the wings as well, translating more roll energy to yaw energy. Therefore, using ailerons against the spin normally has an adverse effect on recovery with all other effects being constant.

The longitudinal location of the center of gravity can have an important influence on the nature of the spin. Generally, a forward CG setting is more resistant to spin entries and is more hesitant to continue rotation, but not always. An airplane can have worse spin and recovery characteristics at a forward CG. Aft CG's contribute more to easier spin entries because the nose-down pitching moment is less and it is easier to obtain higher angles of attack for deeper stalls, often resulting in flatter spins. The destabilizing forward fuselage becomes longer and aft fuselage damping is less, further degrading spin recovery. Nevertheless, center of gravity effects can be unpredictable for the particular aircraft as other inertial and aerodynamic forces/moments may be overriding.

Spinning with flaps deployed can have a very unpredictable effect on the spin. When flaps are deployed the lift curve shifts left and up, increasing the lift coefficient, but at a lower angle of attack. This means that the stall is encountered earlier, but the airfoil possesses a greater nose-down pitching moment, which tends to promote an overall steeper spin attitude. Therefore, it is often assumed that flap-down spins are safer than the flaps-up case, but every airplane may exhibit the opposite effect if other inertial or aerodynamic forces/moments are influenced to be more adverse. In any event, this thesis study will briefly examine what behaviour flaps impose on spin recovery as rolling moments of inertia is changed.

Gyroscopic precession of the aircraft's mass can have a proverse or adverse effect on spin behaviour depending on the airplane's mass distribution. The combined spinning masses of the fuselage and the wing, as they rotate about the roll, pitch and yaw axes, interact with one another to produce either pro-spin or anti-spin moments. If enough force or moment is applied to a spinning mass (gyroscope) in an attempt to tilt the gyroscope, then there will be a reaction 90 degrees downstream from where the force/moment was applied. For example, in the case of a wing-heavy airplane that develops a lot of energy about the roll

axis during a right spin, then the upward pitching moment from centrifugal effects cause a precessional effect on the rolling mass to result in a pro-spin yaw, flattening the spin. However, if the disturbance was a yawing torque (say from increasing pro-spin turn rate) rather than a pitching one, then a nose down pitching moment would result. The same should happen in a left spin, and the overall effect on the spin depends upon the strength of the disturbance. Gyroscopic precession can greatly influence differences between right and left spins during the development stages and especially in oscillatory spins. Thus, gyroscopic influences in the spin are complex and often there can be factors that tend to cancel the precessional effects. To further understand the gyroscopic precessional effects caused by using ailerons-against the spin and from deploying the recovery parachute, see Table 2-3.

Propeller precession has the same principle as aircraft mass gyroscopic precession. Propeller precession normally reacts from disturbances about the yaw and pitch axes, and it depends on the size, weight and rotational speed of the propeller. However, the effects from this are minimal in the radio-controlled model case, as the propeller has little mass compared to the airplane and will be operated at idle speed (~2500 rpm) during all spin events.

In summary, all factors that affect spin behaviour must be considered together to formulate explanations of spin behaviour. For this thesis study, the model's tail configuration and shape of the model are fixed. Its mass distribution and center of gravity were varied causing some predicted outcomes and some anomalies. It was the balance between aerodynamic and inertial forces/moments that were disturbed to cause some unusual behaviour.

For completeness' sake, Figure 2-2 shows the airplane's body axes and rotation rate conventions used in this thesis study.

Experimental Considerations – Dimensional Analysis/Similitude

Aerodynamicists rely on carefully designed experiments to gain insight into complicated aerodynamic problems that cannot be solved analytically or even with a computer (computational fluid dynamics). The complex dynamics of the aircraft spin is one such area that depends greatly on flight test experimentation. Experiments are typically performed on full-scale prototypes or on scaled-down models where time, cost, and risk are

Table 2-3. Gyroscopic Precessional Effects.

Action	Aerodynamic or Inertial Effect	Gyroscopic Disturbance Input	Precessional Output
Ailerons-Against the Spin	Increases spin rotation rate from down-going aileron.	Pro-spin yaw disturbance on roll axis.	Nose-down pitching moment.
	Flattens the fuselage and increases AOA from centrifugal effects as spin rate increases.	Nose-up pitching moment disturbance on yaw axis.	Wings leveling rolling moment.
		Nose-up pitching moment disturbance on roll axis.	Pro-spin yawing moment.
	Flattens the wings from centrifugal effects as spin rate increases and aerodynamic lift changes.	Anti-spin rolling disturbance on yaw axis.	Nose-down pitching moment.
	Increases yaw rate from dissipated rolling rate.	Pro-spin yaw disturbance on roll axis.	Nose-down pitching moment.
Spin Recovery Parachute Deployment	Nose-down pitching moment.	Nose-down pitching moment disturbance on yaw axis.	Pro-spin rolling moment.
		Nose-down pitching moment disturbance on roll axis.	Anti-spin yawing moment.
	Anti-spin yawing moment.	Anti-spin yawing moment disturbance on pitch axis.	Wings leveling rolling moment.
		Anti-spin yawing moment disturbance on roll axis.	Nose-down pitching moment.

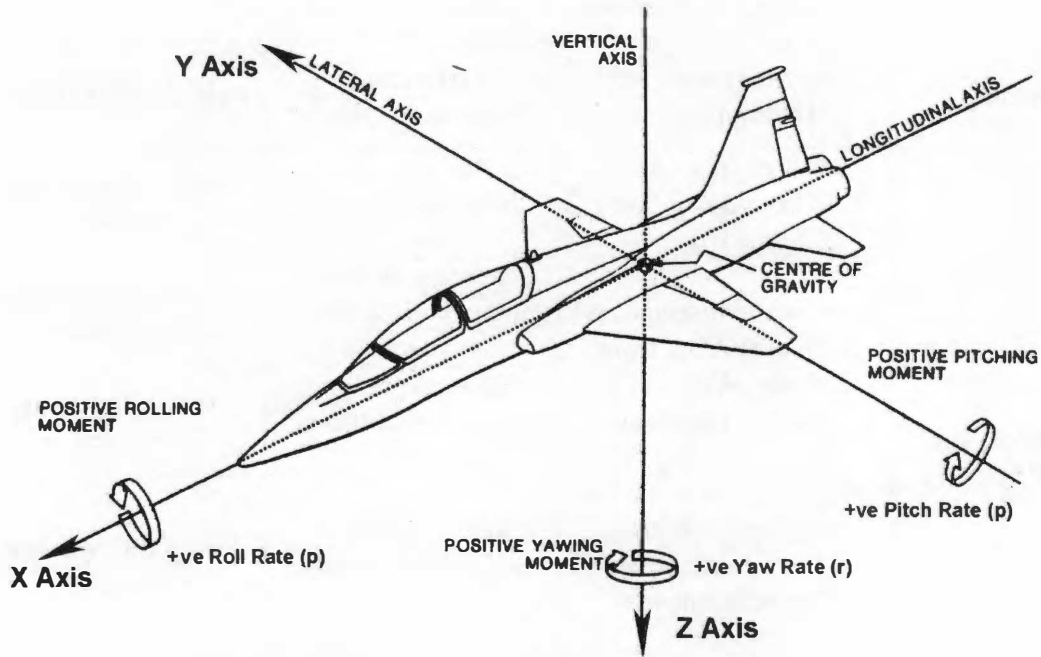


Figure 2-2. Body Axes and Rotation Rate Conventions [39].

constraints. Flight test research using models may augment the full-scale tests by providing a prediction of what to expect during the full-scale tests. This is an especially important consideration for hazardous spin testing of new aircraft designs.

To ensure the experimental results properly reflect the performance of the representative full-scale flow, geometric and dynamic similarity between the full-scale aircraft and the scaled-down model are essential. All the variables that could potentially influence a flow situation can be vast and deciding how to report the effect of all the possible variables on the results can be very difficult. These issues are addressed by the concepts of similitude (the theory of models) and dimensional analysis. Dimensional analysis allows for the consolidation of the numerous variables governing the complex flow into a reduced, more manageable number of dimensionless parameters. Equating the non-dimensional parameters permits the direct comparison of experimental data obtained using a scaled-down model with the full-scale aircraft. *White* [26] details the Buckingham Pi theorem as one such scheme to reduce a number of dimensional variables into a smaller number of dimensionless groups. The variables relevant to this research study can be described by the following function:

$$f_1(\rho, \mu, V, I, W, l, S, g, \Omega, \beta, \alpha, \delta, \Gamma, \theta_T, t, T, P) = 0$$

where:

ρ	is the free stream air density
μ	is the free stream coefficient of viscosity for air
V	is the spin descent velocity
I	is the moment of inertia about a body axis
W	is the gross weight
l	is a linear geometric dimension
S	is the area of a flight surface
g	is the acceleration of gravity
Ω	is the spin rate
β	is the angle of sideslip
α	is the angle of attack
δ	is the angle of deflection for a flight control
Γ	is the dihedral angle
θ_T	is wing twist
t	is time
T	is thrust
P	is engine power

The dimensional analysis problem is one of 17 variables in 3 dimensions: M, L, T (mass, length, and time). Therefore 14 dimensionless variables are expected. Selecting ρ , V , and l as repeating variables, and using a matrix method to simultaneously determine the 14 non-dimensional groups, we get:

$$\Pi_1 = \frac{\mu}{\rho V l} = \frac{1}{\text{Re}} \quad \text{- inverse Reynolds number}$$

$$\Pi_2 = \frac{I}{\rho l^5}$$

$$\Pi_3 = \frac{W}{\rho V^2 l^2}$$

$$\Pi_4 = \frac{S}{l^2}$$

$$\Pi_5 = \frac{gl}{V^2} = \frac{1}{Fr} \quad \text{- inverse Froude number}$$

$$\Pi_6 = \frac{\Omega l}{V^2}$$

$$\Pi_7 = \beta$$

$$\Pi_8 = \alpha$$

$$\Pi_9 = \delta$$

$$\Pi_{10} = \Gamma$$

$$\Pi_{11} = \theta_T$$

$$\Pi_{12} = \frac{tV}{l}$$

$$\Pi_{13} = \frac{T}{\rho V^2 l^2}$$

$$\Pi_{14} = \frac{P}{\rho V^3 l^2}$$

The above can be rearranged and reduced as follows:

$$f_2 \left(\text{Re}, \frac{l}{\rho l^5}, \frac{W}{\rho V^2 l^2}, \frac{S}{l^2}, Fr, \frac{\Omega l}{V^2}, \beta, \alpha, \delta, \Gamma, \theta_T, \frac{tV}{l}, \frac{T}{\rho V^2 l^2}, \frac{P}{\rho V^3 l^2} \right) = 0$$

Of particular importance in this exercise were the two non-dimensional groups – Reynolds number and Froude number. Normally, for incompressible flow situations such as this, the model and full-scale airplane must have equal Reynolds numbers. As discussed later in more detail in the “Reynolds Number Considerations” subsection, Reynolds number equivalence cannot be obtained in air for both the test model and the full-scale airplane. But, dynamic similarity requires the model and the full-scale airplane to have the same length-scale ratio, time-scale ratio and mass-scale ratio. Mass-scale ratio implies weight and inertia scaling. Perfect dynamic similarity is more of a dream than a reality when it comes to obtaining true equivalence of Reynolds number for flight test in air. Since both the velocity

and length scales are constrained by the Froude number, Reynolds number scaling is violated due to viscosity. However, to obtain some adequate similitude scaling formulas to correlate model and full-scale test data, the kinematic similarity provided by the Froude number must be employed, as Reynolds number and Mach number are inappropriate. By demanding equivalent Froude numbers for the model and the full-scale airplane, a velocity scale was obtained. With a length scale and velocity scale available, scaling formulas were derived for weight, spin rate, time, thrust and power. Scaling formulas for area and moments of inertia required use of only the length scale in their derivation.

This method of Froude number equivalence is not commonly seen without free surface flows, but similitude rules for models that must operate in the atmosphere require this method. This was also the method employed by NASA in their radio-controlled model spin testing. Therefore for this thesis study, it is considered that the model is “dynamically Froude number scaled”. Nevertheless, Reynolds number must still be carefully analyzed and not discounted (see next sub-section).

Now, let N be the linear geometric scaling factor for the model. For this thesis study, $N = 6$. Subscript M denotes the model and A the full-scale airplane. Therefore, the similitude formulas that define the proper scaling relationships between the airplane and model can be obtained by equating the non-dimensional parameters for the model and full-scale airplane. They are as follows:

Length Scale:	$l_M = \frac{l_A}{N}$
Area Scale:	$S_M = \frac{S_A}{N^2}$
Weight Scale:	$W_M = \frac{W_A}{N^3} \frac{\rho_M}{\rho_A}$
Moment of Inertia Scale:	$I_M = \frac{I_A}{N^5} \frac{\rho_M}{\rho_A}$
Velocity Scale:	$V_M = \frac{V_A}{\sqrt{N}}$
Spin Rate Scale:	$\Omega_M = \Omega_A \sqrt{N}$

Time Scale:	$t_M = \frac{t_A}{\sqrt{N}}$
Thrust Scale:	$T_M = \frac{T_A}{N^3} \frac{\rho_M}{\rho_A}$
Engine Power Scale:	$P_M = \frac{P_A}{N^{7/2}} \frac{\rho_M}{\rho_A}$
Angle Scales:	$\alpha_M = \alpha_A$ $\beta_M = \beta_A$ $\delta_M = \delta_A$ $\theta_{TM} = \theta_{TA}$ $\Gamma_M = \Gamma_A$

All the above scaling formulas were used except for velocity, thrust and engine power. Velocity data were not collected during the spin tests because of the difficulty in making an accurate sensor for high angle of attack spin maneuvers. Although, not particularly needed for the spin analysis, velocity data would have facilitated the non-dimensionalization of spin rate. Full-scale thrust was unknown for in-flight idle settings, therefore no thrust scaling was carried out, but propeller diameter was properly scaled down. Also, since spin testing was carried out at idle power, it was not necessary to install a scale-sized engine¹. Note that all angles are preserved in geometric similarity.

All the above effort was to obtain scaling formulas so model dimensions, mass properties and spin data could be related to full-scale. After the model spin data are converted to full-scale, it must be made non-dimensional by determining another set of dimensionless groups of parameters. They are:

$$f_3(V, b, m, I, \Omega) = 0$$

where:

V is the spin descent velocity

b is the wing span

¹ If engine power scaling was required, then a model engine with 0.45 hp would be necessary. That is typical of a 0.25 cu.in. displacement two stroke hobby engine, totally underpowered for this thesis study.

- m is the mass of the air vehicle
- I is the moment of inertia about a body axis
- Ω is the spin rate

Following the same procedure as above, the dimensional analysis problem is one of 5 variables in 3 dimensions: M, L, T (mass, length, and time). Therefore 2 dimensionless variables are expected. Selecting V , b and m as repeating variables, and using a matrix method to simultaneously determine the 2 non-dimensional groups, we get:

$$\Pi_1 = \frac{I}{mb^2} \quad \text{and} \quad \Pi_2 = \frac{\Omega b}{V}$$

Π_1 is commonly known as an inertia moment parameter, but usually takes the form as a difference between two moment of inertia values. Most commonly used, and most relevant to this thesis study is the inertia yawing moment parameter (IYMP), which was first conceived in early 1940's. Π_2 is commonly known as the dimensionless spin rate, and is normally divided by 2 (representing a semi-span, which is the distance from the spin axis to the wing tip when the spin axis is aligned at the CG). Therefore, the dimensional analysis equation becomes:

$$f_4 \left(\frac{I_x - I_y}{mb^2}, \frac{\Omega b}{2V} \right) = 0$$

The IYMP parameter was used in this thesis, but the dimensionless spin rate was not, because descent rate data were not collected during the spin events. Therefore, any spin rate data will only be displayed as full-scale values, which should be satisfactory to appreciate the effects caused by variations in the IYMP.

Aeroelastic Similarity

There was one similarity analysis not considered above, aeroelastic similarity. In some cases it is important that a model and its full-scale counterpart have the same structural

stiffness distribution that would reproduce the same natural frequencies and mode shapes. For an airplane's wing, aeroelastic similarity requires the correct area moment of inertia distribution, correct spanwise mass distribution, and correct internal damping. *Bisplinghoff et al* [40] and *Fung* [41] explain and derive the non-dimensional parameters and modeling laws, but one must use engineering judgment to determine the relative importance and applicability of aeroelastic similarity.

For spin testing purposes, a model with aeroelastic similarity was not important compared to the geometric and inertial properties. The flight envelope being explored was well below the flutter speeds where aeroelastic behaviour is important. Additionally, construction of a radio-controlled model with scaled structural stiffness could compromise the moment of inertia distribution, exacerbating the construction challenge.

Reynolds Number Considerations

As indicated above, testing the radio-controlled model in the atmosphere violates the Reynolds number similarity parameter. Reynolds number cannot be discounted as it is one of the most important parameters in fluid mechanics. The Froude number, which is purely a kinematic parameter, was not contravened ensuring that length and time scales are adhered to. Nevertheless, departures from similarity rules may be permissible provided that violations are justified through experimental comparison to show that the full-scale behaviour is not significantly affected. There are two primary components of the radio-controlled model that influence Reynolds number effects, the wing and fuselage. At high angles of attack, various separation phenomena occur, some of which are Reynolds number dependent.

Chambers [2] indicated the effects of Reynolds number on the lift of a typical wing airfoil (NACA 64-series), which can be seen in Figure 2-3. The Reynolds number for the thesis spin model is approximately 0.3×10^6 . Comparison between low and high Reynolds number reveals that effects are predominant on lift coefficient (C_L) below an angle of attack of 30 degrees. This is experienced during the entry and development (incipient) phases of a spin where the angle of attack is below 30 degrees. Above 30 degrees, Reynolds number effects are less significant. This area is characteristic of moderately steep to flat spins. Since coefficient of drag (C_D) is influenced by both Reynolds number and coefficient of lift, the

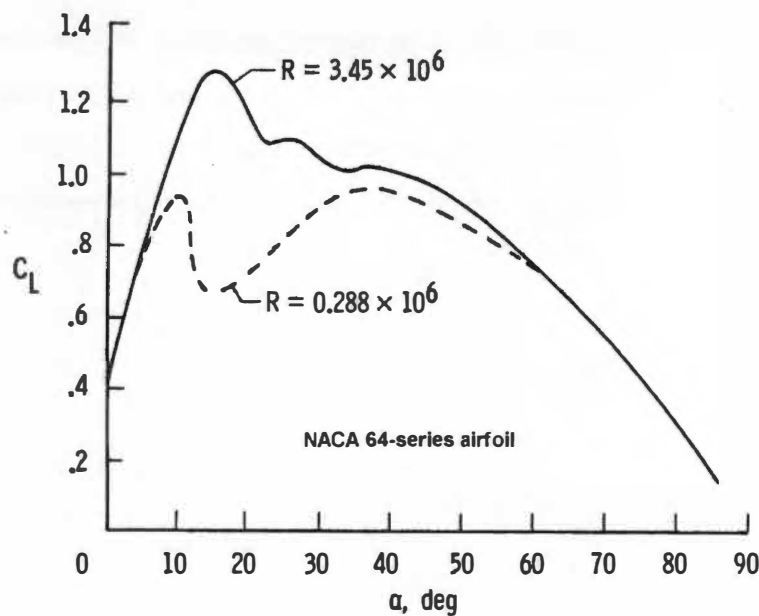


Figure 2-3. Effect of Reynolds Number on Lift [2].

same effect can be assumed. Therefore, to minimize any effects of Reynolds number, spins should be in the developed stage before recovery is initiated. From references [4, 5, 20], it was recommended that spins be allowed to develop into a steady spin by carrying out up to six turns before recovery.

The fuselage aerodynamics during a spin are much different than the wing. Reynolds number effects are always apparent on the fuselage. *Polhamus* [27] in 1959 discovered that Reynolds number and cross sectional shape have large effects on the aerodynamics during a spin. Fuselage side forces in a spin may even change from anti-spin to pro-spin as Reynolds number changes from the model to full-scale. Furthermore, research performed by *Clarkson et al* [28] in 1976 indicated that fuselages with noncircular cross-sections, which have corner radii are particularly susceptible to variations in Reynolds number. *Neihouse* [20] mentioned that these effects might be amplified if the fuselage nose is long and the projected area of the fuselage is large relative to the wing area. These fuselage Reynolds number effects could change the complete balance of forces and moments in a spin, and the autorotative spin rate, thereby complicating the correlation of model results to full-scale. The junction at the wing and fuselage can also pose various Reynolds number effects.

In summary, Reynolds number effects must be evaluated for each particular geometry and results carefully examined. The radio-controlled model used in this thesis study is typical of the models used in references [4, 5, 6, 7], which claimed to have insignificant Reynolds number correlation problems. Nevertheless, some of the spin anomalies encountered in this thesis could be attributed to Reynolds number effects, which are discussed in Chapter IV.

CHAPTER III

EXPERIMENTAL APPROACH

Experimental Objectives

The primary objective of this thesis study was to investigate and determine the general effects of rolling moment of inertia variations upon spin recovery for general-aviation aircraft using a radio-controlled model. A secondary objective was to correlate the test data from the radio-controlled model to the full-scale representative airplane. Also, it was desired to investigate the use of hobby-type angular rate gyros for measuring rates of rotation in spin testing research.

Experimental Set-up and Method

The Test Model

As mentioned earlier, a model fuselage was made available for possible use in this project. It was representative of a Piper PA-28-180 Cherokee of 1970's vintage. Its scale was 1/6, which would be just large enough to be visually seen during the flight tests. Since the Cherokee was typical of general-aviation aircraft, it was decided to use this model design for spin testing.

The model was Froude number dynamically scaled with a wingspan of 5.0 feet and test weight of 14.6 pounds. The model represented the full-scale airplane flying at 10,000 feet MSL. Time permitted only one model to be built by the author, so a spin recovery parachute system was designed and used to ensure the best possible survivability from the more dangerous flat spin events. The model's geometric size was measured against the full-scale airplane and was also built with scale slotted flaps and wheel pants. The wheel pants were later removed as they posed a hazard to the flaps during hard landings where the strut assembly would flex rearward and contact the deployed flap breaking its servo geartrain. The powerplant was a standard two-cycle model airplane engine that had a displacement of 0.61 cubic inches and developed approximately 1.9 horsepower at 19,000 rpm with glow-plug ignition. A hobby 10-channel PCM remote control system with 11 servos was used to

function the flight controls, nose wheel steering, throttle, flight data recorder system, and the spin recovery parachute system. The complete model description, construction techniques, geometric and mass data, fuel system, etc. are contained within Appendix A.

The wing loading of the model was 52 oz/ft². It may not be obvious, but this wing loading is very high, in fact, almost double that of typical radio-controlled models. This presented more of a challenge to the pilot as the handling qualities were much more critical, especially during slow speeds near the ground. Landings dictated use of full-down flaps with some power-on to reduce touchdown speeds and to minimize damage to the landing gear. Cross-wind landings were always a chore and entertaining to the spectators.

One pilot, the author, operated all functions of the model except the spin recovery system, which was activated by an assistant flipping a switch on the pilot's transmitter. *Burk and Wilson* [8] used two pilots to reduce pilot workload, one pilot functioning the longitudinal controls (elevator) while the other pilot operated the lateral-direction controls (ailerons and rudder). It was the opinion of this thesis author that a model cannot be flown well with partial control, especially during maneuvers requiring quickly coordinated responses. Therefore, the one pilot system was used and with much success.

The model was painted white with orange trim and the bottom of one wing was painted orange to provide some visual contrast during the spin events. It was found, however, that white paint provided poor contrast with the background sky and clouds. This problem was very apparent for the videographer, often requiring as much as 30 seconds to locate the model at 800 feet altitude. A darker colour such as black would have been superior.

A photo of the author with the test model prior to taxi is shown in Figure 3-1.

Instrumentation

The model was instrumented with angle of attack, angle of sideslip, rate sensors about the three body axes, and position sensors for the stabilator, ailerons and rudder. The data were collected by an on-board flight data recorder (FDR) at a sampling rate of 5 Hertz. A 9V battery powered the FDR and all the sensors. After each flight, the model was



Figure 3-1. Author with Test Model Prior to Taxi.

connected to a laptop computer to download the data and import into Microsoft Excel for further reduction. Appendix B explains in more detail the components used, how the systems worked and the calibration methods used.

The angle of attack and sideslip vane sensors were mounted on booms projecting one chord length ahead of each wingtip in accordance with recommendations by *Kimberlin* [11]. AOA was on the right tip and sideslip on the left. This was not an ideal set-up for AOA, as it did not provide true AOA data at the center of gravity. Because the down-going (inside) wing during a spin experiences a higher local angle of attack than at the CG or compared to the up-going (outer) wing, AOA results will bias to higher values in right spins than left spins. Normally, AOA sensors are installed at each wingtip and their results averaged, then a correction factor applied [*Moul*, 29]. In retrospect, the sideslip sensor should have been eliminated and used as an angle of attack sensor. Sideslip data were not significantly meaningful for conclusions to be drawn in this study.

Flight control position sensors used were electrical potentiometers that were linked to the output arms of the flight control servos. This system worked well and is described more

in Appendix B. Flight control position recordings were essential to determine when the stall and spin were initiated, when ailerons-against the spin were applied and when recovery action took place. All the flight data were plotted as time histories, so it was easy to extract the pertinent spin data, based on the flight control position recordings.

Rotation rates about the three body axes were sensed by off-the-shelf hobby rate gyros, commonly used in radio-controlled helicopters. The signals from the gyros were converted from pulse width modulation to volts DC so that the FDR could record them. The sensitivity of these gyros was impressive, reacting very quickly to changes in rotation rates. One gyro was oriented in each plane of rotation. Locating the rate gyros at the center of gravity was neither required nor feasible. Unfortunately, the recorded gyro data served limited use, where it could have served immense use. It was discovered during the spin program that the gyros had sensory limits to a maximum of 55-200 deg/s, depending on the gyro. Unfortunately, the cause was not investigated prior to thesis writing. If gyro calibration could have provided rotation rates above 30 deg/s to be near 300 deg/s, then this problem would have surfaced prior to the spin program. The cure would either have been to reduce the gyros' gain or to replace the gyros with a different brand. Accurate body axis rotation rate data would have served to calculate the spin rate (Ω) about the spin axis and to correct for true angle of attack. For further explanation, see the "Data Reduction Procedure" section.

Spin Recovery Parachute System

A spin recovery parachute system was designed and installed on the model's tail. The purpose of the system was to stop any yawing motion and cause a nose-down pitching moment so that controlled flight could be restored. The system was designed so that the parachute could be remotely released from the model at the pilot's convenience after recovery. The system was deployed once in a steep spin to prove that it worked and twice to recover from flatter spins.

The design of the system was partially based on the research by *Burk et al* [30]. Their research determined the tail parachute diameter and canopy distance required for emergency spin recovery. For full-scale recovery from flat spins, a parachute diameter of about 10.5 feet and a canopy distance (riser length plus suspension line length) between 15

and 20 feet were necessary based on spin tunnel testing of a 1/11 scale model. It was determined that if the canopy distance was too short, the parachute canopy may be too close to the airplane and its wake may potentially interfere with the chute, perhaps causing it to collapse. If the canopy distance was too long, the parachute would trail above the airplane on the spin axis, producing a nose-down pitching moment but no yawing moment to stop the spin. Figure 3-2 pictorially shows the effect of parachute line length. It was decided to scale down the parachute diameter to 1/6th scale, but not the canopy distance. Rather, canopy distance was determined as a function of fuselage length, because the distance from the parachute mount to the CG was the important parameter to avoid problems related to too long a canopy distance. The ratio of canopy distance to fuselage length was calculated to be between 3/4 and 1/1. It was decided to average the ratios and use 7/8. The result was a parachute diameter of 24 inches and a canopy distance of 42 inches.

Burk et al [30] had also determined that a parachute with a canopy porosity of 400 or greater was needed to ensure stability with a corresponding drag coefficient of 0.50. Parachute stability was determined to be important so that the parachute will trail with the relative wind and apply an anti-spin yawing moment. An unstable parachute that has high oscillations may apply yawing moments that vary between anti-spin and pro-spin, delaying recovery. Thus, ring-slot or ribbon type parachutes with geometric porosity were recommended for full-scale applications. *Burk and Wilson* [8] followed these recommendations with success for their radio-controlled spin test project. Unfortunately, a 24-inch ring slotted parachute was not readily available on the market, so it was decided to purchase an available 12-inch inexpensive solid parachute. It was 50% smaller than recommended but had less porosity, so its stability was in question. Its drag coefficient was unknown. Nevertheless, it was tested and proved to work well enough. In level flight, there was significant gyrating motion of the parachute behind the model causing approximately $\pm 10^\circ$ oscillations in pitch. Yet, erratic level flight could be maintained due to the power of the engine and the parachute could be released when desired.

For the two cases when the recovery parachute was needed, the recovery parachute ceased the spin and then caused a transfer of yawing and pitching energy to rolling energy complemented by the gyroscopic precessional effects caused by the parachute force. The result was two or three quick axial rolls towards the ground after the spin stopped, which

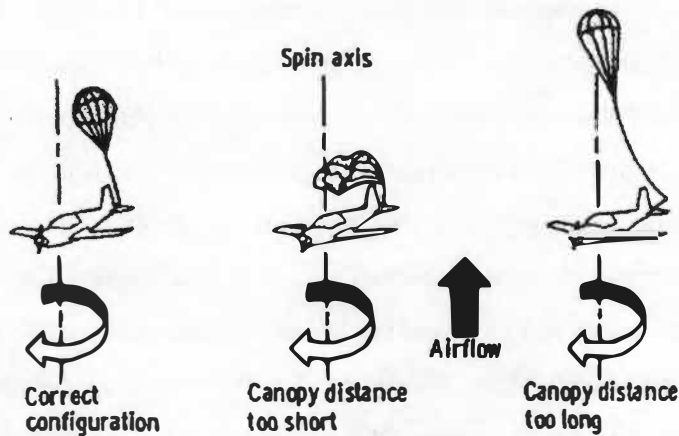


Figure 3-2. Effect of Parachute Line Length [30].

delayed the pull-up for recovery. This was unexpected and caused a loss of sufficient altitude for safe recovery after the last spin event was carried out. The model crashed, which is explained in more details in Chapter IV.

The recovery parachute system's design and photos are contained within Appendix C.

Mass Properties and Moments of Inertia Measurements

As explained in the dynamic similitude section of Chapter II, mass properties must be scaled down properly to reflect the full-scale airplane. Three conditions were important to be simultaneously satisfied for mass properties: total weight of the model, moments of inertia about the three body axes, and center of gravity position. Changing one or two of the properties caused a change to the other(s). Consequently, achieving acceptable mass properties was iterative and consumed much time. Additionally, it was desired to increase only the rolling moment of inertia without disturbing the other moments of inertia, the total weight or the CG position. This was never achieved due to the “bare bones” weight distribution and construction of the model.

To simulate increased rolling moment of inertia, it was decided that the experimental approach would be based on changes in rolling moments of inertia created by variations of fuel capacity in the wing of the full-scale airplane. This approach would enable a “realistic” appreciation of any potential adverse effects on spin recovery. It was decided that a total of 20 additional gallons of aviation fuel would be a typical requirement for a general-aviation

airplane. Therefore, the increased moments of inertia about the three body axes were calculated based on an additional 10 gallons per wing located at mid span. This translated to approximately 21% increase in rolling moment of inertia (I_x) for the full-scale airplane and the model, and an IYMP increase from -56×10^{-4} to 8×10^{-4} . It was also decided to flight test the model in a reduced state of inertia for trend comparisons. For this case, the mass that was added to the wing tip bays for “stock” condition were simply removed causing a reduced rolling moment of inertia.

The method of adding or removing mass from the wing tip bays to achieve the desired rolling moment of inertia (I_x) also caused the yawing moment of inertia (I_z) to change and minor changes resulted to the pitch moment of inertia (I_y). I_z increased up to 10% and I_y 2%, when I_x was increased by 21%. Gross weight increased by 3% (0.48 lbf) over stock weight when the inertia state was increased.

The bifilar torsional pendulum technique was used for moment of inertia measurements about all three axes. Measurements were made for the forward and aft CG settings in the reduced, stock and increased rolling moment inertia states. Appendix D explains the method, along with photos of the operation.

All mass properties and error analyses are also contained in Appendix D. Table 3-1 below shows the mass properties for only the forward CG setting (24.8% MAC).

Stock mass properties were obtained from *McCormick* [31] for the full-scale Piper PA-28-180 Cherokee. It was assumed that *McCormick*'s data were calculated data from the manufacturer, and not actually measured. Success at obtaining the scaled-down moments of inertia was not obtained. In fact, moments of inertia using the bifilar torsional method

Table 3-1. Model Mass Properties at Forward CG Setting (24.8% MAC).

CG Position (% MAC)	Gross Weight (lbf)	Moments of Inertia (slug-ft ²)			$\frac{I_x}{I_y}$	Rolling Moment of Inertia State
		I_x	I_y	I_z		
	14.44	0.2609	0.3836	0.5935	0.680	20% decrease
24.8	14.75	0.3246	0.3795	0.6587	0.855	stock
	15.23	0.3914	0.3822	0.7176	1.024	21% increase
Published Data	14.60	0.1805	0.2107	0.3901	0.857	stock target

revealed differences of up to 80% compared to *McCormick's* data. It was impossible to reduce these values because the model's density could not be reduced any further. As this was a significant departure from published data, it was decided that a different approach was needed to give some confidence with the measured values. Since the model's weight was near its target weight (1% difference), the ratios of I_x/I_y , I_x/I_z , and I_y/I_z better represented the mass distribution. Resulting was 0.2% difference in I_x/I_y , and a 6.6% difference for both I_x/I_z and I_y/I_z . Accuracy of I_x/I_y was deemed to be more important than the other two ratios for the spin testing, just as the inertia yawing moment parameter (IYMP) is often considered to be the important parameter. Hence, the non-dimensional I_x/I_y parameter was used for comparison purposes in lieu of the IYMP. Nevertheless, IYMP was calculated for the full-scale airplane based on the model's values using the derived dynamic similitude formulas. IYMP was also found to be the same for the model and the full-scale airplane. Table 3-2 contains the IYMP values as well as the scaled up weights for the full-scale airplane. One can see that an aft CG may not always be more the critical case in terms of IYMP. For example, the greatest IYMP was at the forward CG position with the increased inertia state.

Aircraft Spin Configurations

Table 3-3 presents the configurations that were spin tested. Not all spin events were conducted due to an unfortunate accident that prevented the model from being repaired in a timely fashion.

Table 3-2. IYMP and Weight Properties for the Full-Scale Airplane.

CG Position (% MAC)	Rolling Moment of Inertia State	Weight (lbf)	IYMP
24.8	Reduced	2378	-109×10^{-4}
	Stock	2429	-48×10^{-4}
	Increased	2508	8×10^{-4}
28.4	Reduced	2378	-118×10^{-4}
	Stock	2429	-56×10^{-4}
	Increased	2508	-4×10^{-4}
Published Data	Stock	2400	-27×10^{-4}

Table 3-3. Aircraft Spin Configurations (L = left, R = right).

Flap Position, Aileron Position	Rolling Moment of Inertia State	CG Position		
		Fwd (24.8% MAC)	Mid (26.6% MAC)	Aft (28.4% MAC)
Flaps Up, Ailerons Neutral	Reduced	L, R	L, R	L, R
	Stock	L, R	L, R	L, R
	Increased	L, R	L, R	L, R
Flaps Down, Ailerons Neutral	Reduced	L, R	L, R	-
	Stock	L, R	L, R	L, R
	Increased	L, R	L, R	-
Flaps Up, Ailerons Against	Reduced	-	-	L, R
	Stock	L, R	-	-
	Increased	-	-	L

Flight Test Technique

The flight test procedure was as follows:

- For the first flight of the day, a range check of the radio-control system was carried out to verify radio integrity;
- A serviceability check of the FDR system was carried out with it connected to the laptop computer;
- Model was fueled, started and engine tuned for best performance;
- Model was taxied, then taken-off;
- Model was climbed to approximately 800 feet AGL and trimmed for level flight in the desired aircraft configuration;
- Spin event number was captured on video;
- Model was then captured on video;
- FDR was switched on at the transmitter;
- Throttle was reduced to idle and the pitch control eased back to slowly stall the model;

- j. Just before the model stalled, full rudder was inputted and full up-stick was held with ailerons neutral to commence spin maneuver;
- k. After $\frac{1}{4}$ turn, opposite aileron was inputted, if applicable for spin event;
- l. Recovery was initiated after letting the model spin for 2-3 turns, to allow sufficient altitude for pull-out and possible deployment of the spin recovery parachute. When recovery was initiated, the pilot called out "Recovery Now", to have the audio captured on the video recording;
- m. Level flight was regained;
- n. FDR was switched off;
- o. Altitude was re-gained and the above steps repeated for the next spin event in the configuration desired;
- p. Up to four spin events per flight were possible at a flight time of approximately 6.5 minutes before the fuel was consumed;
- q. Model landed and taxied back to be downloaded;
- r. After downloading, the 9V FDR battery was disconnected at the model's access door;
- s. Model was refueled and its receiver batteries charged, if required; and
- t. Model and instrumentation were visually checked for serviceability.

Data Requirements

The following data were collected prior to start-up:

- a. Model's weight, CG position, and inertia state; and
- b. Date.

The following data parameters were collected after each spin event for documentation purposes and further analysis:

- a. Spin rate, pro-spin turns, and turns for recovery from the video recording;
- b. Roll rate;
- c. Pitch rate;
- d. Yaw rate;
- e. Angle of attack;

- f. Angle of sideslip;
- g. Elevator position;
- h. Rudder position;
- i. Aileron position; and
- j. Spin and recovery control inputs using the Stone Spin Shorthand Method [Kimberlin, 11].

Test Conditions

The minimum weather requirements demanded no rain, no wind greater than 15 knots, and a ceiling of 800 feet AGL.

Test Facility

Flight tests were carried out at Tullahoma Regional Airport, Tullahoma, Tennessee. Tullahoma airport was originally built for the U.S. Army Air Corps in 1942. Today, the airport is a civilian facility operating with uncontrolled airspace. Model flights were conducted on a decommissioned runway away from the active runways. The runway area for the model was approximately 150 feet wide and 1000 feet long. The airspace was shared with full-scale aircraft, so it was mandatory to have someone else act as a spotter to alert the model pilot of nearby air traffic.

The surrounding grass was approximately three feet high and aided any emergencies off the runway. However, a four-wheel drive truck was required for model search and recovery.

The airport also had an automated weather service to provide real-time weather information to the test team.

Data Reduction Procedure

Data reduction was required for all data parameters collected. Each parameter is discussed separately in the following paragraphs.

Angle of Attack Data Reduction

The raw AOA downloaded from the FDR were converted to degrees using the calibration curve in Appendix B. The calibration of the AOA vane was based on the angle of the boom, which was installed at 2-degrees negative incidence, parallel to the tip washout angle. Thus, 2 degrees were added to the calibrated data, which represented the angle of attack of the wing root. This corrected data was then plotted as a time history with data at every 0.2-second intervals (5 Hertz).

As mentioned earlier, an angle of attack sensor was only located at the right wing tip resulting in higher local AOA for right spins and lower local AOA for left spins. *Moul* [29] determined a data correction procedure where data from the AOA sensors at each wingtip were averaged to determine the AOA at the airplane's center of gravity. To determine the true angle of attack of the airplane, corrections must be applied to the measured local AOA to account for sideslip effects and for the change in flow direction at the sensor location because of the presence of the airplane and sensor pod. *Moul* explained that there were three methods to estimate the errors, but none could be utilized for this test program because of insufficient and inaccurate data to calculate the corrections. Also, AOA corrections caused by spin rate effects were deemed insignificant. Overall, *Moul* found that up to 15% error between the measured and true AOA could be caused by the presence of the airplane and sideslip effects. Figure 3-3 shows *Moul's* correction plot versus measured AOA. Over the range of 10° to 40° AOA, the correction would be approximately -3.8°, and at 50° the error would be approximately -8°. For this thesis study, it was decided that raw AOA data be left uncorrected since the range of AOA would generally have a constant error correction. This error correction would, however, require validation in a wind tunnel for this particular podded design of AOA vane sensors. Therefore, the reduction process for AOA was to plot the measured local AOA versus time and to calculate an average value over the most developed portion of each spin event. It was common practice by the USAF [23] to average out any AOA oscillations to arrive at a more meaningful AOA. Each of these averaged AOA values were then plotted versus CG position and inertia state for trend analysis. Note that the reduced AOA results did not represent AOA at the model's center of gravity. In an attempt to convert AOA data to the model's CG, the left spin event data were averaged with the right spin data and plotted versus CG position and inertia state.

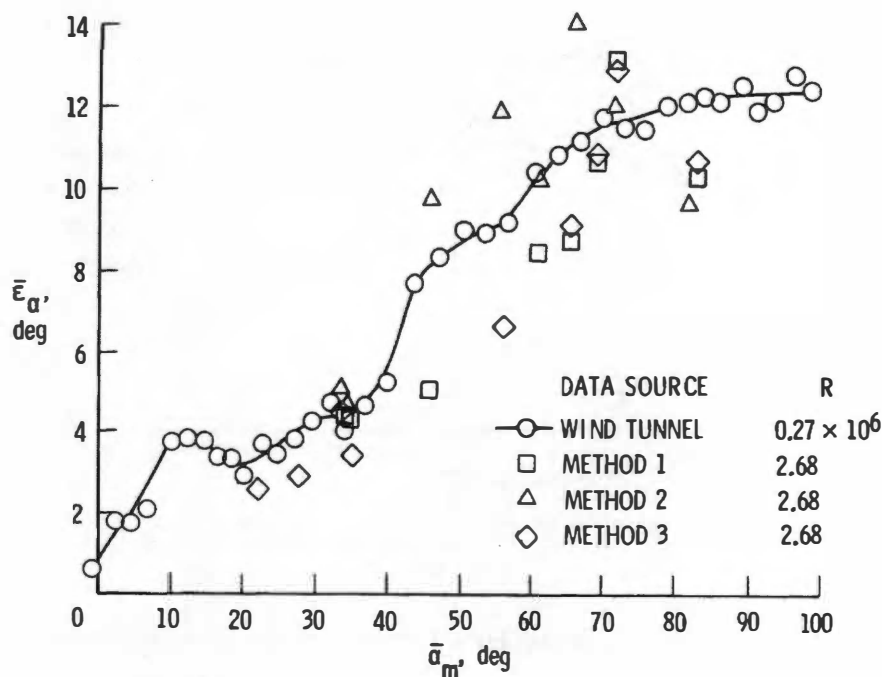


Figure 3-3. Average Angle of Attack Flow Corrections for Spinning Aircraft with Vane Type Sensors Mounted on Wingtip Booms [29].

Angle of Sideslip Data Reduction

The same calibration procedure was used for sideslip as AOA. Measured sideslip values must be corrected for the presence of the model and pod assembly, like the AOA sensor. *Moul* shows in Figure 3-4 that AOS is particularly sensitive to angle of attack and sideslip. Errors can be as high as 7° at a flight attitude of 85° AOA and 17° AOS.

Nevertheless, sideslip data were not corrected because a broken vane that was not discovered until near the end of the test program corrupted most sideslip data. Therefore, only time history plots of AOS were plotted for only several spin events and the values averaged over the most developed portion of each spin event.

Control Position Data Reduction

The raw control position data (elevator, rudder and aileron) downloaded from the FDR were converted to degrees using the calibration curves in Appendix B. Control position data were corrected for trim position by subtracting the level flight data (see Table 4-2).

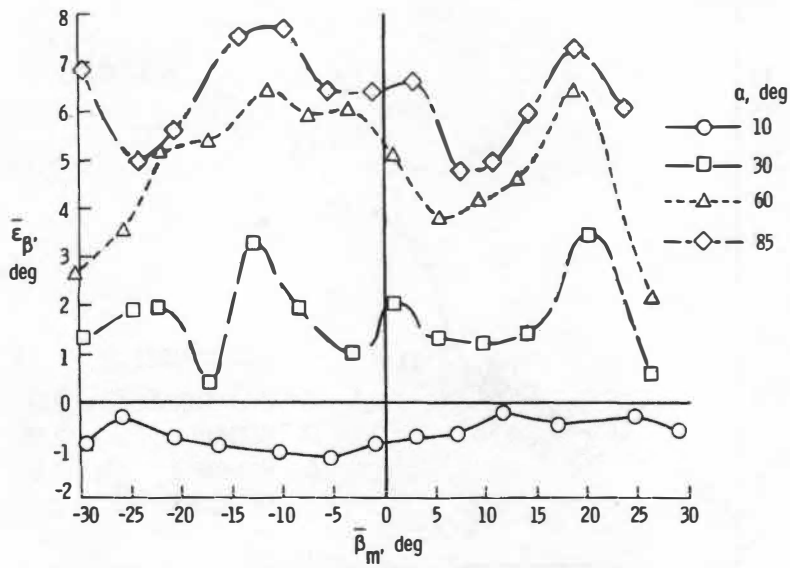


Figure 3-4. Average Angle of Sideslip Flow Corrections for Spinning Aircraft with Vane Type Sensors Mounted on Wingtip Booms [29].

Time history plots were simply carried out for each of the control positions. The control position plots were all put on the same history plots for AOA and AOS.

Rotation Rate Data Reduction

The raw rotation rate data (p , q , r) downloaded from the FDR were converted to degrees per second using the calibration curves in Appendix B. One correction had to be made for the rotation rate data to correct for shifts in the calibration curves, as explained in Appendix B. The pre-flight FDR serviceability check served this purpose to provide rotation rate “zeros” that were applied to the flight data. Therefore, the calibrated data were corrected by subtracting the pre-flight data.

Time histories of all rate data were plotted together for each spin event. The rate data were averaged over the most developed portion of each spin event, as was done for AOA and AOS. Spin rate (Ω) about the spin axis can be computed by taking the vectorial summation of these rotation rates about each body axis:

$$\text{Spin Rate } (\Omega) = \sqrt{p^2 + q^2 + r^2}$$

As detailed by *Moul* [29], rotation rate data can be used to transfer the AOA and AOS measured at each wing tip to the center of gravity, however descent velocity would have been required, which was not collected. In addition, rotation rate data can estimate the true AOA and AOS at the CG by one of the methods by *Moul* [29]. The simplest estimate of true AOA for a steady spin is:

$$\alpha_t = \tan^{-1} \left(\frac{r}{p} \right)$$

However, insufficient gyro range did not provide proper rate data to calculate Ω and α_t .

Video Data Reduction

Spin rate (Ω), spin turns, and turns for recovery were determined from the video recordings. Spin rate (Ω) was calculated using the following formula:

$$\Omega = \frac{360 \text{ deg}}{\text{time for one rotation (sec)}} = \frac{\text{deg}}{\text{sec}}$$

A stopwatch was used to measure the spin rotation time immediately preceding spin recovery. This was carried out twice and then the time averaged for each spin event. The spin turns and turns for recovery were also counted from the video recording. The recorded audio of the pilot calling “Recovery Now” indicated when recovery action was initiated and the subsequent cessation of the spinning motion indicated spin recovery.

Test Plan

A test plan was created to establish the flight test technique, preliminary tests, data requirements, expected spin behaviour, emergency procedures, personnel requirements and duties, contact information, and the test matrix to be conducted. Appendix E documents the test plan employed. 60 spin events were planned.

Precision and Accuracy

The model was manufactured and measured per the following precision:

- a. Linear dimensions and fuselage contours: $\pm 1/32^{\text{nd}}$ of an inch;
- b. Airfoil contours: $\pm 1/64^{\text{th}}$ of an inch;
- c. Wing washout twist: $\pm 1/4$ degree;
- d. All angles of assembled components: $\pm 1/4$ degree;
- e. Flight control rigging: $\pm 1/2$ degree;
- f. Weight: ± 1 ounce;
- g. Center of Gravity location: $\pm 1/16$ inches or 0.6% MAC; and
- h. Moment of Inertia values: $\pm 1\%$

Flight data were reduced to the following accuracy:

- a. Roll rate: ± 2 deg/s below 60 deg/s, ± 10 deg/s above 60 deg/s;
- b. Pitch rate: ± 2 deg/s below 60 deg/s, ± 10 deg/s above 60 deg/s;
- c. Yaw rate: ± 2 deg/s below 60 deg/s, ± 10 deg/s above 60 deg/s;
- d. Local angle of attack: $\pm 0.5^\circ$;
- e. Local angle of sideslip: $\pm 0.5^\circ$;
- f. Flight control positions: $\pm 1^\circ$;
- g. Pro-spin turns and turns to recovery: $\pm 1/8^{\text{th}}$ of a turn;
- h. Spin turns: $\pm 1/8^{\text{th}}$ of a turn; and
- i. Spin Rate: ± 2 deg/s or $\pm 3\%$ relative error.

Consequently, analyses of the reduced data were considered realistic and not compromised by system and calibration errors.

CHAPTER IV

RESULTS AND ANALYSIS

Test Flight Data

Data Flights

A total of 11 flights and 38 spins were carried out on 27, 28 May and 4 June 2003. The majority of spins were not repeated due to the large quantity of spins to be carried out and the desire to avoid jeopardizing the aircraft. Table 4-1 below details an overview of the spin events carried out and the corresponding aircraft's configuration.

Of the 38 spin events, 19 were to the left and 19 to the right, 14 had flaps in the full down position, and 6 were carried out with ailerons against the spin direction. Not all of the flights laid out in the test plan were carried out. This was primarily due to the fact that the test model suffered damage to its wing structure preventing continued flight testing. The damage was caused by a crash into tall grass surrounding the runway as result of insufficient altitude for recovery from a left spin (Spin #B2UA), even with the spin chute deployed. Nevertheless, the flight test program previous to the crash provided sufficient data for productive analysis.

Table 4-1. Number of Spin Events versus Aircraft Configuration.

Aircraft's Center of Gravity Position	Aircraft's Rolling Moment of Inertia State		
	Reduced	Stock	Increased
24.8% MAC	4	6	4
26.6% MAC	4	4	4
28.4% MAC	5	4	3

Test Flight Data – General

Data were successfully collected after all flights and reduced as described in the preceding Chapter. Appendix F contains the time history plots for the reduced data for each spin event. From these plots Tables G-1 to G-6 in Appendix G were constructed containing the following data for each spin event:

- Spin Number
- Date
- Center of Gravity Position
- Inertia Configuration
- Direction of Spin
- Flap Position
- Aileron Position
- Stone Spin Block
- Pro-Spin Turns (from video reduction)
- Turns for Recovery (full-scale)
- Average AOA (full-scale)
- Average β (full-scale)
- Average Roll Rate (full-scale)
- Average Pitch Rate (full-scale)
- Average Yaw Rate (full-scale)
- Spin Rate (from video reduction, full-scale)
- Recovery Chute Required?
- Spin Mode (from criteria in Table 2-1)
- Description of Recovery (from criteria in Table 2-2)

All data in Tables G-1 to G-6 were converted to full-scale per the Dimensional Analysis section in Chapter II.

Ground Video Data

Video data were successful for all the flights, though with varying degrees of clarity. Difficulty was encountered with tracking, focus control and steadiness. Flying steady circuits to allow the videographer to regain track prior to entering a spin event solved the tracking challenge. The camera's auto-focus system had difficulty choosing to focus between the moving aircraft and the background, which was greatly improved by using manual control. Extracting visual data from the videotape proved acceptable when using manual focus recordings. Additionally, although not essential, the camera was not equipped to remove any

unsteadiness while recording. The resulting un-stabilized recordings were acceptable but not ideal. A camera with “tracking-focus” and “steady-shot” capabilities would have been more suitable for this project.

From the video recordings, the number of turns for recovery and spin rate (Ω) about the spin axis were obtained using the data reduction process of the previous Chapter.

On-Board Recorded Flight Data

As detailed in the preceding chapter, the model aircraft was instrumented and calibrated to measure p , q , r , α , β , δ_e , δ_r , and δ_a . Success was experienced in downloading the data from the onboard FDR for all flights. However, there was varied success with the serviceability and capability of the systems. Each parameter will be discussed separately in the following paragraphs.

The rotational rates about the body axes (p , q , r) proved to have limited use. Both the roll and yaw angular rate gyros reached their maximum range during most spin events, consequently eliminating the method to calculate spin rotation rates using p , q , and r . Roll rate maximized at +90 deg/s and -95 deg/s, while yaw rate maximized at +52 deg/s to the right and -120 deg/s to the left². Otherwise, the gyros provided exceptional data and resolution within their operating ranges. The causes for range limitations were not explored before the time of writing due to the unavailability of a calibration rate table capable of rotation speeds greater than 30 deg/s. Another problem appeared to be with the operation of the gyro for roll rate. The data recorded were pegged at its limit suggesting that the gyro or FDR could not sense any higher rates of rotation. Again, the causes for this anomaly have not yet been explored, but it is suspected that the gyro was faulty or had its gain control improperly adjusted.

The angle of attack and sideslip sensors worked well and provided good data. With the sensors located at the wingtips, the only difficulty encountered was if a ground strike occurred to the sensor during aircraft landing. There was one occasion (landing after spin #B4D) when the β vane was inconspicuously damaged resulting in no sideslip data for the next 19 spins. The sensor was field repaired thereafter and recalibrated, but the spins were not repeated.

² Rates quoted are actual model rotation rates and not converted to full-scale rates.

The flight control position sensors also worked very well. Unfortunately, the rudder sensor was connected in reverse to the FDR causing strange readings. After first believing that the problem was a calibration one that could be corrected after the flight program, the real problem wasn't realized and corrected until before the last flight (two spins).

Spin Behaviour

General

Some qualitative comments are made below regarding the behaviour experienced for each of the spin phases from what was seen first-hand. Spin entry (and the incipient phase), the steady developed phase and recovery phase are discussed. Bearing in mind the primary objective of this project is to study the recovery phase, poor spin entry and unsteady equilibrium can influence the recovery phase.

Spin Entry

Spin entry was successful using the technique described in the preceding chapter. However, it was found that rudder application was required just before the stall, otherwise departure would not easily occur. This technique repeatedly put the model into a spin. Generally, as the center of gravity was moved aft, the model entered the spin slightly more quickly. In the state of increased rolling moment of inertia, spin entry was slightly slower, although all spin attempts were successful. Spin entry was initiated at approximately 700-850 feet AGL.

Steady Spin

Holding pro-spin controls, the model autorotated about both its spin axis and center of gravity axis. The perfectly steady spin was rarely observed, but it was found that the spins with faster rotation rates had much less oscillations. Oscillations about each axis were visually apparent for most spins, especially about the pitch axis with the nose pitching up and down. Unsteady rotational speeds were encountered for some right spins. FDR data also collaborated the visual data in great detail of any oscillatory nature. *Mason* [21] explained that variable spin patterns may occur from entering the spin with too much airspeed, but usually dissipates after two or three rotations after which the steady spin develops. *Mason*

also stated that some aircraft have inherent oscillatory spin patterns where the aerodynamic and gyroscopic forces are not in balance, and that these spins may rotate slower than the steady smooth spin and recover quicker. It is believed that the test model exhibited the later inherent oscillatory spin nature for some spins.

Although three or four rotations before recovery would have been preferred, altitude was a constraint for this test program and spin recovery was normally initiated after two to three turns to permit adequate altitude for recovery.

Spin Recovery

The normal NASA recovery technique was successful at overcoming the spin equilibrium and arresting the autorotation, except for two cases when ailerons were used against the left spin. These two cases (Spin #s J5A and B2UA) required use of the spin recovery parachute for successful recovery. For spin #B2UA, in an attempt to ensure spin equilibrium (four turns before recovery initiated), recovery had indeed occurred after the deploying the spin chute, but altitude was insufficient to regain controlled flight resulting in a crash.

It was observed that in both cases when the spin chute was deployed, the rapidly decayed pitching and yawing energy was transferred to the roll axis causing several quick axial rolls. It was this response of the model that exacerbated the difficulty at regaining controlled flight after spin #B2UA.

Data Analysis

General

The downloaded instrumentation data are examined in the paragraphs below. First, level flight data are analyzed to appreciate the aerodynamic characteristics for level flight. Followed are analysis of body spin rates, AOA and sideslip behaviour in the spin. Trends and comparisons are then made of AOA, spin rate and turns to recovery versus CG positions and wing rolling moment of inertia changes. Lastly, comments regarding correlation of model results to full-scale are made.

Level Flight Data

Data were collected in steady level flight at the model's maximum level speed to be used as a reference flight condition, and to capture any fluctuations in sensor readings for that flight condition. The configuration of the model was at maximum forward CG (24.8% MAC) for gross weight, and in its stock inertia state. The data were plotted against time and are displayed as Figure H-1 in Appendix H. Each of the parameters was averaged to give a representative value during the level cruise configuration. The control position values were used to normalize the spin data in accordance with the data reduction procedure described in the preceding Chapter. Table 4-2 contains the level flight parameter values.

Examining Figure H-1, it was apparent that the flight parameters had some fluctuations despite the presumed steady flight conditions, as the standard deviations indicate. Even though level flight was attempted, some minor corrections were inputted by the pilot to maintain level flight. AOA and sideslip fluctuations were attributed to the design of the sensors where turbulent/separated flow from the pods may have disturbed the vanes. Wind tunnel tests would have to be carried out to confirm this. Body axes rotation rate fluctuations were attributable to disturbances caused by the pilot to correct level flight or from external turbulence on the aircraft. The rate gyros were obviously very sensitive. Flight control position fluctuations were due to pilot's level flight corrections and sensor pushrod free-play. In all cases, these fluctuations (standard deviations) were deemed acceptable since the spin flight data of importance were also averaged for analysis.

Table 4-2. Level Flight Instrumentation Parameters.

Parameter	α (deg)	β (deg)	p (deg/s)	q (deg/s)	r (deg/s)	δ_e (deg)	δ_a (deg)	δ_r (deg)
Average ³ Value	7.5	0.5	-4.2	-1.1	-0.6	-0.8	-2.2	2.1
Standard Deviation	1.2	2.3	9.8	3.9	5.7	0.0	1.6	0.7

³ All values represent full-scale.

Body Axes Spin Rate Data

Roll rate. In all spin events roll rate data started in a trim condition, then when the model was pitched up for the stall, roll rate typically spiked once to the left and then to the right followed by pegging itself to a constant rate in the corresponding right or left spin. As stated earlier, behaviour of the roll rate instrumentation system was abnormal during the spin, the cause of which cannot be explained without more bench testing. Post spin recovery always showed fluctuating right and left roll rates, which decayed as the model re-established controlled flight.

Pitch Rate. The data collected showed that the model exhibited oscillatory pitch modes for all spin events. Typically with flaps up, two oscillations occurred during a two-turn spin prior to recovery. Pitch rate values varied and were not consistent between model spin CG and M₀I configurations. Flap-down spins had significant pitch oscillations with pulsations in the order of 130 deg/s/pulsation⁴. Four to five oscillations typically occurred in all flap-down spins both to the left and right, and the magnitudes of pitch rates were 30% greater than with flaps up. Pitch rate oscillations decayed faster with the flaps up as well, and more spin rotations (5-6) before recovery may have resulted in a near equilibrium, especially for the flaps up case. Therefore, the model design (and full-scale airplane) has an inherent oscillatory pitch nature during the spin, worse with flaps down. Analysis of the AOA data below collaborated the pitch rate findings. Perfect equilibrium (spin trim points) between inertia and aerodynamic forces was thus never obtained in this test program.

Yaw Rate. Generally, no oscillatory motion occurred in yaw. After pro-spin rudder input, the yaw rate gradually increased until a steady yaw equilibrium occurred (within ± 5 deg/s). Yaw equilibrium occurred after approximately 1-1½ rotations in the reduced inertia state and for some stock inertia states. However, for most spin events in the stock and all spins in the increased inertia states, yaw equilibrium did not occur but was still increasing at the time when recovery action was initiated. This suggests that the two to three pro-spin rotations prior to recovery were insufficient, especially for the increased inertia state. It was intended to repeat these spins by going to a higher altitude and recovering the model after 4-5 rotations. Unfortunately, the model was damaged preventing this examination.

⁴ Model rotation rate quoted (not full-scale).

There was also an apparent problem with the yaw rate gyro like the roll rate gyro. In the right spin, the yaw gyro system would limit itself at approximately 53 deg/s and to approximately 120 deg/s in the left spin⁵. Further bench testing would be required once a calibration rate table capable of rotation speeds greater than 30 deg/s was available.

Due to the gyro limitations, spin rate data calculated from the video were used instead to analyze inertia effects on the spin.

Angle of Attack Data

AOA data were very good with no significant problems in the AOA instrumentation system. AOA data contained very useful information. It was easy to distinguish when pitch-up occurred to initiate the stall, identify any pitch oscillations and influences of spin technique (ailerons against spin for example), and recognize when recovery had occurred. The AOA data also collaborated the pitch rate data for any oscillations. There were no true trends of decaying AOA for certain aircraft configurations during the spin. The spins that had decaying AOA were generally the flaps-down spins, but not all flap-down spins had this characteristic. The ailerons-against spin events had dramatically increasing AOA during the spins, especially in the left direction.

Right spins with flaps up consistently experienced higher AOA than left spins, as much as 60% more. This was expected due to the location of the AOA sensor, as explained in the previous Chapter.

Angle of Sideslip Data

Sideslip behaviour consisted of a trim condition followed by sideslip in the direction of pro-spin rudder application. Once rotation had started, sideslip went to the opposite direction of the spin and then oscillated back and forth, then decayed as equilibrium was attempting to establish. Unfortunately, sideslip data were only collected for seven left spins and four right. After an initial examination of the data, no trends could be determined to aid the objectives of this study. Therefore, angle of sideslip will not be examined as a function of CG position and wing rolling moment of inertia state.

⁵ Model rotation rate quoted (not full-scale).

Effects of Center of Gravity and Moment of Inertia Changes on Spin Angle of Attack

As AOA data contained much information about spin behaviour, it was decided to plot the average AOA for each spin event in relation to its corresponding CG position and rolling moment of inertia state. Alternative to using averaged AOA data, AOA peaks could have been analyzed but with oscillatory motion in pitch, the relative “strength” of the spin’s AOA attitude could not be appreciated. Left and right spins (flaps up) are shown below in Figure 4-1.

In both spin directions, the spin became flatter (higher AOA) as the CG was moved aft. This was because of less nose-down pitching moment as the CG was moved aft, less aft fuselage damping and a longer de-stabilizing lever arm forward of the CG (see Spin Theory in Chapter II). For right spins, higher wing inertias caused trend increases (7-16%) in spin AOA (flatter spins) compared to the reduced inertia case. It was the upward pitching moment from centrifugal effects that likely caused a precessional effect on the rolling mass to result in a pro-spin yaw, which will cause the spin to flatten. Also, physics requires that centrifugal forces will pull the added wing tip mass outward, raising the lower wing and causing an overall flatter spin.

The opposite occurred for left spins with increased wing inertia causing trend decreases (8-15%) in AOA (steeper spins). An explanation follows. From the yaw rate data for left spins in the stock and increased inertia states, the yaw rate was still building momentum when recovery was initiated. In other words, the anti-spin forces present in the left spin were delaying the development of a “quasi-steady” spin and AOA position. The author’s theory was that both greater AOA and spin rate would have resulted if the spin were allowed to continue an additional two or three turns to the left before recovery action.

Bowman et al [4], *DiCarlo et al* [5] and *Neihouse et al* [13] suggested that six turns are usually required for a spin to fully develop.

When full opposite ailerons were used against the spin, this had a dramatic effect on the spin’s AOA. Despite only performing six of these spins, it was apparent that the spins were considerably flattened by as much as 85% increase in AOA compared to normal spins. As explained in the spin theory section of this paper, aileron against the spin induces a lower effective local AOA on the up-going wing causing a decrease in lift, leveling the wings and potentially flattening the spin’s AOA through increased spin rate. The greatest change in

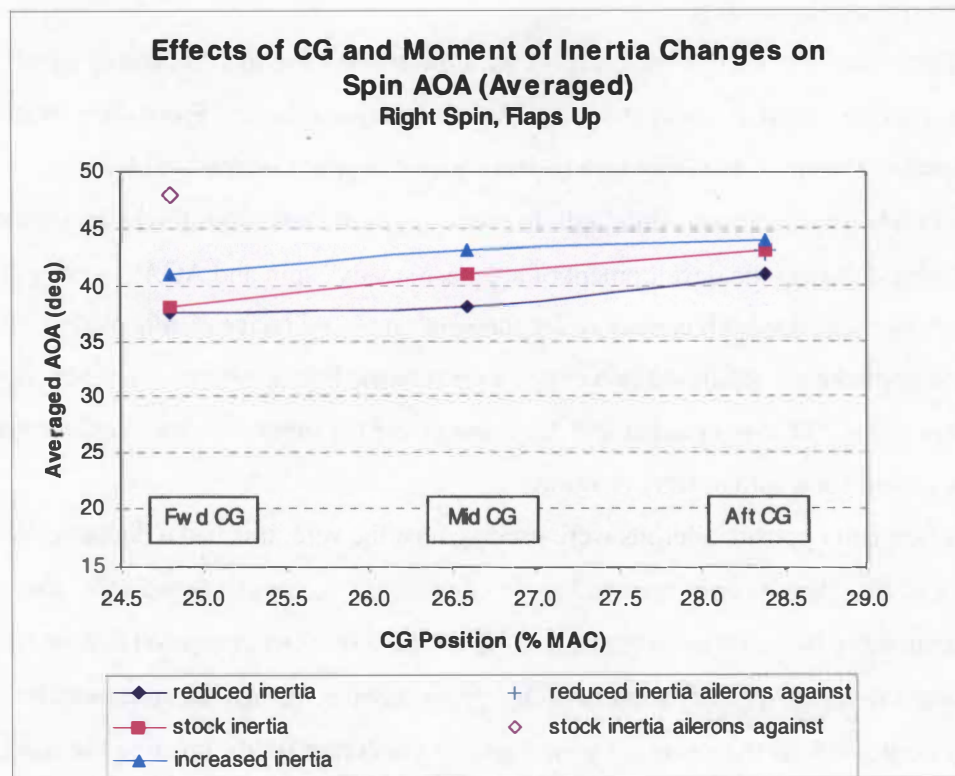
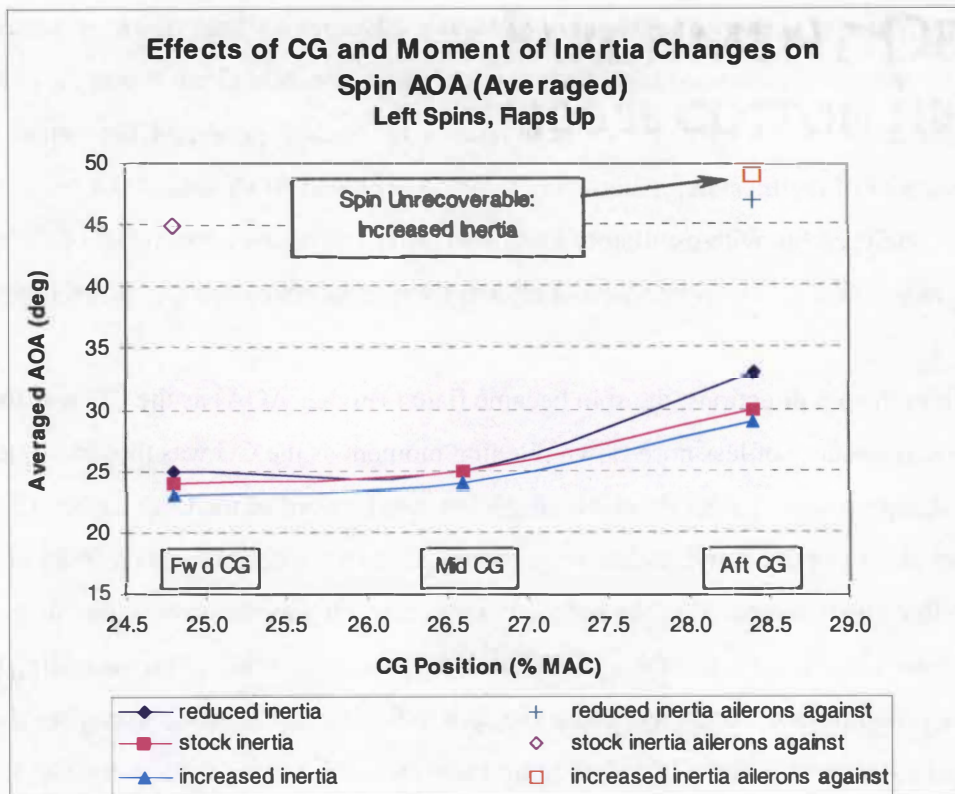


Figure 4-1. Effects of CG Position and Inertia States on Spin AOA.

Effects of Center of Gravity and Moment of Inertia Changes on Spin Rate

Spin rate analysis was based on video data and was an important factor in determining the overall effects of wing rolling moment of inertia changes. Left and right spin rate data are plotted below in Figure 4-3, against their corresponding CG positions and inertia states. Both figures have spin rates converted to full-scale results, but were not non-dimensionalized because descent velocity was not collected.

For left spins, spin rate generally increased as the CG was moved aft and as inertias were increased. There was one spin, at reduced inertia and mid CG, which did not follow this pattern and had a higher spin rate than both stock and increased inertia spins at the same CG setting. This was attributable to recoveries being executed prematurely, preventing the stock and increased inertia spins from developing higher steady spin rates (and AOAs). Therefore, one would expect the complete curve for stock and increased rolling moments of inertias to shift up to higher spin rates. The reason for higher spin rates as wing inertias were increased was as follows. As previously discovered, spin AOA generally rose as inertias increased causing the spin to become flatter. This flatter helical trajectory caused the spin radius to shorten due to the inertial forces becoming more vertical. From the conservation of angular momentum theory [32], angular momentum⁶ is a function of radius and angular velocity. If the spin radius shortens (or the moment of inertia about the spin axis decreases) and angular momentum remains constant, then the angular velocity must increase⁷. Therefore, the inertial forces and moments that flatten a spin result in a shorter spin radius and a faster rotation rate due to energy conservation.

For right spins, the spin rate behaviour was as predicted, with increased wing inertias having higher spin rates for a given CG position and inertia setting. Interestingly, the mid CG setting was consistently more severe, and the aft CG setting more benign. This is a unique characteristic of this model/aircraft. Granted, right spins had healthy spin rates no matter the CG position.

Overall for normal spins, increased rolling moments of inertia caused trend increases (by up to 19%) in spin rate compared to the reduced inertia case. When full opposite ailerons were used against the spin, this had a powerful effect on the spin rate as it did with AOA. As explained in the Spin Theory section of Chapter II, ailerons applied against the spin direction

⁶ Angular momentum = $m\omega r^2 = \omega I_{\text{spin axis}}$

⁷ Often called the “Ballerina Effect”.

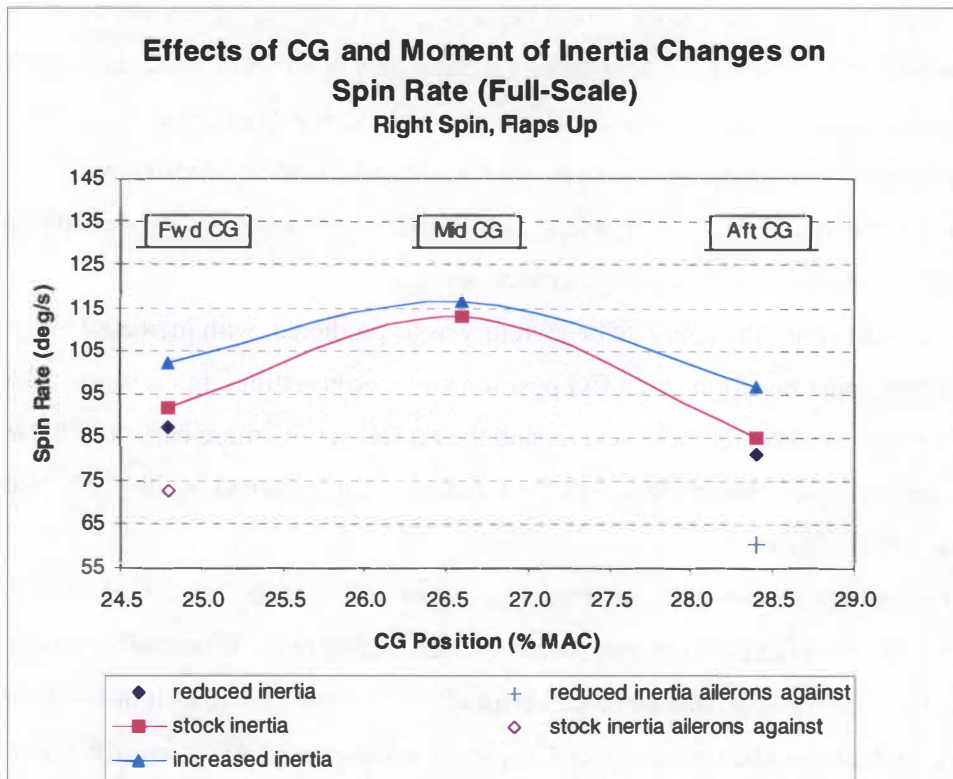
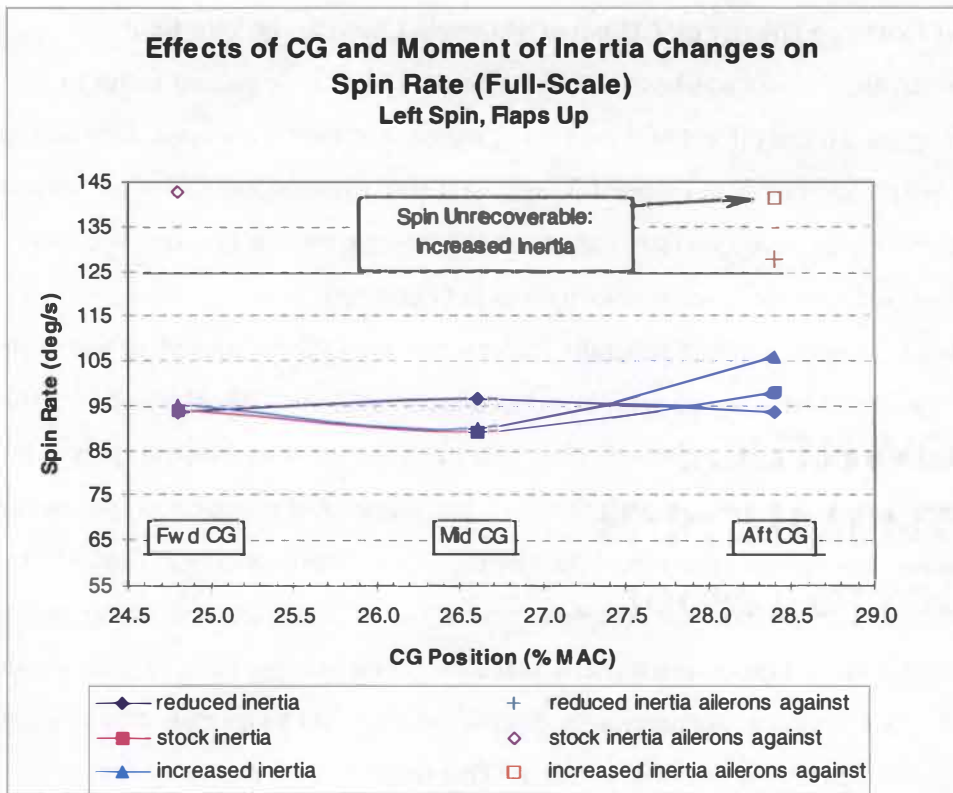


Figure 4-3. Effects of CG Position and Inertia States on Spin Rate.

spin AOA occurred with left spins, but both right and left spins with ailerons-against produced similar AOA values for a given CG position and inertia state. However, in the left spin direction with stock and increased rolling moments of inertias resulted in unrecoverable spins. There were other factors at play that contributed to this, most notably the high left spin rate as a result of using ailerons against the spin (explained below). Note also that the one aileron-against spin carried out with reduced inertia produced as flat a spin as the increased inertia spin, but it was recoverable because it had less energy with a 12% reduced spin rate (see next section).

Spins with flaps down had considerable pitch oscillations. Average AOA was always lower than the flaps-up case for the same direction, CG setting and inertia state. This was primarily because of the increased nose down pitching moment created by the effectively increased airfoil camber. Unfortunately due to the flight program being cut short, there were not as many flap-down spins carried out, resulting in insufficient data to make any concrete conclusions. For this reason, flap-down spins were considered to be more benign than the flaps-up case.

The forgoing discussion included analysis of left spins compared to right spins. However, it was already stated that AOA values were greater (by up to 65%) for right spins than left spins because the AOA sensor was mounted at the right wingtip. If there had been a left AOA sensor too, then both of the sensors' data would have been averaged to provide AOA data at the model's CG. Since this was not possible, let's examine the average of the AOA data from the left and right spins, flaps up. This seems appropriate because spins in both directions were very similar. Figure 4-2 shows the results. Interestingly, the AOA curves are essentially on top of each other, except for the ailerons-against spins. If one assumes that these curves estimate the AOA at the model's CG, then variations in rolling moments of inertia have little effect on spin AOA. Granted, it was decided that stock and increased inertia states did not have enough time to develop into their steady-state attitudes, which were assumed to be at higher AOA's and spin rates. Nevertheless, it can be concluded that increased rolling moments of inertia cause higher AOA's at the airplane's center of gravity, but not significantly (up to 6% compared to the reduced inertia case). Additionally, ailerons-against spins still exhibit greater AOA's, but not much divergence was experienced when rolling moments of inertia were changed.

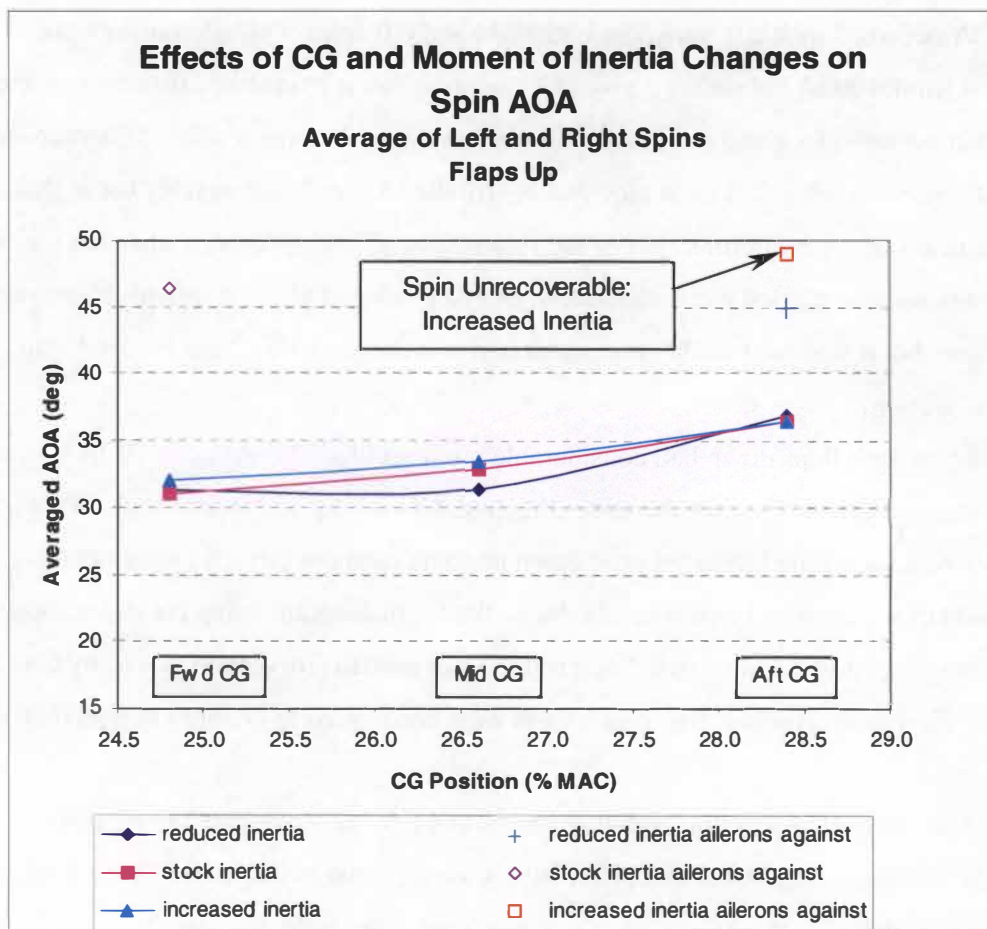


Figure 4-2. Angle of Attack Averaged Between Left and Right Spins.

are normally spin rate excitors due to the increased drag of the down going wing from the down aileron deflection. Interestingly, this occurred for the left spin but not for the right. Left spins had pronounced increases in spin rate, by as much as 50% over standard spins. The reduced inertia case exhibited 12% less spin rate than the higher wing inertias. This may be a contributing factor as to why the one-aileron-against spin with reduced inertia was recoverable, yet had as flat a spin as the ones that did not recover.

As mentioned, ailerons-against spins to the right possessed reduced spin rates. Spin rate dropped by as much as 27% over standard spins. Here the ailerons-against maneuver had the opposite effect compared to the left. Even though AOA had remained the same or increased for the ailerons-against maneuver, it increased the yaw damping, slowing the spin. This explains the easy recovery for these right spins. When the ailerons were deflected to the left bank, the overall gyroscopic balance must have resulted in anti-spin yawing moments to slow the right spins.

Effects of Center of Gravity and Moment of Inertia Changes on Turns for Recovery

Figure 4-4 plots the turns to recovery versus CG position and wing inertia states, for left and right spins, respectively. Using the standard recovery technique, most recoveries were fairly quick. Turns for recovery never exceeded more than 1 turn, except for one case in the right spin at mid CG and stock inertia state that required $1\frac{3}{4}$ turns. It would have been expected that turns to recovery may have been higher for increased inertia spins to the left had they not been prematurely recovered. CG effects on recovery were not consistent, especially in the right spin, but degraded left spin recoveries by as much as an extra $\frac{3}{4}$ turn as CG was moved aft.

Ailerons-against the spin to the left greatly degraded spin recovery. Recovery never occurred for the spin at increased inertia state with aft CG, requiring the use of the spin recovery parachute. Recovery for the stock inertia state was at four turns. For this spin, the video data showed that recovery was imminent without the spin chute, even though the spin chute was used. Recovery at the reduced inertia state was quicker at 3 turns using the normal technique. For right spins, ailerons-against the spin aided spin recovery. Both right spins carried out in the reduced and stock inertia cases resulted in only $\frac{1}{4}$ turns. The lower spin rates explain the quick recovery.

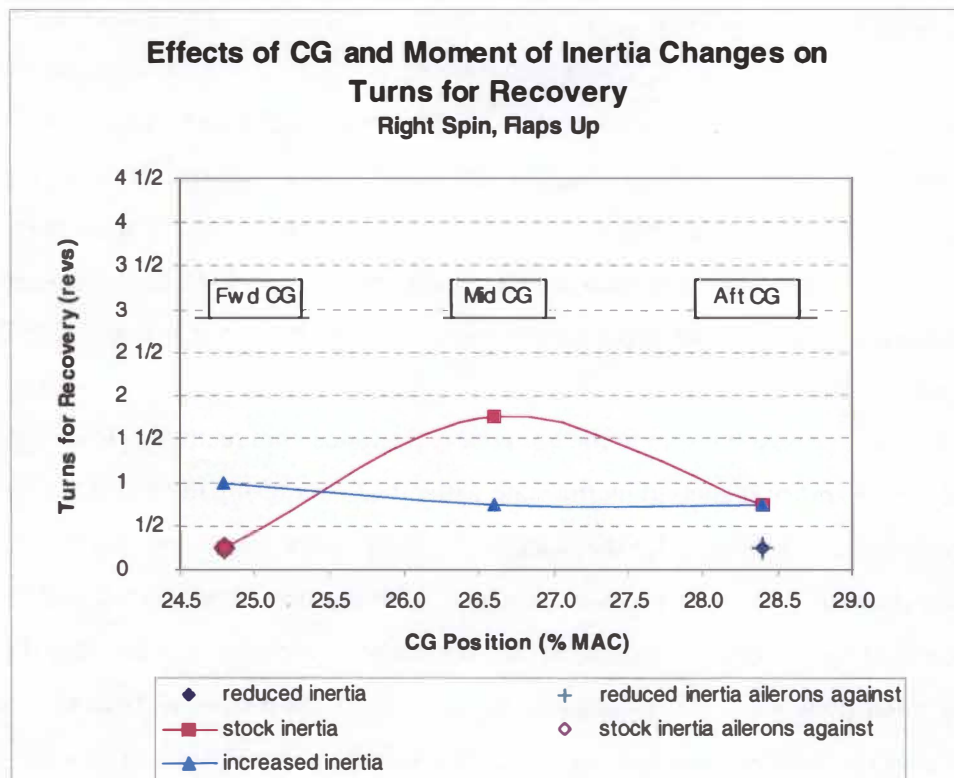
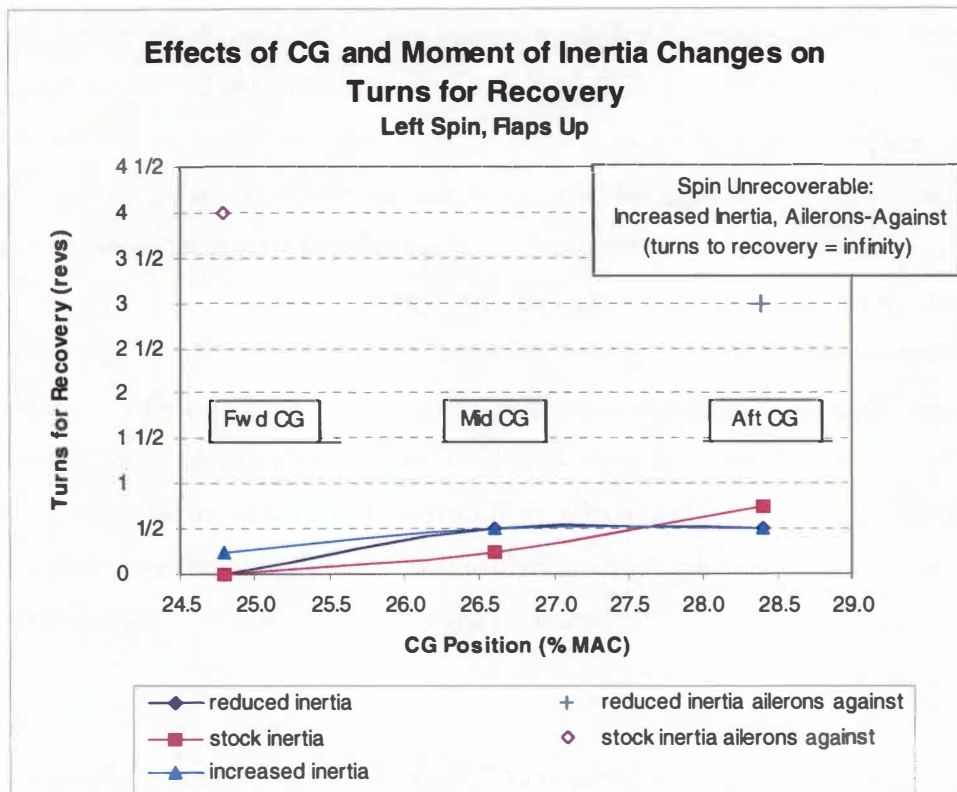


Figure 4-4. Effects of CG Position and Inertia States on Turns for Recovery.

Overall Effect of Moment of Inertia Changes on Spin Recovery

As complicated as aircraft spin dynamics are, no single aerodynamic or inertial factor could explain or predict how an aircraft would spin and recover. After examining how inertia variations affect spin angle of attack, spin rate, and turns to recovery, an overall perspective and explanation can be obtained by combining the individual analyses.

For this aircraft design, spin behaviour was generally consistent for each spin direction tested. Without using ailerons-against the spin, all left and right spins recovered within $1\frac{3}{4}$ turns. However, turns to recovery did not reveal anything that was happening aerodynamically or indicate the “severity” of the spin.

Let’s first examine the complete picture for left spins. AOA and spin rate data generally showed that as rolling moments of inertia were increased, AOA slightly increased, the spin flattened and the spin rate increased. However, without using ailerons-against the spin, spin “severity” or energy level was not sufficiently high enough to cause delayed recoveries. The ailerons-against spins amplified the spin behaviour, especially the inertial effects. Table 4-3 below compiles relevant left spin characteristic data for discussion. The reduced inertia case showed strong AOA (47 deg) but a weaker spin rate. This spin recovered without external assistance of a chute. The stock inertia case had slightly less AOA (45 deg) but the highest spin rate at 143 deg/s. Its recovery was at the brink of being unrecoverable. Here is where the “cliff” occurred for this inertia study. Any extra inertia increases in the wing would have caused further degradations in spin recovery, which was the

Table 4-3. Left Spin Aerodynamic Elements – Ailerons-Against the Spin.

Rolling Moment of Inertia State	CG Position	AOA (α) (deg)	Spin Rate (Ω) (deg/s)	Turns to Recovery	Parachute Required?
Reduced	28.4% MAC	47	128	3	No
Stock	24.8% MAC	45	143	4	No/Yes ⁸
Increased	28.4% MAC	49	141	∞	Yes

⁸ The spin chute was used in recovery, but video reduction determined that recovery was imminent without the chute.

case for the increased inertia state representing 20 gallons of extra fuel in the wings at mid-span. For this spin, AOA reached a maximum of 49 degrees and a high spin rate of 141 deg/s. The combination of high AOA and spin rate caused by the rolling moment of inertia increase resulted in degraded spin recovery to the point of being unrecoverable.

Now consider right spins. The same spin nature occurred with respect to inertia increases. That is, AOA slightly increased, the spin flattened, and the spin rate increased as inertia increased. However, the right spin was not aggravated by ailerons-against the spin. Ailerons-against the spin damped the spin rate and hence reduced the turns required for recovery.

It is apparent that spin rate was the key element in determining whether or not a spin would become more severe by increasing the rolling moment of inertia. It is debatable whether the AOA at the airplane's center of gravity exhibited little change or not as inertias were varied. In the ailerons-against cases, AOA had increased for both left and right spins over standard spins, but only left spin rates had increased, leading to significantly more turns to recovery.

In comparing these findings to previous research (see Chapter II), not all results completely agreed. From spin tunnel tests, *Neihouse* [14] in 1948 found that simultaneously increasing all body moments of inertia led to flatter spins, slower spin rates and slower recoveries. *Kerr* [17] in 1953 also discovered that recovery standards worsened as the I_y/I_x ratio decreased. Full-scale flight tests by *Stough and Patton* [19] in 1979 found that adding mass to the wings caused slower recoveries but slightly slowed spin rate and slightly decreased spin AOA. The findings of this thesis study confirmed the slower recovery, but showed slightly higher spin rates and AOA as rolling moments of inertia were increased. This was even with premature recoveries and a much less IYMP (8×10^{-4} versus 50×10^{-4}) for this study compared to *Stough and Patton*. It is suspected that results differed because of the differences in geometry, that is, results may be specific to aircraft shape. Overall, all studies concluded that increasing wing mass degrades spin recovery given the right circumstances. The effects on spin rate and AOA can be unpredictable because of the dependence upon the airplane's design and other influencing aerodynamic and inertial forces/moments that vary from aircraft to aircraft. The aircraft spin, indeed, is a complex maneuver that cannot always be generalized.

Correlation of Model Results to the Full-Scale Airplane

Chapter II indicated that previous research found that correlation of spin results between radio-controlled models and their full-size counterparts were generally good. To avoid Reynolds number effects, spin recovery must be beyond the early phases of the spin, and spins with angles of attack above 30 degrees have less Reynolds number effects. This was generally the case for the spins conducted under this thesis study.

There was, however, one divergence of dynamic similitude that may alter the correlation. The measured moments of inertia values were as much as 80% greater than the published data, but two different methods were used to obtain the full-scale and model values. Thus, the ratios of I_x/I_y , I_x/I_z , and I_y/I_z better represented the mass distribution, since the model was essentially at its target weight.

It is concluded that correlation to the full-scale airplane should be accurate. Therefore, the spin characteristics of the model and its configuration of an additional scale 20 gallons of fuel at midspan are representative of the full-scale airplane.

CHAPTER V

CONCLUSIONS AND RECOMMENDATIONS

Conclusions

An experimental study of the effects of variations in rolling moments of inertia on aircraft spin recovery was carried out. The experiment utilized flight tests of a Froude number dynamically scaled radio-controlled model to obtain results. Ground video recordings and on-board instrumentation produced data that allowed the conclusions to be reached concerning the spin behaviour, correlation with the full-scale airplane, the radio-controlled model, and the hobby-type rate gyros. Conclusions for each specific issue follow:

Spin Behaviour Results

Conclusions specific to the spin results are:

- a. 11 flights and 38 spin events were marginally sufficient to provide the data required;
- b. Angle of attack, spin rate about the spin axis, and turns to recovery were mandatory data requirements to analyze spin behaviour for this thesis study;
- c. No single aerodynamic nor inertial factor could explain or predict how the aircraft would spin and recover;
- d. Spin behaviour results were generally consistent for each spin direction;
- e. Flap-down spins were considered more benign than the flaps up case;
- f. Flap-down spins were always oscillatory in pitch, recovering more quickly;
- g. Premature recoveries prevented the stock and increased inertia spins from developing their potential energy level (higher AOA and spin rates). Higher inertia spins required more spin turns than lower inertia spins to reach equilibrium;
- h. Increased rolling moments of inertia generally caused slight increases in AOA for all CG settings;
- i. Increased rolling moments of inertia caused higher angles of attack at the airplane's center of gravity, but not significantly;

- j. Increased rolling moments of inertia generally caused increases in spin rate for all CG settings;
- k. When using the standard recovery technique, the number of turns for recovery did not exhibit any significant trends when rolling moments of inertia were increased. This was partly due to premature spin recoveries in the higher inertia states;
- l. Ailerons-against spin maneuvers amplified the inertial effects and stimulated the gyroscopic effects on spin behaviour and recovery. Overall effects of ailerons against the spin were more severe for left spins and more benign for right spins compared to the normal spins;
- m. Ailerons applied against spins to the left greatly degraded recovery with higher AOA and faster spin rates;
- n. Ailerons applied against spins to the right aided spin recovery with slower rotation rates, even with high angles of attack;
- o. Spin rate and angle of attack were the key elements in determining if a spin would be more severe from increasing the rolling moment of inertia;
- p. Increased rolling moments of inertia may not always cause spin recovery to degrade. However, given enough spin turns, suitable additional wing inertia, and the right control deflections, there may be a point where the spin will become unrecoverable;
- q. The representative increase in 20 gallons of fuel load in the wing caused unrecoverable spins in only the ailerons-against left spin; and
- r. Non-dimensional moments of inertia ratio parameters provided an alternate means of correlating between full-scale and model values.

Full-Scale Correlation and the Radio-Controlled Model

Conclusions specific to correlation to the full-scale airplane and the radio-controlled model are:

- a. Correlation to the full-scale Piper PA-28-180 Cherokee should be accurate;
- b. General-aviation airplanes similar to the Piper PA-28-180 Cherokee should exhibit worsening spin recovery characteristics as fuel capacity in the wing is

increased to the point where approximately 20 additional gallons of fuel may trigger unrecoverable spins;

- c. The experimental approach of using a radio-controlled model proved to be cost-effective and valuable for obtaining high-risk flight test data;
- d. A black painted model would have improved video recordings;
- e. The sideslip sensor should have been eliminated and used as an additional angle of attack sensor to allow calculations of angle of attack at the model's center of gravity;
- f. An engine with more power would have improved the model's climb performance reducing the flight test time;
- g. A ring-slotted spin recovery parachute would have improved spin chute and model flight stability; and
- h. A video camera with "tracking-focus" and "steady-shot" capabilities would have been more suitable for this project.

Hobby-Type Rate Gyros

Conclusions specific to the hobby-type rate gyros are:

- a. They are suitable for spin testing in radio-controlled models;
- b. They must be calibrated over their complete dynamic range to ensure the gain setting is correct; and
- c. They must be corrected for temperature changes by pre-flight data or other means.

Recommendations

The following recommendations are made concerning the thesis study:

- a. More evaluation should be carried out to verify that increased rolling moment of inertia spins require at least four to six turns to establish a developed spin with greater AOA and faster turn rates than obtained in this study;
- b. Follow-on research and testing to further explore the usefulness and applications for hobby-type piezo-electric gyros should be considered;

- c. Pilots must avoid applying ailerons against the spin during entry or recovery for this aircraft design, as recovery may never occur; and
- d. Precautions must be exercised when spin testing or certifying an airplane that has fuel in the wings, or has been modified with additional fuel capacity in the wings, as unrecoverable spins may result.

LIST OF REFERENCES

LIST OF REFERENCES

1. Anderson, S.B., "An Historical Overview of Stall/Spin Characteristics of General Aviation Aircraft", AIAA Conference on Air Transportation: Technical Perspectives and Forecasts, Los Angeles, CA, AIAA Paper 78-1551, August 1978.
2. Chambers, J.R. and Stough, H.P. III, "Summary of NASA Stall/Spin Research for General Aviation Configurations", AIAA General Aviation Technology Conference, Anaheim, CA, AIAA Paper No. 86-2597, October 1986.
3. Layton G.P., "A New Experimental Flight Research Technique: The Remotely Piloted Airplane", AGARD Conference Proceedings, No 187, April 1975.
4. Bowman, T.S. Jr, Burk, S.M. Jr, Stough, H.P. and Patton, J.M. Jr, "Correlation of Model and Airplane Spin Characteristics for a Low-Wing General Aviation Research Airplane", AIAA Aircraft Systems and Technology Conference, Los Angeles, CA, AIAA Paper 78-1477, August 1978.
5. DiCarlo, D.J. and Johnson J.L. Jr, "Exploratory Study of the Influence of Wing Leading Edge Modifications on the Spin Characteristics of a Low-Wing Single-Engine General Aviation Airplane", AIAA Aircraft Systems and Technology Meeting, New York, AIAA Paper 79-1837, August 1979.
6. McCormick, B.W., "Equilibrium Spinning of a Typical Single-Engine Low-Wing Light Aircraft", AIAA Paper 81-4076, March 1981.
7. Yip L.P., Ross H.M. and Robelen, D.B., "Model Flight Tests of a Spin Resistant Trainer Configuration", AIAA Journal of Aircraft, Vol. 29, No. 5, September-October 1992.
8. Burk, S.M. Jr, and Wilson, C.F. Jr., "Radio-Controlled Model Design and Testing Techniques for Stall/Spin Evaluation of General-Aviation Aircraft", National Aeronautics and Space Administration, NASA TM-80510, April 1975.
9. Holcomb, M.L., "YT-34C Radio-Controlled Model Spin Research Program", Beech Aircraft Corporation Report No. 104E210 A, September 1975.

10. Kershner, D.D., "Miniature Flow-Direction and Airspeed Sensor for Airplanes and Radio-Controlled Models in Spin Studies", National Aeronautics and Space Administration, NASA TP 1467, May 1979.
11. Kimberlin, R.D., "Flight Test of Fixed Wing Aircraft", American Institute of Aeronautics and Astronautics, Inc., 2003.
12. Neihouse, A.I., "A Mass-Distribution Criterion for Predicting the Effect of Control Manipulation on the Recovery from a Spin", National Advisory Committee For Aeronautics, NACA ARR, Aug 1942.
13. Neihouse, A.I., Lichtenstein, J.H. and Pepoon, P.W., "Tail-Design Requirements for Satisfactory Spin Recovery", National Advisory Committee For Aeronautics, NACA Technical Note No. 1045, April 1946.
14. Neilhouse, A.I., "The Effect of Variations in Moments of Inertia on Spin and Recovery Characteristics of a Single-Engine Low-Wing Monoplane with Various Tail Arrangements", National Advisory Committee For Aeronautics, NACA Technical Note No. 1575, May 1948.
15. Seidman, O. and Neihouse, A.I., "Free-Spinning Wind-Tunnel Tests of a Low-Wing Monoplane with Systematic Changes in Wings and Tails. III. Mass Distribution along the Wings. NACA TN No. 664, 1938.
16. Bowman, J.S. Jr, "Summary of Spin Technology as Related to Light General-Aviation Airplanes", National Aeronautics and Space Administration, NASA TN D-6575, December 1971.
17. Kerr, T.H., "A CRITERION FOR THE PREDICTION OF THE RECOVERY CHARACTERISTICS OF SPINNING AIRCRAFT", Technical Note No. Aero 2251, Royal Aircraft Establishment, Farnborough, U.K., August 1953.
18. Bowman, J.S. Jr and Burk, S.M. Jr, "Stall/Spin Studies Relating To Light General-Aviation Aircraft", SAE Paper No. 730320 Presented at the SAE Business Aircraft Meeting, Wichita, Kansas, Society of Automotive Engineers, April 1973.
19. Stough, H.P. III and Patton, J.M., "The Effects of Configuration Changes on Spin and Recovery Characteristics of a Low-Wing General Aviation Research

- Airplane”, AIAA Aircraft Systems and Technology Meeting, New York, New York, AIAA Paper 79-1786, August 1979.
20. Neihouse, A.I., Klinar, W.J. and Scher, S.H., “Status of Spin Research For Recent Airplane Designs”, National Aeronautics and Space Administration, NASA TR R-57, 1960.
 21. Mason, S., “Stalls, Spins, and Safety”, McGraw-Hill, Inc., 1982.
 22. Kerr, T.H., edited by Perkins, C.D., Dommasch, D.O., and Durbin, E.J., Advisory Group for Aeronautical Research and Development (AGARD) Flight Test Manual, Vol. II, 2nd edition, Stability and Control, Chapter 8, “Part I - General Principals of Spinning”, Pergamon Press Ltd., New York, 1959.
 23. USAF Test Pilot School Flight Test Handbook, “Flying Qualities Theory and Flight Test Techniques”, AFFTC-TIH-79-2, Defense Technical Information Center, Alexandria, Virginia, 1980.
 24. Bowman, J.S., “Airplane Spinning”, Astronautics & Aeronautics, March 1966.
 25. Pamadi, B.N., “Performance, Stability, Dynamics, and Control of Airplanes”, American Institute of Aeronautics and Astronautics, Inc., 1998.
 26. White, F.M., “Fluid Mechanics”, 2nd edition, McGraw-Hill Inc., 1986.
 27. Polhamus, E.C., “Effect of Flow Incidence and Reynolds Number on Low-Speed Aerodynamic Characteristics of Several Noncircular Cylinders with Applications to Directional Stability and Spinning”, National Aeronautics and Space Administration, NASA Technical Report R-29, 1959.
 28. Clarkson, M.H., Malcolm, G.N., and Chapman, G.T., “Experimental Poststall Rotary Aerodynamic Coefficients for Airplane-Like Configurations”, AIAA Journal of Aircraft, Vol. 13, No. 8, August 1976.
 29. Moul, T.M., “Determination of Corrections to Flow Direction Sensor Measurements Over an Angle-of-Attack Range From 0° to 85°, National Aeronautics and Space Administration, NASA TM-86402, December 1985.
 30. Burk, S.M. Jr, Bowman, J.S. Jr and White, W.L., “Spin-Tunnel Investigation of the Spinning Characteristics of Typical Single-Engine General Aviation Airplane Designs, II - Low Wing Model A: Tail Parachute Diameter and Canopy

Distance for Emergency Spin Recovery”, National Aeronautics and Space Administration, NASA TP-1076, November 1977.

31. McCormick, B.W., “Aerodynamics and Flight Mechanics”, 2nd edition, John Wiley and Sons, 1994.
32. Sears, F.W., Zemansky, M.W. and Young, H.D., “University Physics”, Addison-Wesley Publishing Company, 1984.
33. Shigley, J.E. and Uicker, J.J. Jr., “Theory of Machines and Mechanisms”, McGraw-Hill, Inc., 1980.
34. Green, M.W., “Measurement of the Moments of Inertia of Full Scale Airplanes”, National Advisory Committee For Aeronautics, NACA Technical Note No. 265, September 1927.
35. Miller, M.P., “An Accurate Method of Measuring the Moments of Inertia of Airplanes”, National Advisory Committee For Aeronautics, NACA Technical Note No. 351, October 1930.
36. Gracey, W., “The Experimental Determination of the Moments of Inertia of Airplanes By a Simplified Compound-Pendulum Method”, National Advisory Committee For Aeronautics, NACA Technical Note No. 1629, June 1948.
37. Sanders, E., CompuFoil 2000 ®, SoarSoft Software, 7682 Winfield Dr N.E., Brighton, MI 48116, (810) 225-1165.
38. Piper Aircraft, “PA-28-140 Cherokee Service Manual”, June 1961.
39. Canadian Forces Publication (CFP) 169(1), “Aerodynamics”, Volume 1, Manual of Training, 1975.
40. Bisplinghoff, R.L., Ashley, H., Halfman, R.L., “Aeroelasticity”, Dover Publications Inc., 1996.
41. Fung, Y.C., “An Introduction to the Theory of Aeroelasticity”, Dover Publications Inc., 2002.

APPENDICES

APPENDIX A: The Test Model

The Test Model

Model and Full-Scale Specifications

The model was a Froude number $1/6^{\text{th}}$ dynamically scaled version of a Piper PA-28-180 Cherokee. Based on the specifications of the full size airplane [McCormick, 31], the model was built to the geometric size and mass properties listed in Table A-1. Figure A-1 shows the complete model and radio transmitter.

Model Construction

Fuselage

The provided fuselage was constructed of fiberglass and polyester resin. It was a solid design that included two plywood formers ahead and aft of the wing section. A rugged engine mount was made from solid hardwood and aluminum, and permanently installed. The vertical fin was molded into the fuselage for additional rigidity.

The author installed a hinged door on the left side of the fuselage (Figure A-2) for access to the FDR battery and download connector without removing the wing. The wing was removable by unscrewing two nylon bolts. The rudder was hinged with a removable hinge pin to allow for pushrod connections and servicing in that area. The rudder was not mass balanced.

An all-moving horizontal stabilizer (stablator) was made by the author using typical radio-controlled modeling techniques. It had a foam core (1 oz/ft^2 density) with an internal hardwood support for anchoring a 5/16-inch diameter aluminum shaft, which was the pivot shaft for the all-moving horizontal stab. Nylon pivot bearings were installed in the fuselage for the stablator shafts and a cast-aluminum crank facilitated pushrod activation of the stablator. The airfoil used was a NACA 0011 at 11.5 % thickness ratio. Its profile was made using Compufoil 2000® software [37], which produced paper templates for the airfoil, that were transferred to a phenolic material. The airfoil was cut out of a 2-inch thick foam block using a typical hot-wire method. A 1/4-inch deep balsa piece was shaped to form the leading edge. Compufoil also enabled leading edge templates to be made. The foam core was laminated with a 1/16-inch thick balsa wood using epoxy glue to bond the skin to the cores. Carbon-fiber reinforcement, 0.007 inches thick by 0.5 inches wide, was sandwiched

between the wing skins along the trailing edge of the stabilator to increase “ding” resistance. Fiberglass cloth, 0.75-oz/yd², was adhered to the outer surface of the wing skins with epoxy finishing resin (PN PAAR2240)⁹, and prepared to provide a suitable surface for paint. The stabilator was mass balanced in the leading edge to 100% static balance.

A steerable nose gear assembly (PN GPMQ4261) was incorporated into the fuselage nose at the scale position with approximately 5 degrees of forward rake. The strut was made of 5/32-inch steel and was custom bent to the correct height to provide approximately 3 degrees of ground angle of attack for the wing. Height of the nose gear was also sized to represent the full-scale oleo in the extended position. A 2½-inch nose wheel (PN DUB250T) was used and a scale wheel pant fitted (PN GPMQ1750), but later removed.

The engine bay was designed to mount the engine on its right side. A hole was required in the right fuselage side to allow cooling air to exit from the engine bay. Thus a 2½ inch x 1½ inch hole was not covered. This may have had an effect upon spin recovery, but was never verified due to the unscheduled cessation of the flight program.

Wing

The complete wing assembly was made by the author. The identical construction technique for the stabilator was used for the wing. Each wing half was made from three separate foam panels to give the wing its proper planform shape. The wing was also fitted with ½-inch square balsa spars on the upper and lower surfaces of the wing. The spars were located at the maximum airfoil thickness was for the outer panels, which was 50% of the local chord. Landing gear mounts were fabricated out of hardwood and imbedded into the lower wing just aft of the lower spar. Chord-wise 1/8-inch thick plywood was also imbedded into the foam to strengthen the landing gear mounts. A planform view is shown in Figure A-3.

The airfoil used was a NACA 65₂-415, of which templates were produced using Compufoil 2000® software [37]. A sample airfoil for the outer wing panel is shown at Figure A-4. For the wing washout, 2-degrees of twist was programmed into the template design. The wing was sheeted with 1/16-inch thick balsawood and the leading edge shaped from ¼-inch balsa sheet. The flap and aileron sections were cut out using a band saw and

⁹ Unless, otherwise stated, all part numbers were from Tower Hobbies, P.O. Box 9078, Champaign, IL, 61826, 1-800-637-4989.

then their hinge surfaces faced with ½ inch balsa sheet to facilitate hinge mounting. The leading edges of the ailerons were shaped like a bevel to allow up and down deflection resulting in a gapless hinge line. The flap's leading edges were shaped to be like the scale slotted flaps with external hinge points. All trailing edges of the wing, ailerons and flaps were reinforced with 0.007-inch carbon-fiber as used for the stabilator. The wing's surface, ailerons and flaps were finished with 0.75-oz/yd² fiberglass and painted. The ailerons and flaps were not mass balanced.

The landing gear configuration was fixed. It was custom bent using 3/16-inch diameter steel rod with its length representing the full-scale oleo in the extended position. Main wheels of 2½-inch diameter (PN ROBQ1512) were used and scale wheel pants fitted, but later removed. The chordwise location of the main gear relative to the center of gravity was followed as closely as possible to the full-scale airplane. No problems were encountered with lift off at a 3-degree ground angle of attack.

Four bays were made in the wing to house two servos for actuating the ailerons and two servos for the flaps. An additional two bays, one at each wing tip aligned along the longitudinal center of gravity, were made to accommodate lead weight for increasing the rolling moments of inertia. All six bays had removable covers for easy access. Figure A-5 shows a bottom view of the wing and the bays. The ailerons were actuated via solid pushrods that were exposed to the airflow, whereas the flaps were actuated through internal solid pushrods. The hinges used for the ailerons were heavy-duty pinless hinges (PN HAYQ1105) that tended to provide a restoring moment to the flight surface. The flap's external hinges were custom made using carbon fiber control horns (Bob Violet Models PN BVM5555).

The whole model was painted with a fuel proof paint, TopFlight Lustrekote brand. A spinner, 2¼-inch diameter, was also painted and fitted to the model.

Engine and Fuel System

The engine used was an O.S. Max 61FX (PN OSMG0561). It was a two-cycle single-cylinder model airplane engine equipped with an adjustable carburetor. Ignition was by glow plug (PN OS #8), which was heated by a 1.2-volt NiCad battery for starting. A special exhaust "Pitts style" muffler (PN SLIG2217) was purchased to vent the exhaust down below the airplane. The propeller used was a 12-inch diameter with a 6-inch pitch Master

Airscrew propeller (PN MASQ1360). A fuel filter (PN GPMQ4150) and silicone fuel line were also essential.

The fuel system was a typical model system that was pressurized from the exhaust system. The tank was a 12-ounce plastic tank (PN DUBQ0212) and was located at the model's center of gravity. The engine had no difficulty drawing fuel from the tank at all spin attitudes. Also installed was a 2-ounce hopper tank in the engine bay. The main tank fed the hopper tank, which had a center pick-up and no clunk. The purpose of the hopper tank was to ensure a fuel supply was always available for the engine during spin maneuvers when the main tank's clunk might not be covered by fuel. The center pickup of the hopper tank always ensured bubble-free fuel supply to the engine.

The fuel used was model airplane fuel. Specifically, it was Sig Champion fuel composed of 5% nitro methane, 20% oil content, and 75% methyl alcohol. It proved quite suitable for engine performance.

Although performance was adequate with the engine used, climbing to 800 feet altitude to commence spin testing consumed up to 2 minutes and ¼ of the fuel load. It would have been more efficient for testing to have used the more powerful OS MAX 91FX, which actually weighs less and retains the same external dimensions as the OS MAX 61FX.

Radio Control System

A JR 10X PCM (Horizon Hobby PN JRP164TX) remote control transmitter and a 10 channel JR S-PCM receiver (PN JRPR955) were used for the model because of the large number of remote systems on-board. Pulse Code Modulation (PCM) provided the best radio link integrity with programmable "fail-safe" in case of contact loss with the model. The following functions were carried out by 11 servos (PNs provided):

- a. stabilator – high torque coreless ball-bearing servo (PN JRPS4721);
- b. rudder – standard ball-bearing servo (PN JRPS537);
- c. ailerons – two miniature servos (PN HRCM3124);
- d. flaps – two miniature servos (PN HRCM3124);
- e. nose wheel steering – standard servo (PN JRPS527);
- f. throttle – standard servo (PN JRPS527);
- g. spin chute deployment and release – standard servo (PN JRPS527);

- h. flight data recorder on/off – standard servo (PN JRPS527); and
- i. aileron position sensor – standard servo (PN JRPS527);

All servos were mounted in the fuselage center section with the exception of the flap and aileron servos being mounted within bays made in the wing. The elevator and rudder were connected to the servos using rigid fiberglass pushrods (PN DAVQ3000) and heavy-duty model hardware. The throttle servo actuated the engine's carburetor via a flex cable (PN DUBQ1425) and nose wheel steering was connected to its servo with a solid pushrod (PN GPMQ3750). To switch the FDR on and off, a micro switch (Radio Shack PN 275-016A) was siliconed to the top of its servo for easy actuation.

A high capacity 1100 mah 4.8V battery (PN JRPB4240) was used for powering all the servos, gyros and receiver. The receiver's antenna was mounted along the inside top of the fuselage. Electrical Y connectors were required to connect the flap servos together and the aileron position servo with one of the aileron servo channels. Each aileron servo was connected to the receiver to make it easier to set up the high differential throw of the ailerons. All other servos directly connected to the receiver for individual control throw adjustments.

The transmitter used was very sophisticated, but made the flight much easier. It allowed the flight controls to be set up to the maximum desired control throw yet allowed an exponential increase in control movement. This permitted small flight control movements around neutral stick ("soft center"), yet maximum throw at the stick limits. Unique to the system was its flight modes. Three flight modes were used, each having its own trim settings that were individually adjustable. The flight modes used were: normal flight (for spin events), flaps at 20°, and flaps at 42°. These modes were activated at the flip of a switch and any adverse pitch, yaw, or roll effects could be trimmed out and memorized by the transmitter for that individual flight configuration (mode).

Figure A-6 shows a bottom view of the fuselage with the wing removed.

Control Surface Throws

Control surface throws were set on the model at their tolerance to cause the worst-case scenario for the spin tests. Table A-2 contains the throw limits, tolerances and actual model settings. Reference [38] was the source for this information.

Ground Support Equipment

The following equipment was necessary for the flight program:

- a. Video camcorder (Samsung Hi8, PN SCL810);
- b. Fuel and fuel pump (PN HAN108);
- c. 12 volt battery for fuel pump and starter motor (if necessary);
- d. Fast charger (PN HAN114) for receiver battery;
- e. Tools for assembly and minor repairs;
- f. Spares including props, glow plugs, etc;
- g. Laptop for downloading data from the FDR; and
- h. Shelter from the sun.

Figures A-7 and A-8 show the setup and a FDR download in progress.

Model Components Not Made to Scale

Some of the features and components of the model were or could not be made to scale. They are listed below and it is the opinion of the author that the results were not compromised because of these divergences:

- a. Cooling hole for the engine in the left fuselage;
- b. External aileron pushrods;
- c. Idle engine thrust;
- d. Exhaust outlet;
- e. Spinner shape;
- f. Wheel pants not installed;
- g. Antenna, door handles, hatches, etc. not installed;
- h. Spin recovery parachute installation; and
- i. Wingtip booms for angle of attack and sideslip.

Table A-1. Full-Scale Airplane and Model Specifications.

Item		Full Size Piper PA-28-180 Cherokee [31]	1/6 Scale Model
Wing	Span (b)	30 ft	60 in
	MAC (ft)	5.5 ft	10.8 in
	Mid-span chord	5.25 ft	10.5 in
	Root chord	6.2 ft	12.31 in
	Taper Ratio (λ)	1.0	1.0
	LE sweep (Λ)	0 deg	0 deg
	Dihedral (Γ)	7.5 deg	7.5 deg
	Twist (θ_T)	-2.0 deg	-2.0 deg
	Planform Area (S)	163.2 ft ²	646 in ² (4.48 ft ²)
	Aspect Ratio ¹⁰ (A)	5.71	5.71
	Airfoil	NACA 65 ₂ -415	NACA 65 ₂ -415
Horizontal Tail (all-moving)	Span (b _t)	10.0 ft	20 in
	MAC (c _t)	2.5 ft	5 in
	Taper Ratio (λ_t)	1.0	1.0
	LE sweep (Λ_t)	0 deg	0 deg
	Dihedral (Γ_t)	0 deg	0 deg
	Twist (θ_{Tt})	0 deg	0 deg
	Planform Area (S _t)	25 ft ²	100 in ²
	Aspect Ratio (A _t)	4.0	4.0
	Airfoil	symmetrical (unknown)	NACA 0011
Vertical Tail	Span (b _v)	4.47 ft	8.94 in
	MAC (c _v)	3.31 ft	6.62 in
	Taper Ratio (λ_v)	0.54	0.54
	LE sweep (Λ_v)	35.0 deg	35.0 deg
	Planform Area (S _v)	11.4 ft ²	45.6 in ²
	Aspect Ratio (A _v)	3.5	3.5
	Airfoil	symmetrical (unknown)	symmetrical (unknown)
Fuselage	Length	23.9 ft	47.8 in

¹⁰ Based on mid-span chord.

Table A-1. Continued.

Item		Full Size Piper PA-28-180 Cherokee [31]	1/6 Scale Model
	Nose to Wing LE	5.0 ft	10 in
Propeller	Diameter	6.17 ft	12 in
	Prop to Wing LE	5.5 ft	11 in
Engine	Brake Horsepower	180 hp	1.9 hp
Total Airplane	Gross Weight	2400 lbf	14.6 lbf (233 oz)
	Wing Loading (W/S)	15.2 lbf/ft ²	52 oz/ft ²
	Power Loading	13.3 lb/hp	7.68 lb/hp
	Moment of Inertia (I _x)	1070 slug-ft ²	0.1805 slug-ft ²
	Moment of Inertia (I _y)	1249 slug-ft ²	0.2107 slug-ft ²
	Moment of Inertia (I _z)	2312 slug-ft ²	0.3901 slug-ft ²
	CG Range (Max Gross Weight) ¹¹	24.8 % MAC to 28.4 % MAC	24.8 % MAC to 28.4 % MAC

Table A-2. Control Surface Throws, Tolerances and Settings [38].

Flight Control	Throw Limits	Model Settings
Stabilator	18° ± 1° up 2° ± 1° down	19° up 1° down
Ailerons	30° ± 2° up 15° ± 2° down	32° up 17° down
Rudder	27° ± 2° right and left	29° right and left
Flaps	10°, 25°, 40° ± 2°	20° and 42°

¹¹ From Pilot's Operating Manual



Figure A-1. Model of the 1/6th Scale Piper PA-28-180 Cherokee with Radio Transmitter.



Figure A-2. Photo of Model's Access Door.

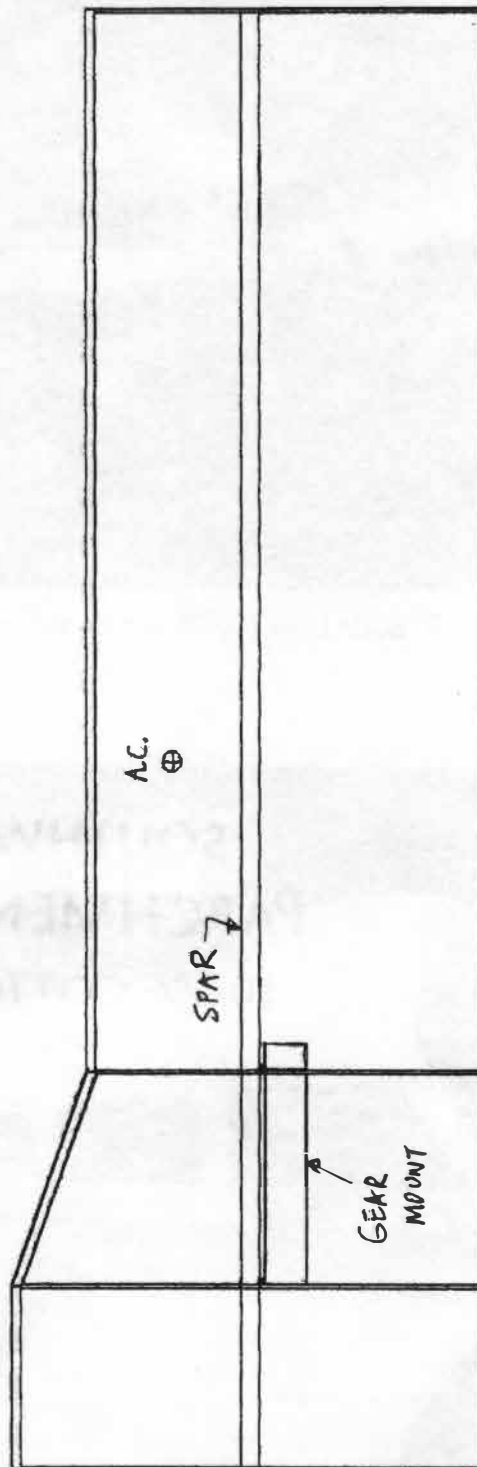


Figure A-3. Semi-Span Wing Planform Layout.

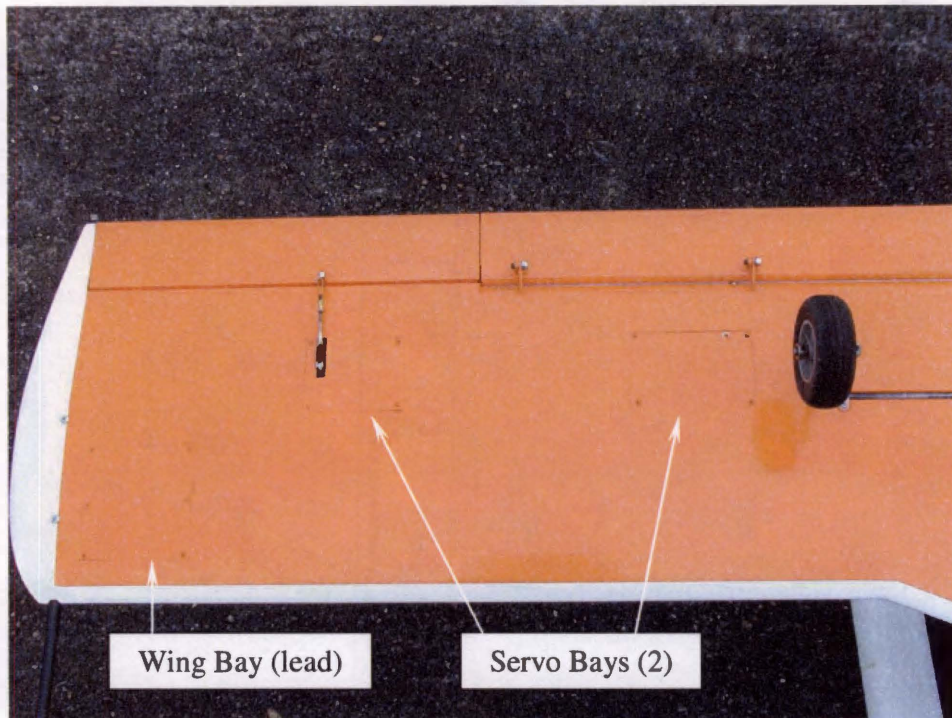


Figure A-5. Bottom View of Wing.

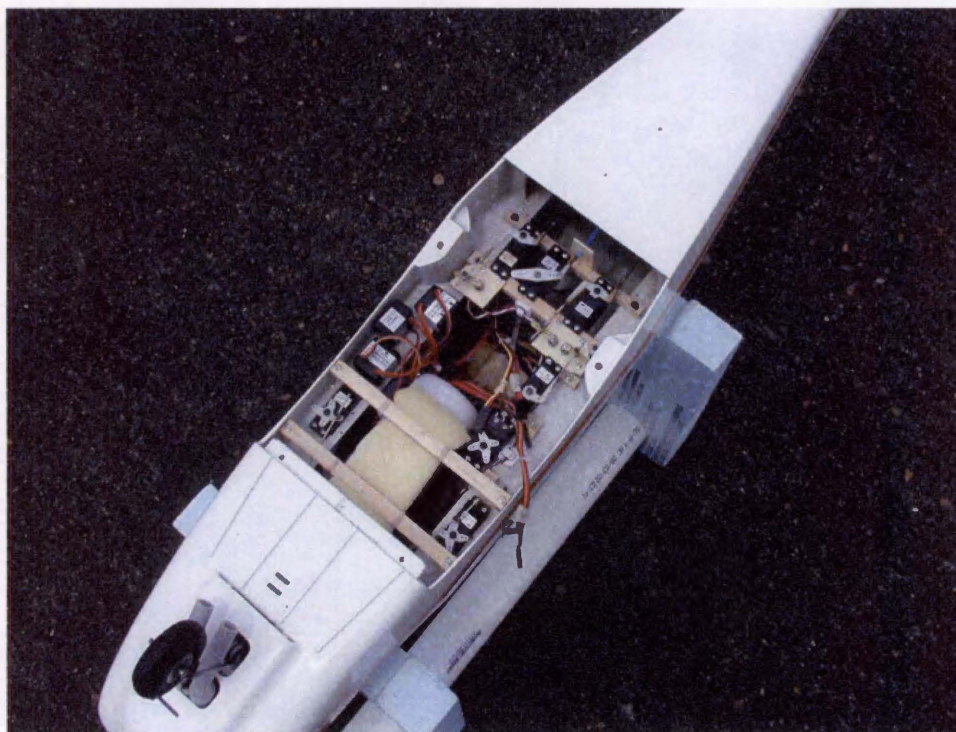


Figure A-6. Bottom View of Fuselage with Wing Removed.



Figure A-7. Setup and Downloading FDR Data.



Figure A-8. Author (right) with Thesis Advisor (left), Model and Recovery Vehicle.

APPENDIX B: Instrumentation

Instrumentation

This appendix details the creation of the instrumentation system and its calibration. Instrumentation includes the video system, the flight data recorder system, three control position systems, three rotation rate systems, and two angle sensor systems. Each is described separately.

Video System

The video system used was a Samsung Hi8 8mm camcorder (PN SCL810). It operated on either DC battery or AC power. It featured the following capabilities that were desirable for the test program:

- a. 22x high ratio zoom lens;
- b. Liquid crystal colour display;
- c. Black and white viewfinder;
- d. Speaker with volume control;
- e. Excellent battery life;
- f. Date and time recording; and
- g. Manual and auto focus control.

It did not have the following desirable features:

- a. Digital image stabilization to compensate for unstable images caused by hand shake, particularly at high magnification;
- b. Focus tracking to lock onto the model's movements so that focus is not easily lost; and
- c. Counter accuracy at $1/100^{\text{th}}$ of a second to facilitate spin rate calculations.

Flight Data Recorder

A flight data recorder made by Onset Computer Corporation was used for this project. It was the Tattletale TFX-11v2, which was a data logger ideal for embedded data acquisition or control applications. It was portable, had fast sampling capability over multiple channels, small size and weight, low power, and non-volatile data storage. It was

programmed with TFBASIC code, enabling the user to develop and implement custom solutions to the most challenging data acquisition or control tasks. The Tattletale's specifications are contained in Table B-1.

Mr. Michael Rigsby performed the programming and building of the FDR system. A 9V battery supplied power for the FDR and the battery was mounted at the model's access door with Velcro. To download data, a stereo phono plug was connected to a laptop computer. Each flight recording contained up to 150 kilobytes of data, which required up to 15 seconds to download. This was based on a sampling rate of 5 Hertz. The FDR had limitations to the range it could record. In "Tattletale units", the range was approximately 9,000 to 70,000. This required the sensors to be calibrated within that range, otherwise the data would peg itself at the limit.

The author installed the FDR in the upper fuselage above the fuel tank. The FDR was wrapped in foam rubber and secured to the fuselage using #64 rubber bands. Pictures of the Tattletale and its installation are shown in Figures B-1 to B-3.

Flight Control Position Sensors

The flight control position sensors were electrical potentiometers (pots) that were linked to the output arms of the flight control servos. Each pot was mounted onto a 1/8-inch thick light plywood plate. A piece of 1/8-inch diameter brass tubing was cut to desired length, then flattened and soldered onto a 1/8-inch wheel collar (PN DUBQ1180). Special connectors (PN DUBQ1860) were fitted to the brass tube and then a steel pushrod connected to it and to each flight control servo. The pots used had 5000-ohm resistance.

Electrical cable connected the pots to the FDR using a 3-pin Molex connector. Photos of the flight control position sensors can be seen in Figures B-3 and B-4.

Rotation Rate Sensors

Rotation rates about the three body axes were sensed by off-the-shelf hobby rate gyros, commonly used in radio-controlled helicopters. Traditionally, model helicopter gyro devices have been operated by an actual mechanical gyro with a spinning flywheel driven by a small electric motor. That old technology was surpassed by gyros using a piezo-electric crystal, which has no moving parts, is much more compact, lighter, more durable, and uses

less battery power than a mechanical gyro. Furthermore, a piezo-electric gyro offers faster response time and more accurate control than a mechanical gyro. However, not all piezo-electric gyros are created equal. Some have higher dynamic ranges (higher than 720 deg/s), more sophisticated software to correct for thermal drift, features to isolate RF and dissipate heat, and options for either manual or remote gain controls. The way the gyro works is by sensing motion about the axis that it controls, and sending a signal to the servo instructing it to move in the opposite direction so as to stabilize the air vehicle. The gain control changes the sensitivity of the gyro resulting in more or less effect on the servo that it's controlling. More gain causes more stability, but less immediate control by the pilot.

One drawback with piezo-electric gyros is that they are sensitive to temperature changes causing the gyro's neutral position to shift. This was very evident during the calibration process.

The idea used for this thesis study was to use piezo-electric gyros to provide rotation rate data to a flight data recorder rather than to servos. The gyros selected were single-axis piezo-electric angular rate gyros made by Heli-Max Performance Parts (PN HMXM1010), claimed to be the world's smallest gyros on the market. They featured manual gain control and a centering adjustment to manually correct for drift rather than internal software. Their specifications are contained within Table B-2. The gyros were mounted using 1/8-inch thick double-sided foam tape (PN KYOQ0603), one gyro oriented in each plane of rotation along the left fuselage side. Figure B-5 shows a close-up of their installation.

The signals from the gyros were converted from pulse width modulation to volts DC so that the FDR could record them. Three converters were purchased from RealDesign Ltd. in Finland. This company specialized in miniaturized sensors and data loggers for remote-control airplanes. Power for the converters came from the 9V FDR battery, and the converter's specifications are in Table B-3.

Angle Sensors

The angle of attack and sideslip vane sensors were mounted on booms projecting one chord length ahead of each wingtip, as recommended by *Kimberlin* [11]. AOA was on the right tip and sideslip on the left.

The booms were made from fiberglass pushrod, the same pushrod material used for the stabilator and rudder controls. Each boom was mounted in a hole drilled into the solid balsa wing tips and held in with two screws. The booms were hollow allowing for electrical wire to pass through to the sensors mounted at the forward ends. Conduit was built into the wing during construction to allow wiring to be routed from the wing's center-section to the tip booms.

The angular sensors were another product from RealDesign Ltd. in Finland. The sensor worked without any mechanical contact and measured the rotation of a magnetic field. Each sensor was composed of a tiny magnet (approx 3mm in diameter) and an electrical board. The sensor's specifications are in Table B-4. Because of the size of the board, it was not feasible to install it inside the boom assembly. Therefore, "pods" were designed and made from aluminum. The pods had a diameter of 7/8 inches and a length of 3.8 inches. The board assembly was siliconed inside the boom pod and the tiny magnet attached to the end of the vane's shaft. The pods were also designed with removable fore and aft sections to allow installation and service of the electrical and magnetic components. All up weight of each pod was 2.5 ounces with all components and the boom installed.

The vane assemblies were made from 1/8-inch diameter brass tubing and 0.010 inch thick "Polyply" (Bob Violet Models BVM PN 5710). Polyply is an epoxy impregnated fiberglass product available in sheets of several thicknesses. The Polyply was used to make the wing section of the vane and the brass tubing was the vane's body. The vanes were 100% mass balanced by soldering 4-40 size steel rod inside the forward section of the brass tube body. The solder at the tip was also filed into an aerodynamic shape. The vane's pivot shaft was made from 2-56 steel pushrod material and cut to a length of 7/8 inches, the diameter of the pod's body. It was soldered to the vane's brass body at a 90° angle. The bearing on the pod for the vane's pivot shaft was made of brass and was press fit into the pod's housing.

Pictures of the angle sensors are shown in Figures B-6 and B-7.

Calibration Procedures

All instrumentation sensors required calibration. For calibration of an individual system, all sensor systems had to be connected to the FDR as if it were the final installation. Otherwise, a voltage rise would occur across the DC power bus of the FDR, which powered

the sensors. A voltage rise or drop would directly change the calibration. Each sensor system is described separately below.

Flight Control Position Sensors

Flight control position sensors were calibrated by deflecting the control stick on the transmitter to a set amount, which drove the servos and pots. A ruler at the trailing edge of the flight control was measuring the deflection while the servo held position and the FDR captured the readings. The readings were plotted as a time history and values averaged for each deflection amount. These values were then converted to degrees of deflection and plotted versus the original FDR data. Figure B-8 shows the FDR data and Figure B-9 shows the calibration curve for the elevator sensor. The calibration curve was a third order function as servo rotational movement was translated into a linear action at the sensor. Note that the aileron calibration curve uses a 5th order curve fit as aileron differential required this.

Calibration curves for the aileron and rudder deflections are shown as Figures B-10 and B-11, respectively.

Rotation Rate Sensors

Calibration of the rate gyros required use of a calibrated rate table. To do this the three gyros were placed on the rate table with the whole aircraft, as all other systems had to be connected to the FDR. The rate table was only capable of 3.75, 7.5, 15 and 30 deg/s rotation rates in both directions. The desired range was up to 300 deg/s. Resulting were calibrations in only 10% of the desired range with extrapolation out to the other 90%. A record turntable at 33 rpm would have provided 198 deg/s, and 75 rpm would have provided 450 deg/s. At these speeds, a more accurate calibration could have been done as well as a functional check at those speeds. The gyro used did not have a dynamic range specification provided.

It was found that the gyro gain setting was important. Decreasing the gain flattened the calibration curve, but if too low, the FDR would not pick up the higher rotation rates. If the gain was too high, the FDR would not be able to pick up rotation rates at the low end of the scale. Unfortunately, without a rate table capable of higher speeds, the gyro properties above 30 deg/s could not have been observed.

As mentioned, these piezo-electric gyros were particularly sensitive to temperature changes causing the gyro's neutral position to shift. Applying a heat gun to the air around the gyro for approximately five seconds caused as much as a 20% shift in the curve. However, this problem was overcome by two procedures. First, the gyro system was given several minutes to warm up. Second, the values prior to each flight were captured with the model motionless on the ground. This data served to be the "zero" that accounted for all adverse effects on the gyros. The data reduction procedure was to subtract the "zero" readings from the flight data. This, however, did not correct for any thermal drift that took place after the pre-flight measurements.

Each calibration was carried out twice and the results averaged. The gyros' responses were linear. The rate table specifications are listed in Table B-5. A picture of the gyro calibration procedure is shown in Figure B-12. The three gyro calibration curves are in Figures B-13 to B-15.

Angle Sensors

The angle sensors were calibrated using the same method as the position sensors. Instead of a ruler, a protractor was mounted to the sensor boom under the vane and used to calibrate the angle sensors. Calibration curves were 2nd order. Figure B-16 shows the mounted protractor and Figures B-17 and B-18 are the calibration curves for AOA and AOS, respectively.

Table B-1. Tattletale Flight Data Acquisition Unit Specifications.

Item	Specification
Name	Tattletale TFX-11v2 Data Logger
Manufacturer	Onset Computer Corporation
Size (inches)	1.2 x 2.75 x 0.5
Weight (ounces)	0.6
Processors	68HC11 and PIC 16F873A
Capacity (RAM)	128K
Capacity (Flash EEPROM)	2MB (program and data)
Analog Channels	11 @ 12-bit resolution 8 @ 8-bit resolution
Analog Input Voltage Range	0 - 5 VDC
Maximum Sampling Rate	3200 Hz for 12-bit 6400 Hz for 8-bit
Digital Lines	16 input/Output
Power Drain	Less than 100 μ A
Peak Current	150 mA
Power Supply Range	5.5 to 18.5 VDC
Operating Temperature	-40°C to +85°C
Relative Humidity	0 to 95%

Table B-2. Rate Gyro Specifications.

Item	Specification
Name	Micro Piezo Gyro
Manufacturer	HeliMax Performance Parts
Dimensions	1.1 x 1.1 x 0.6 inches
Weight	0.49 ounces
Operating Voltage	3.3-7.0 VDC
Current Consumption	35 milli-Amps
Temperature Range	50-95°F
Dynamic range	unknown

Table B-3. AOA and AOS Sensor Specifications.

Item	Specification
Name	Contactless Angle Sensor
Manufacturer	RealDesign Ltd., Finland
Dimensions	58 x 14 x 7 mm
Weight	10 grams
Operating Voltage	5.2-10 VDC
Current Consumption	14 milli-Amps
Voltage Output Range ¹²	0.6-4.74 VDC
Volts/Degree ¹²	0.041
Measurement Range ¹²	100 degrees

¹² Measured by Mr. Mike Rigsby on 2 April, 2003.

Table B-4. Pulse Width Modulation Converter Specifications.

Item	Specification
Name	Servo Pulse Meter
Manufacturer	RealDesign Ltd., Finland
Dimensions	50 x 16 x 10 mm
Weight	10 grams
Operating Voltage	5.2-10 VDC
Current Consumption	2 milli-Amps
Voltage Output Range ¹³	2.0-3.5 VDC

Table B-5. Rate Table Specifications

Item	Specification
Name	Turntable, Inst Test
Manufacturer	Ideal-Aerosmith Inc.
Speeds	225, 450, 900, 1800 deg/min
CAT No.	12525
S/N	7016
Calibration Date	Aug 30, 1962.

¹³ Measured by Mr. Mike Rigsby on 2 April, 2003.

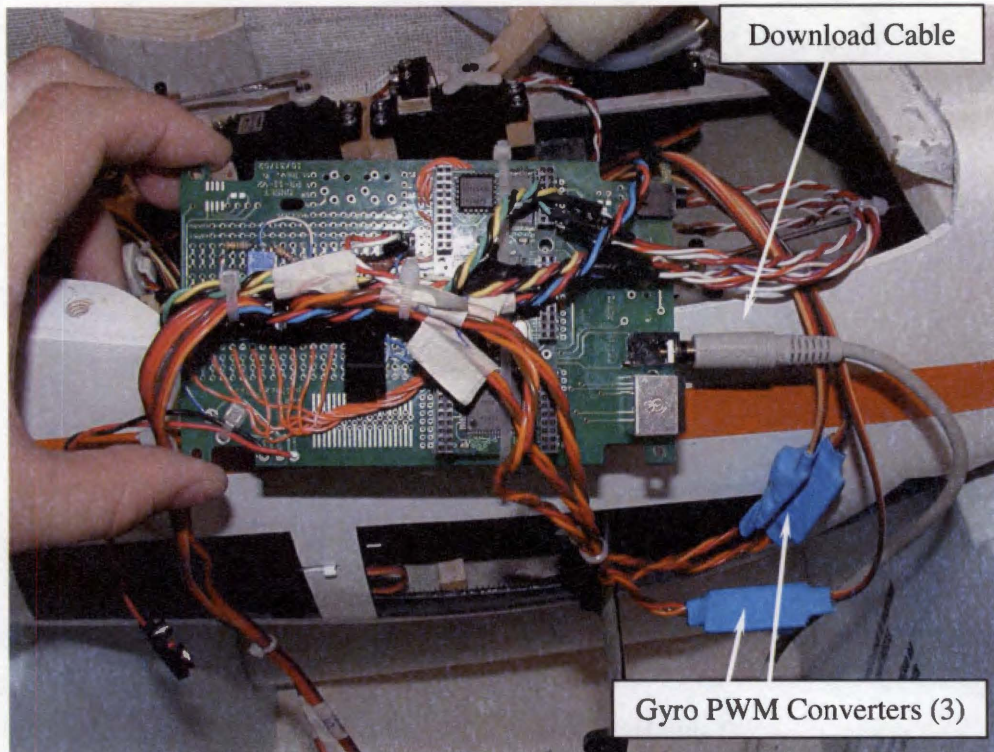


Figure B-1. Tattletale Flight Data Acquisition Unit.

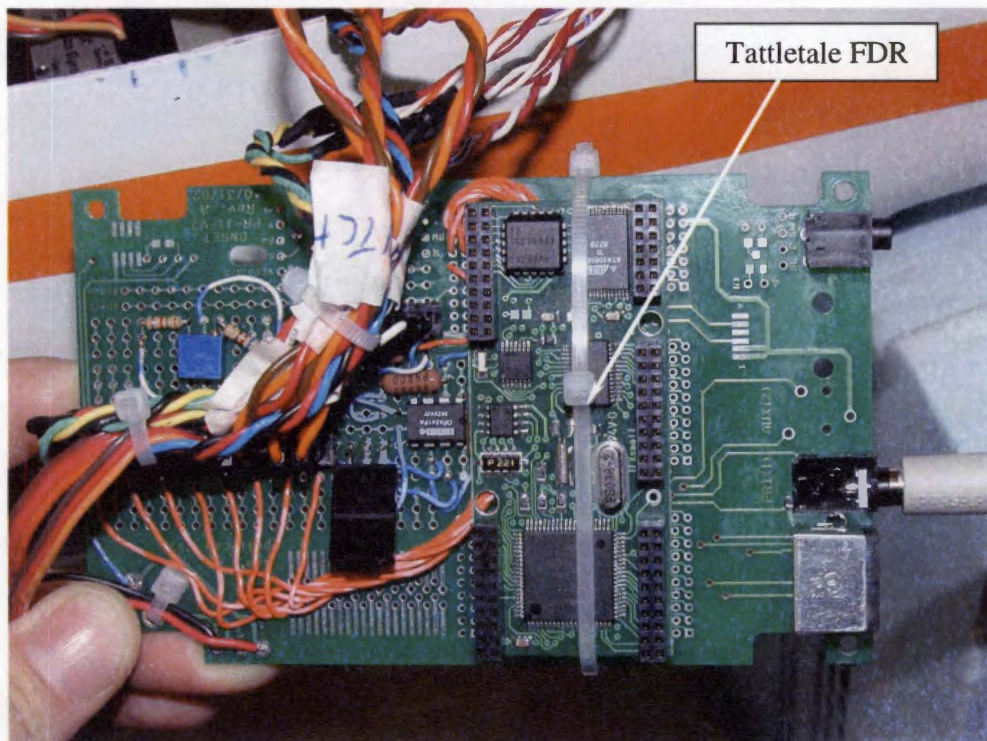


Figure B-2. Close-up of Tattletale Acquisition Unit.

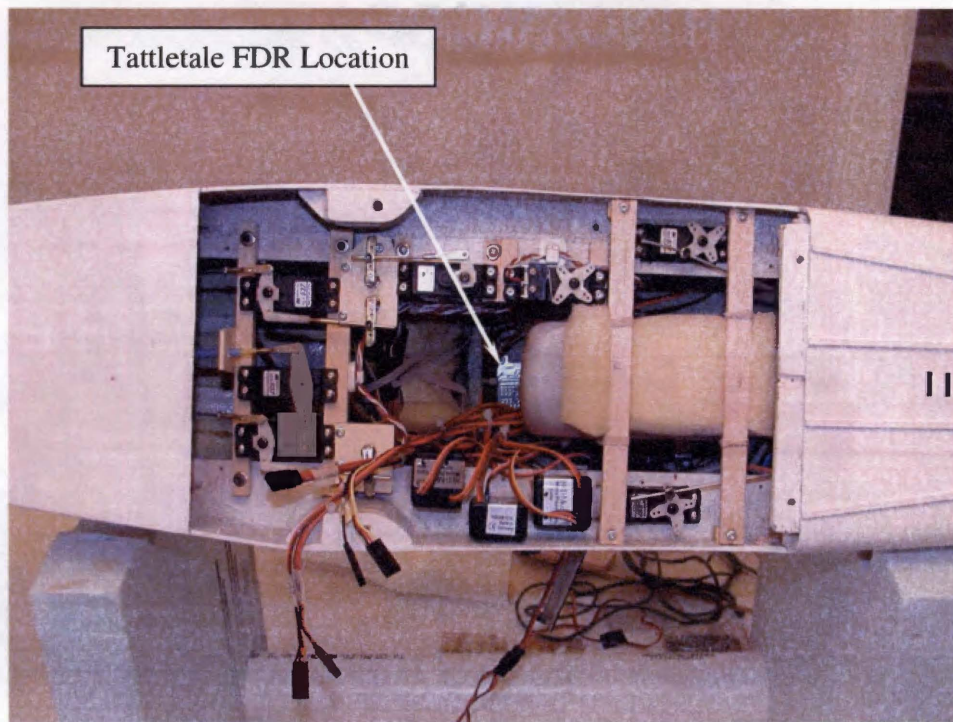


Figure B-3. Tattletale FDR Installation.

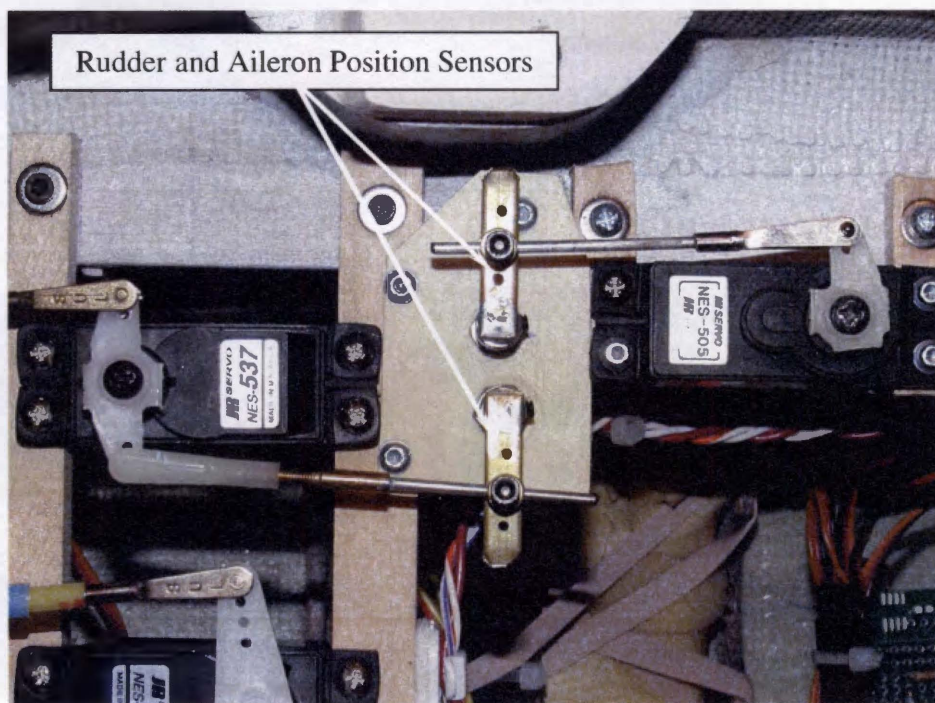


Figure B-4. View of the Rudder (left) and Aileron (right) Position Sensors.

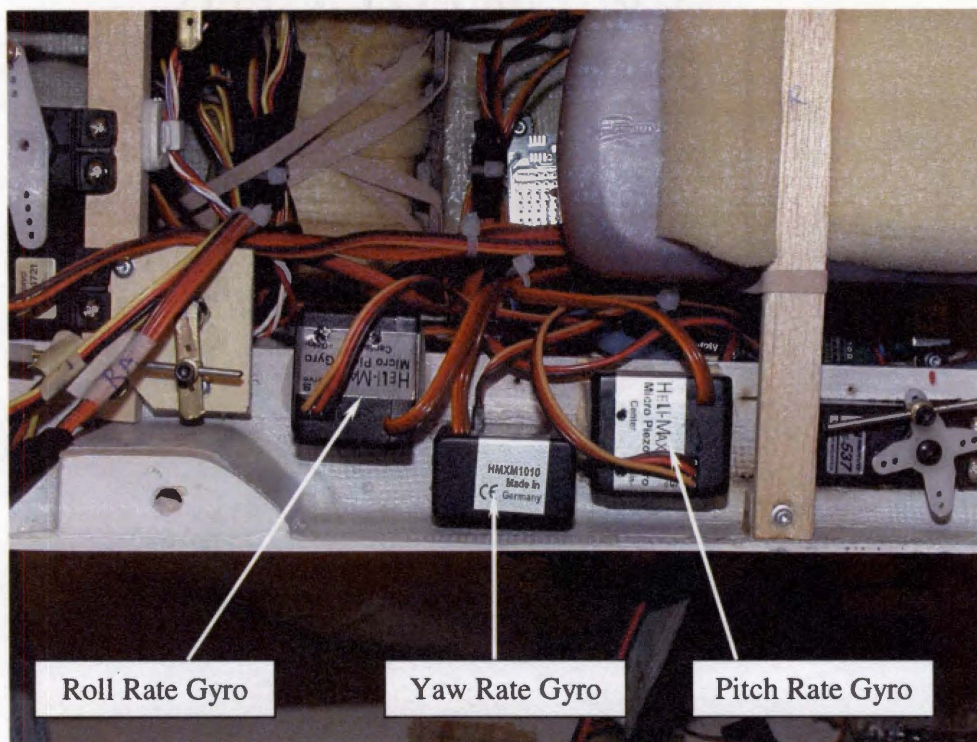


Figure B-5. Gyro Installation on Left Fuselage Side.

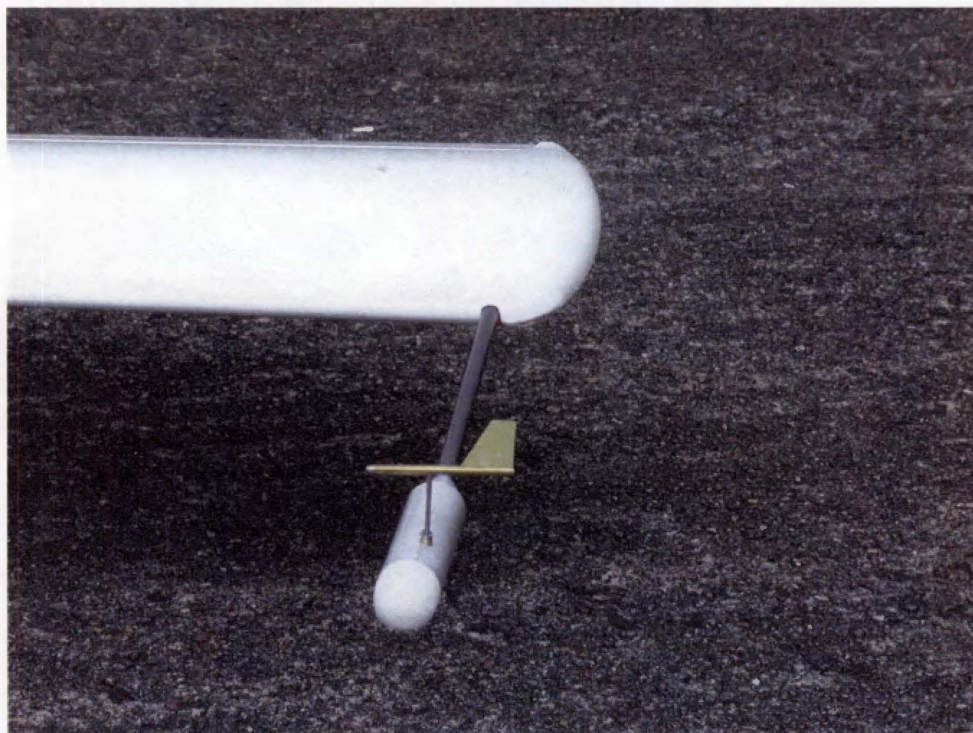


Figure B-6. Sideslip Sensor at Left Wingtip.

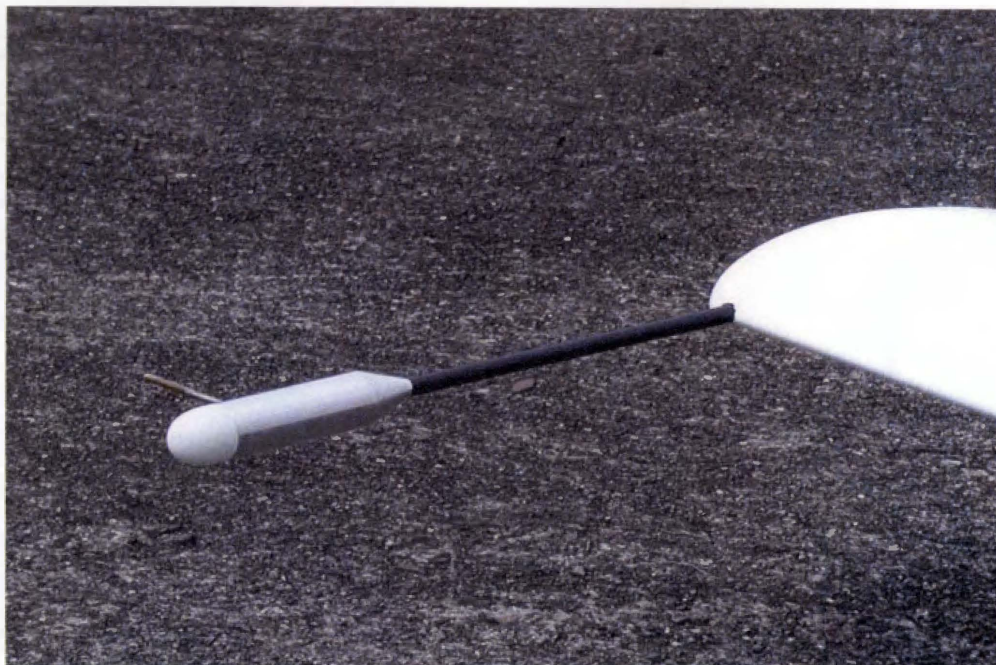


Figure B-7. Angle of Attack Sensor at Right Wingtip.

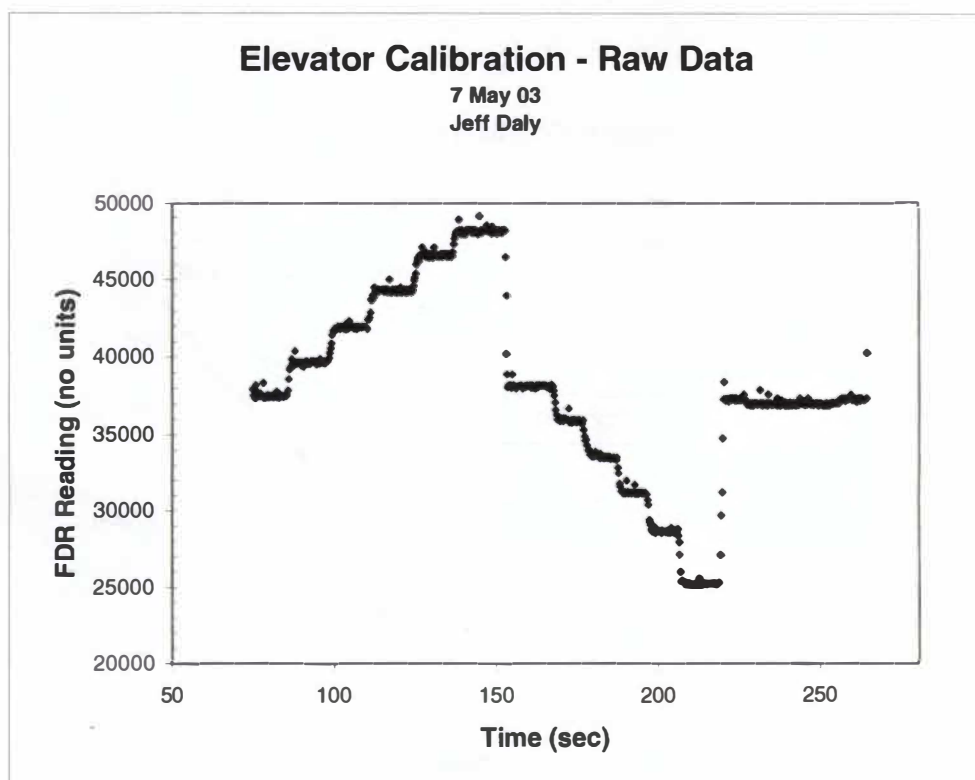


Figure B-8. Sample of Calibration Raw Data from FDR.

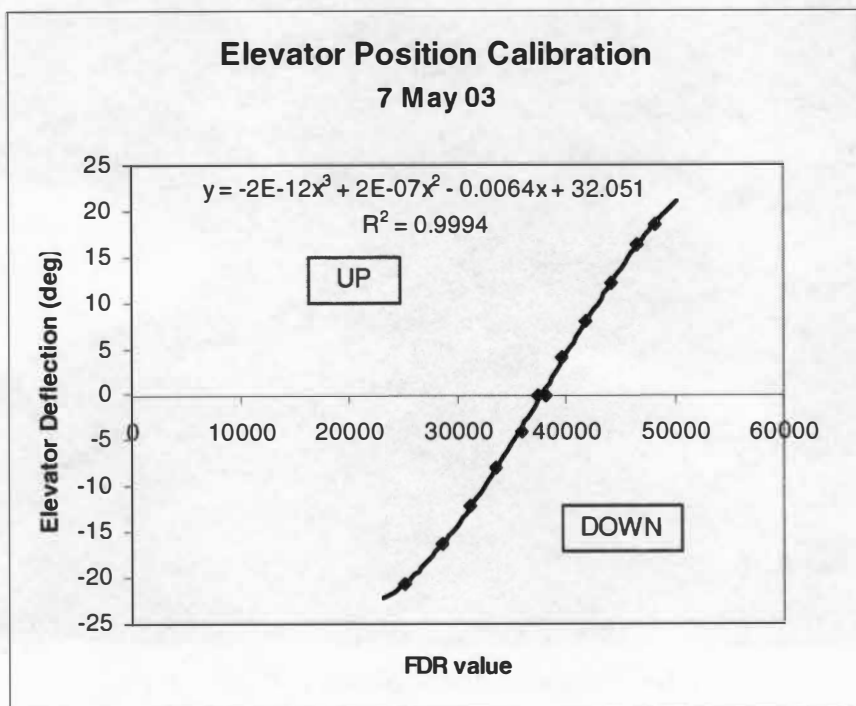


Figure B-9. Elevator Position Calibration Curve.

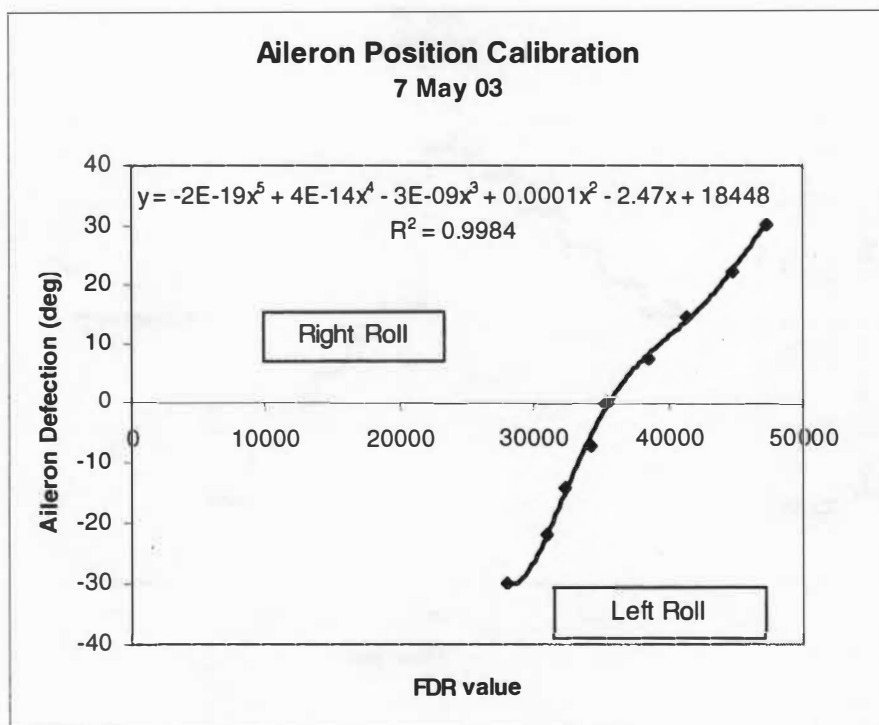


Figure B-10. Aileron Position Calibration Curve.

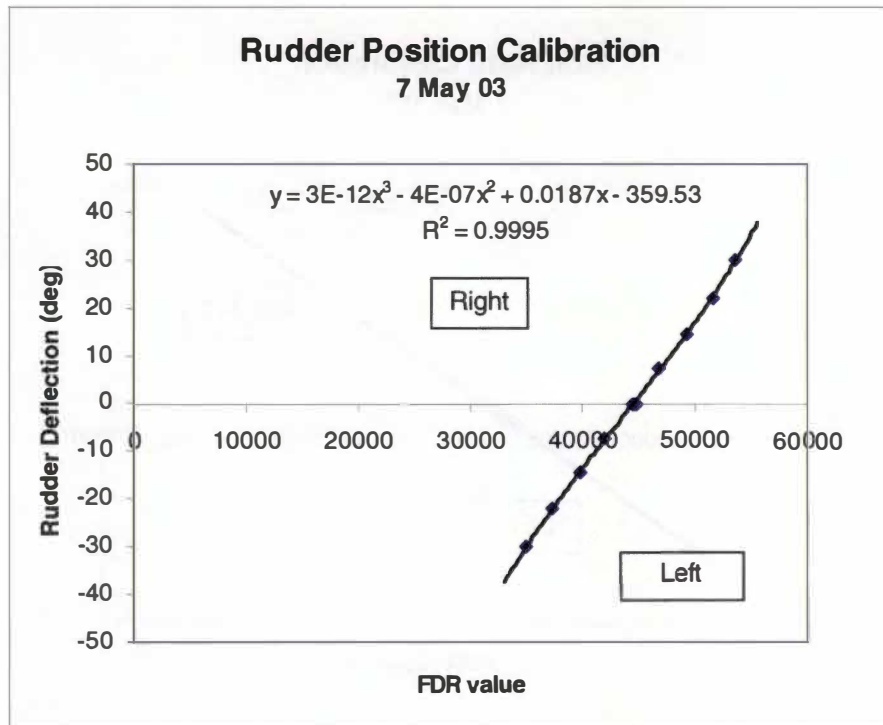


Figure B-11. Rudder Position Calibration Curve.



Figure B-12. Gyro Calibration Operation.

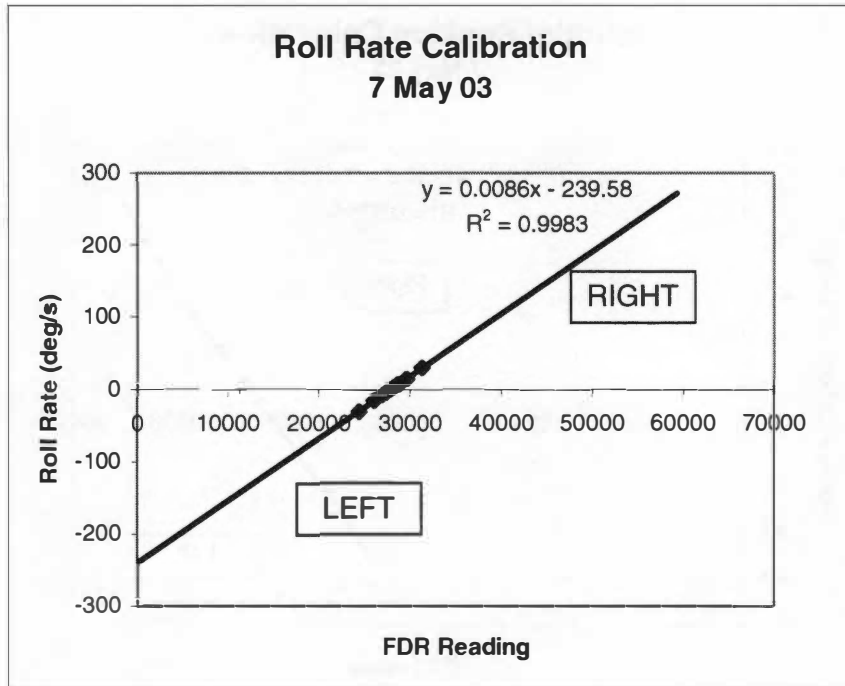


Figure B-13. Roll Rate Calibration Curve.

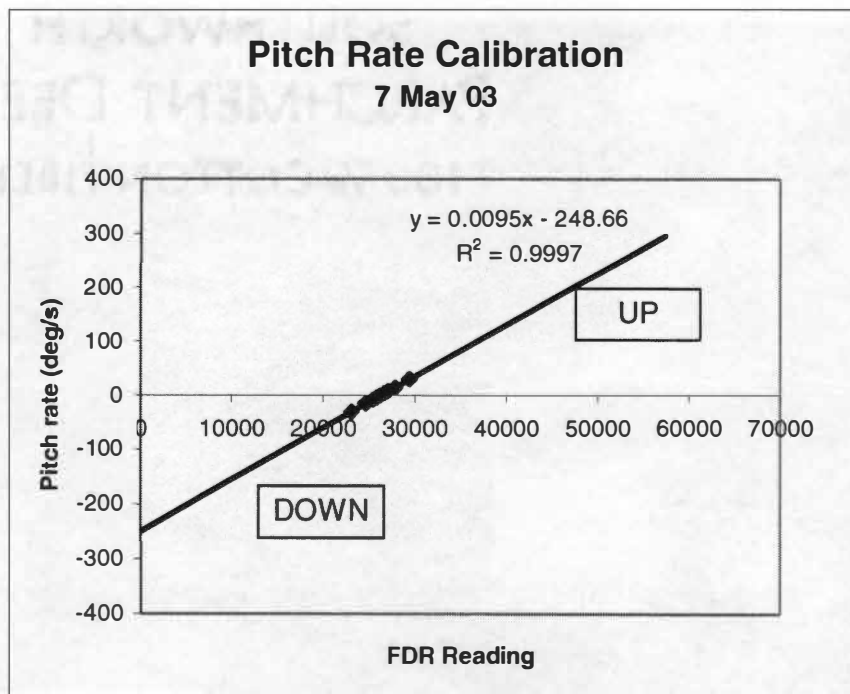


Figure B-14. Pitch Rate Calibration Curve.

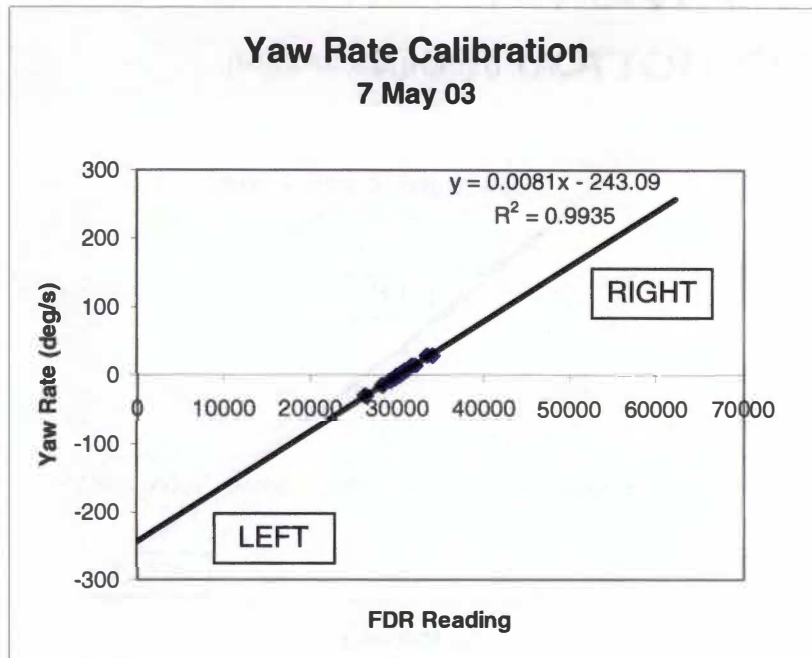


Figure B-15. Yaw Rate Calibration Curve.

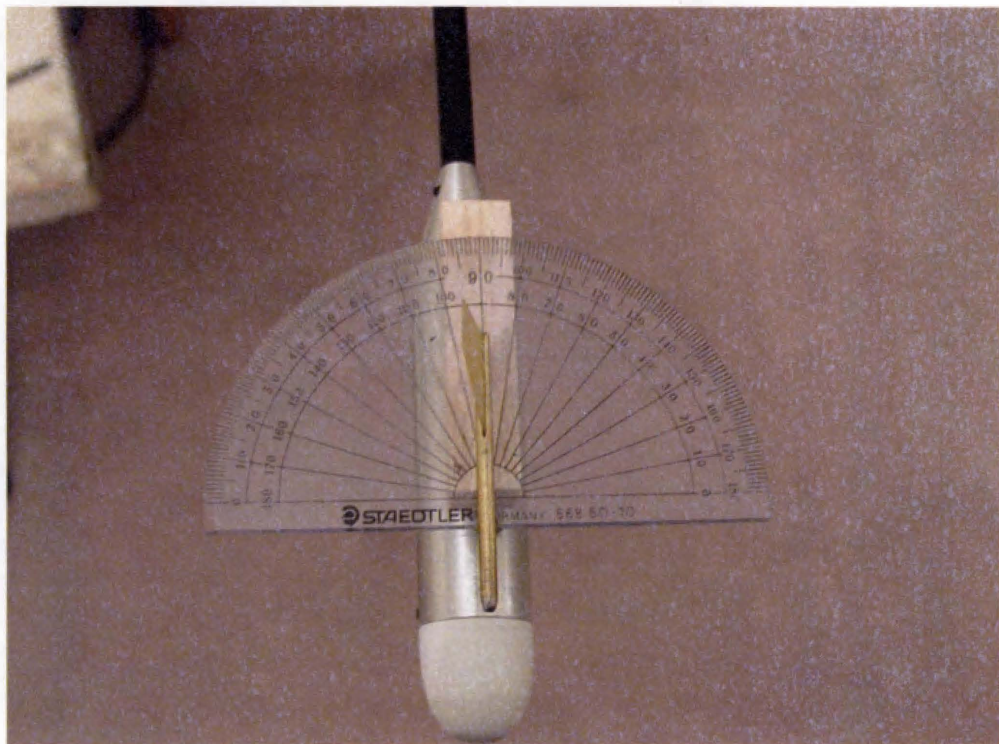


Figure B-16. Angle of Sideslip Calibration.

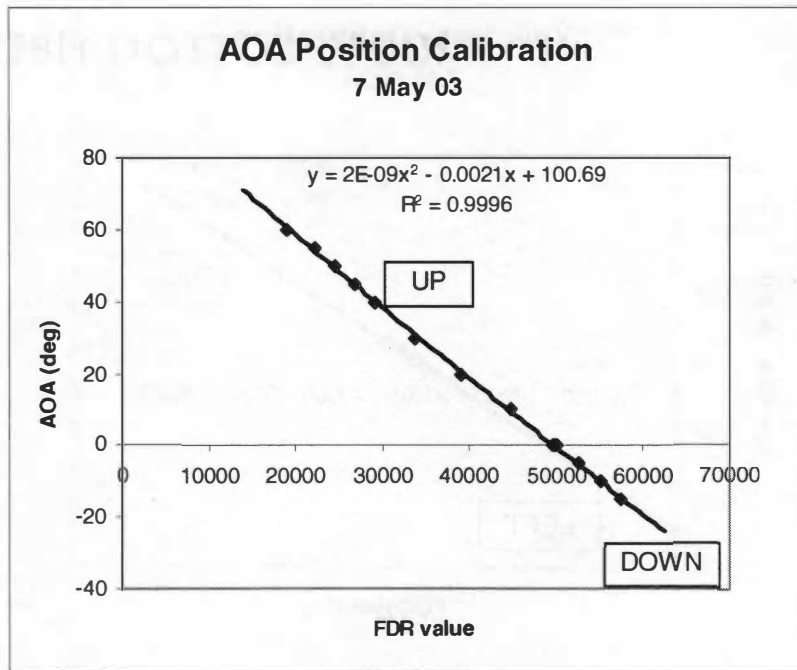


Figure B-17. Angle of Attack Calibration Curve.

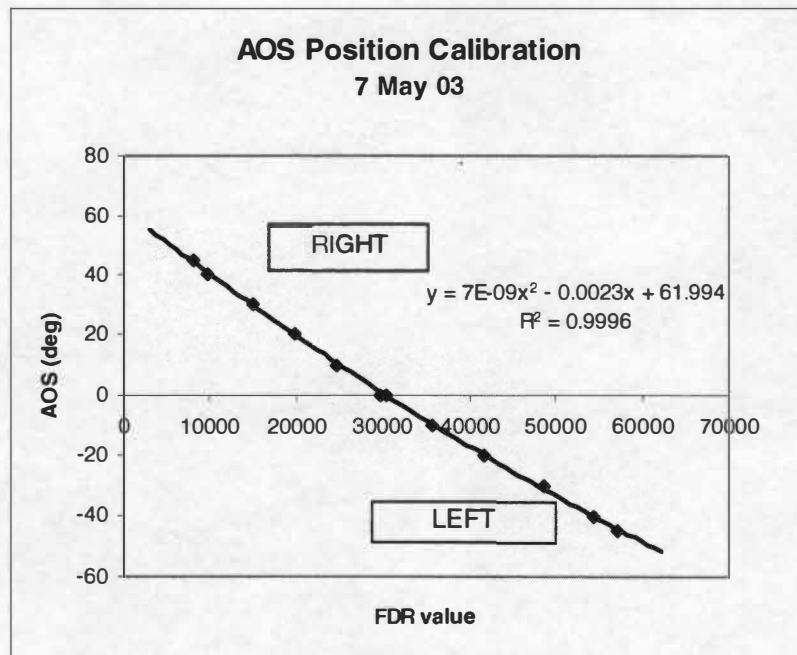


Figure B-18. Angle of Sideslip Calibration Curve.

APPENDIX C: Spin Recovery Parachute System

Spin Recovery Parachute System

Spin recovery parachute systems have been used on full-scale airplanes and radio-controlled models in the past. As partially described in Chapter III, a spin recovery parachute system was designed and installed on the model's tail.

The system design consisted of three parts: the boom and mount, the actuator, and the parachute. They are discussed below:

Boom and Mount

A boom was fabricated from 7/16-inch diameter brass tubing and it projected 6¼ inches aft of the stabilator. It was mounted into a hardwood block that was fastened to the inside of the fuselage with four sheet metal screws. The boom was fixed in place by one small #4 sheet metal screw, which passed through the fuselage wall, through the mounting block and into the brass tube to lock it into position. The boom was located at the lowest point of the fuselage to permit maximum stabilator travel. Pictures of the boom are shown in Figures C-1 and C-2.

The parachute's mount was made from 1/8-inch thick light plywood and ¼-inch thick basswood. The mount was glued together using cyanoacrylate instant adhesive. The center block was also bolted together with 4-40 sized bolts and blind nuts because it sustained all the stress of the parachute deployments. The mount's overall dimensions were 2½ x 1¼ x 11/16 inches. It was attached to the boom using two 4-40 sized bolts and blind nuts. Pictures of the mount are shown in Figures C-3 to C-5.

System Actuator

A "Nyrod" pushrod (PN SULQ3005) was used to deploy the parachute and release it. Figure C-6 shows the Nyrod attached to its servo. The Nyrod was mounted inside the boom and held in place with some basswood inside the boom. A steel 2-56 pushrod was threaded into the end of the Nyrod, which served to be an actuator pin for deploying and releasing the parachute. The parachute was mounted onto the top of the mount and an elastic band held it in place. The actuator pin held each end of the elastic band, so that when a switch was flipped on the transmitter, the servo pulled the spin approximately ½ inch and the elastic

sprung free allowing the parachute to deploy. Flipping another switch on the transmitter pulled the spin an additional 5/8-inch to release the parachute's lines from the actuator pin. This system worked well and was simple. A photo of the releasing pin can be seen at Figure C-2.

Parachute

A 12-inch diameter parachute was purchased (PN DYFP8708). It was a solid type and not a ring slot parachute, commonly used for controlled descent of a radio-controlled glider high-start system. The parachute material was nylon and its risers came attached to the parachute, being 20 inches long. All eight risers were tied to a steel ring that was attached to a fishing line swivel. Two suspension lines were made from nylon cord, cut to 21 inches long, then attached to the swivel. At each end of the suspension lines was a fishing line clip that served to slide over the actuator pin. To stow the parachute, it was folded in half and placed on top of its risers and suspension lines, which were coiled-up using three fingers. The elastic band was wrapped around the parachute and lines and held in place by the actuator pin. It was important to mount the parachute with its opened end facing the direction of flight to aid its deployment and opening.

A picture of the stowed parachute can be seen in Figure C-7. Figures C-8 to C-10 show the parts of the spin recovery parachute system.



Figure C-1. Side View of Spin Recovery Parachute Assembly.

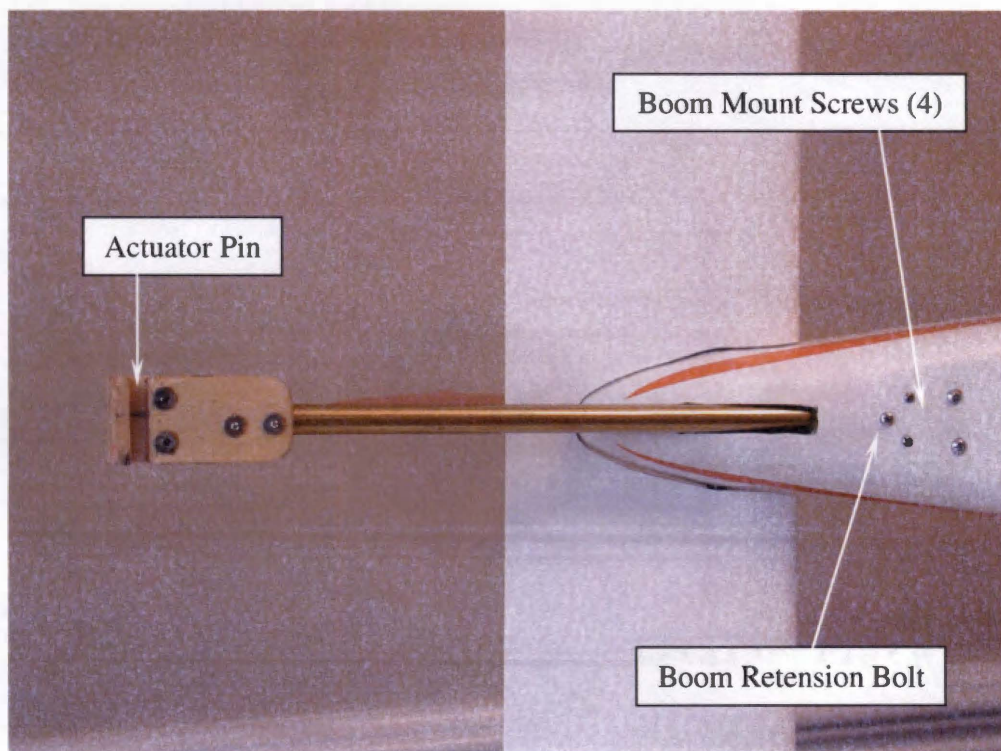


Figure C-2. Bottom View of Spin Recovery Parachute Boom and Mount.

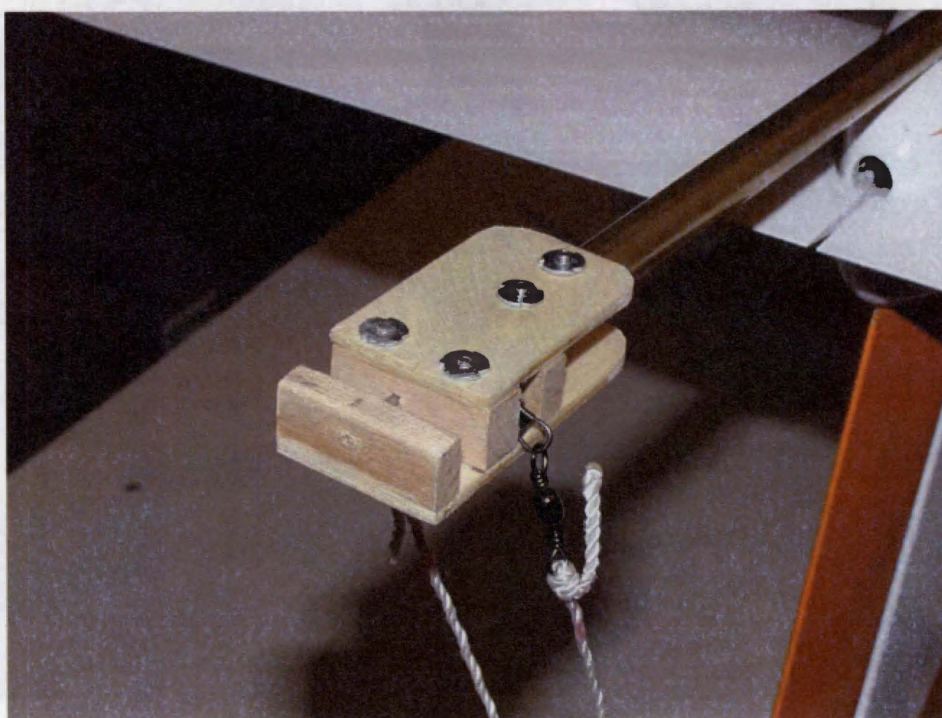


Figure C-3. Spin Recovery Parachute Mount – Bottom View.

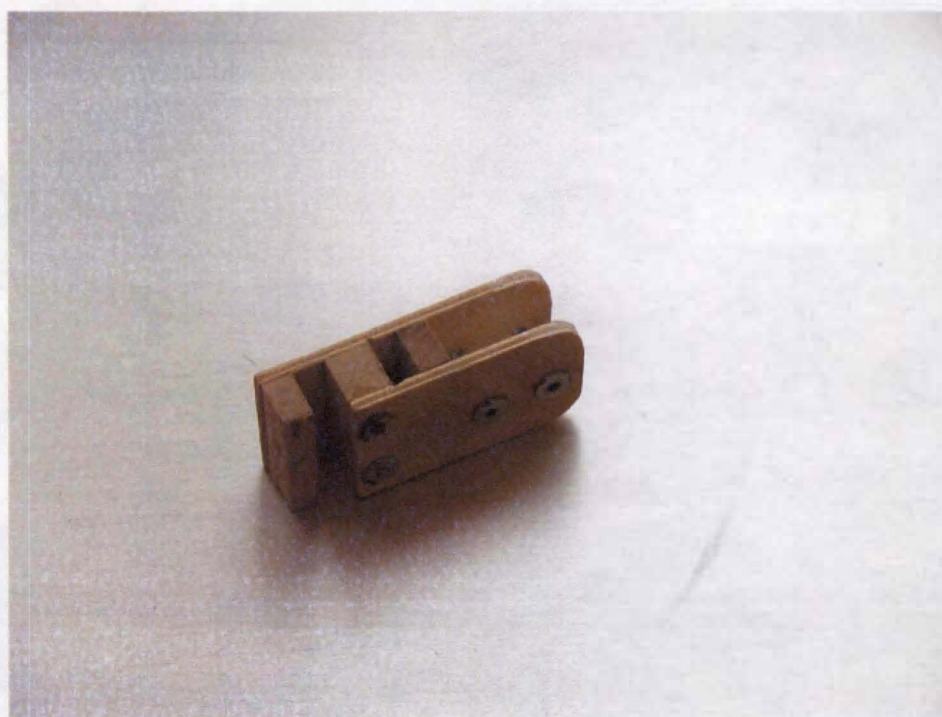


Figure C-4. Spin Recovery Mount – Side View

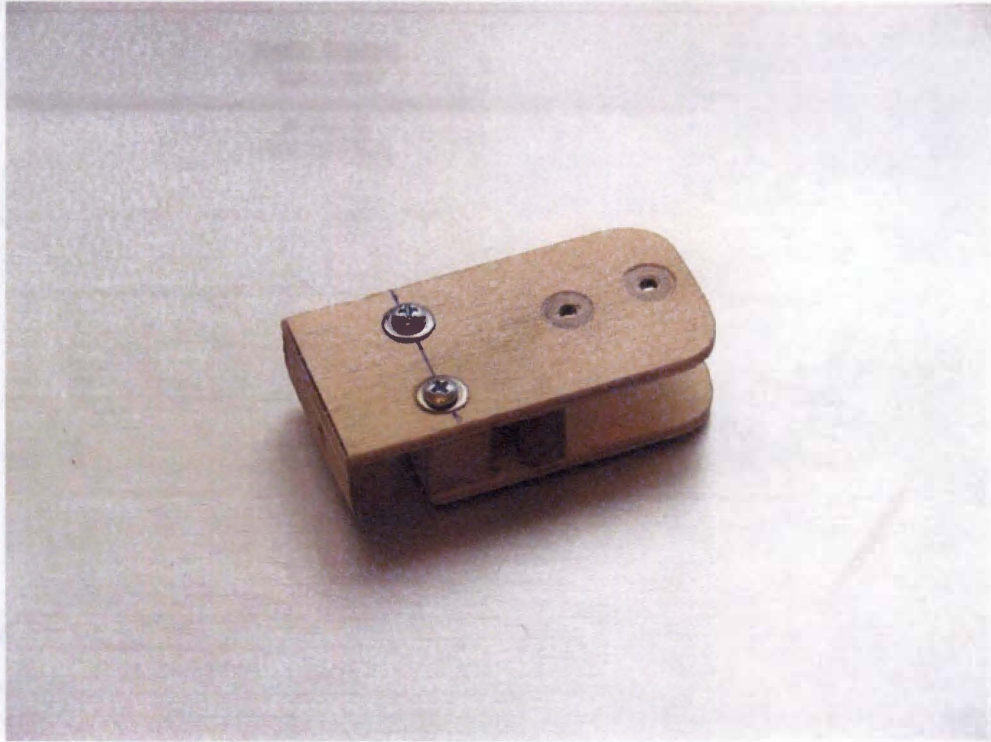


Figure C-5. Spin Recovery Mount – Top View.

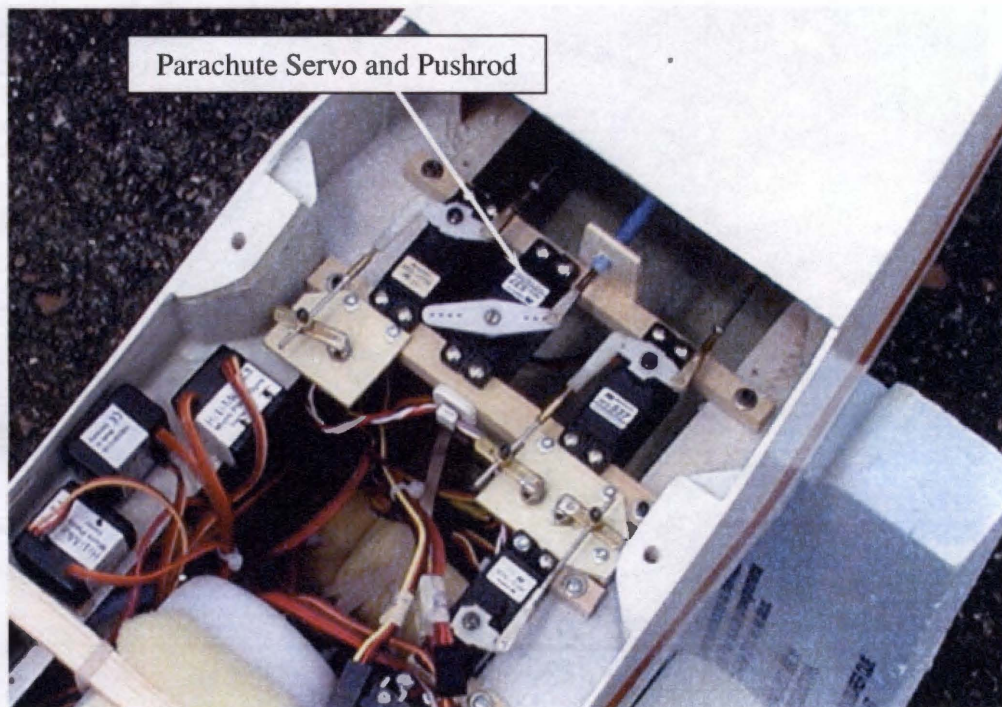


Figure C-6. Spin Recovery Parachute Servo and Pushrod.



Figure C-7. Spin Parachute Mounted.



Figure C-8. Spin Parachute.

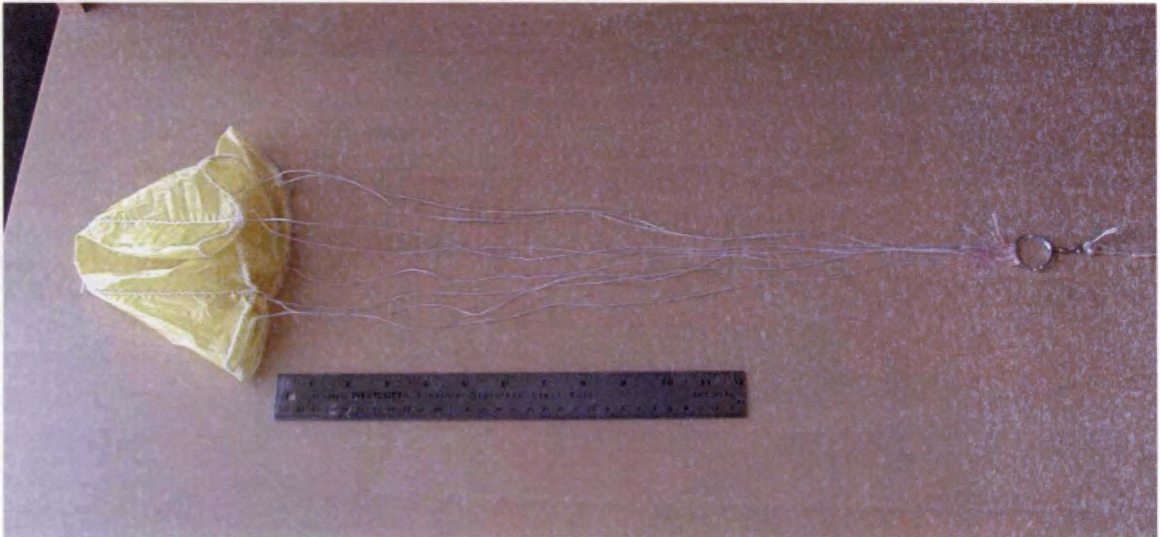


Figure C-9. Spin Recovery Parachute and Risers.

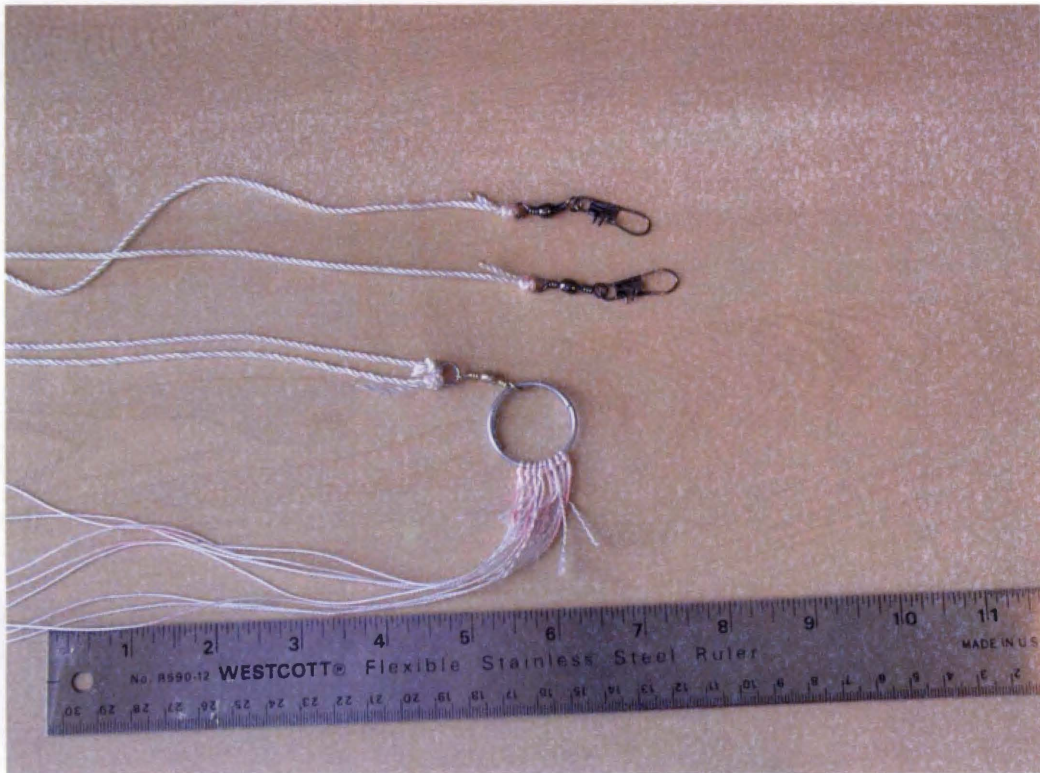


Figure C-10. Spin Recovery Parachute Attachments.

APPENDIX D: Mass Properties and Moments of Inertia Measurements

Mass Properties and Moments of Inertia Measurements

This appendix details the methods used to determine the mass properties of the radio-controlled model. Mass properties entailed the model's weight and moments of inertia. Three conditions were important to be simultaneously satisfied for mass properties: total weight of the model, moments of inertia about the three body axes, and center of gravity position. Each is described below.

Determination of Aircraft Weight and Center of Gravity Position

The model's weight was calculated using the formula derived in the Dynamic Similitude section in Chapter II. The model's weight was also a function of the test altitudes (air densities) of both the model and full-scale representative airplane. The model's weight was measured using a postal scale. Its specifications are contained in Table D-1.

Center of gravity position was measured by inverting the aircraft and balancing the model with one's fingers at the desired center of gravity position. This may seem unscientific, but the CG position was sensed very easily with this method. Accuracy was within 1/16th of an inch. Relocating the model's weight brought the CG to the desired location. The use of a solid brass hub (which weighed 2 ounces, PN HIGQ1320) mounted on the propeller shaft under the spinner was very useful to easily alter the CG setting for the three CG positions used for the flight test program.

Determination of the Moments of Inertia

A literature search was carried out to determine the methods historically employed to determine full-scale and model moments of inertia of their body axes. Prior to the 1950's, small full-scale aircraft were measured using the compound pendulum method where the whole airplane was swung like a child's swing followed by data conversions to translate results to the aircraft's center of gravity. *Green* [34] in 1927 published the methodology, followed by *Miller* [35] and *Gracey* [36] in 1930 and 1948 who improved the method's accuracy. Because of the difficulty of suspending an airplane from an axis parallel to the z axis, the compound pendulum method was not used to measure I_z , but rather the torsional

pendulum method was utilized. *Burk and Wilson* [8] used the bifilar torsional pendulum for their radio-controlled model. Figure D-1 shows the basic method.

It was decided to employ the bifilar torsional method for this thesis project. Two strings of equal length supported the model with the model's CG centered between the supports. Braided 30-pound fishing line (Remington brand) was used for the support strings. The model was then oscillated about the axis of rotation parallel to the string supports and the number of oscillations counted over a specified period of time. A stopwatch was used to time the number of complete oscillations, and the procedure repeated three times and the results averaged. The period of oscillation was calculated by dividing the total number of complete oscillations by the total time. The moment of inertia was calculated from the model's weight, period, and dimensions of the bifilar set-up. The formula used was derived using theory from *Shigley and Uicker* [33]. Thus, moments of inertia were calculated using the following formula:

$$I_{x, y, z} = \frac{W D^2 \tau^2}{16 L \pi^2} \text{ (slugs-ft}^2\text{)}$$

where:

W = model's weight (lbf);

D = distance between the string supports (feet);

τ = period of oscillation (seconds); and

L = length of the string supports (feet).

Correcting the M_oI values for buoyancy and entrapped air was deemed unnecessary for a model of such small size.

Moments of inertia were measured for six different combinations of CG and wing mass. Specifically, the forward and aft CG settings, and wing inertia states at reduced, stock and increased configurations were measured. It was an iterative approach where the model's mass had to be shifted many times and re-measured in order not to change the CG position nor exceed the desired weight, and to obtain the desired M_oI . Solving simultaneous equations would have determined the ideal mass and location corrections, however, that would have

been time consuming and would still have required an actual final measurement for verification. Once the M_0I results were close to the desired values, then small mass additions were made to tune the results. Locations for mass additions were at the outer wing bays. A simple calculation of $I = md^2$ (d = the moment arm from the moment axis, m = mass added) for the mass adjustment determined the additional mass required. Since the adjustment mass size was physically very small, the inertia about its own body axis was very small and therefore neglected in the inertia adjustments.

It was found that the distance between the bifilar support strings was not arbitrary. References [34, 35, 36] commented that $L \geq D$, however, secondary natural oscillations would develop if D was too large, even if $L \geq D$. It was found that D was ideal at 35% of L . Also, the number of oscillations was not important to calculate the period. Ten cycles were used for this method with initial amplitude of approximately 5 degrees.

Table D-2 shows the M_0I results and Table D-3 the error analysis for the forward CG position (24.8% MAC). Figures D-2 to D-4 show the actual moments of inertia operation.

Table D-1. Postal Scale Specifications.

Item	Specification
Name	Postal Scale
Manufacturer	Pitney-Bowes
Range	0 - 10 lbf
Model No.	0051
Serial No.	29840
Calibration Date	March 1984

Table D-2. Moment of Inertia Results.

CG Position	Inertia State	Moment of Inertia (slug-ft ²)			Weight (lbf)	I_x/I_y	I_x/I_z	I_y/I_z
		I_x	I_y	I_z				
Unknown	Published Stock Inertia	0.1805	0.2107	0.3901	14.56	0.857	0.463	0.540
	Calculated Increased Inertia	0.3885	0.3795	0.7187	15.30	1.024	0.541	0.528
Fwd CG 24.8% MAC	Reduced Inertia	0.2609	0.3836	0.5935	14.44	0.680	0.440	0.646
	Stock Inertia	0.3246	0.3795	0.6587	14.75	0.855	0.493	0.576
	Increased Inertia	0.3914	0.3822	0.7176	15.23	1.024	0.545	0.533
Aft CG 28.4% MAC	Reduced Inertia	0.2609	0.3938	0.6077	14.44	0.663	0.429	0.648
	Stock Inertia	0.3246	0.3886	0.6674	14.75	0.835	0.486	0.582
	Increased Inertia	0.3914	0.3958	0.7327	15.23	0.989	0.534	0.540

Table D-3. Moment of Inertia Error Analysis at the Forward CG Setting.

Item	Stock Inertia	Increased Inertia
Weight	1.3%	0.5%
I_x	79.8%	0.7%
I_y	80.1%	0.7%
I_z	68.9%	-0.2%
I_x/I_y	-0.2%	0.0%
I_x/I_z	6.5%	0.9%
I_y/I_z	6.7%	0.9%

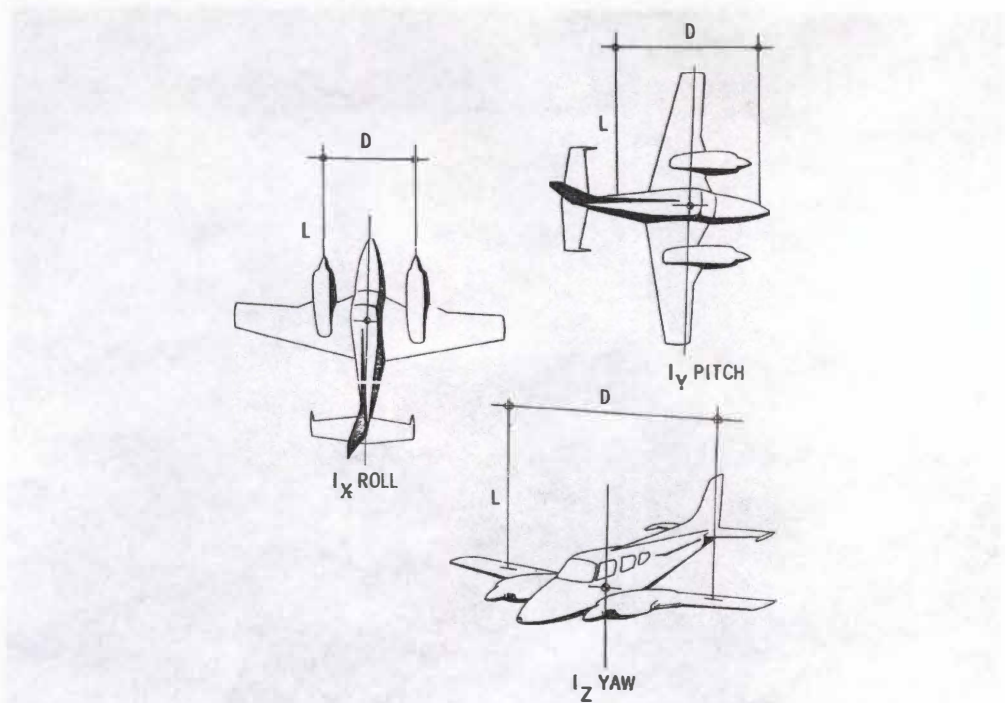


Figure D-1. Torsional Bifilar Swinging Method to Determine Inertial Properties [8].

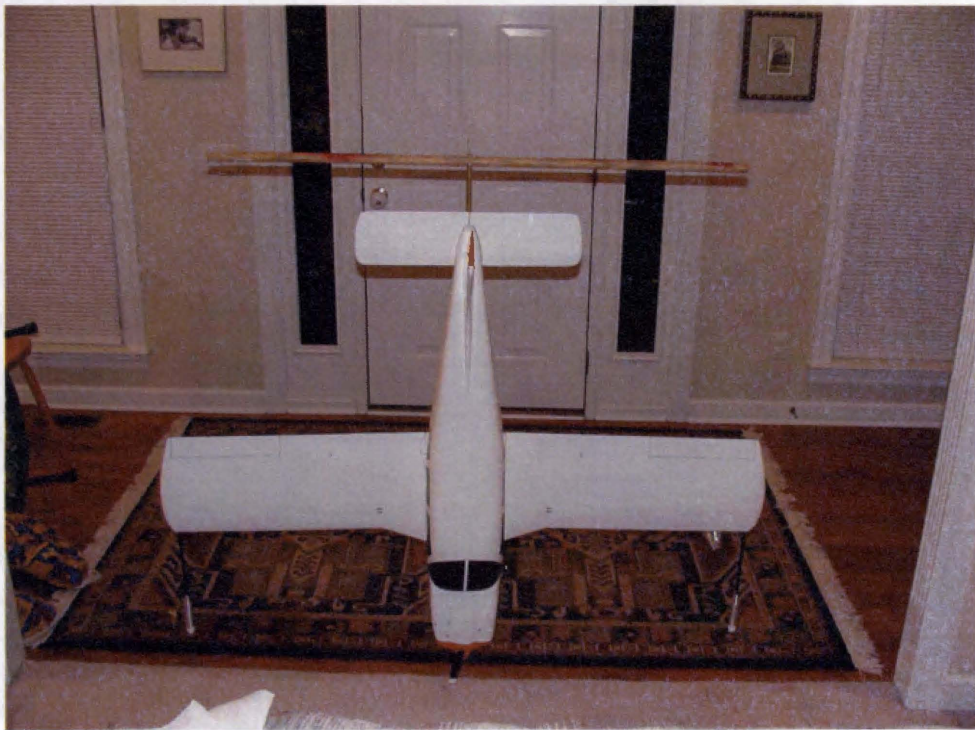


Figure D-2. Moment of Inertia about the X Axis.

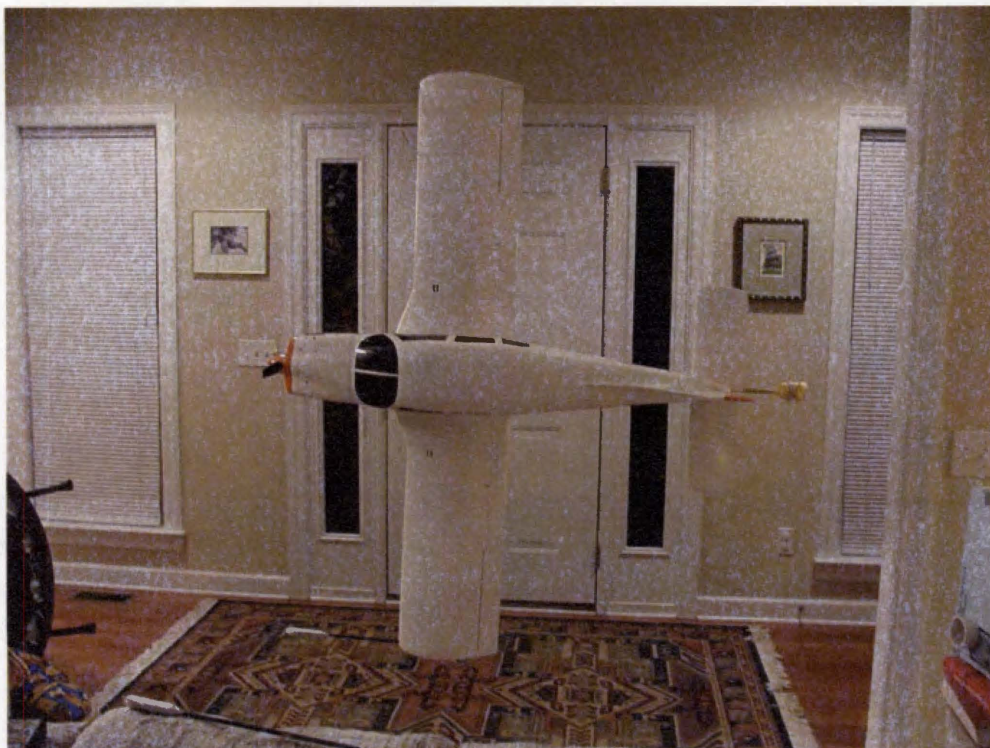


Figure D-3. Moment of Inertia about the Y Axis.

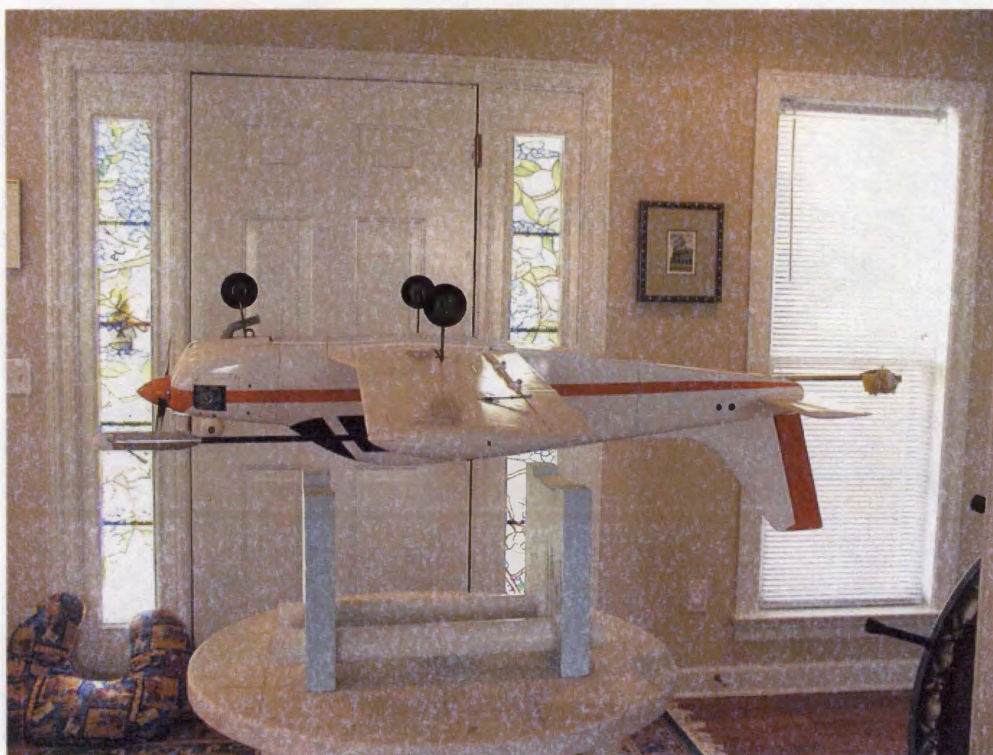


Figure D-4. Moment of Inertia about the Z Axis.

APPENDIX E: Flight Test Plan

Test Plan

The Effects of Wing Inertia Variations on Spin Recovery Characteristics of Single-Engine General-Aviation Aircraft

- Objective:** To obtain flight test data for the above thesis project. A radio controlled model aircraft is to undergo several steady spin configurations, after which recovery is to be initiated and data collected.
- Method:** The model's spin recovery is to be characterized by the number of rotations required to cease the spin. First hand visual data and videotaping each spin event using a ground-based camera should facilitate the determination of the number of recovery rotations required. An on-board flight data recorder will capture positions of the flight controls, angle of sideslip, angle of attack, and rotation rates about each axis with respect to time. This data will supplement the visual data by characterizing the spin dynamics. Flight tests are to be carried out at various inertia states at constant gross weight, various CG positions, and in both spin directions. A build-up technique will be used with the aircraft loaded to forward CG with reduced moments of inertia followed by aft CG settings and increased moments of inertia. A build-up technique will also be followed for spin recovery where recovery will be initiated after half a rotation and build up to 1+ rotations, as required.
- Technique:**
1. The following preliminary tests shall be carried out prior to carrying out the spin testing:
 - a. High speed taxi tests to ensure taxi stability;
 - b. Flight at max speed to ensure no flutter or trim problems;
 - c. Flight at lightest weight for confirmation of flight control rigging;
 - d. Stall aircraft without inducing a spin to get a feel for the aircraft's stall speed (visually);
 - e. High speed taxi deployment and release of the spin parachute to ensure proper function; and
 - f. Deployment check of spin chute during a test spin

2. The first configuration is to set the CG at the maximum forward position (24.8% MAC) and at reduced rolling moments of inertia. After take-off, the aircraft will be trimmed for level flight at medium speed at approx 800 ft AGL. The aircraft is to be slowed in level flight by reducing throttle to idle. At the stall speed, pro-spin controls should be initiated and maintained (full up elevator and full rudder in the spin direction, ailerons neutral) until the model obtains a developed steady spin. (Note that Reynold's Number effects are minimal in the developed spin). It is expected that a developed spin will occur within one spin rotation. Spin recovery should be initiated in accordance with the "NACA Recovery" technique - full opposite rudder and neutral aileron, followed by applying full down elevator. If the aircraft is configured such that its moments of inertia $I_x > I_y$, then full down elevator should be applied at the same time as full opposite rudder. If a flat spin is expected, then consider initiating spin recovery sooner than one spin rotation.
3. The above procedures should be repeated in the other spin direction.
4. The model should be configured at the other CG positions and moments of inertia settings, and the above tests repeated.
5. If time permits, the above procedure should be repeated for the flaps down and ailerons against configurations, as required.

Data Requirements:

1. Take-off:
 - a. Date;
 - b. Wind speed and direction;
2. For each test configuration:
 - a. Test Configuration number;
 - b. Weight, CG position, I_x , I_y , and I_z values;
 - c. Visual rotations for recovery (first-hand);
 - d. Aileron position versus time;
 - e. Elevator position versus time;
 - f. Rudder position versus time;
 - g. Angle of attack versus time;
 - h. Sideslip angle versus time;
 - i. Yaw rate versus time;
 - j. Pitch rate versus time; and

k. Roll rate versus time.

Expected Spin
Recovery Behaviour:

1. Changing I_x , I_z : By increasing the moments of inertia I_x and I_z , it is expected that spin recovery will be adversely affected with longer recovery and more rotations. A flatter spin is anticipated as these moments of inertia are increased.
2. Moving CG aft: This may be unpredictable, but generally the spin recovery degrades as the CG is moved rearward (adverse effect). Recovery may be quicker, but the spin may be flatter.
3. Power on recoveries (if applicable): No predictions can be made as it can have a favourable or adverse effect on spin recovery. Although, power increase would most likely increase spin rate.
4. Flap down recoveries (if applicable): No predictions can be made as inertia are changed.

Emergency
Procedures:

1. Engine failure – land immediately deploying flaps once the landing area has been made.
2. Spin recovery controls ineffective:
 - a. High rates – select high rate controls if time permits;
 - b. Max power – attempt to use prop blast on the tail surfaces to aid recovery, if time permits;
 - c. Spin chute deployment and release – deploy the spin chute above 300 feet AGL, and release it as soon as the aircraft recovers.
3. Parachute hang-up that prevents controlled flight – shut off engine and hope for the best.

Personnel Required:

1. Pilot
2. Flight assistant
3. Video duty

Flight Assistant's
Responsibilities:

1. Initiate high rate control, as requested by pilot;
2. Activate spin chute deployment, as requested by pilot;
3. Activate spin chute release, as requested by pilot;

4. Time countdown call, as requested by pilot.
5. Count spin rotations.

Contact Info: Not included.

Checklists

Pre-Flight Checklist

1. 1st flight of day, range check RC system with FDR operating,
2. fuel aircraft
3. verify FDR works with PC, disconnect 9V battery
4. start aircraft and adjust engine
5. connect and stow 9V battery
6. go fly

Post-Flight Checklist

1. shut down engine and shut off RC system
2. hook-up PC and download data from FDR
3. disconnect 9V battery from FDR
4. record visual data on sheet
5. fast charge any batteries if required (video, RC system)

Spin Checklist (assistant may call out these steps)

1. film spin card with video camera
2. adjust video focus on manual setting for flight recording
3. pilot switch on FDR system prior to spin entry
4. assistant call out to pilot the spin maneuver
5. pilot call out "spin now" when ready
6. pilot call out "recovery now"
7. assistant count number of spins for recovery
8. pilot switch off FDR system
9. end filming
10. repeat for next spin

Table E-1. Test Matrix

Sortie #	Spin #	CG Position	Moment of Inertia State	Direction (left, right)	Flaps (up, down)	Spin Turns	Turns for recovery	Recovery Chute Required?	Qualitative comments	Control Positions (Stone Spin Shorthand)	Date
1	A1U	Max fwd	reduced	left	up						
	A2U	Max fwd	reduced	right	up						
	A3D	Max fwd	reduced	left	down						
	A4D	Max fwd	reduced	right	down						
2	B1U	Max fwd	stock	left	up						
	B2U	Max fwd	stock	right	up						
	B3D	Max fwd	stock	left	down						
	B4D	Max fwd	stock	right	down						
3	C1U	Max fwd	increased	left	up						
	C2U	Max fwd	increased	right	up						
	C3D	Max fwd	increased	left	down						
	C4D	Max fwd	increased	right	down						
4	D1U	Mid	reduced	left	up						
	D2U	Mid	reduced	right	up						
	D3D	Mid	reduced	left	down						
	D4D	Mid	reduced	right	down						
5	E1U	Mid	stock	left	up						
	E2U	Mid	stock	right	up						
	E3D	Mid	stock	left	down						
	E4D	Mid	stock	right	down						
6	F1U	Mid	increased	left	up						
	F2U	Mid	increased	right	up						

Table E-1. Continued.

Sortie #	Spin #	CG Position	Moment of Inertia State	Direction (left, right)	Flaps (up, down)	Spin Turns	Turns for recovery	Recovery Chute Required?	Qualitative comments	Control Positions (Stone Spin Shorthand)	Date
	F3D	Mid	increased	left	down						
	F4D	Mid	increased	right	down						
7	G1U	Max aft	reduced	left	up						
	G2U	Max aft	reduced	right	up						
	G3D	Max aft	reduced	left	down	Not carried out					
	G4D	Max aft	reduced	right	down	Not carried out					
8	H1U	Max aft	stock	left	up						
	H2U	Max aft	Stock	right	up						
	H3D	Max aft	stock	left	down						
	H4D	Max aft	stock	right	down						
9	J1U	Max aft	increased	left	up						
	J2U	Max aft	increased	right	up						
	J3D	Max aft	increased	left	down	Not carried out					
	J4D	Max aft	increased	right	down	Not carried out					
	J5A	Max aft	increased	left	up			Ailerons against			
10	K1U	Max aft	reduced	left	up			Ailerons against			
	K2U	Max aft	reduced	right	up			Ailerons against			
11	Level	Max fwd	stock	na	up						
	B1UA	Max fwd	stock	right	up			Ailerons against			
	B2UA	Max fwd	stock	left	up			Ailerons against			
12	C1U	Max fwd	increased	left	up			High up, redo	Not carried out.		
	C3D	Max fwd	increased	left	down						

Table E-1. Continued.

Sortie #	Spin #	CG Position	Moment of Inertia State	Direction (left, right)	Flaps (up, down)	Spin Turns	Turns for recovery	Recovery Chute Required?	Qualitative comments	Control Positions (Stone Spin Shorthand)	Date
	C4D	Max fwd	increased	right	down			High up, redo			
	C2UA	Max fwd	increased	right	up			Ailerons against			
	C1UA	Max fwd	increased	left	up			Ailerons against			
13	G1U	Max aft	reduced	left	up				redo		
	G3D	Max aft	reduced	left	down						
	G4D	Max aft	reduced	right	down						
	G2UA	Max aft	reduced	right	up			Ailerons against			
	G1UA	Max aft	reduced	left	up			Ailerons against			
14	H1U	Max aft	stock	left	down			High up redo			
	H1UA	Max aft	stock	left	up			Ailerons against			
	H2UA	Max aft	Stock	right	up			Ailerons against			
	H3DA	Max aft	stock	left	down			Ailerons against			
	H4DA	Max aft	stock	right	down			Ailerons against			
15	J1U	Max aft	increased	left	up			High up, Redo			
	J1UA	Max aft	increased	left	up			Aileron against			
	J2UA	Max aft	increased	right	up			Aileron against			
	J3DA	Max aft	increased	right	down			Aileron against			

APPENDIX F: Flight Data

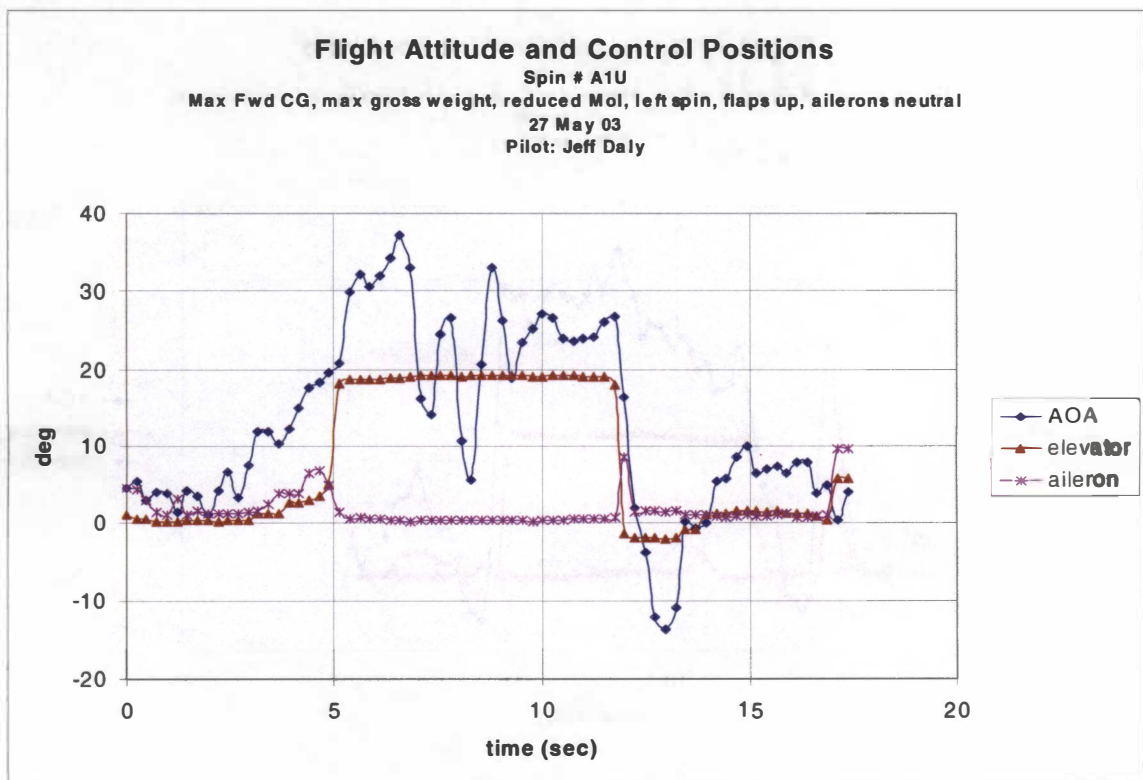
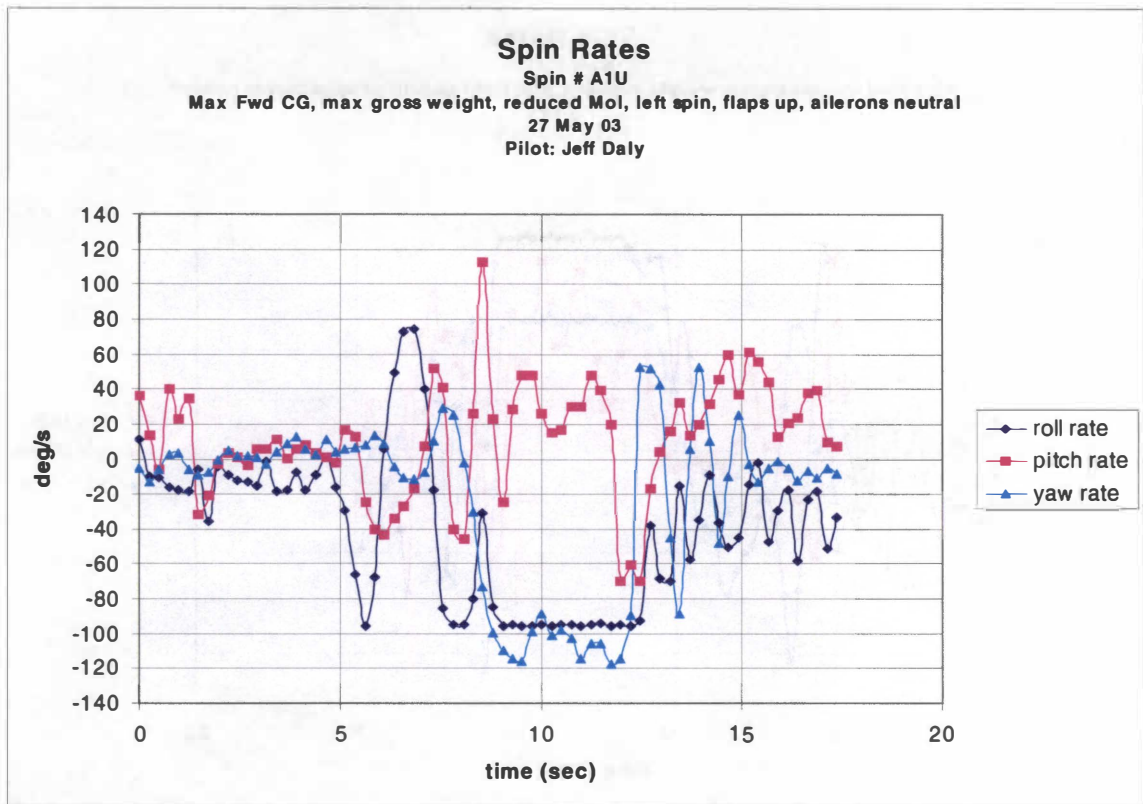


Figure F-1. Spin #A1U.

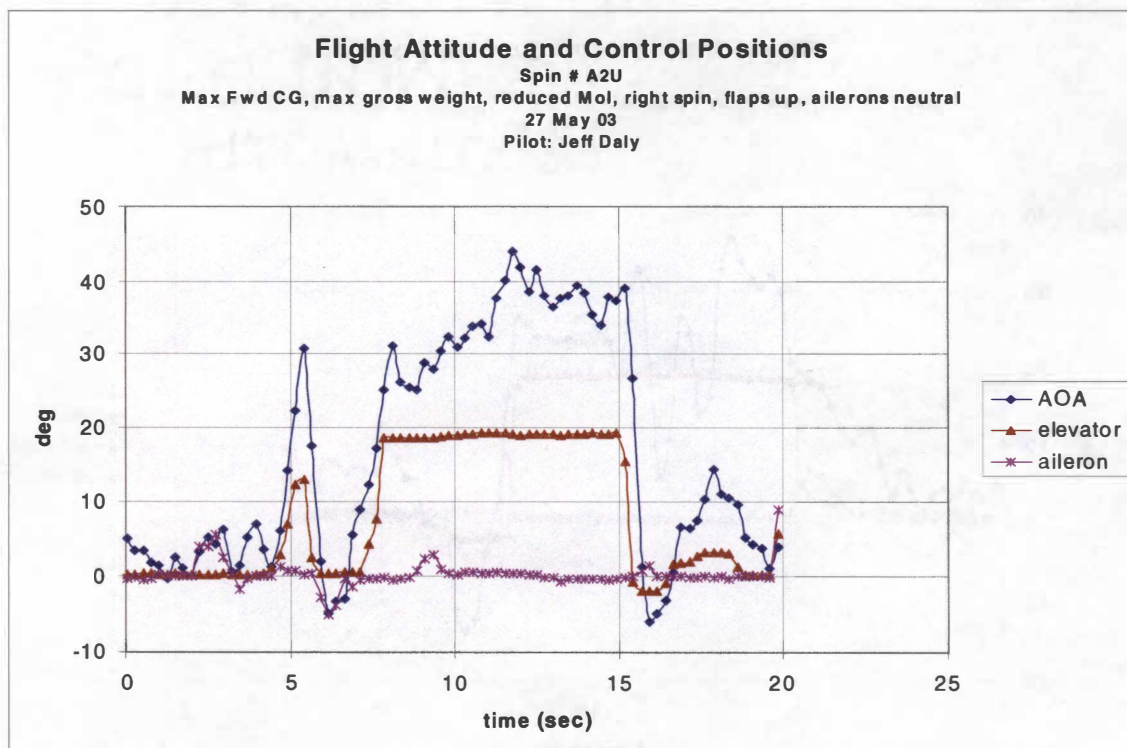
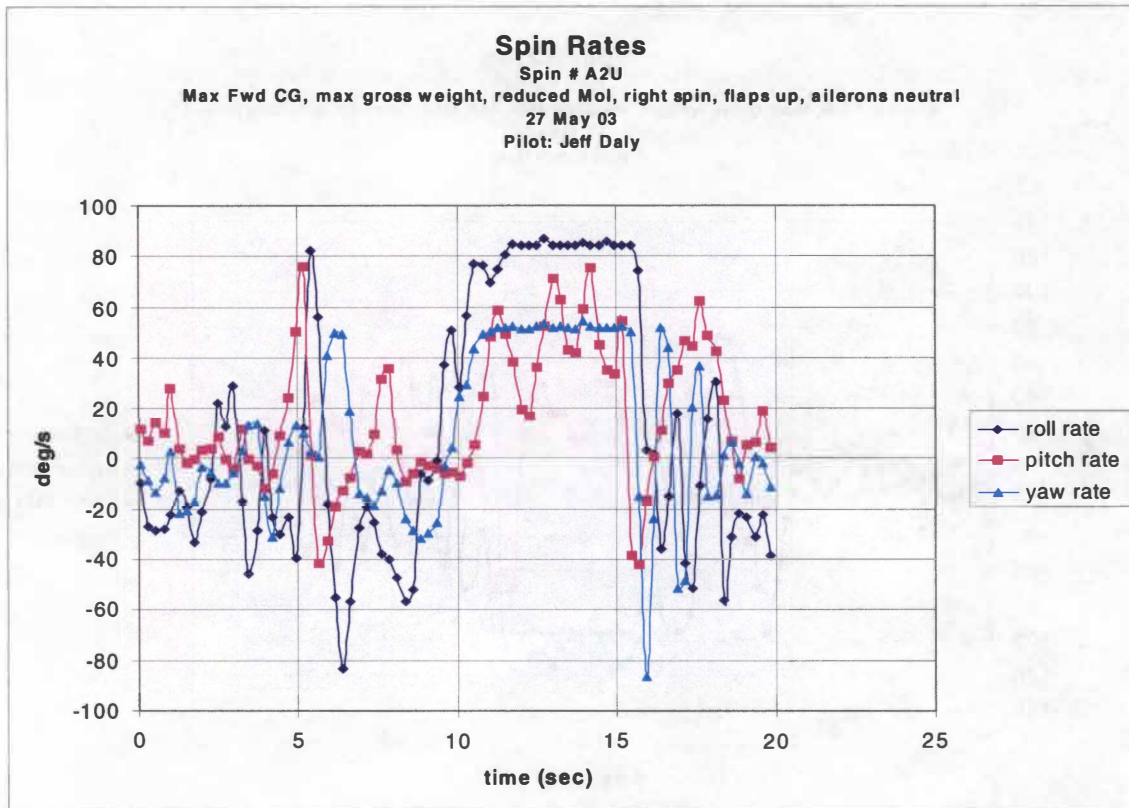


Figure F-2. Spin # A2U.

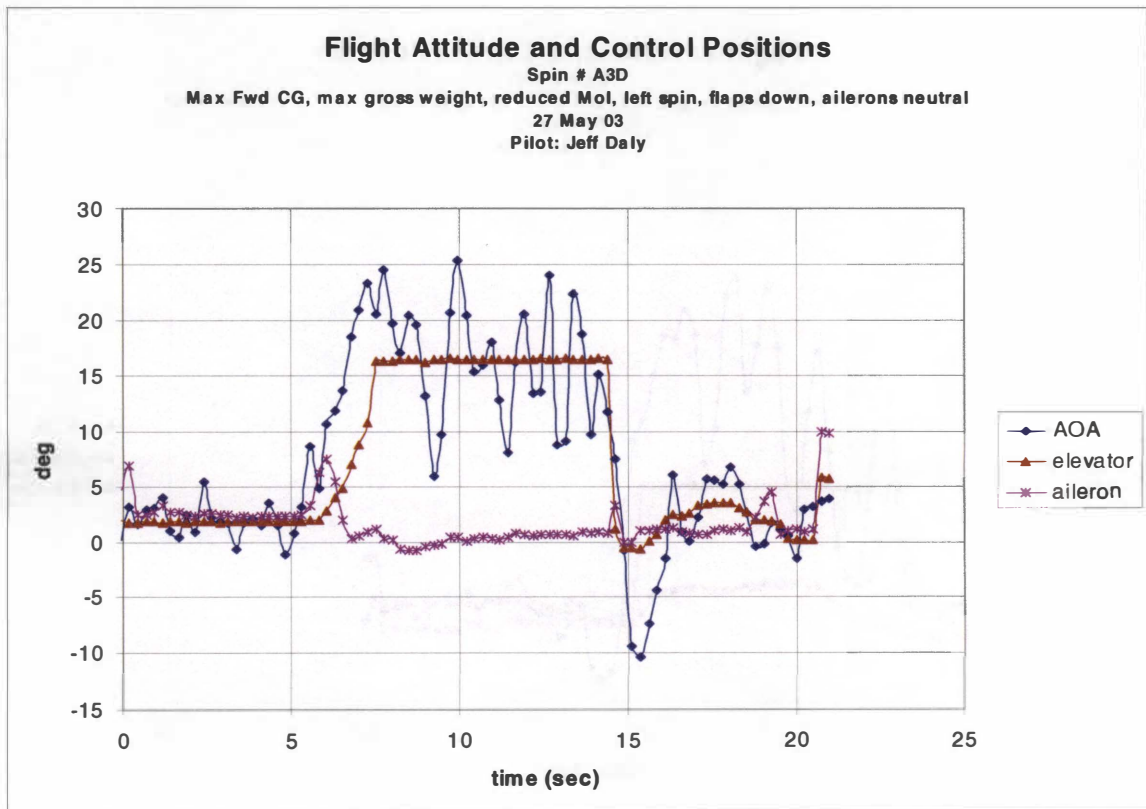
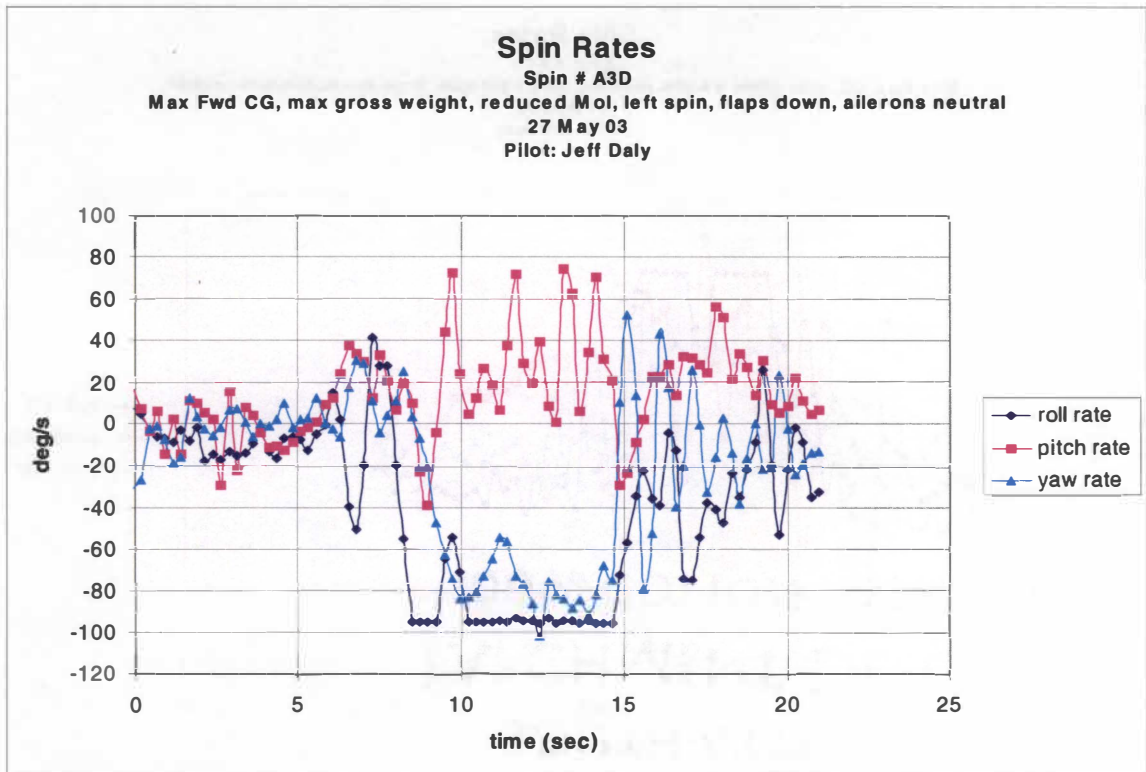


Figure F-3. Spin # A3D.

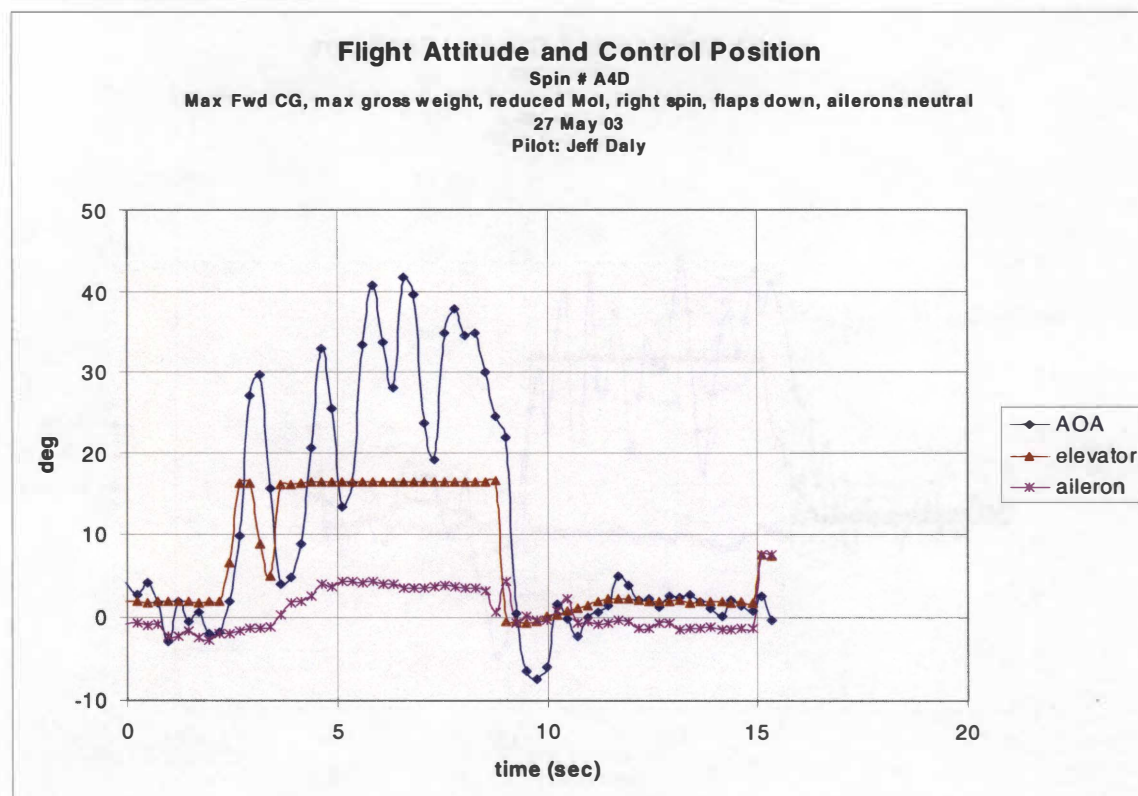
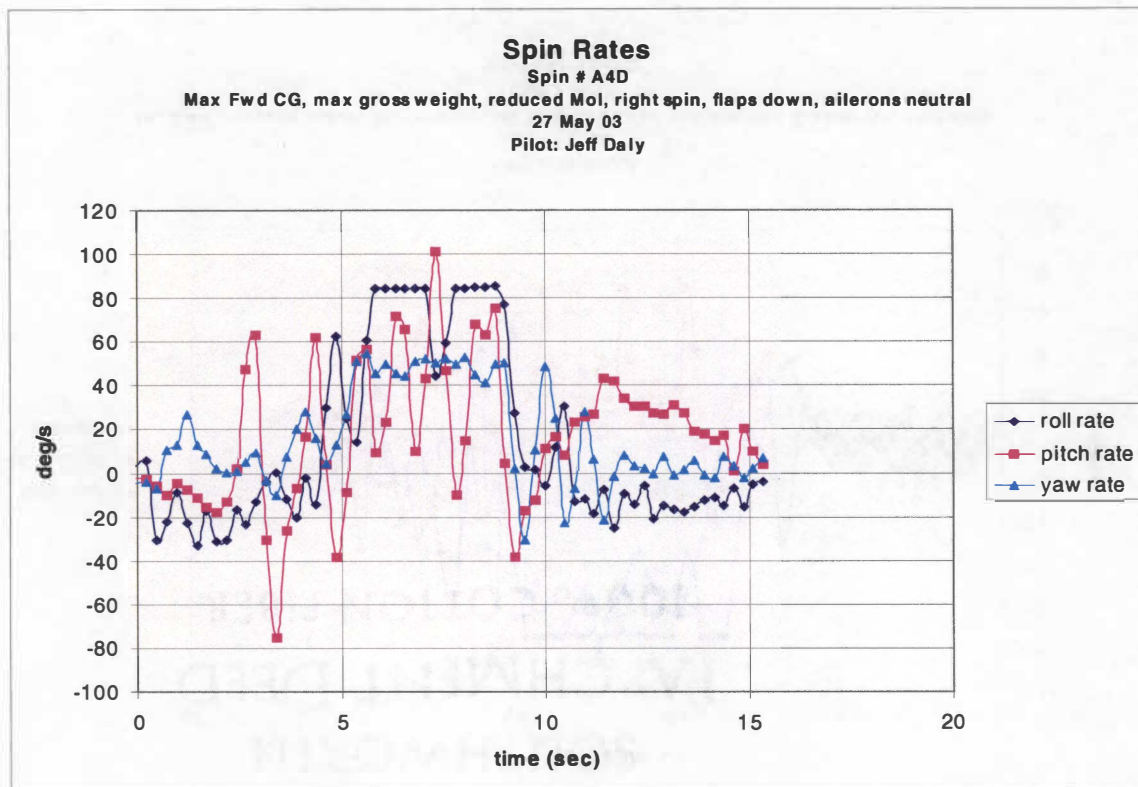


Figure F-4. Spin # A4D.

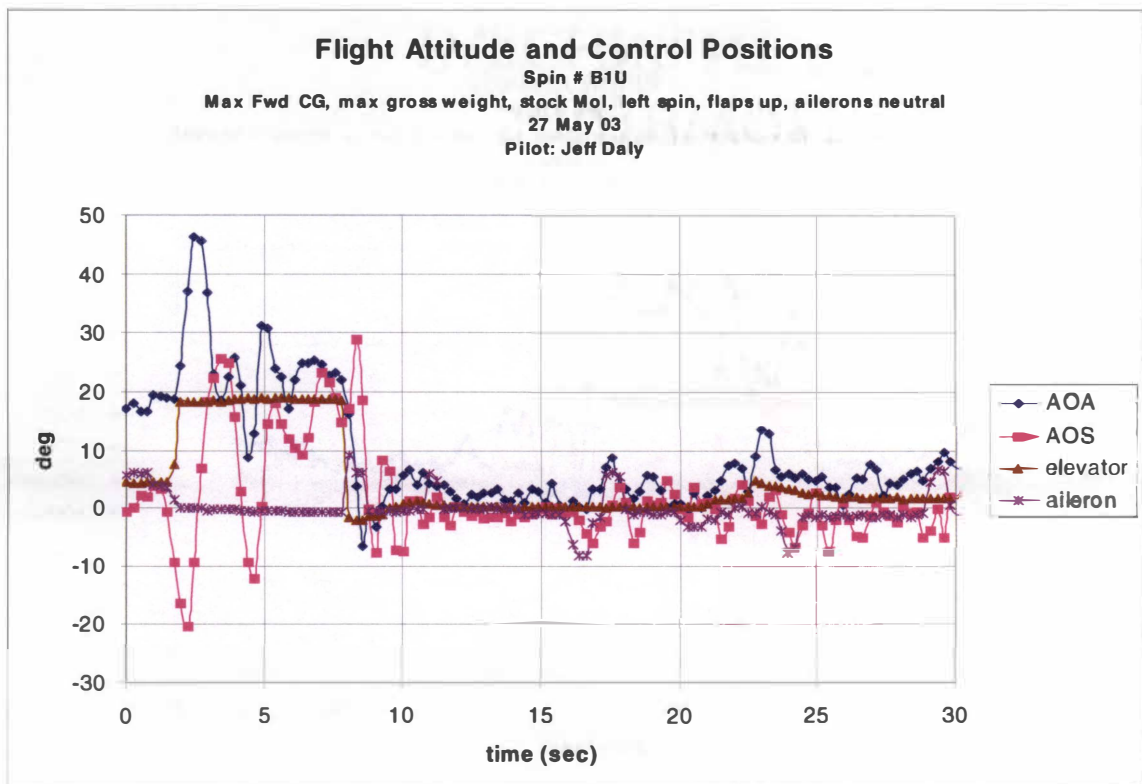
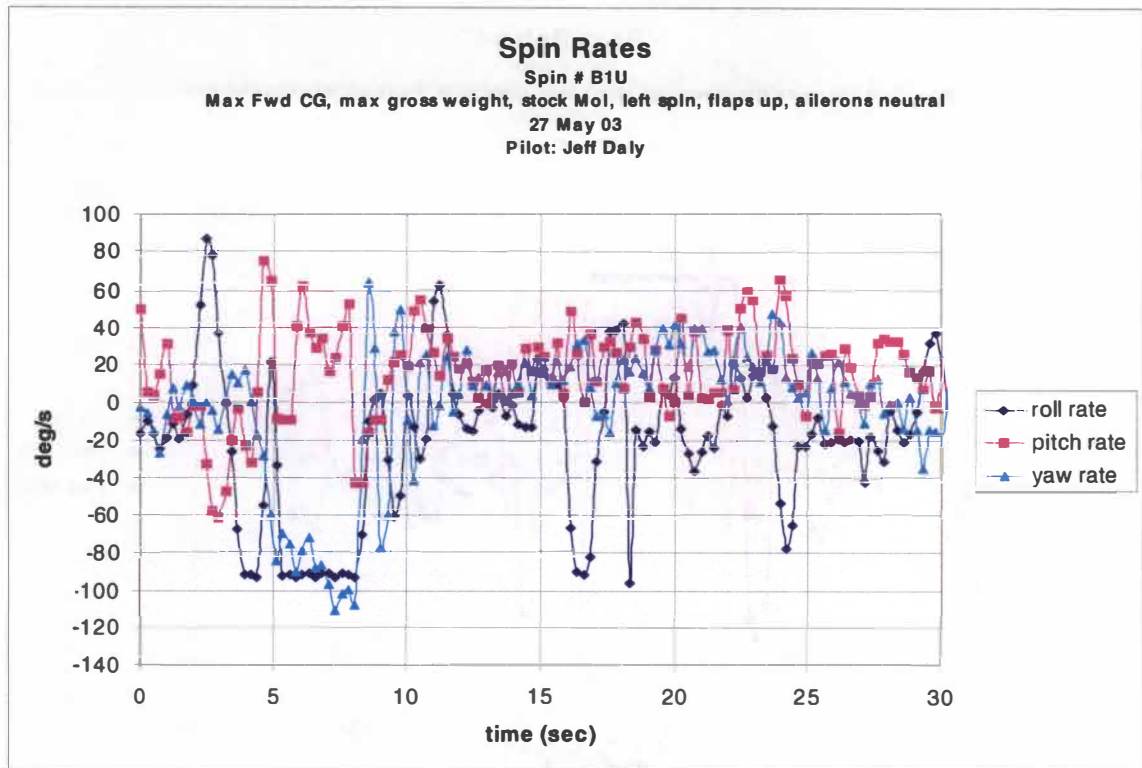


Figure F-5. Spin # B1U.

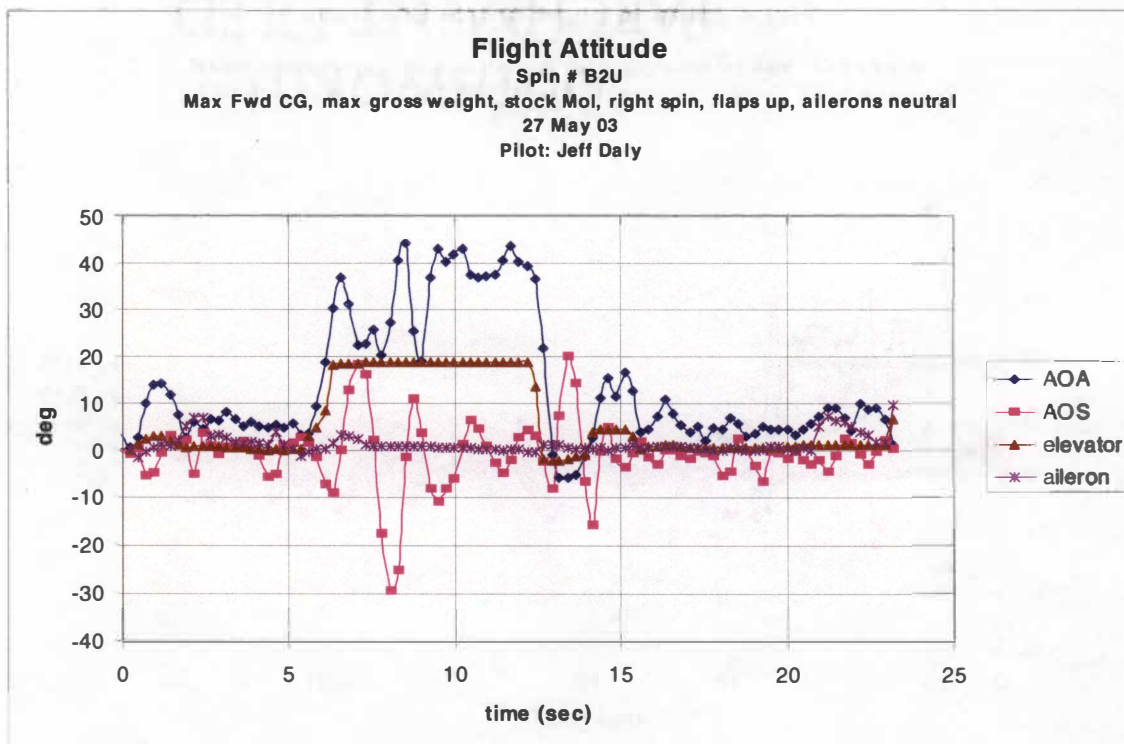
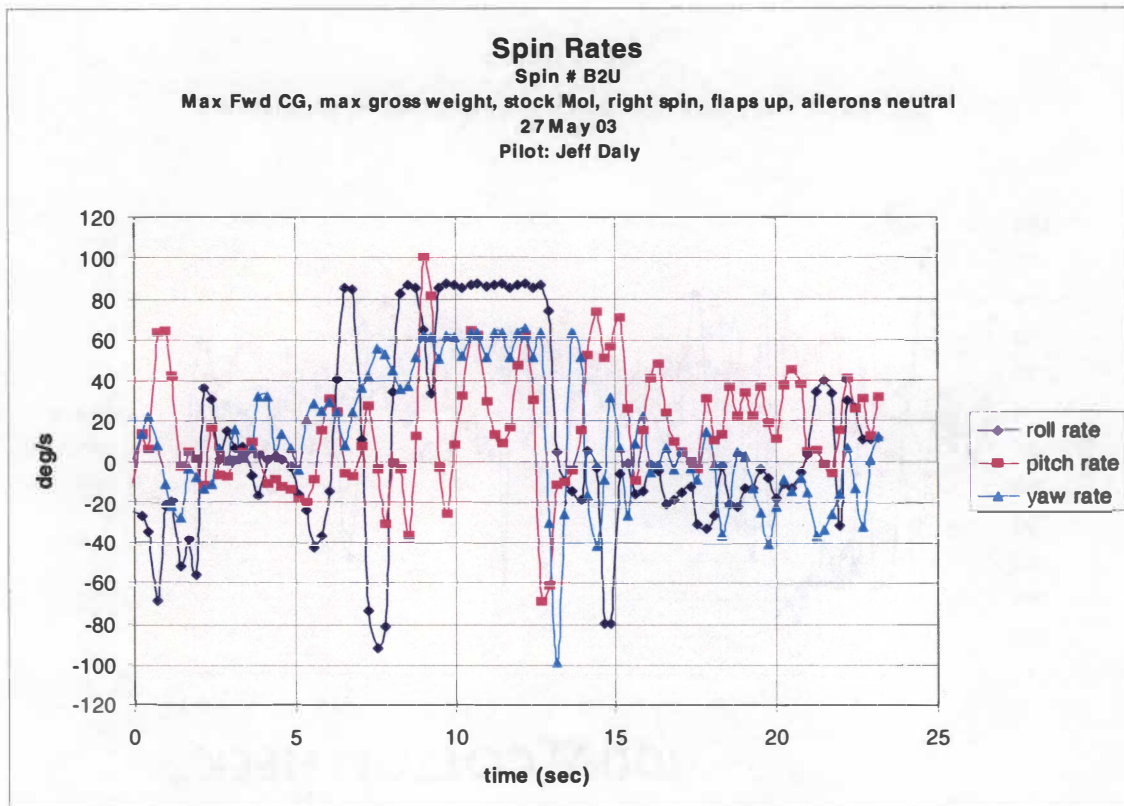


Figure F-6. Spin # B2U.

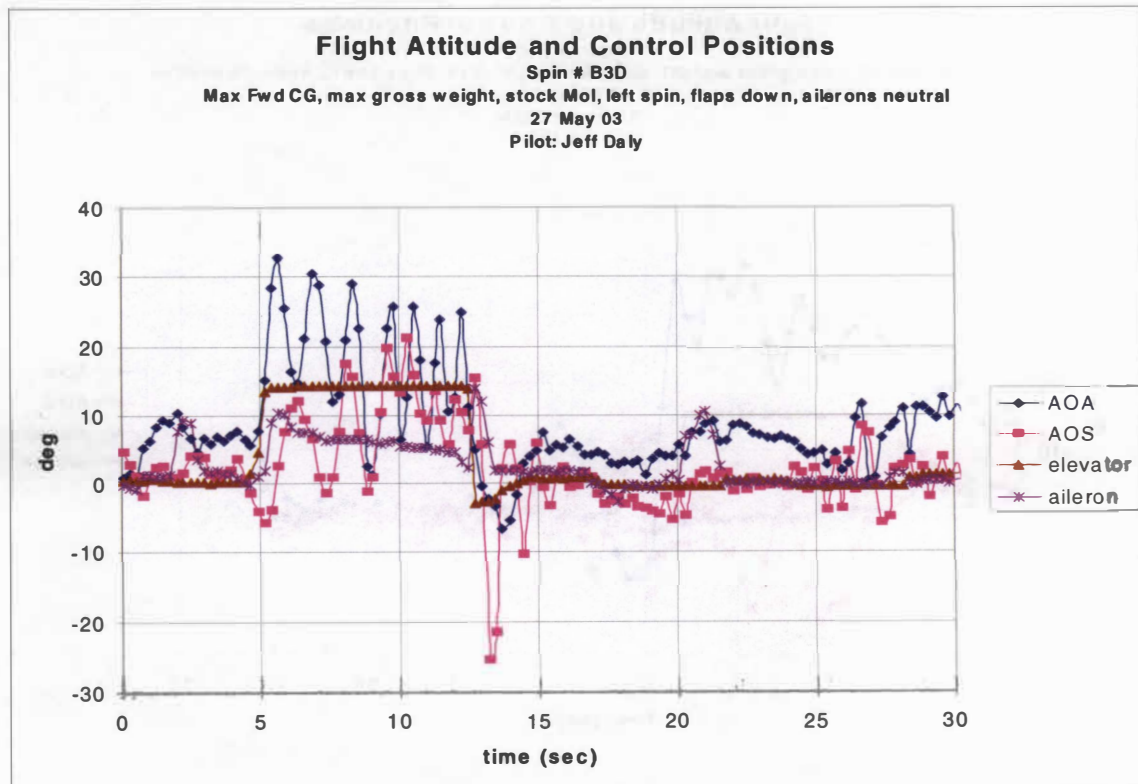
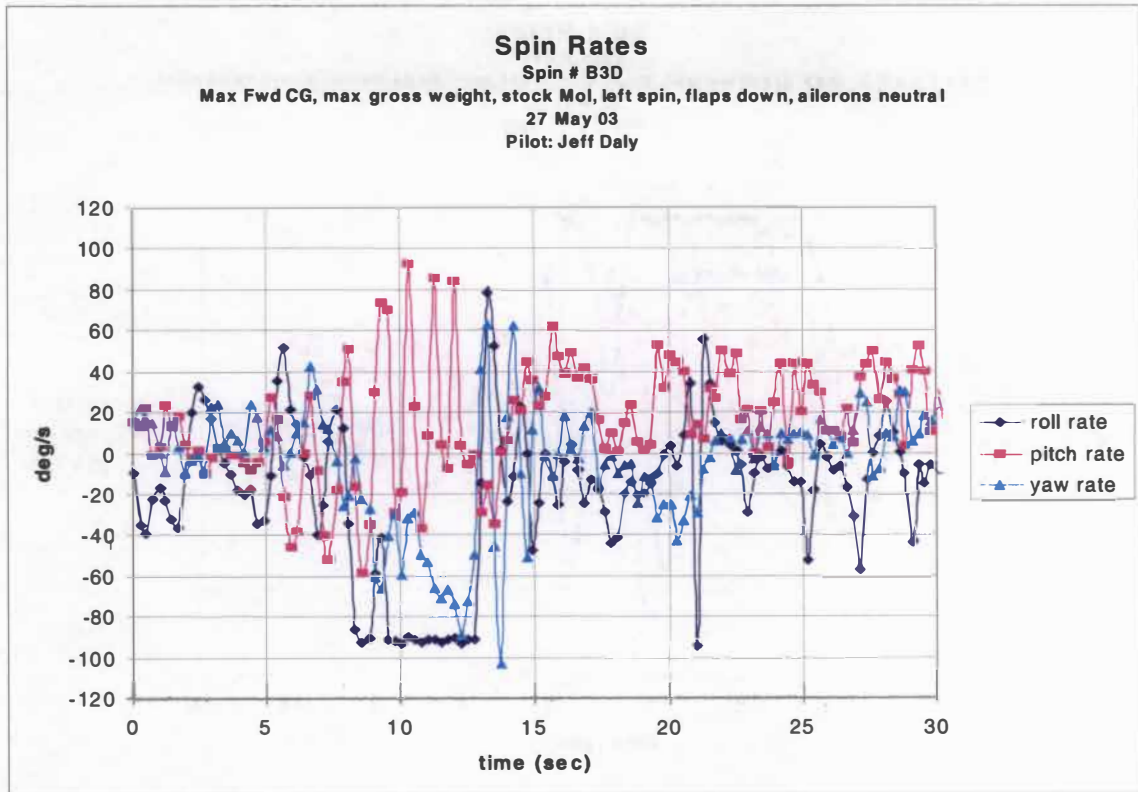


Figure F-7. Spin # B3D.

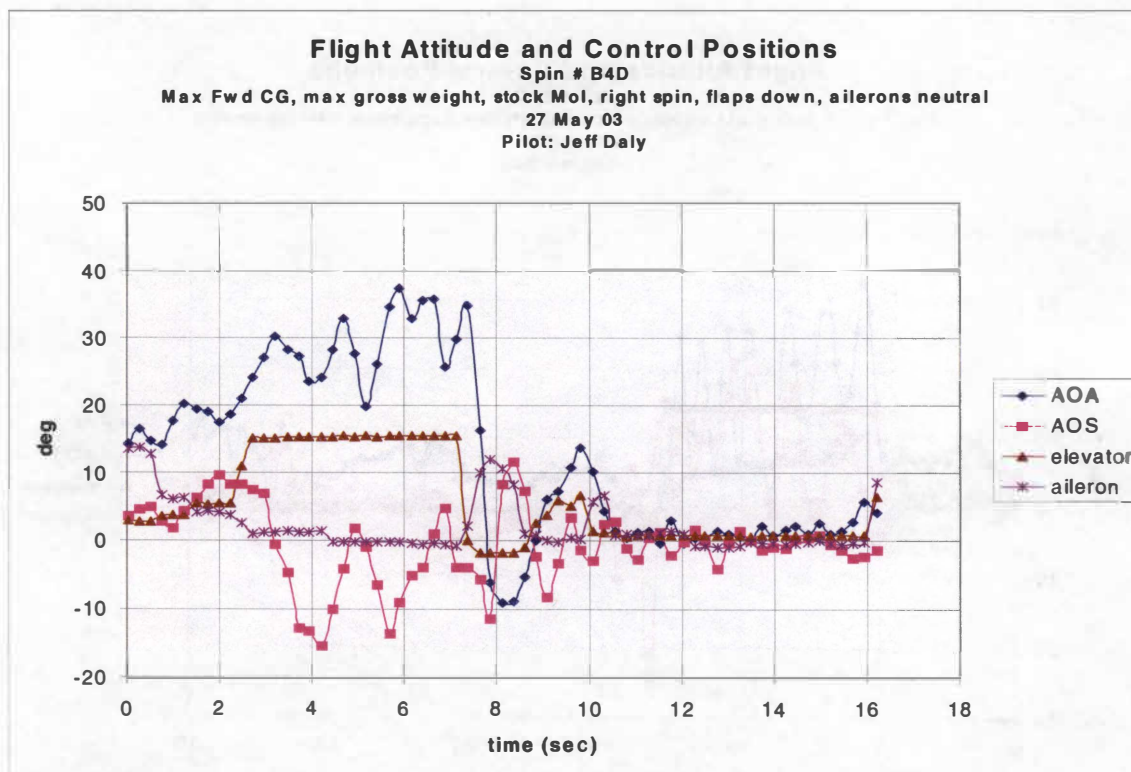
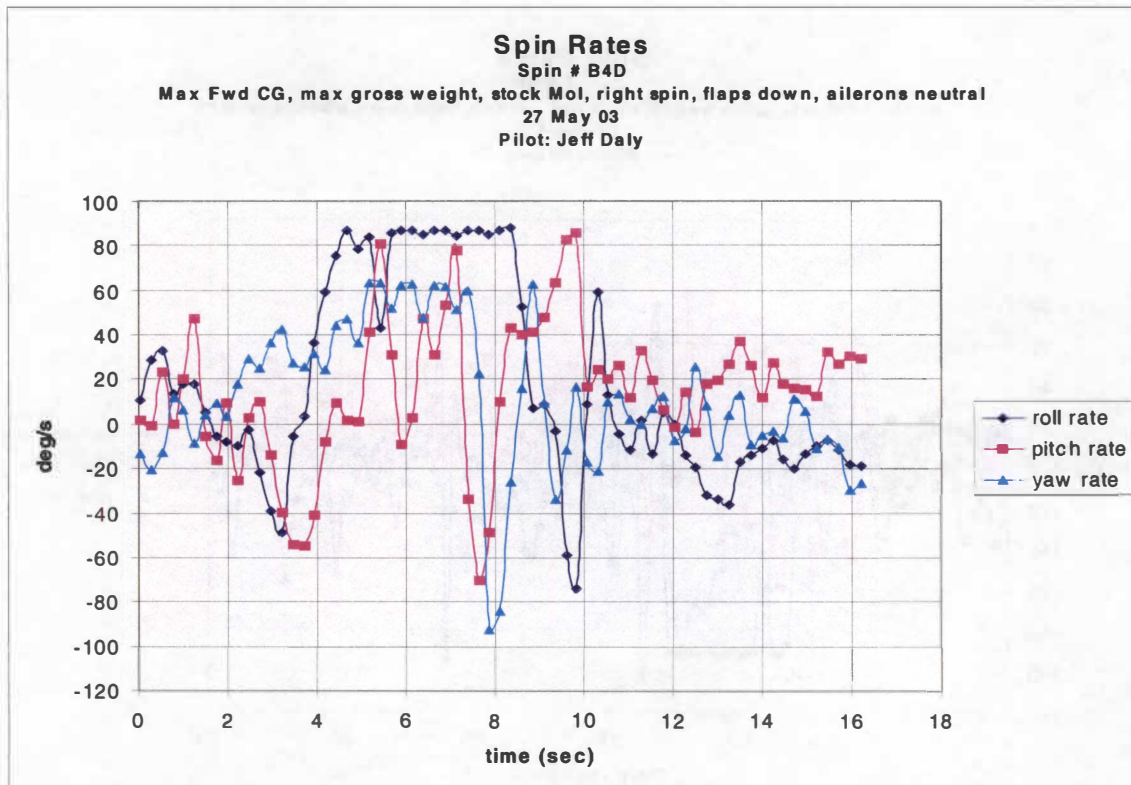


Figure F-8. Spin # B4D.

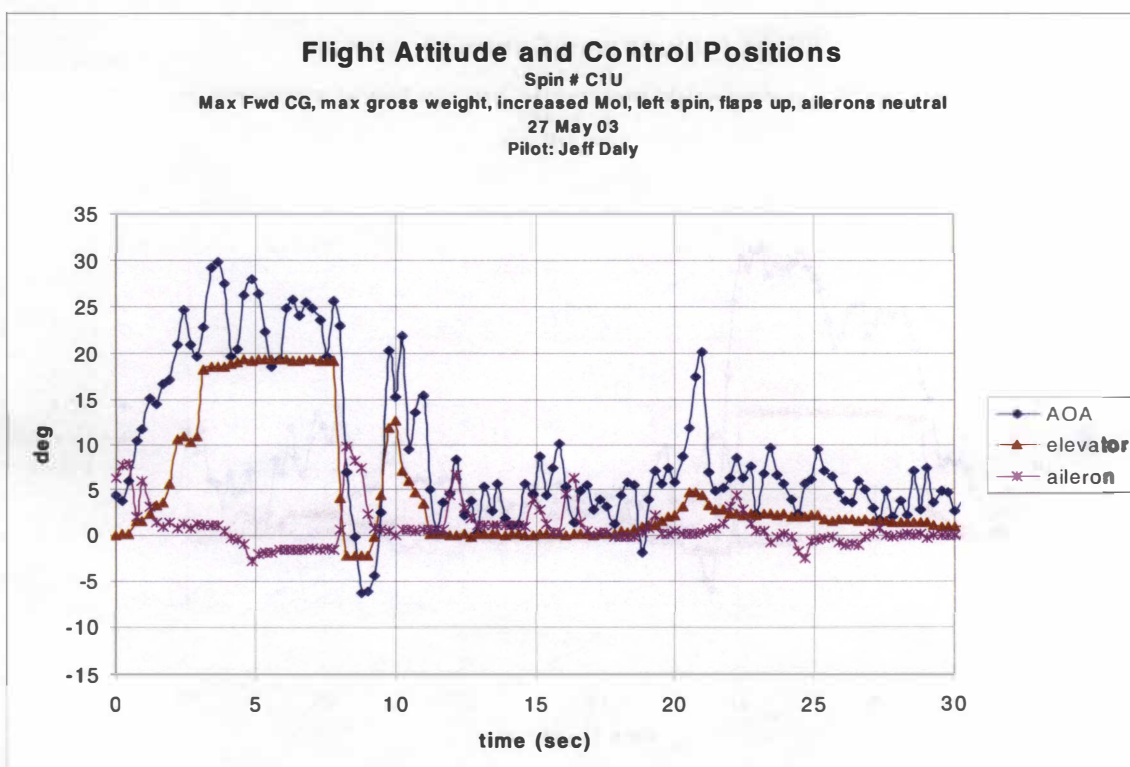
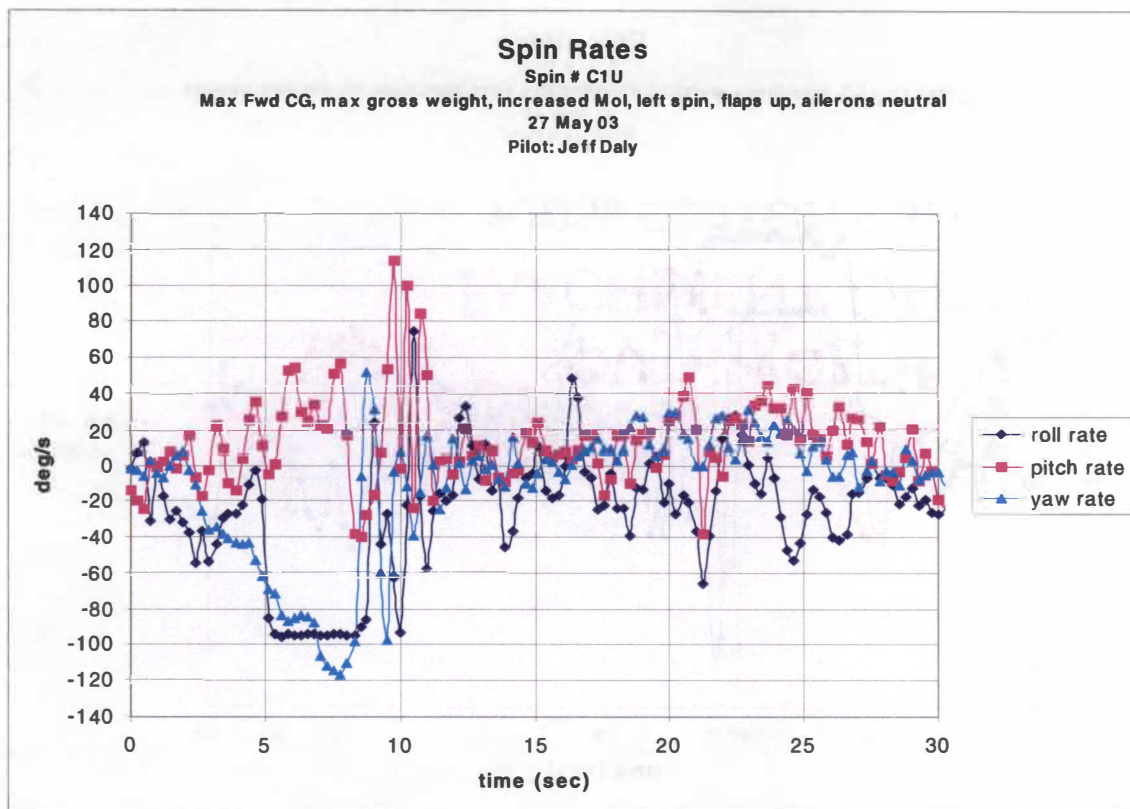


Figure F-9. Spin # C1U.

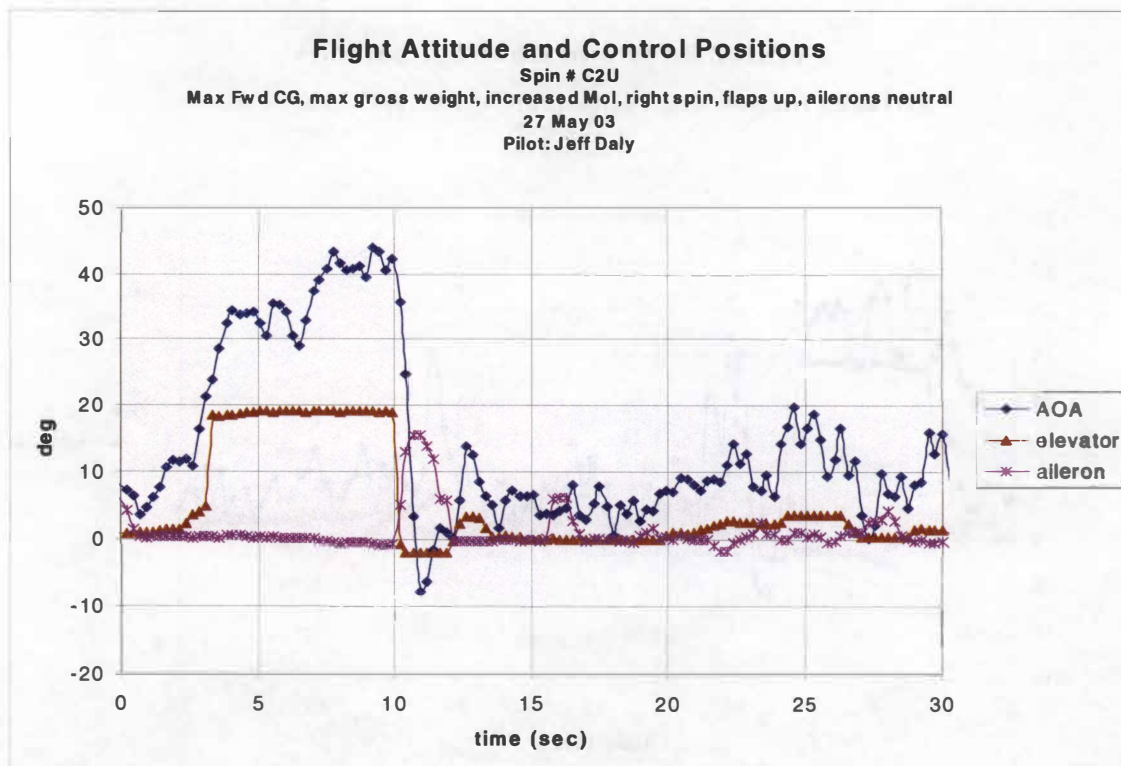
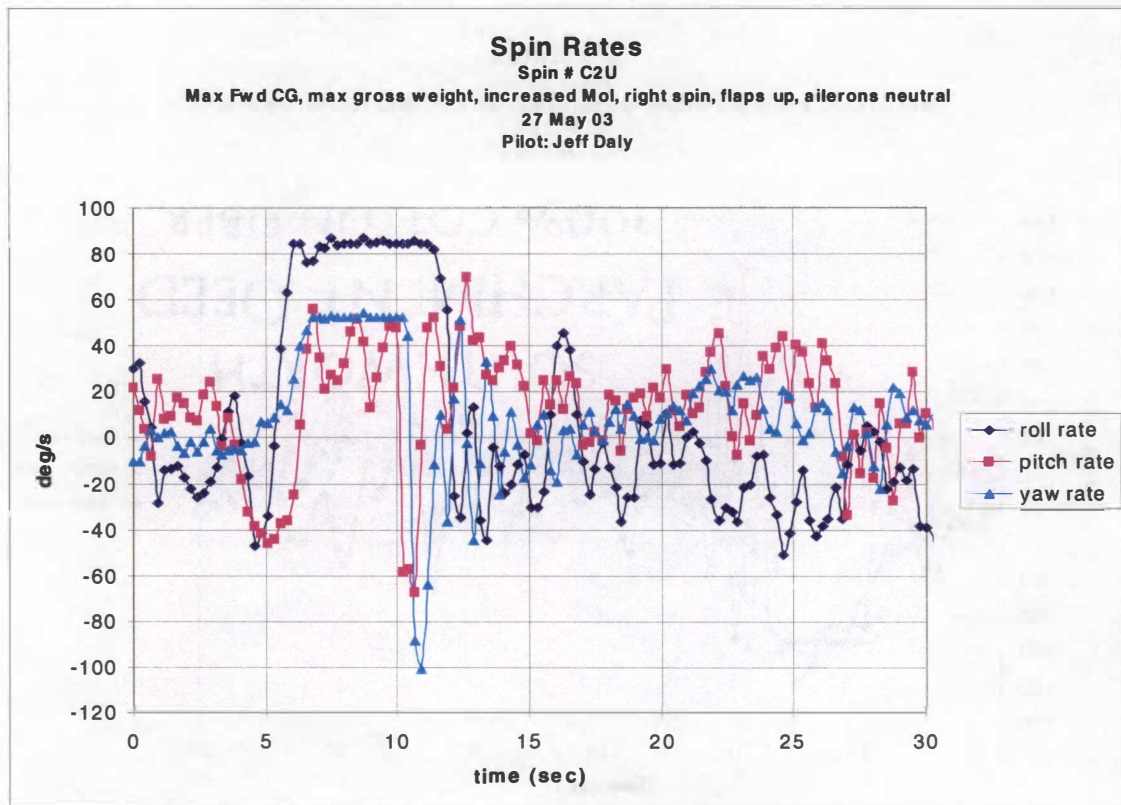


Figure F-10. Spin # C2U.

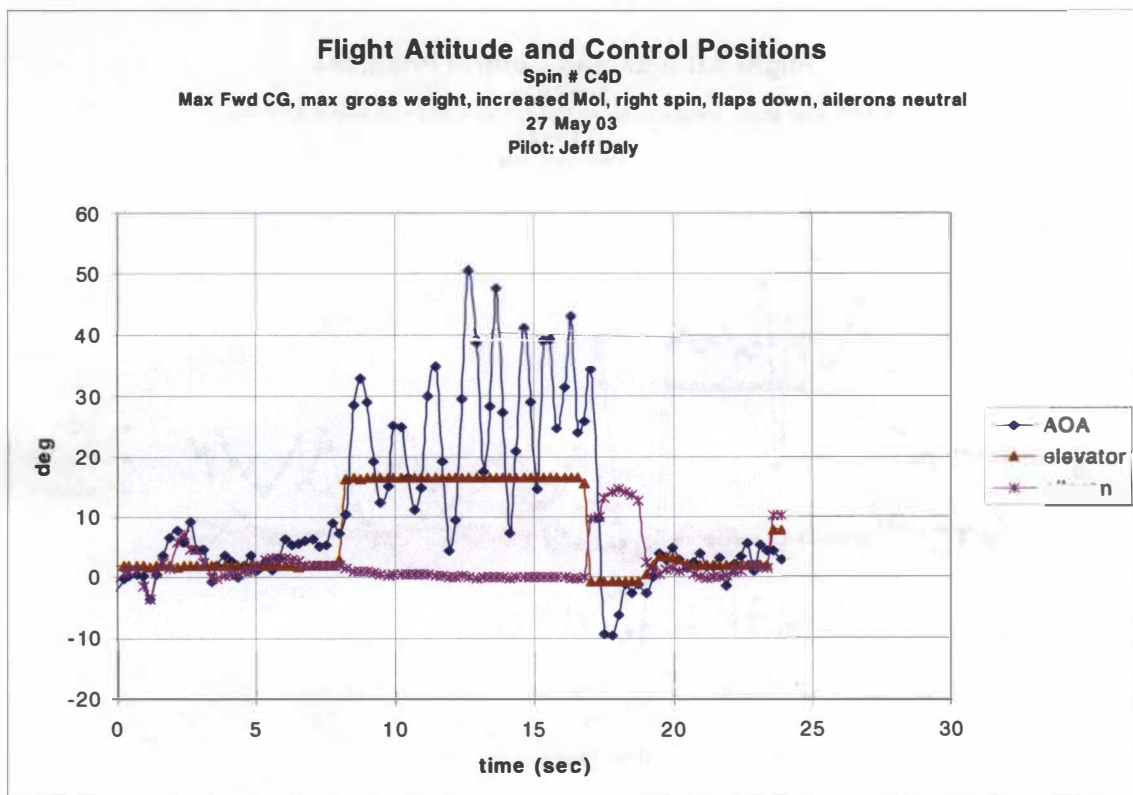
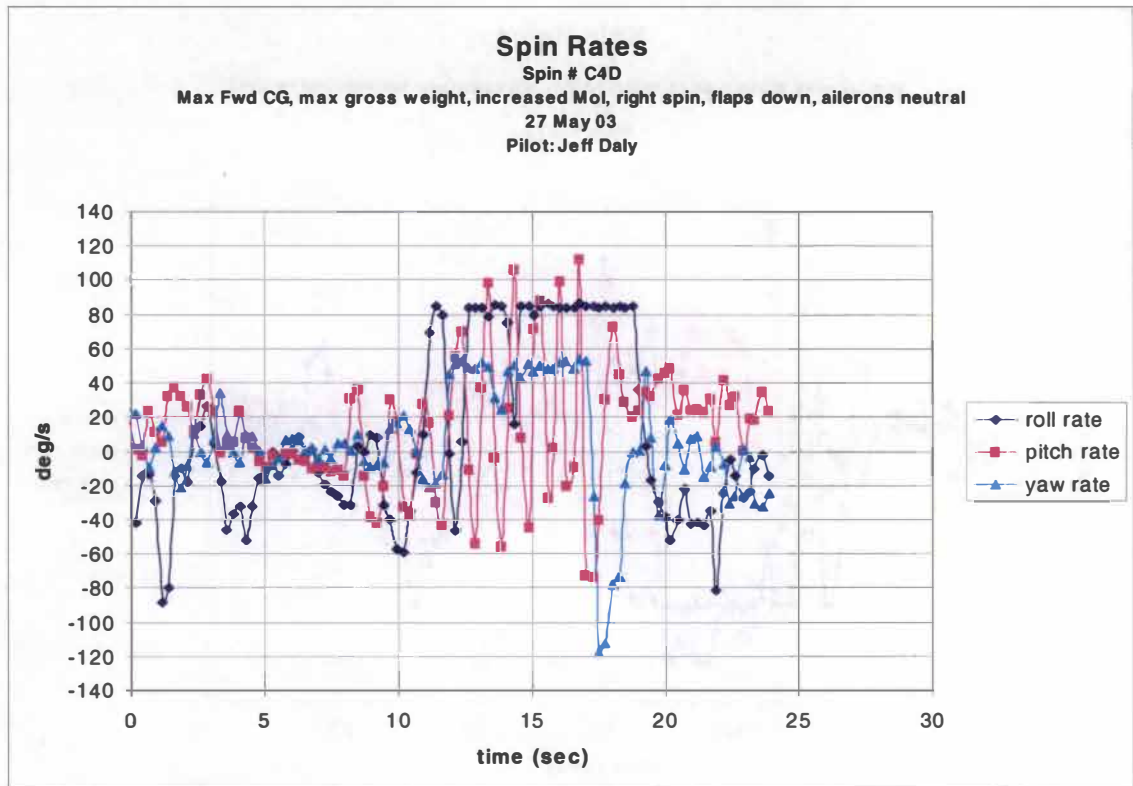


Figure F-11. Spin # C4D.

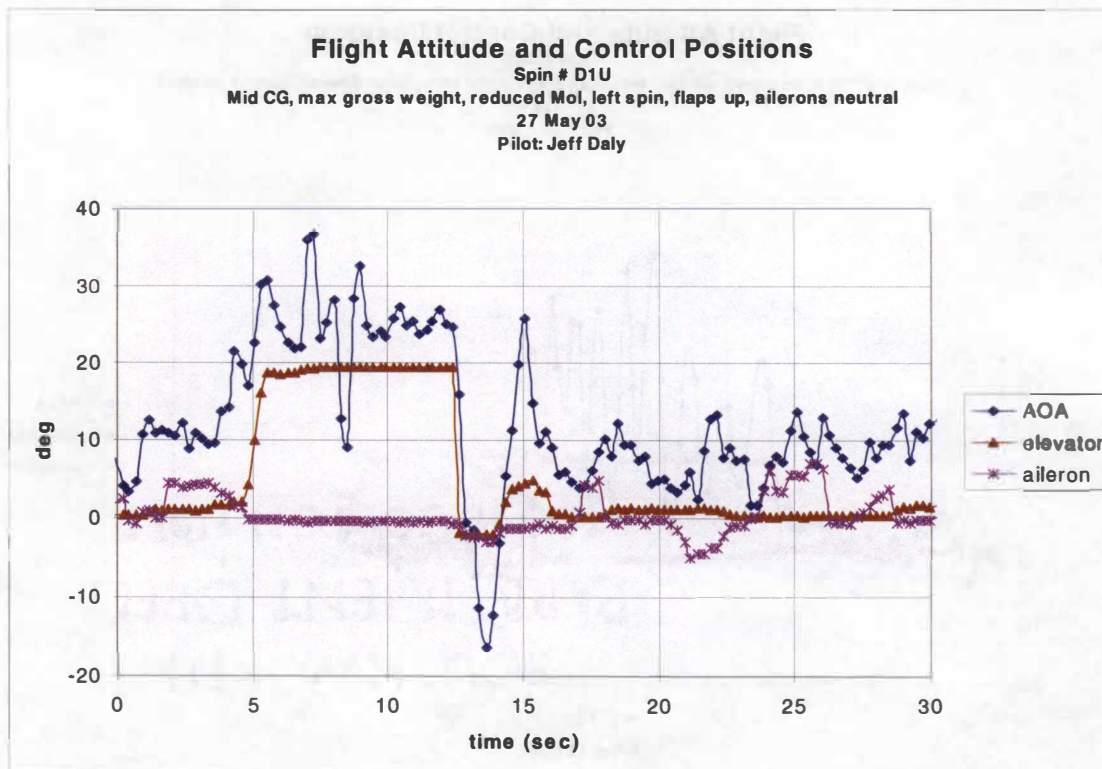
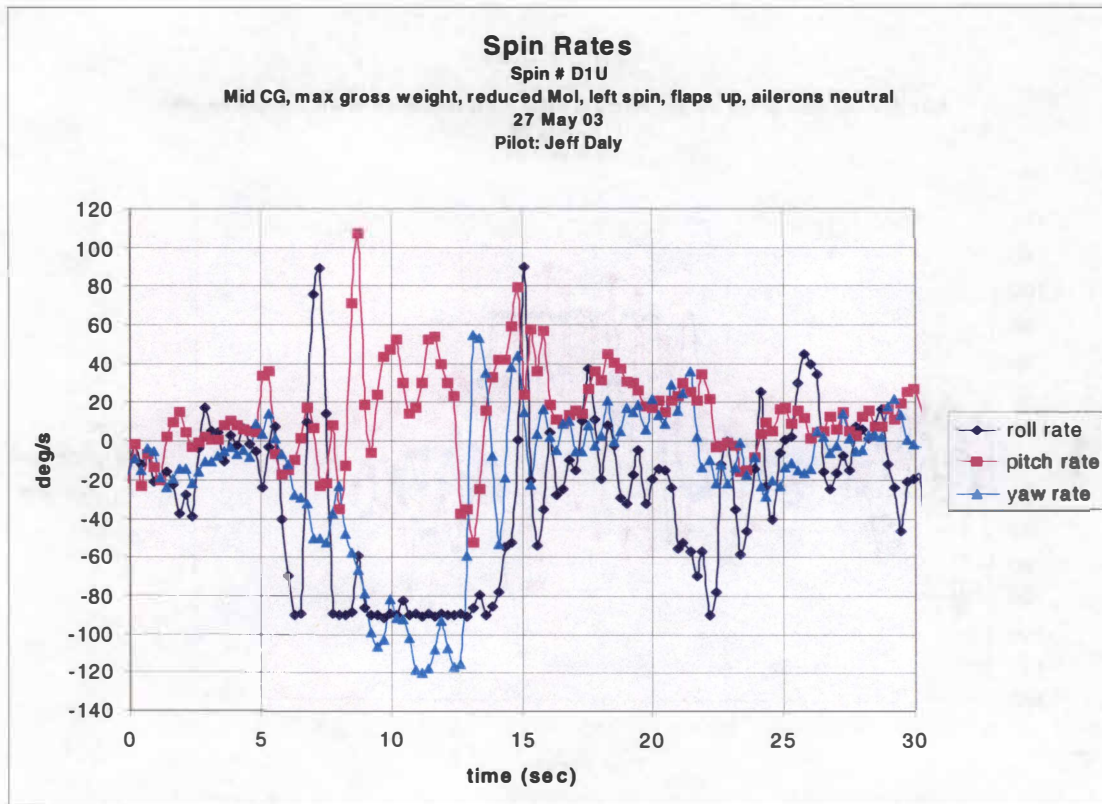


Figure F-12. Spin # D1U.

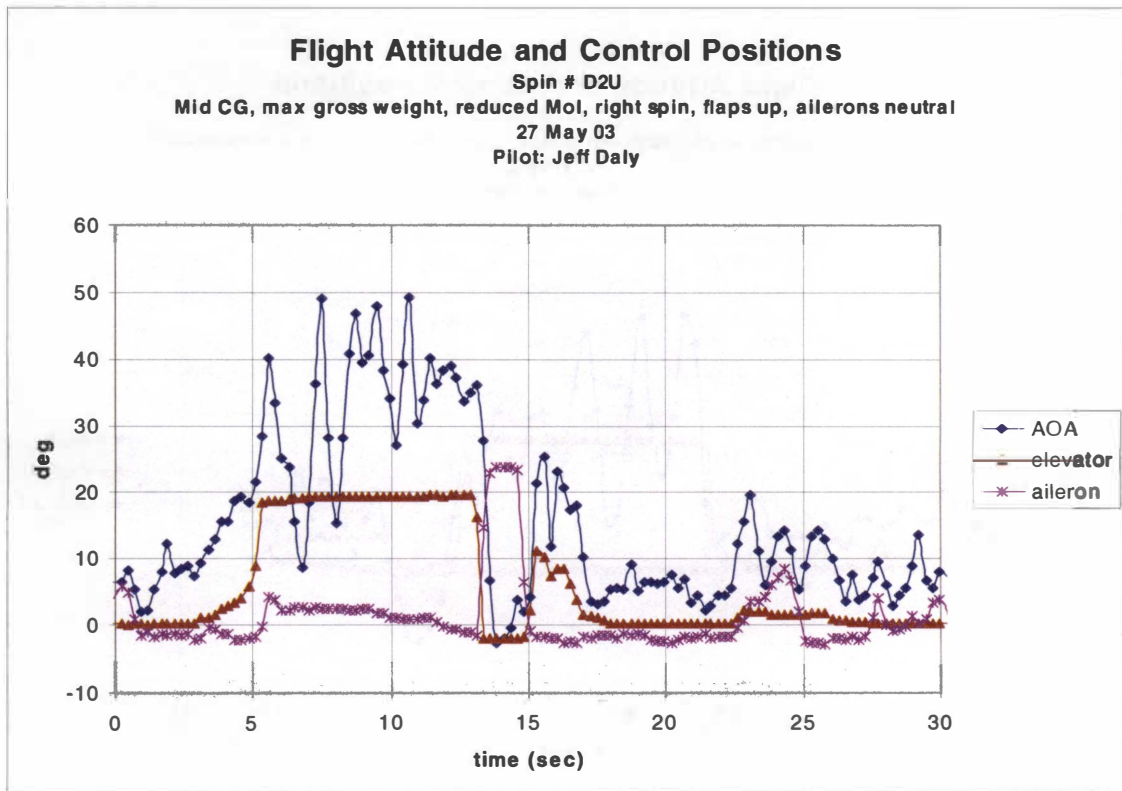
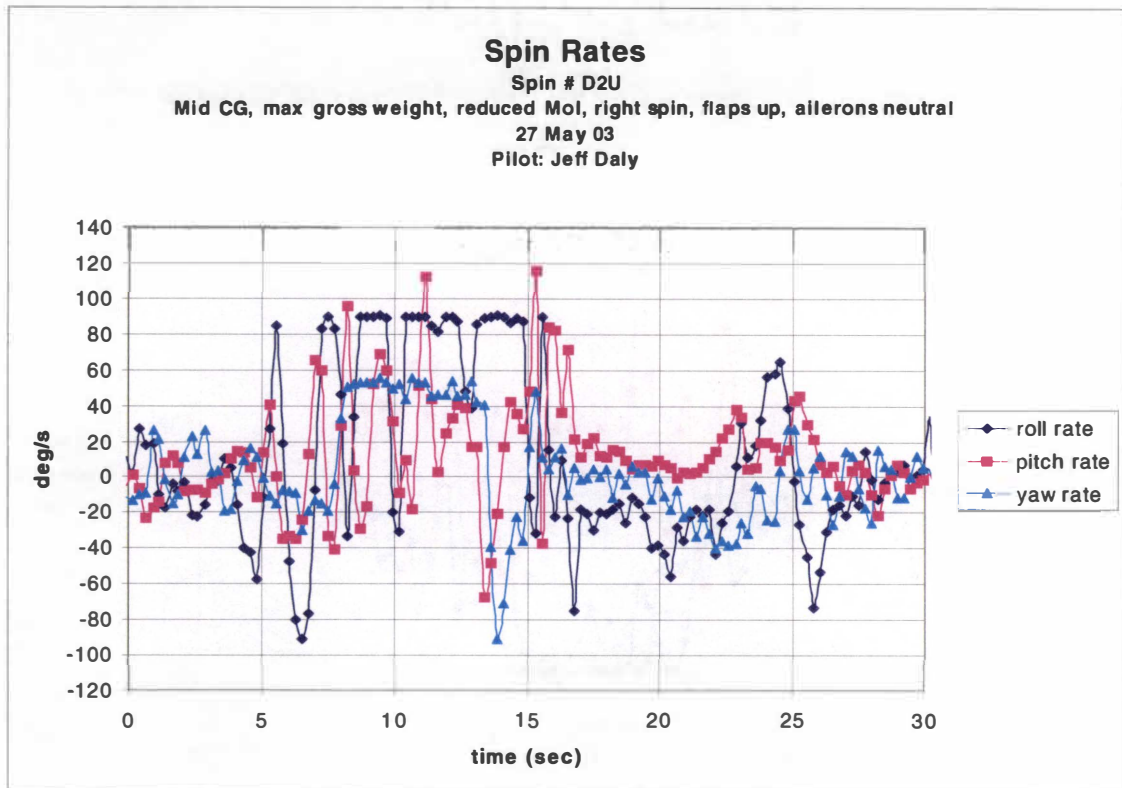


Figure F-13. Spin # D2U.

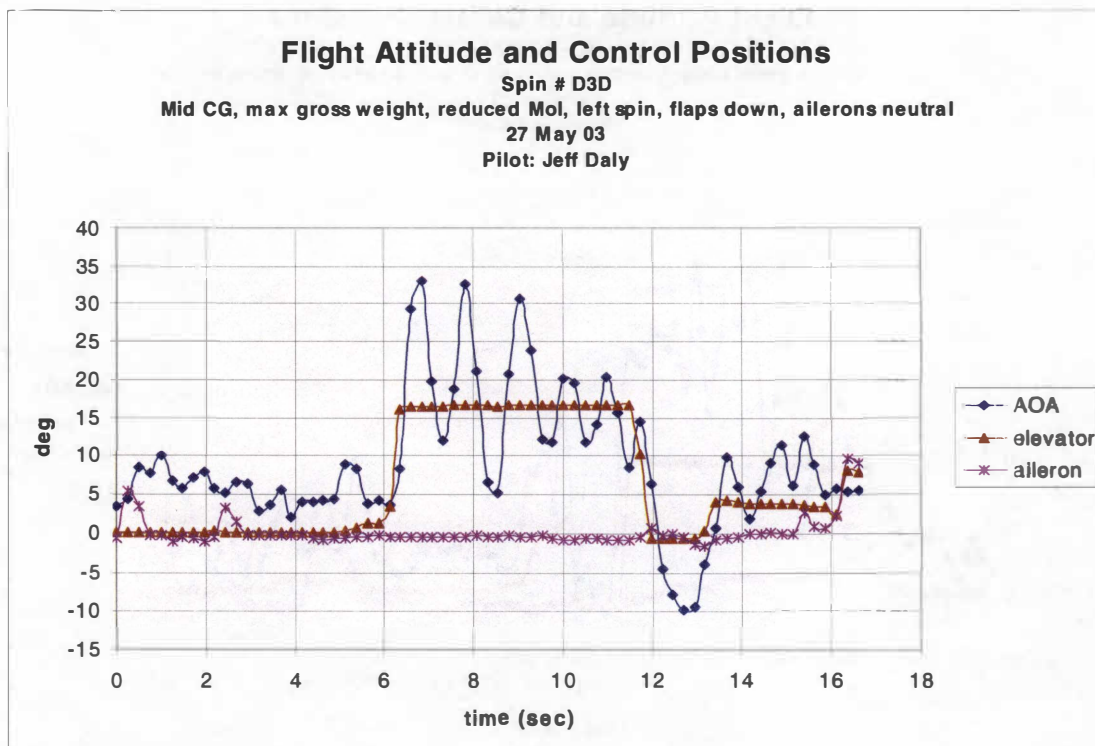
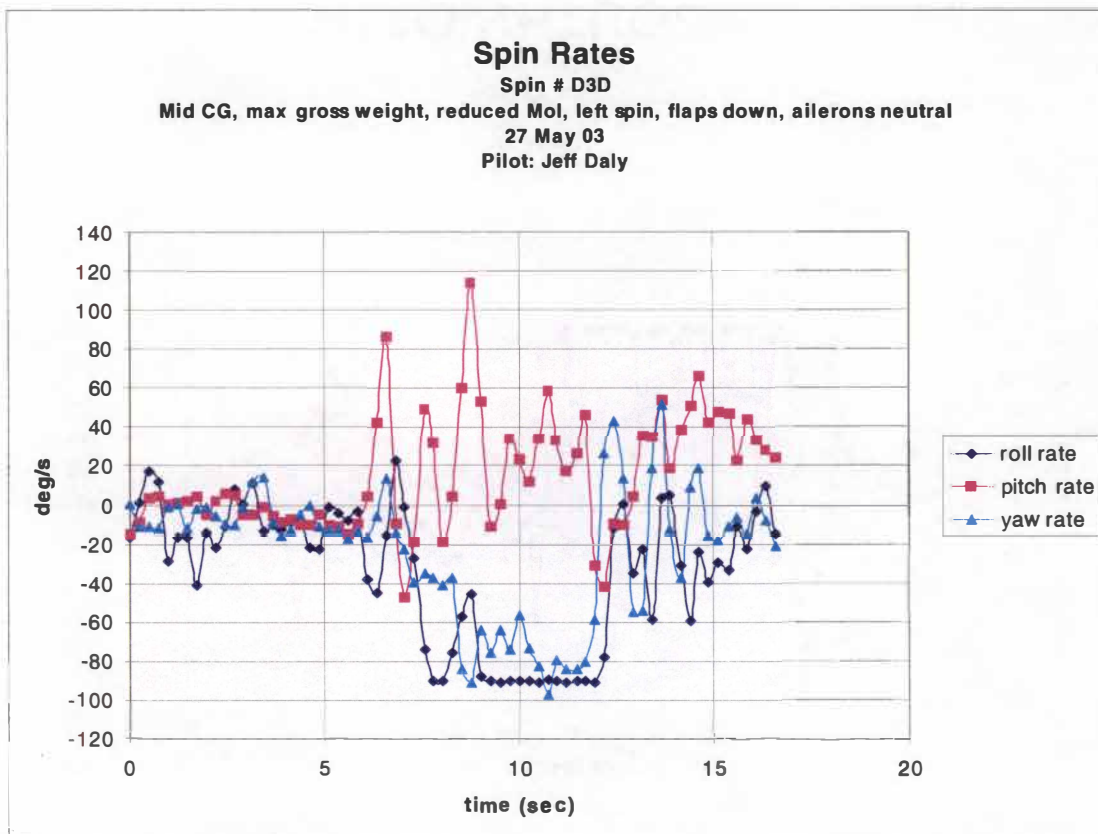


Figure F-14. Spin # D3D.

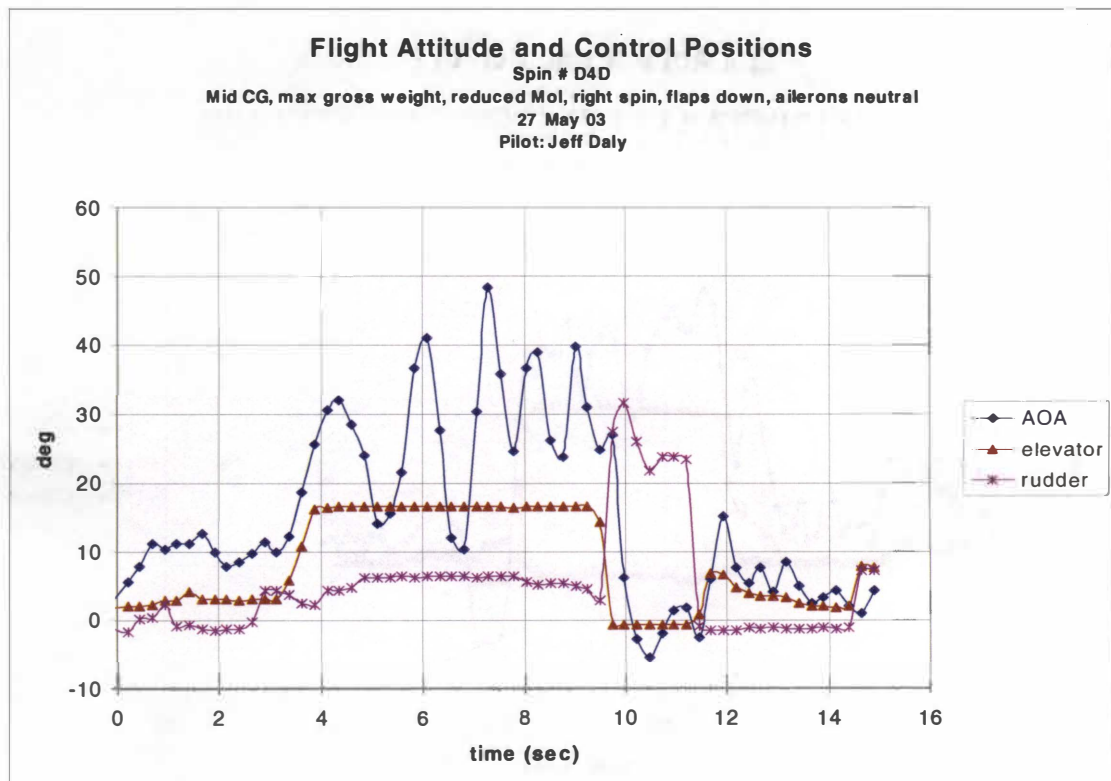
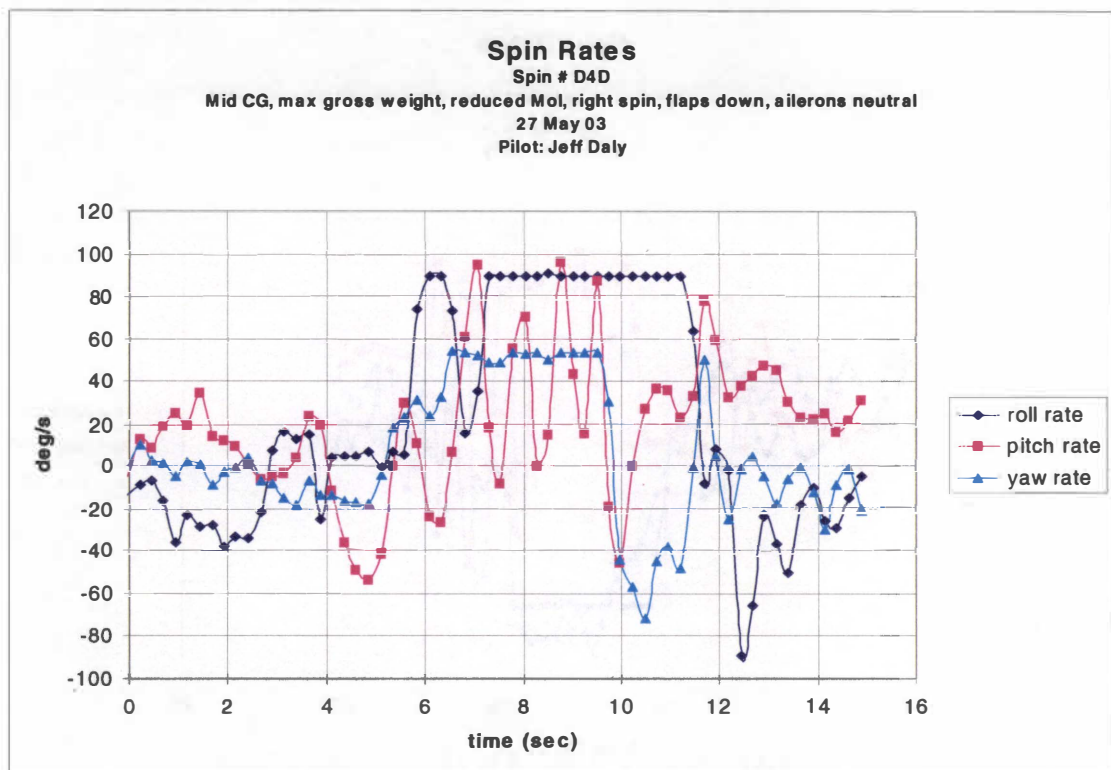


Figure F-15. Spin # D4D.

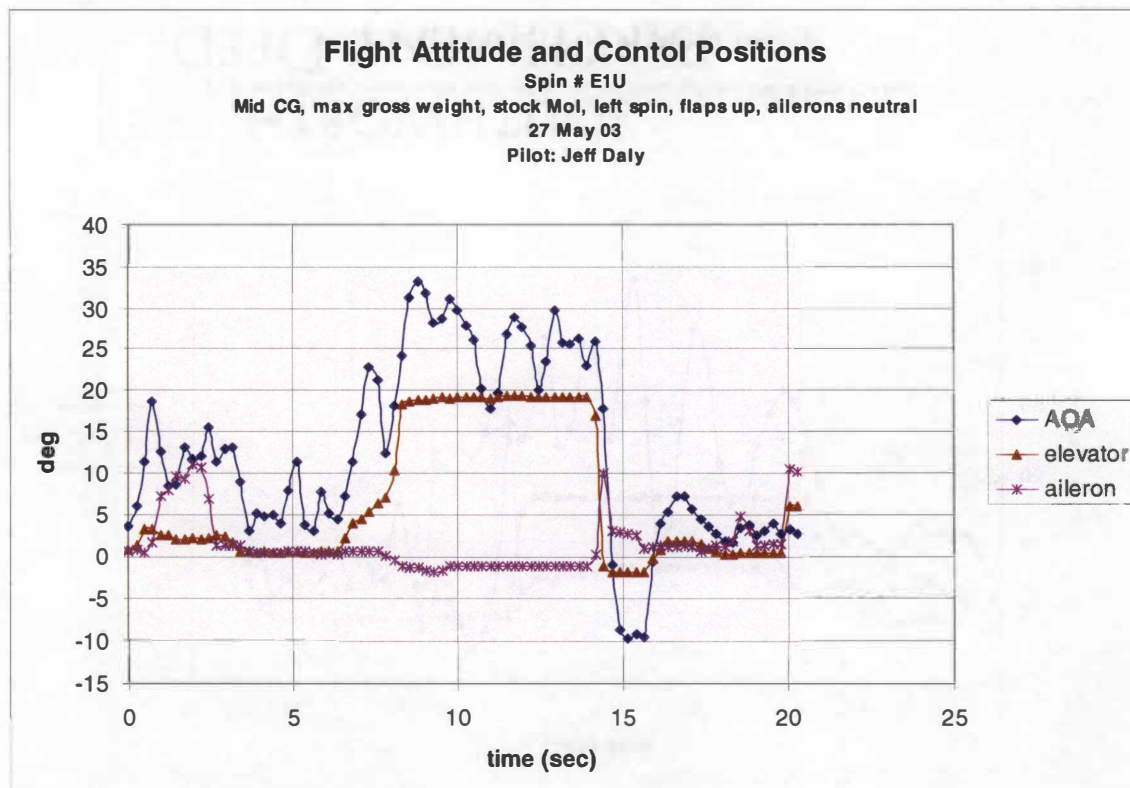
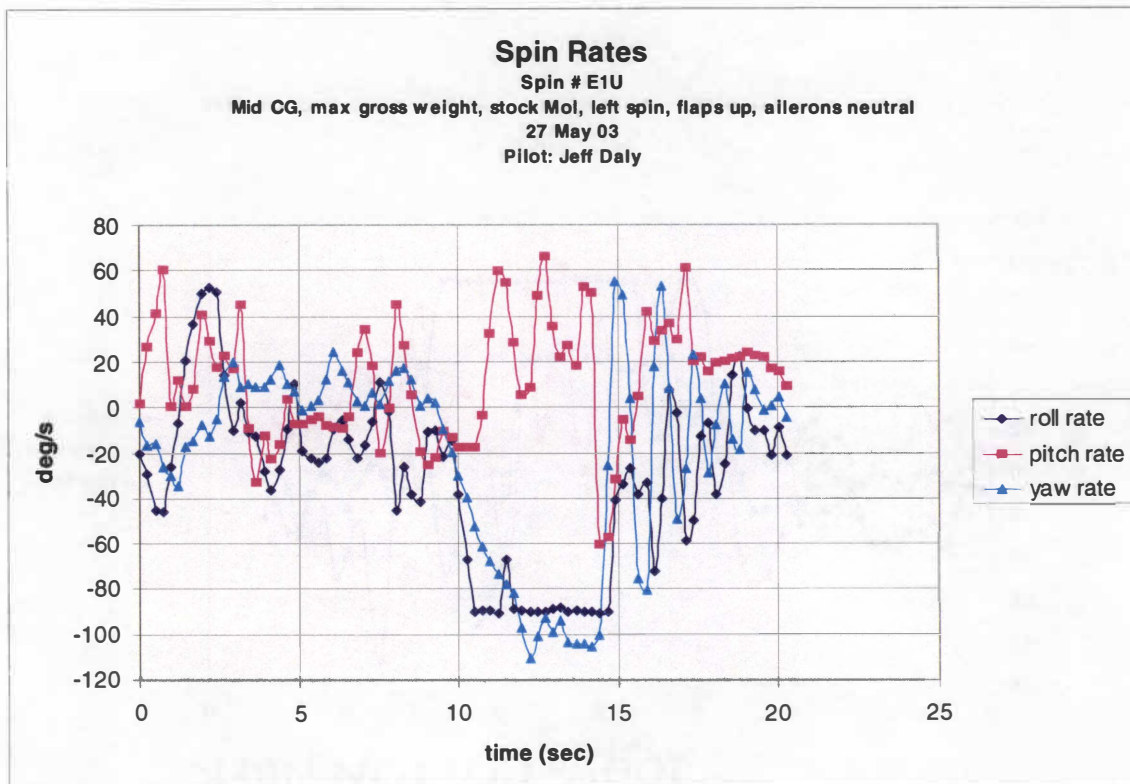


Figure F-16. Spin # E1U.

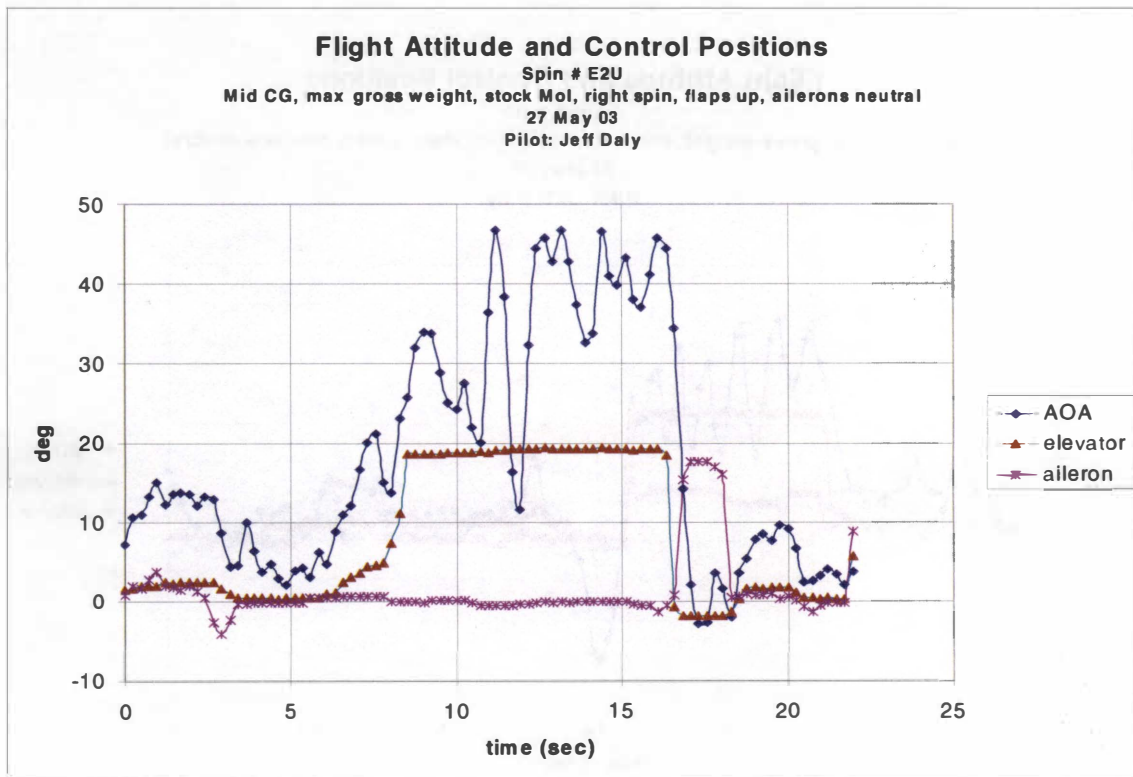
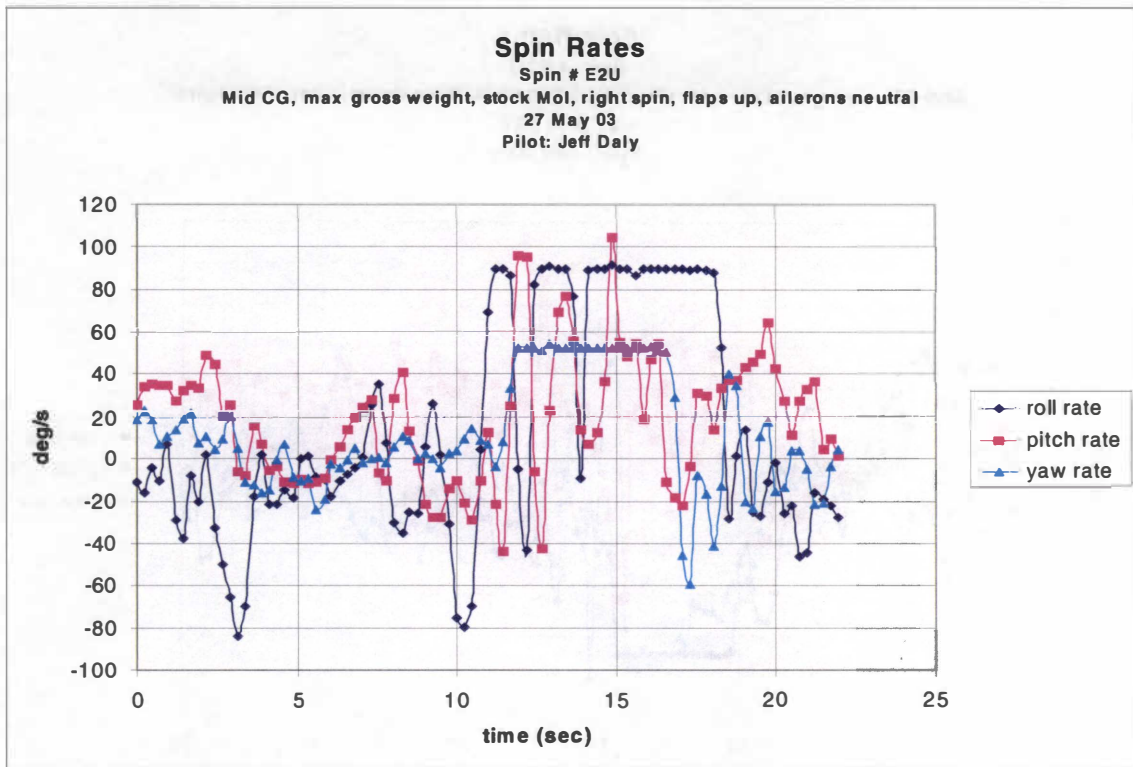


Figure F-17. Spin # E2U.

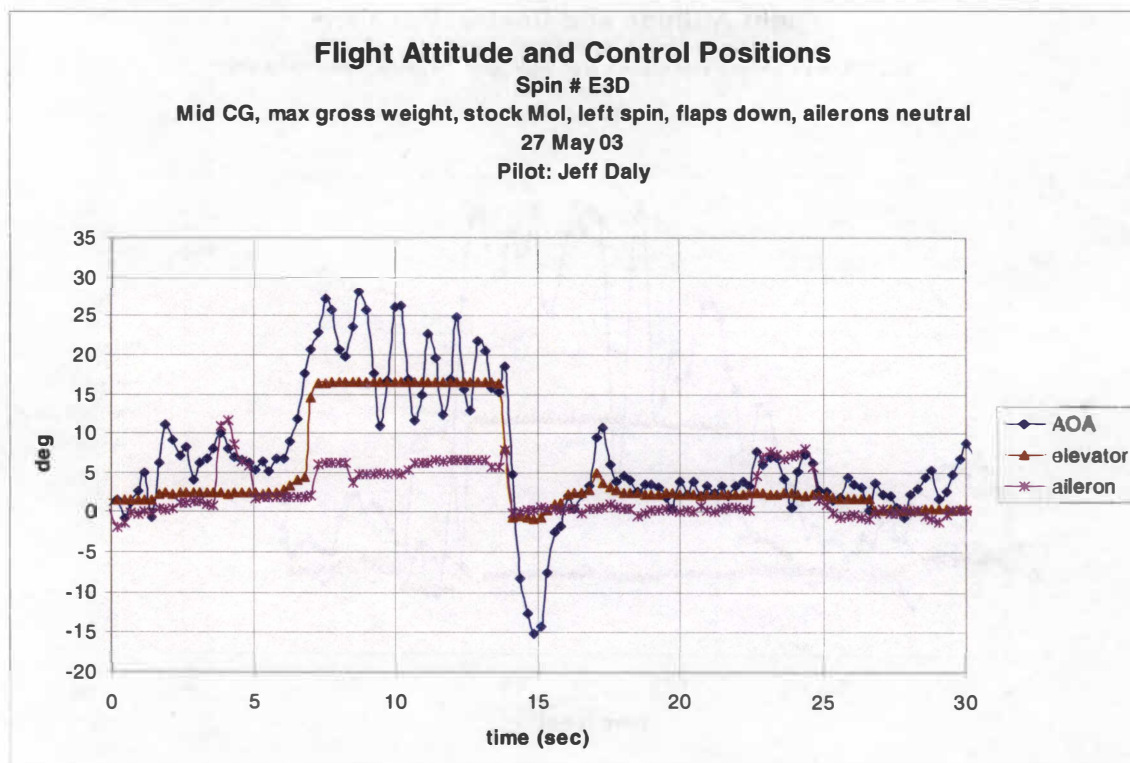
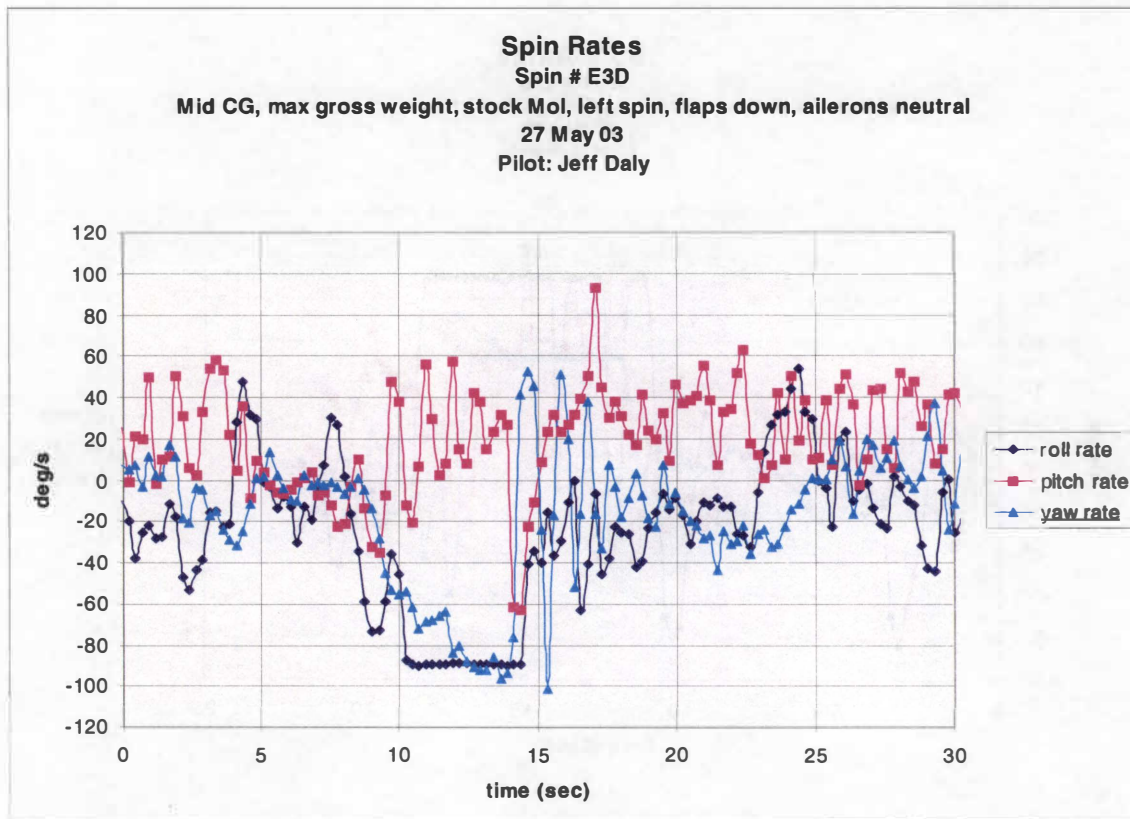


Figure F-18. Spin # E3D.

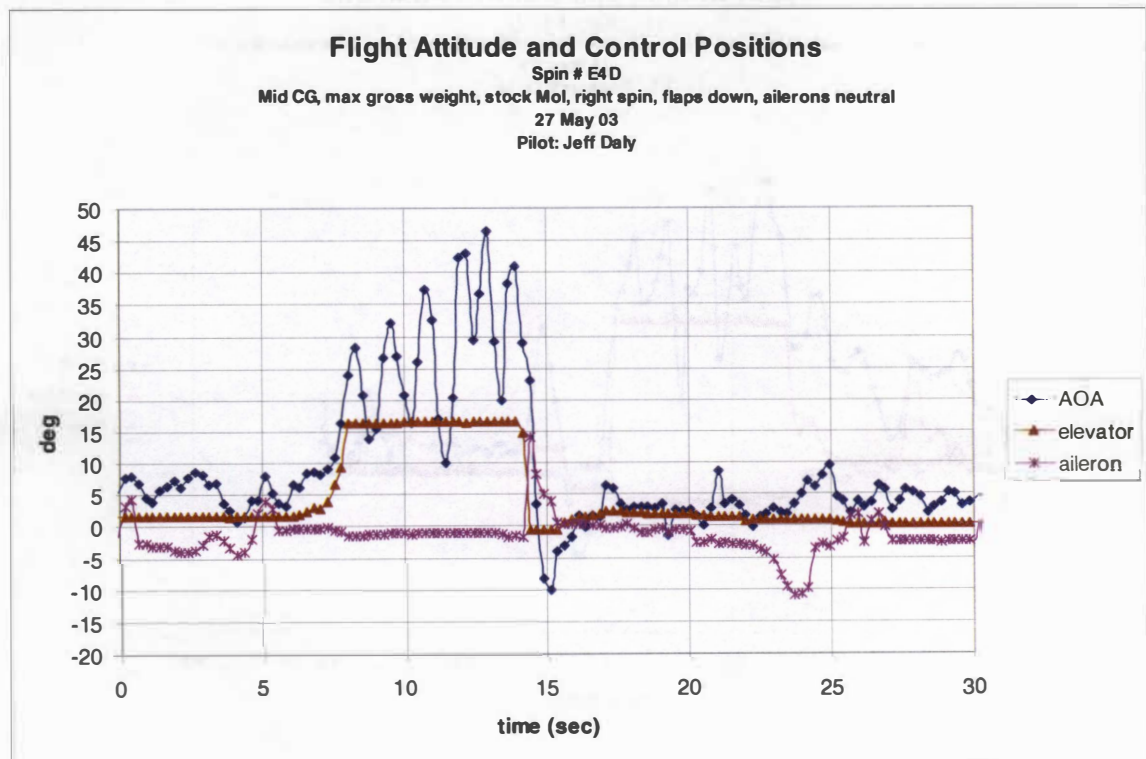
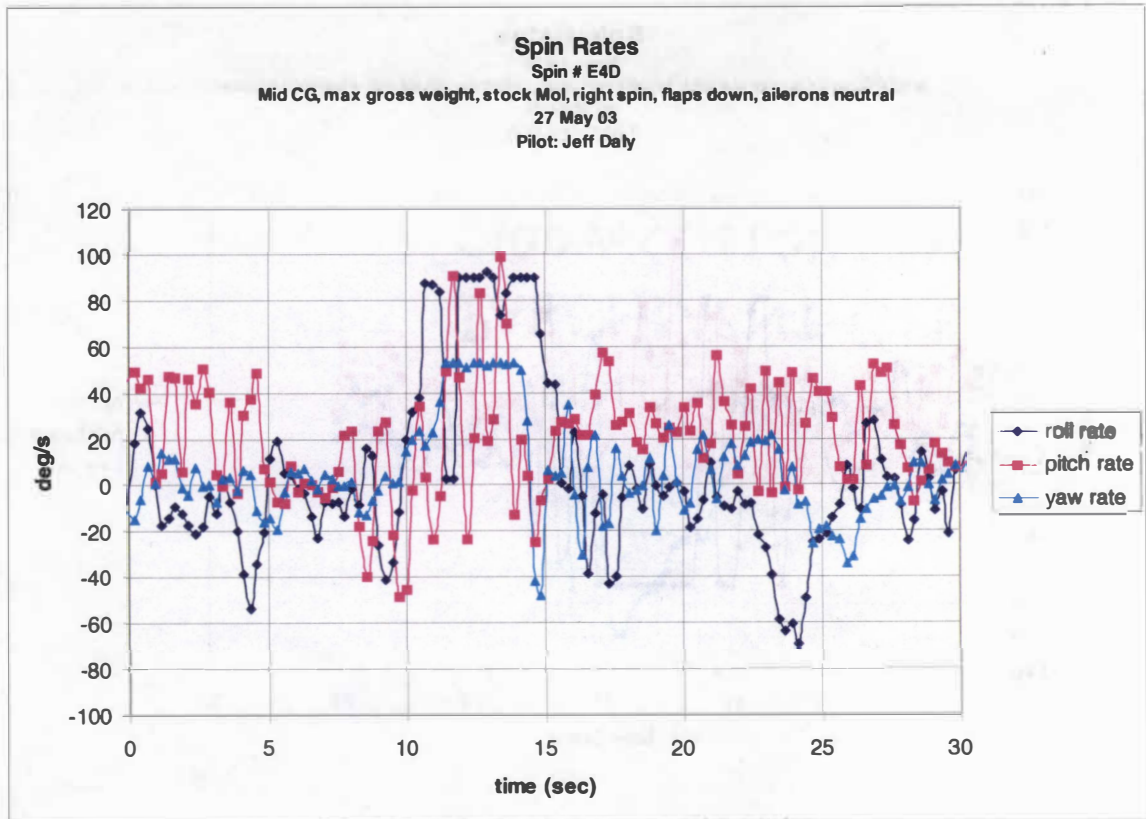


Figure F-19. Spin # E4D.

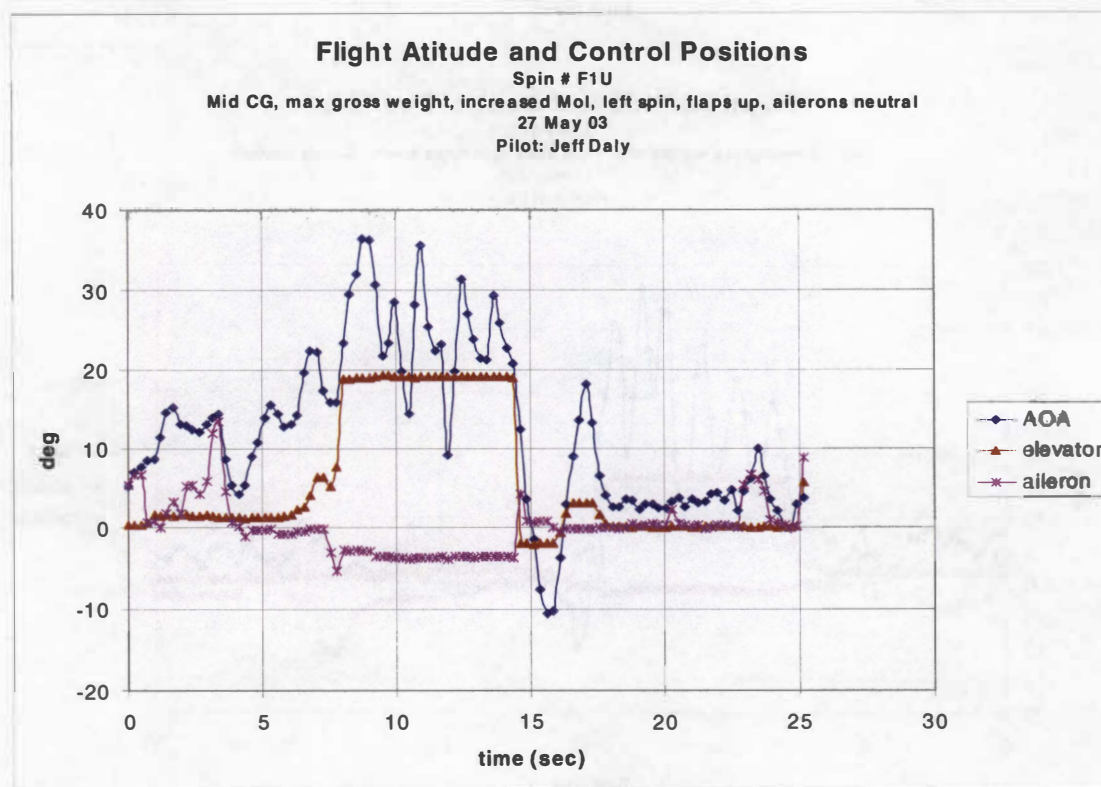
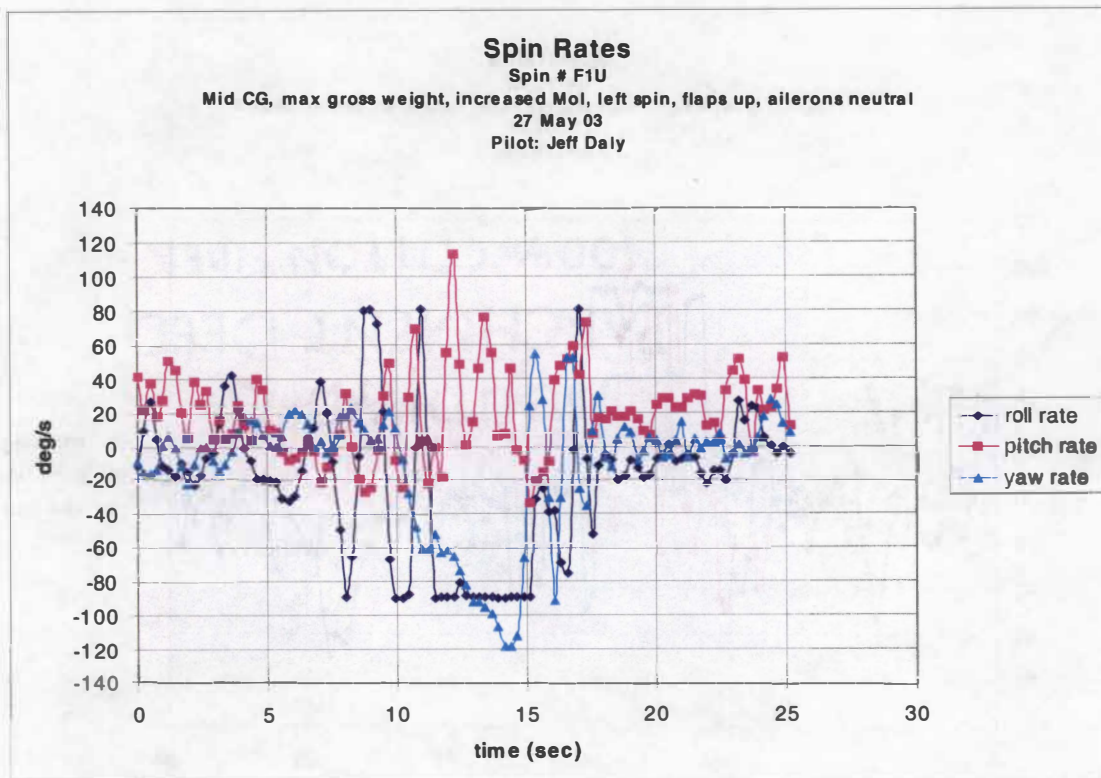


Figure F-20. Spin # F1U.

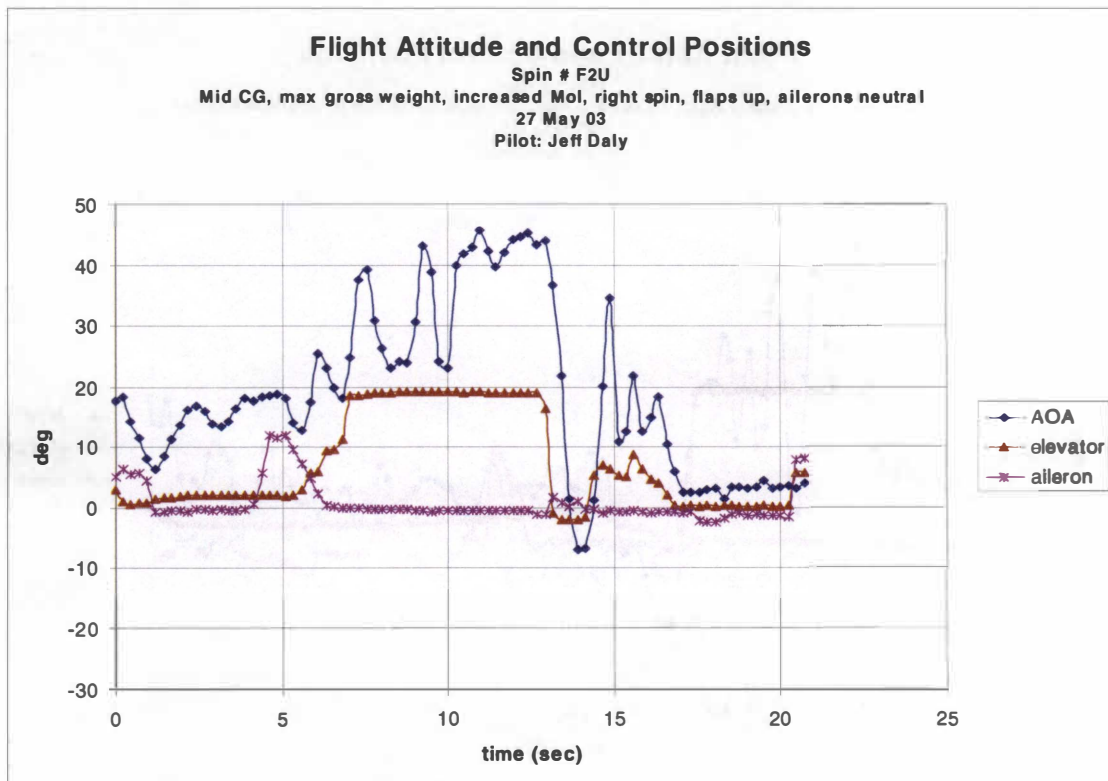
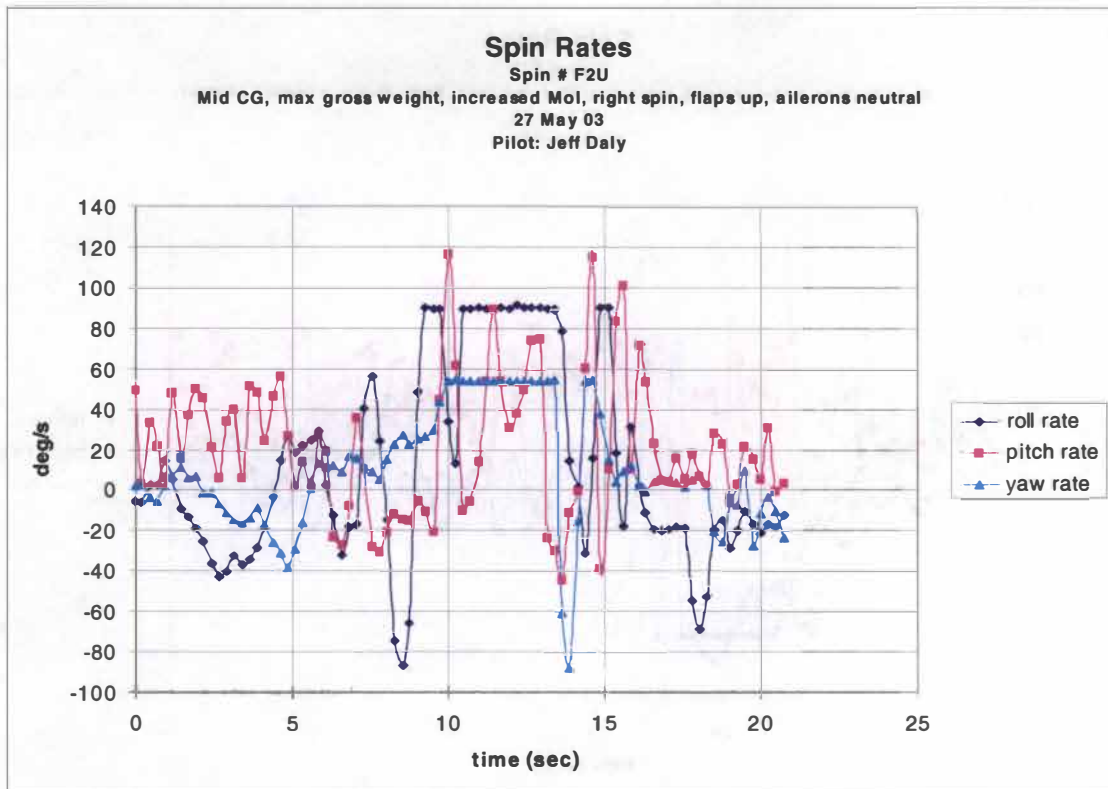


Figure F-21. Spin # F2U.

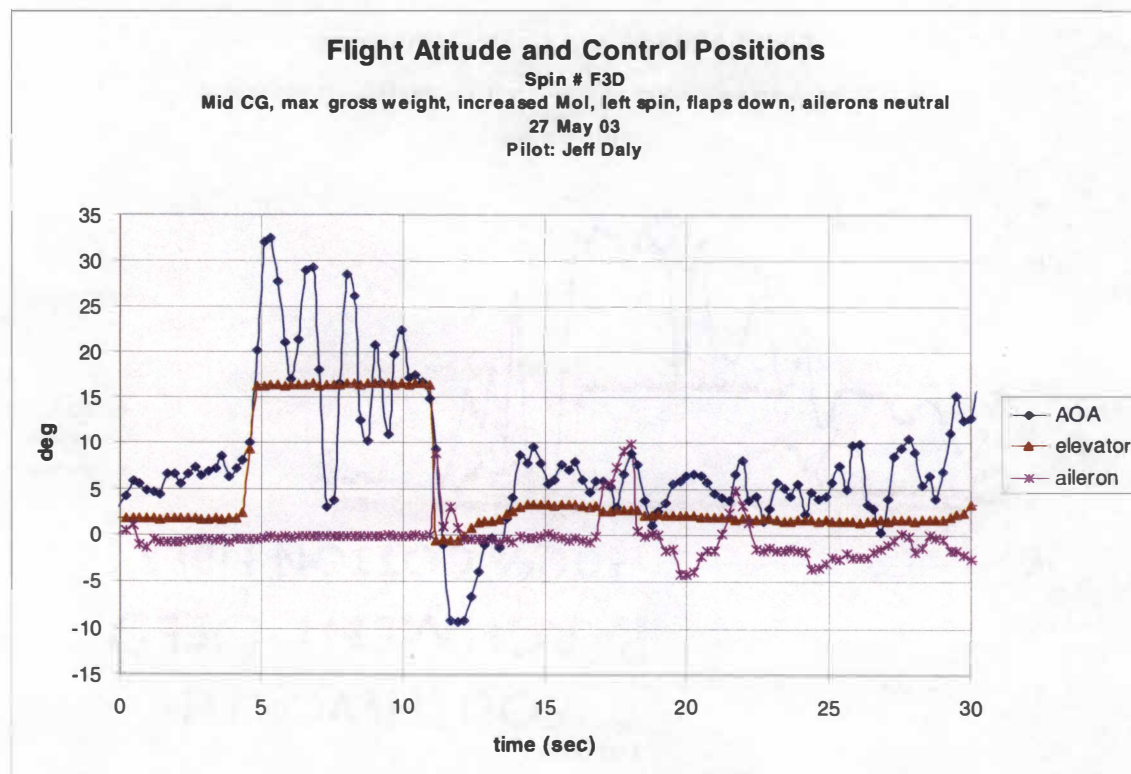
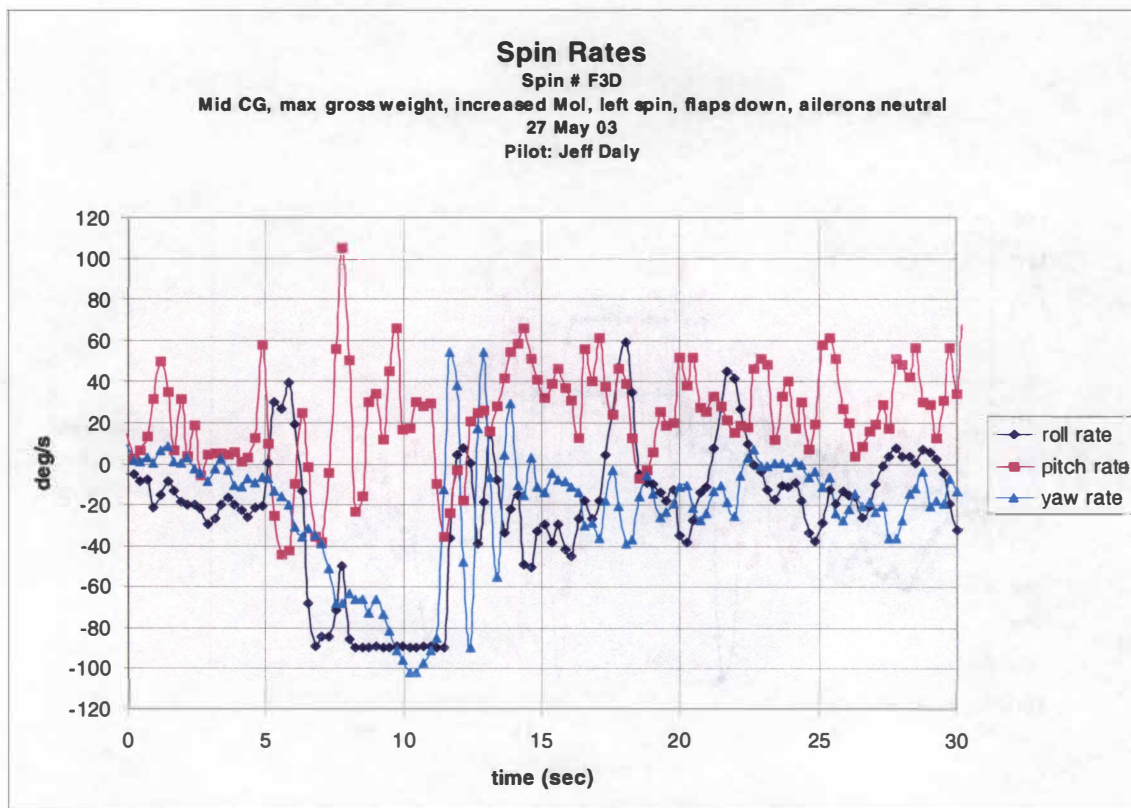


Figure F-22. Spin # F3D.

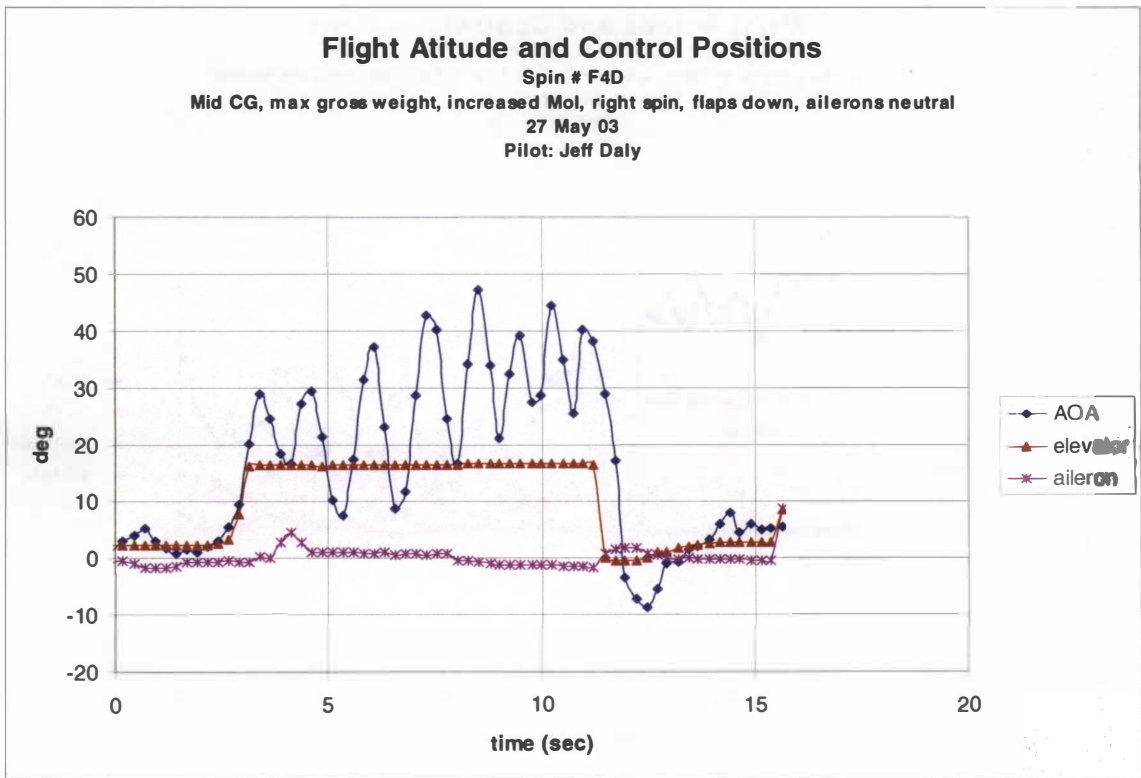
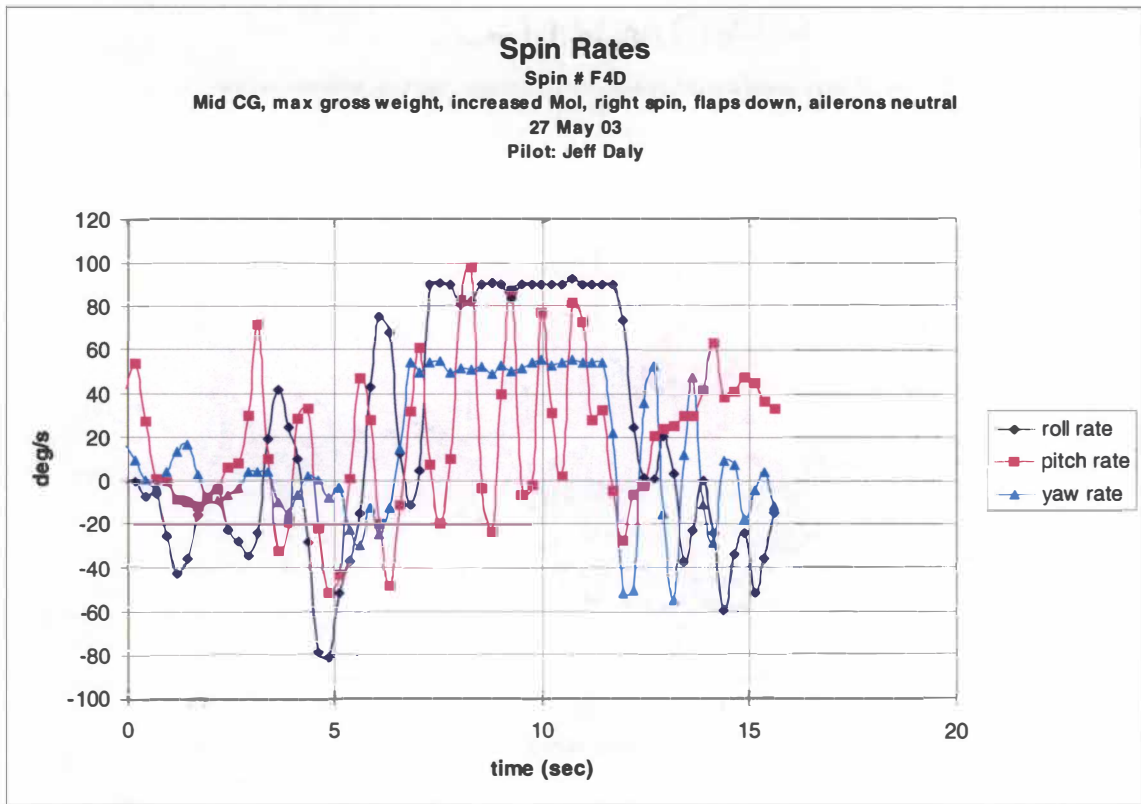


Figure F-23. Spin # F4D.

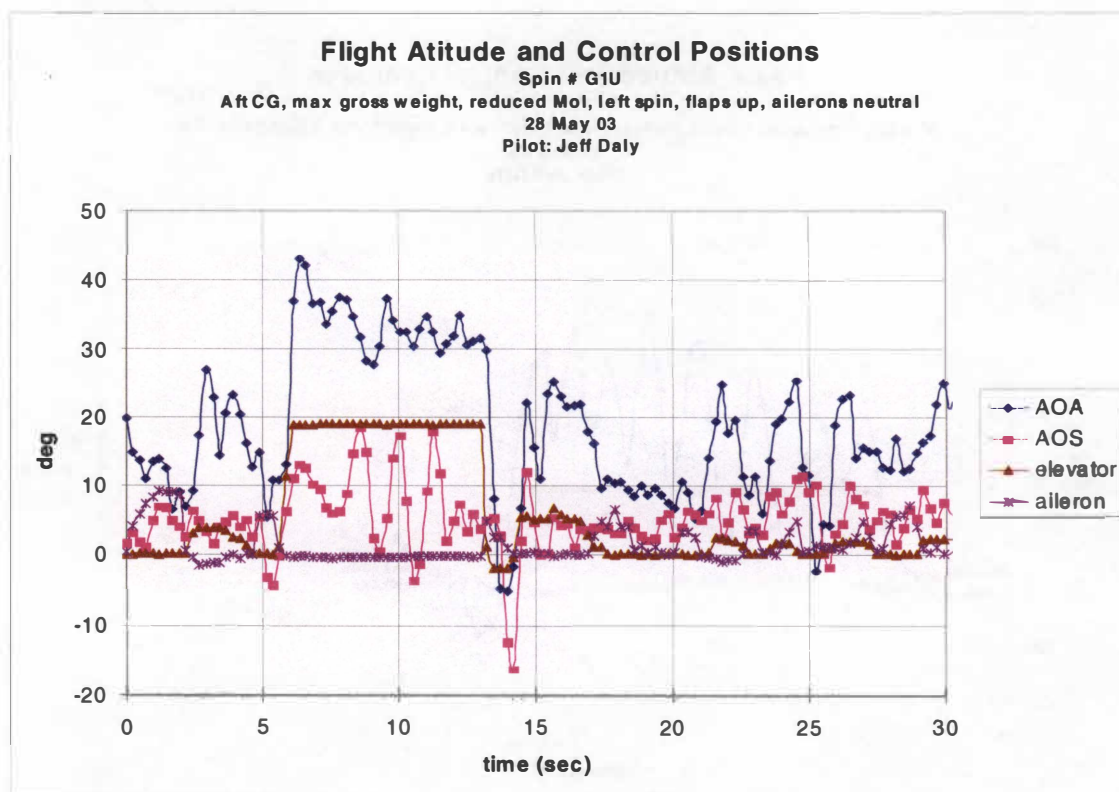
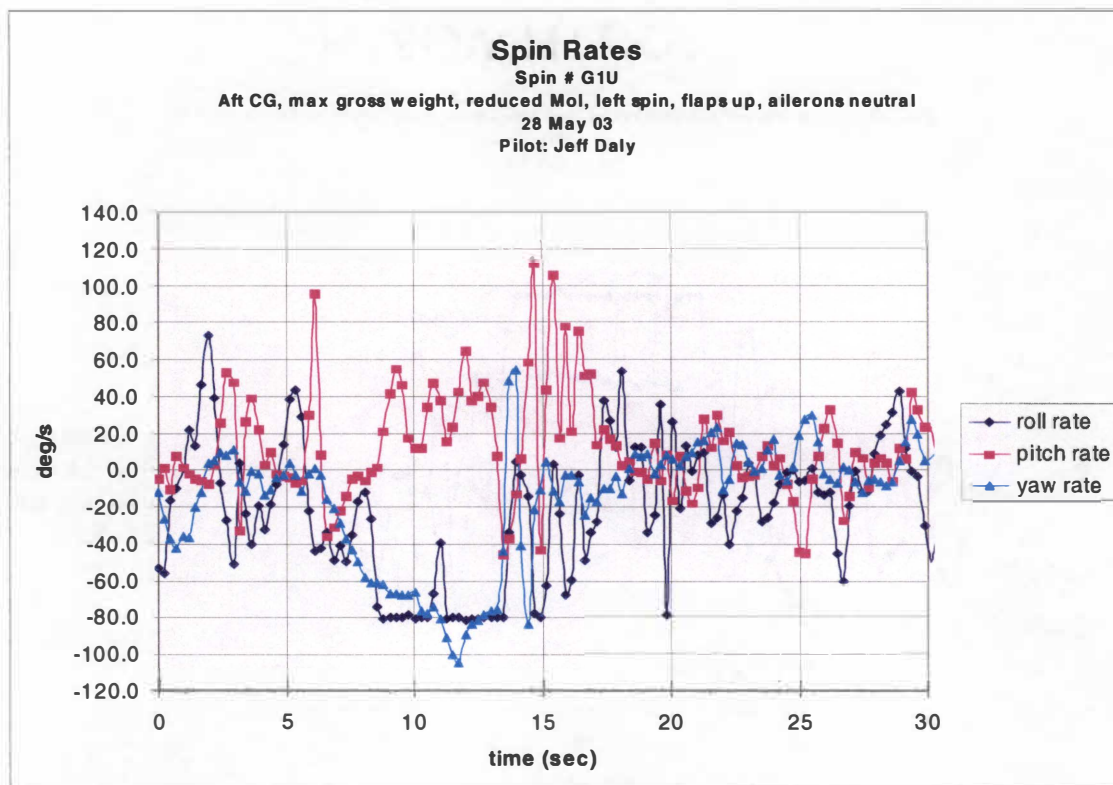


Figure F-24. Spin # G1U.

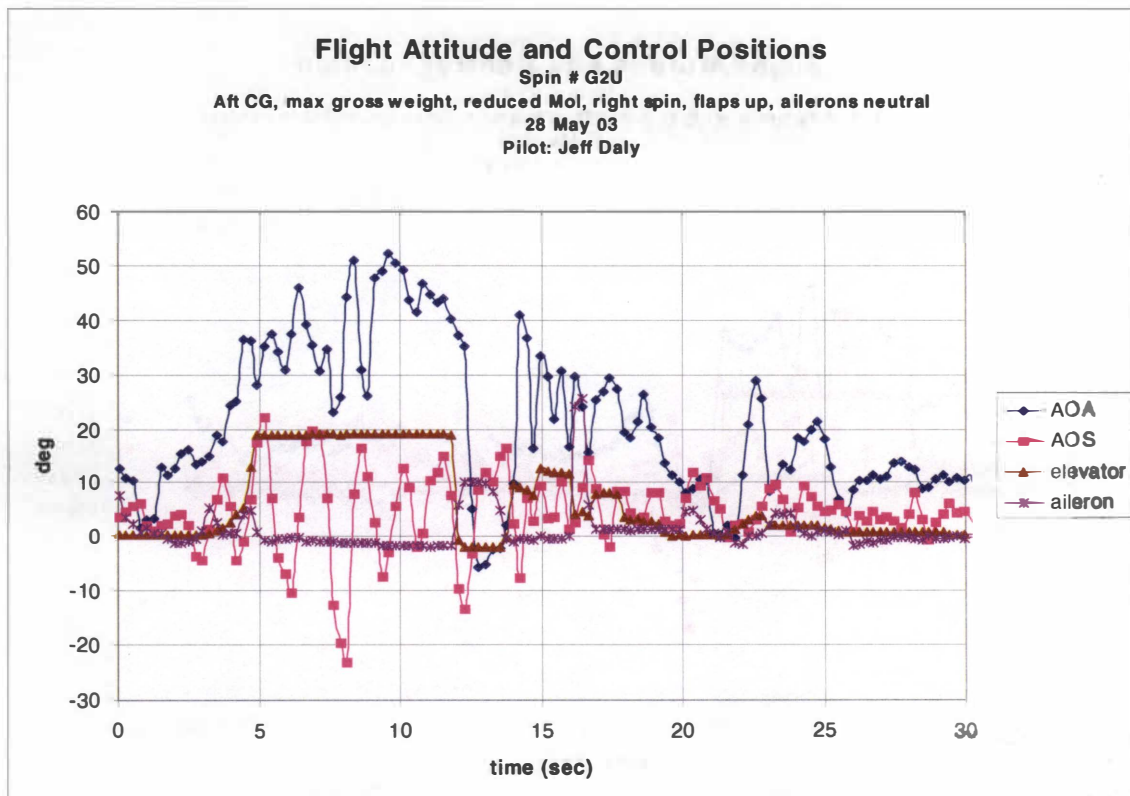
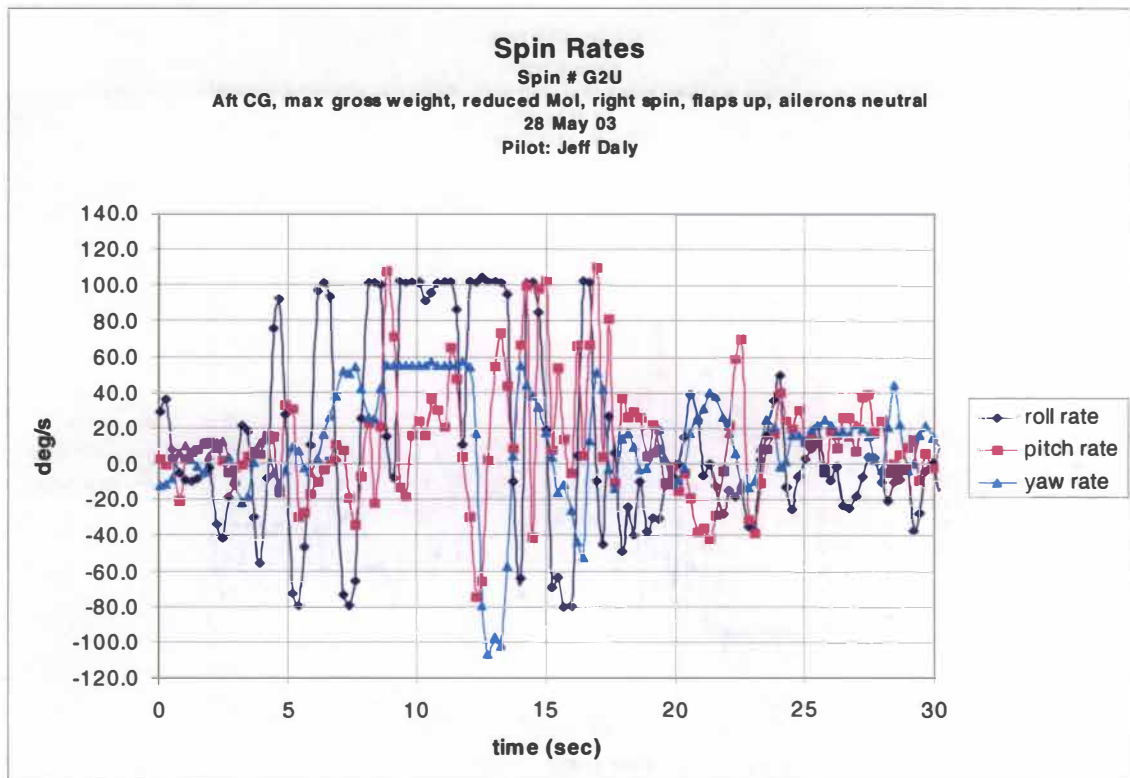


Figure F-25. Spin # G2U.

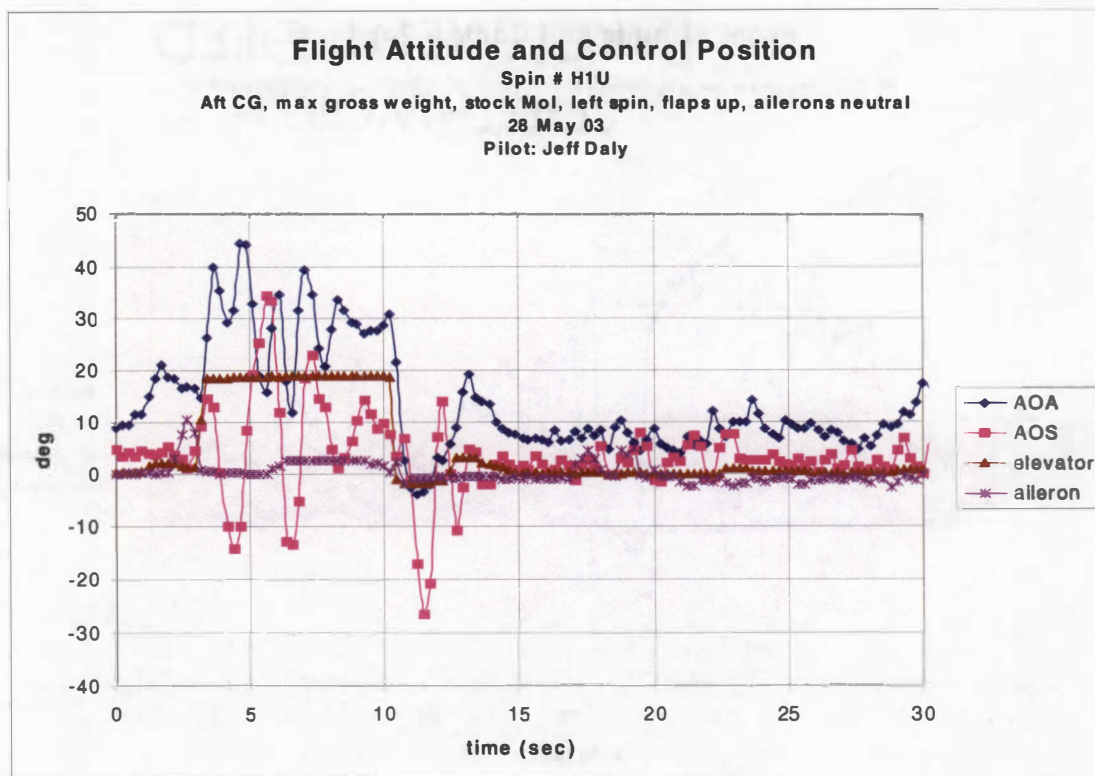
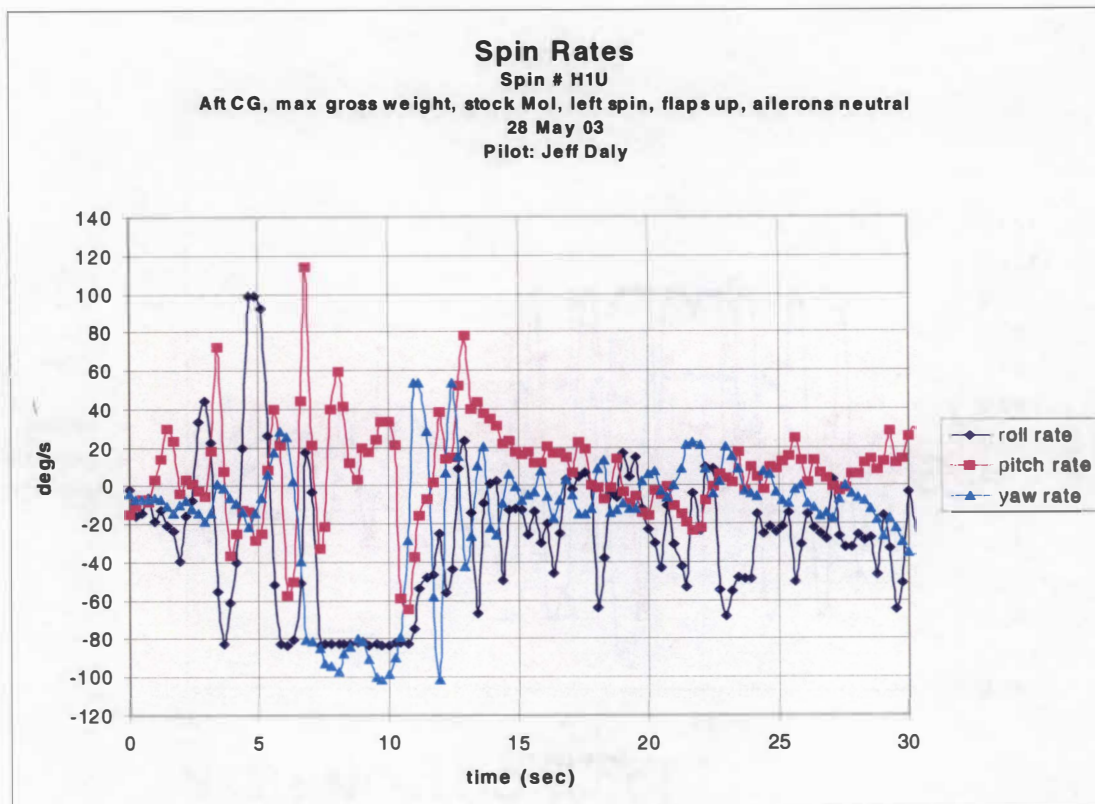


Figure F-26. Spin # H1U.

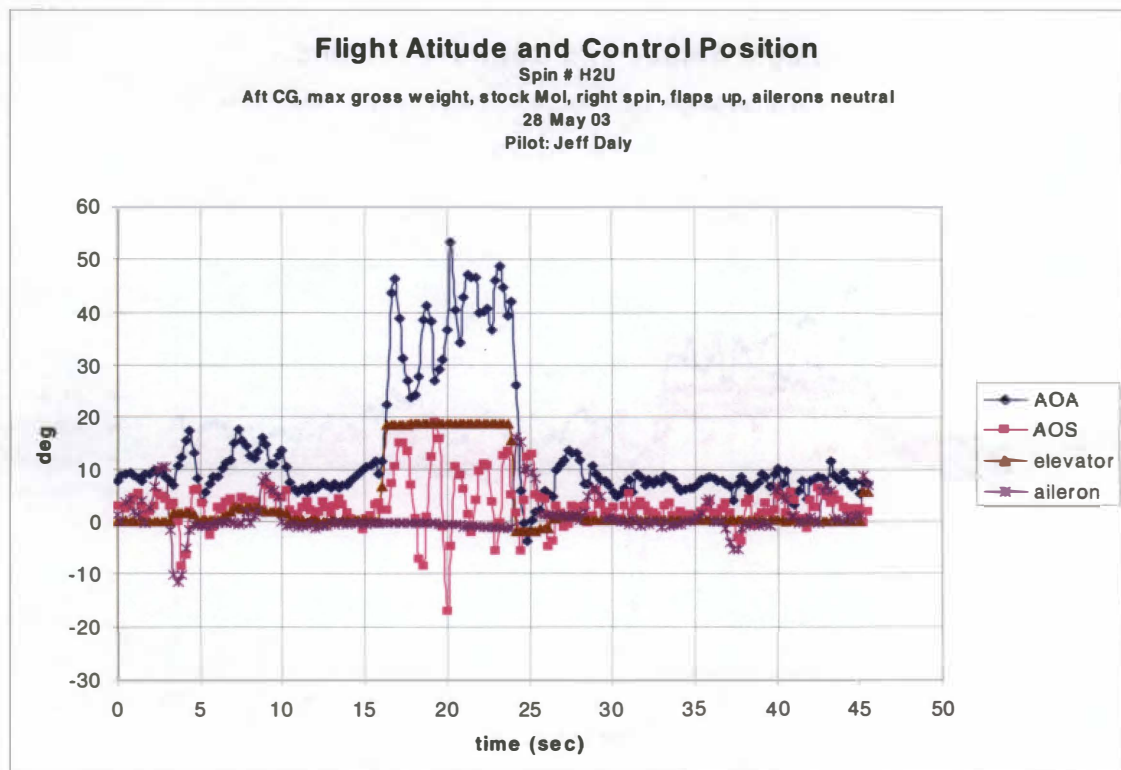
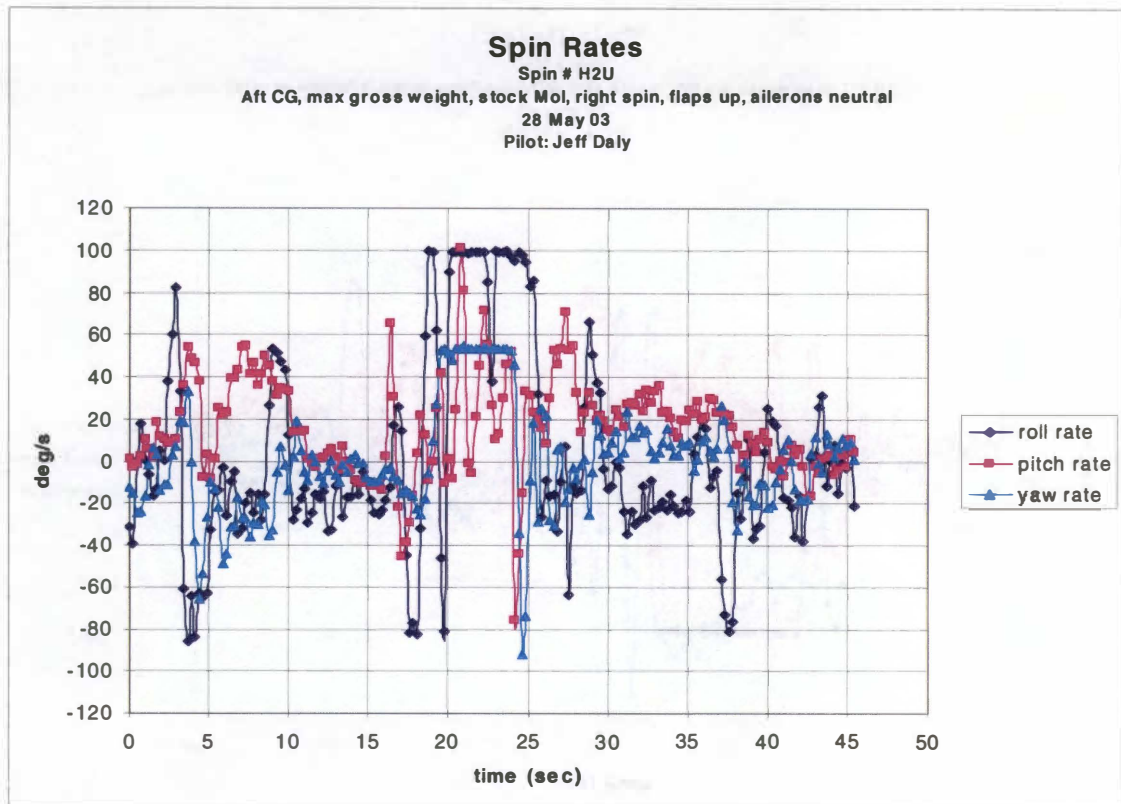


Figure F-27. Spin # H2U.

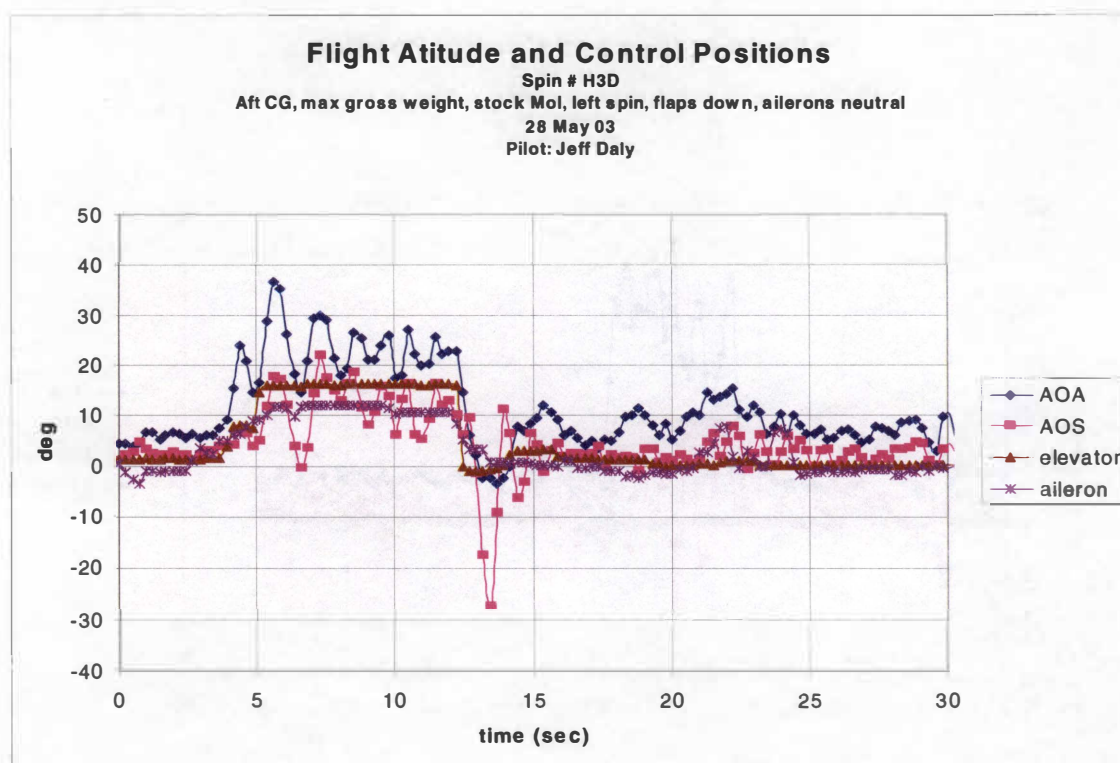
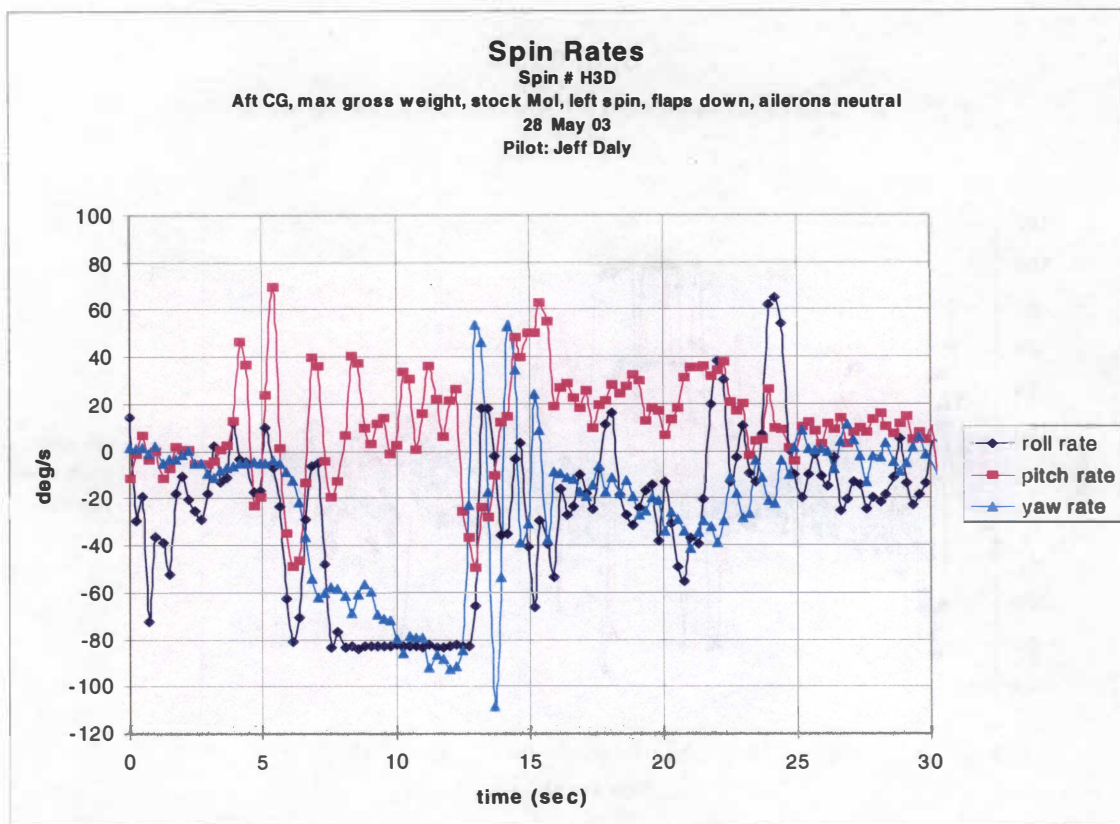


Figure F-28. Spin # H3D.

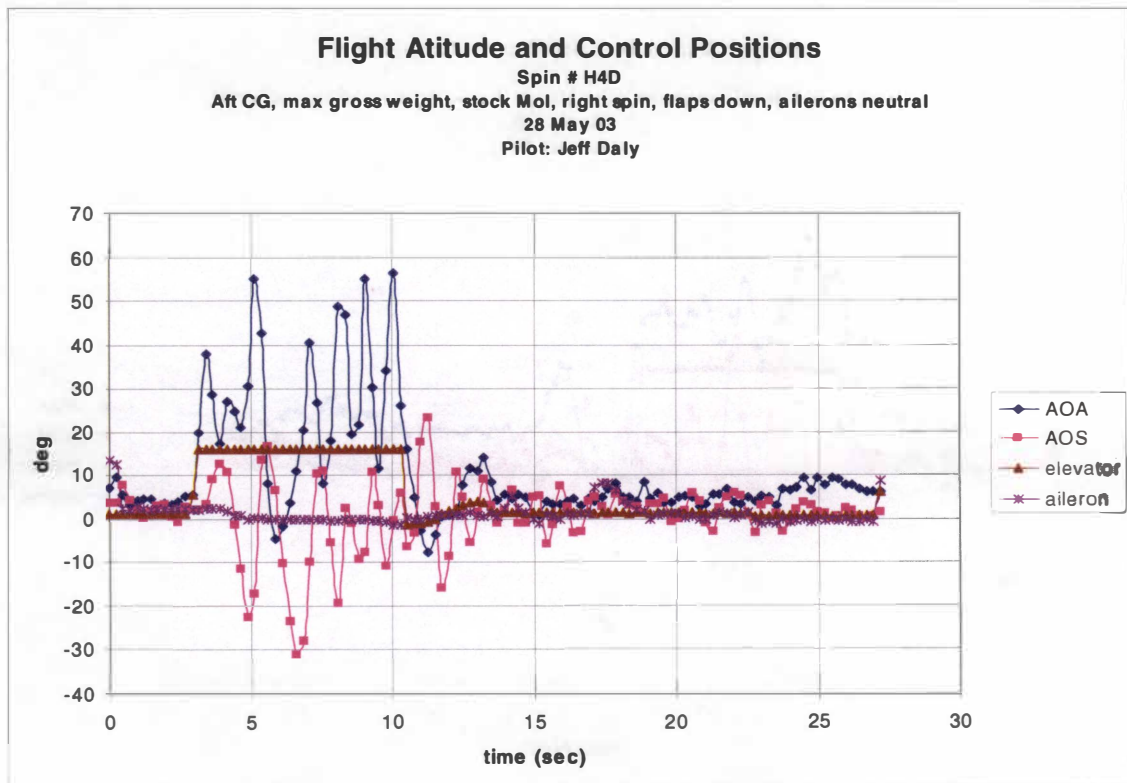
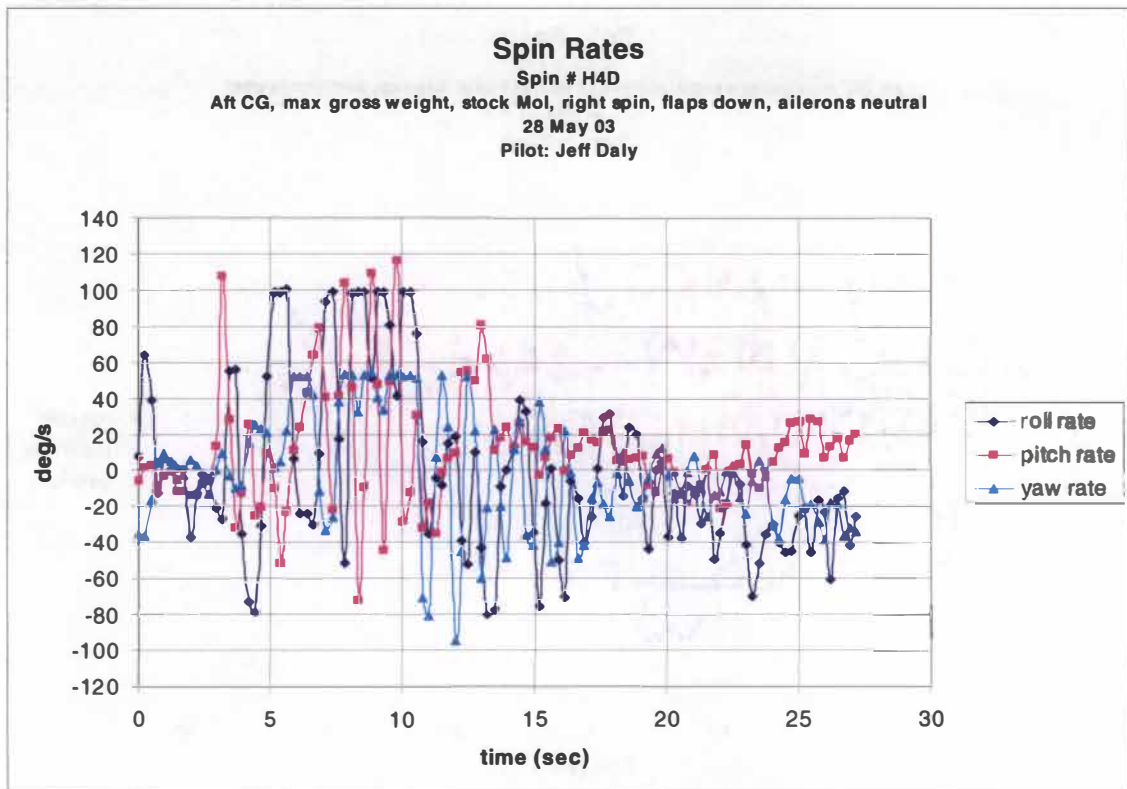


Figure F-29. Spin # H4D.

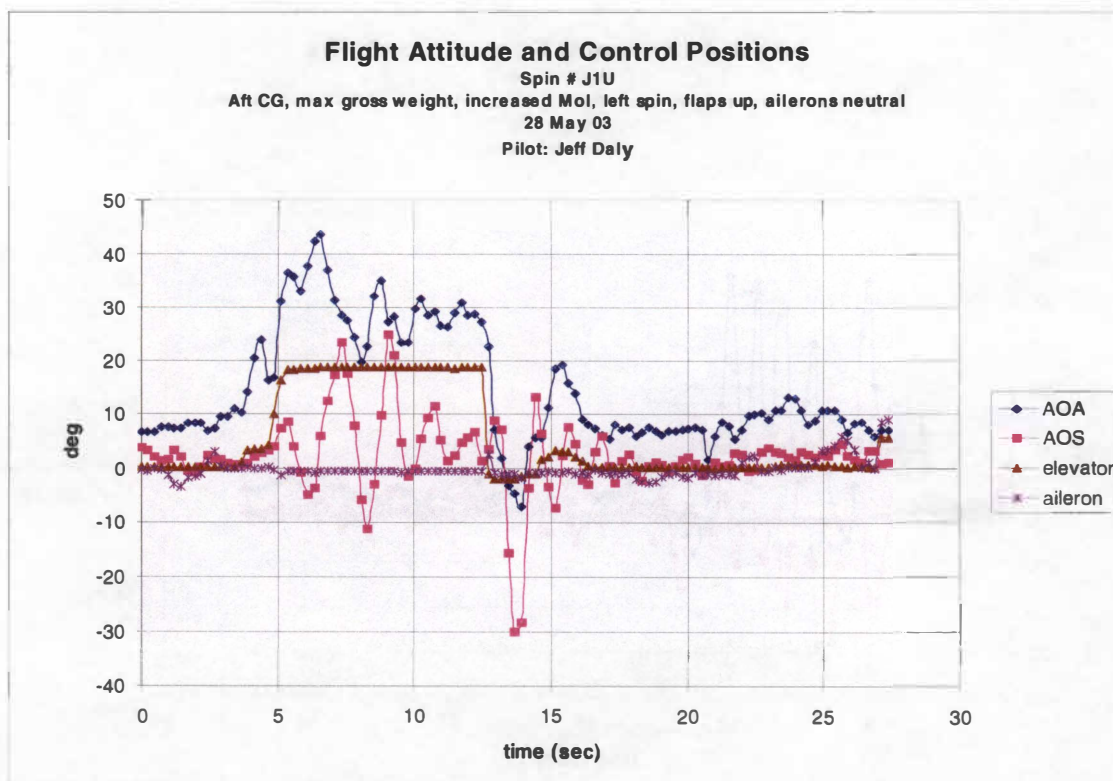
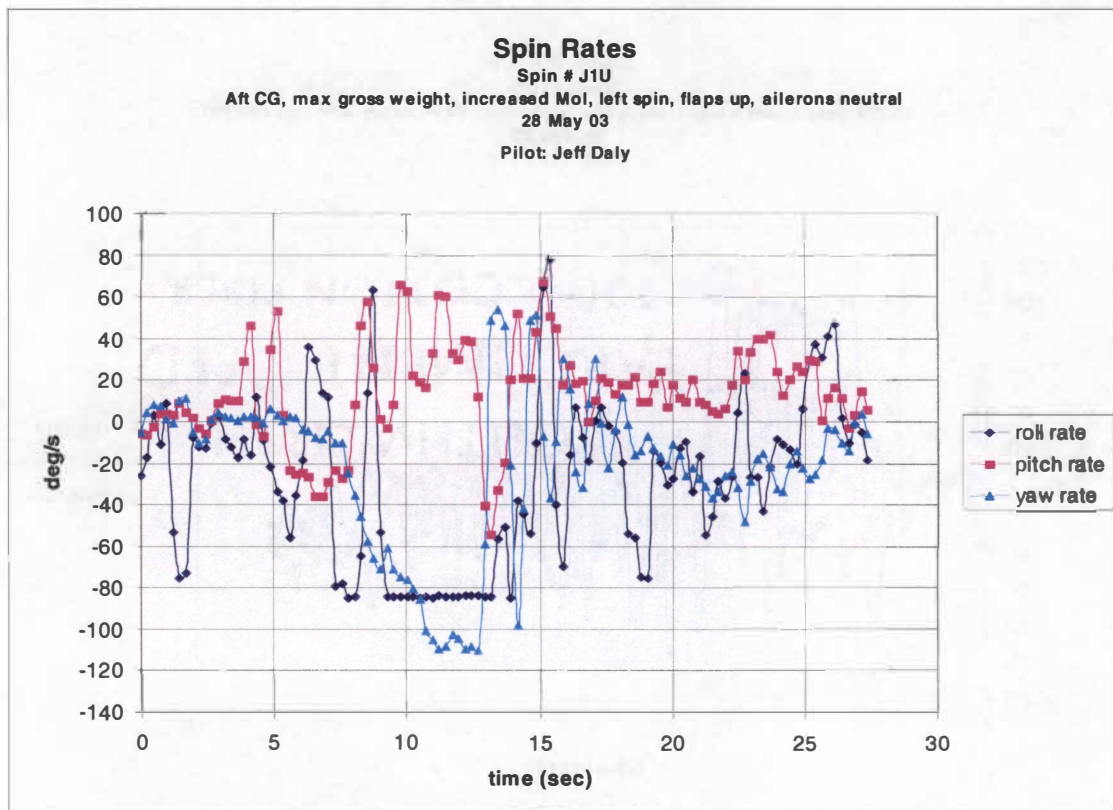


Figure F-30. Spin # J1U.

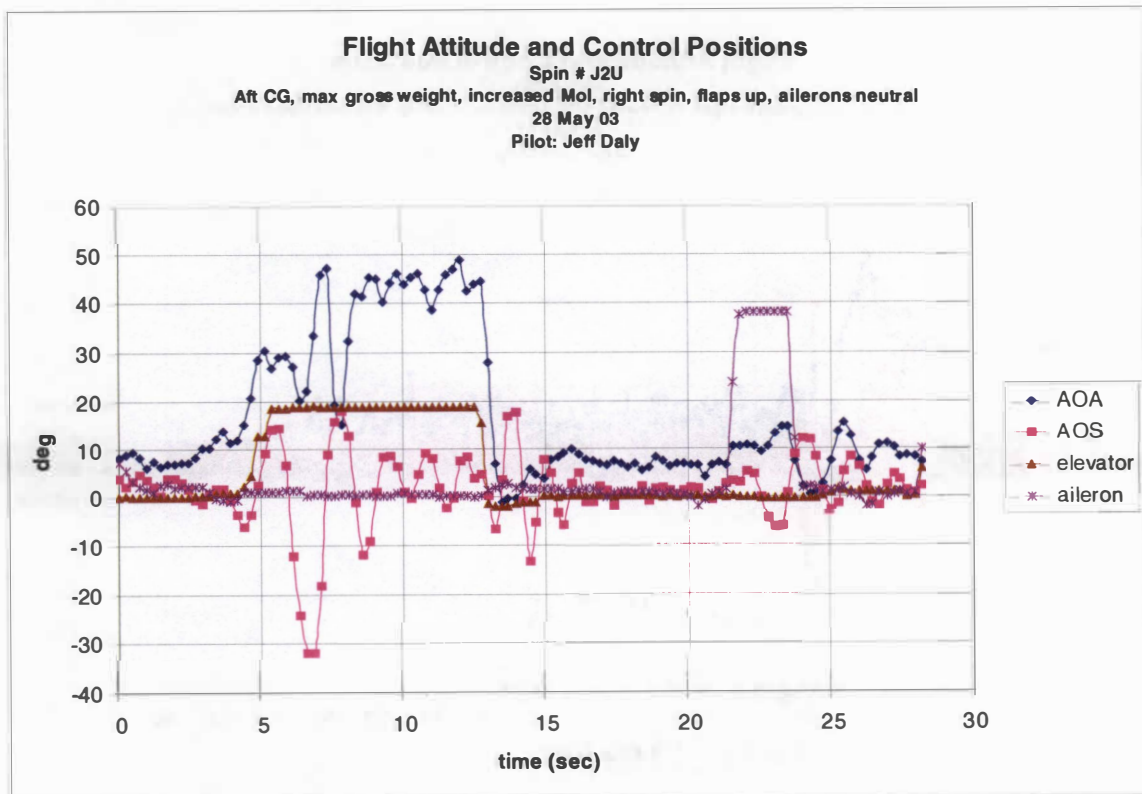
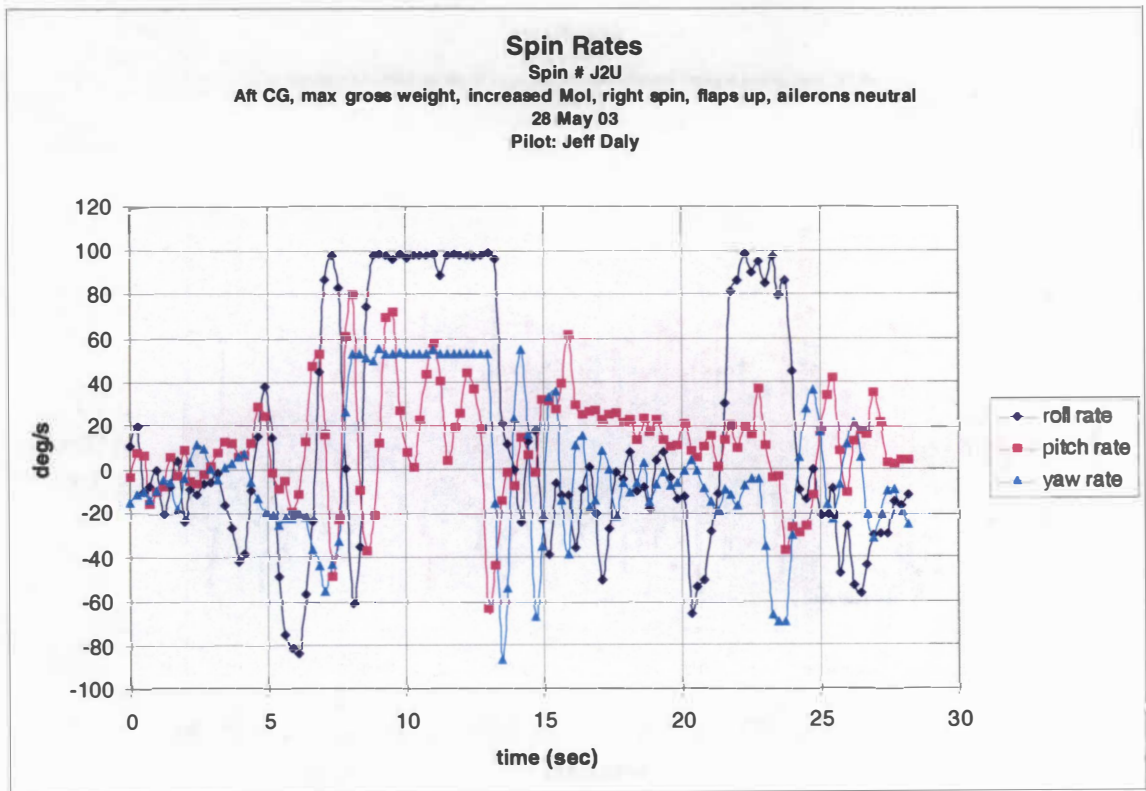


Figure F-31. Spin # J2U.

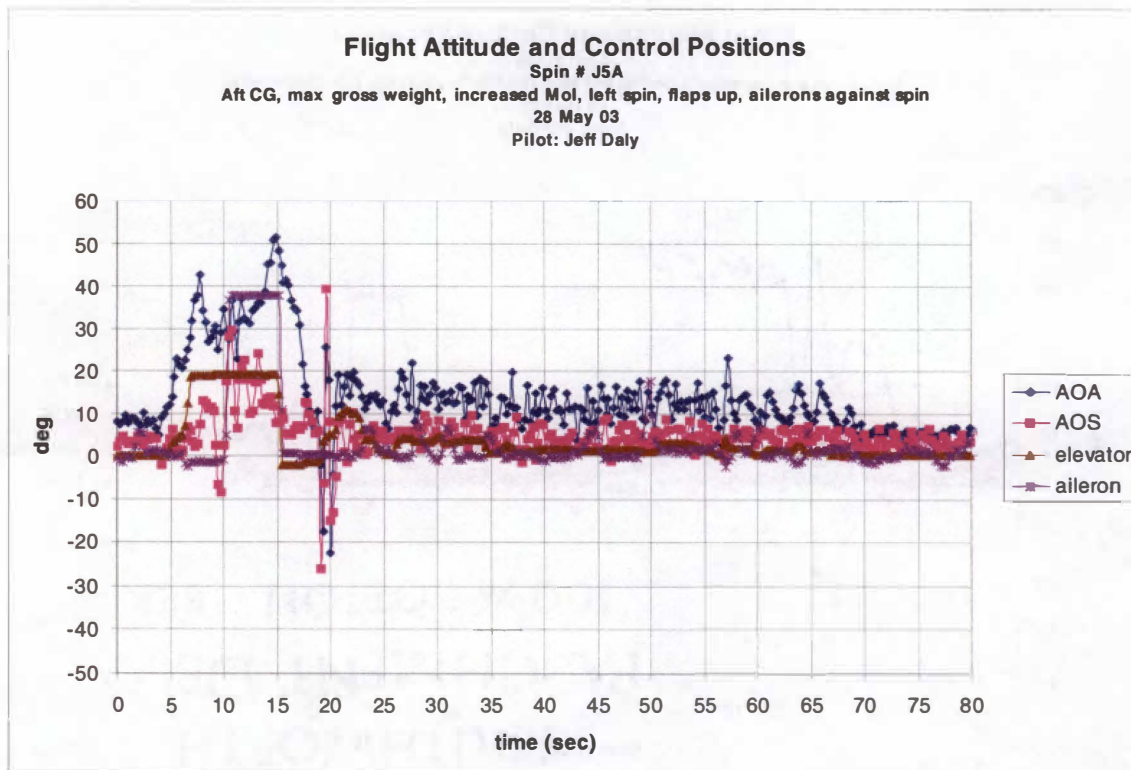
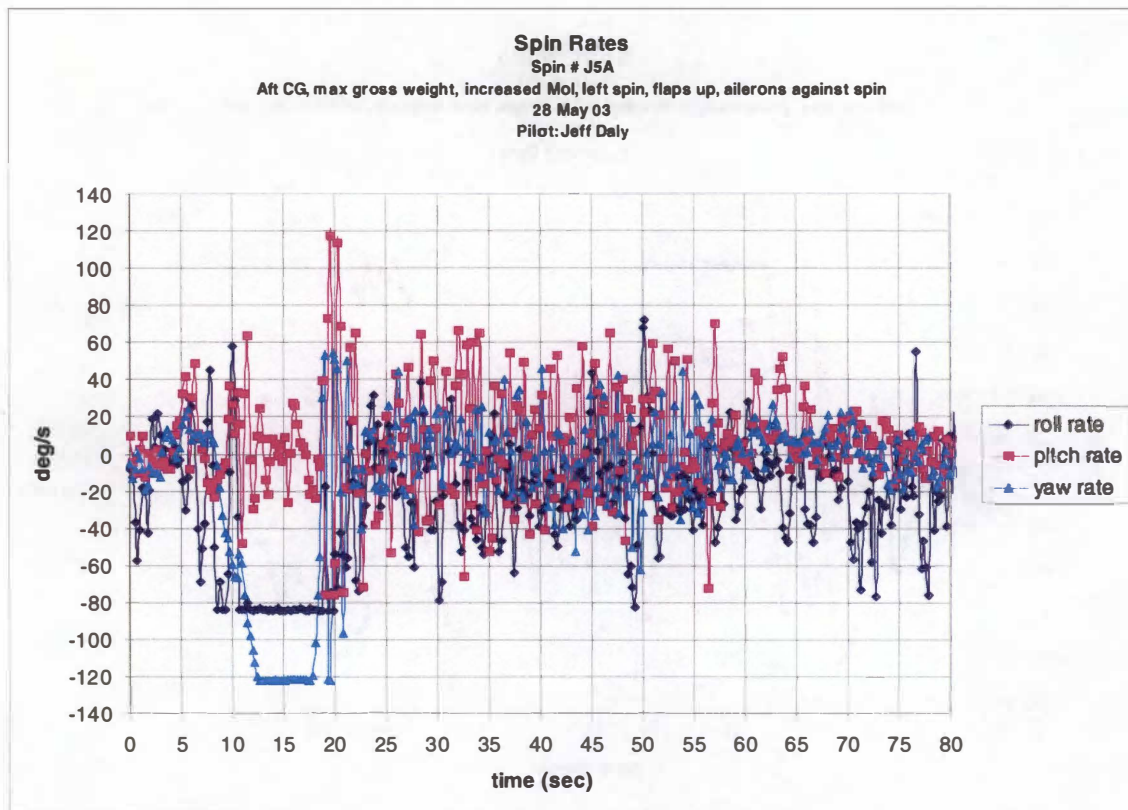


Figure F-32. Spin # J5A.

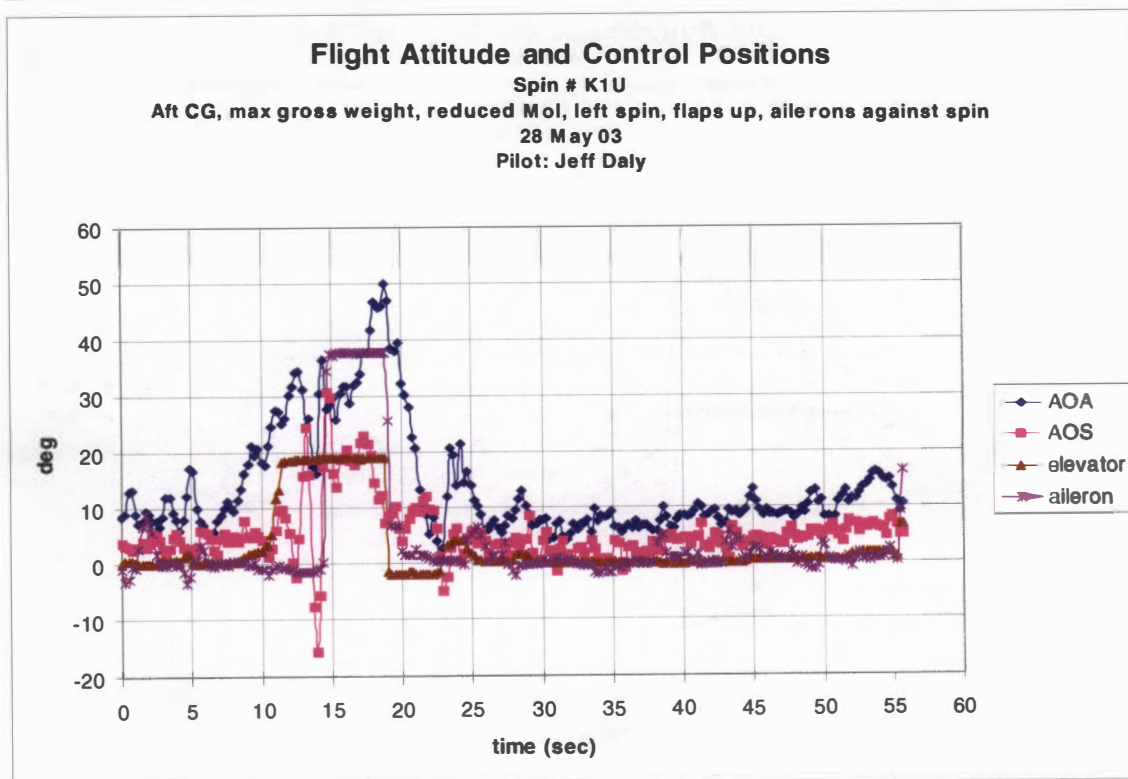
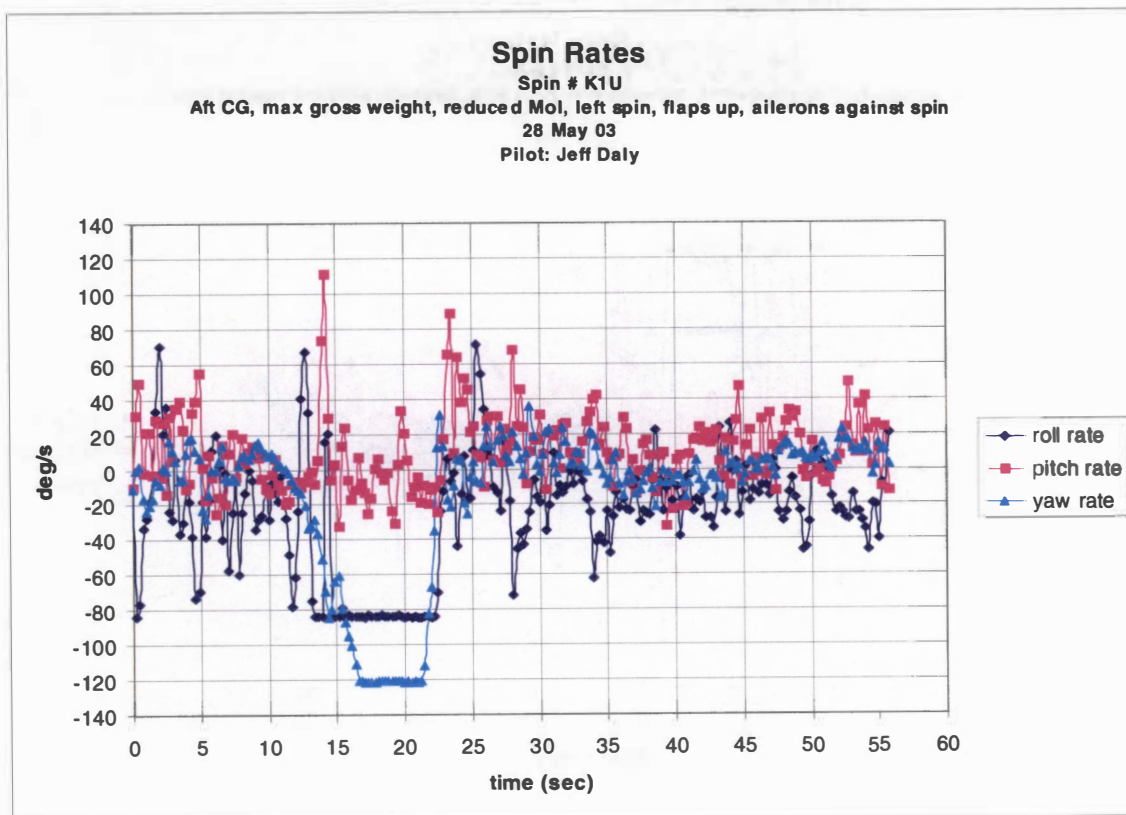


Figure F-33. Spin # K1U.

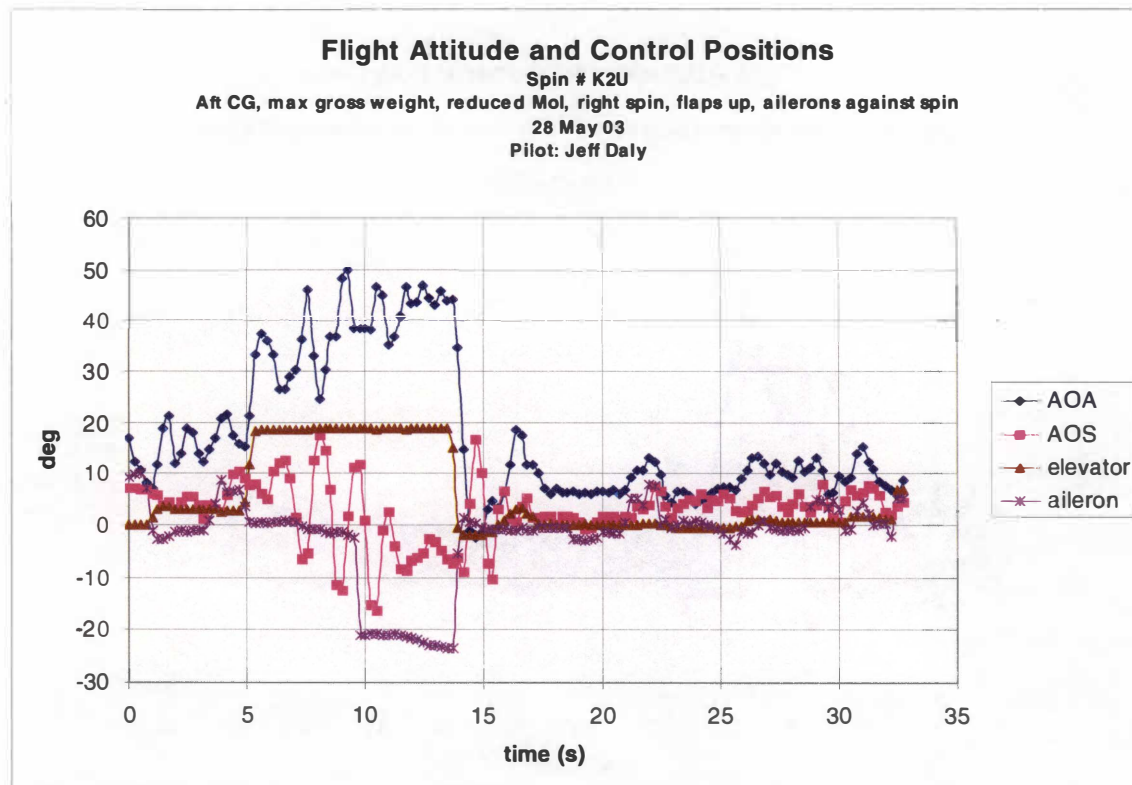
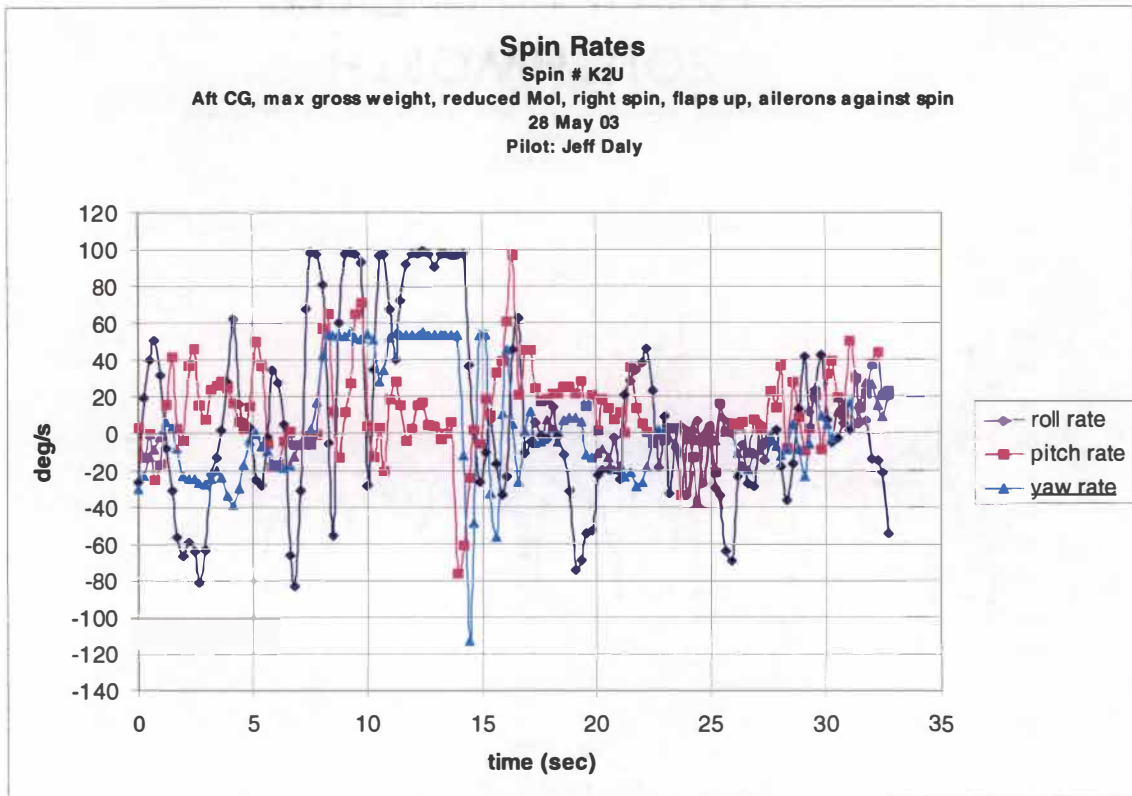


Figure F-34. Spin # K2U.

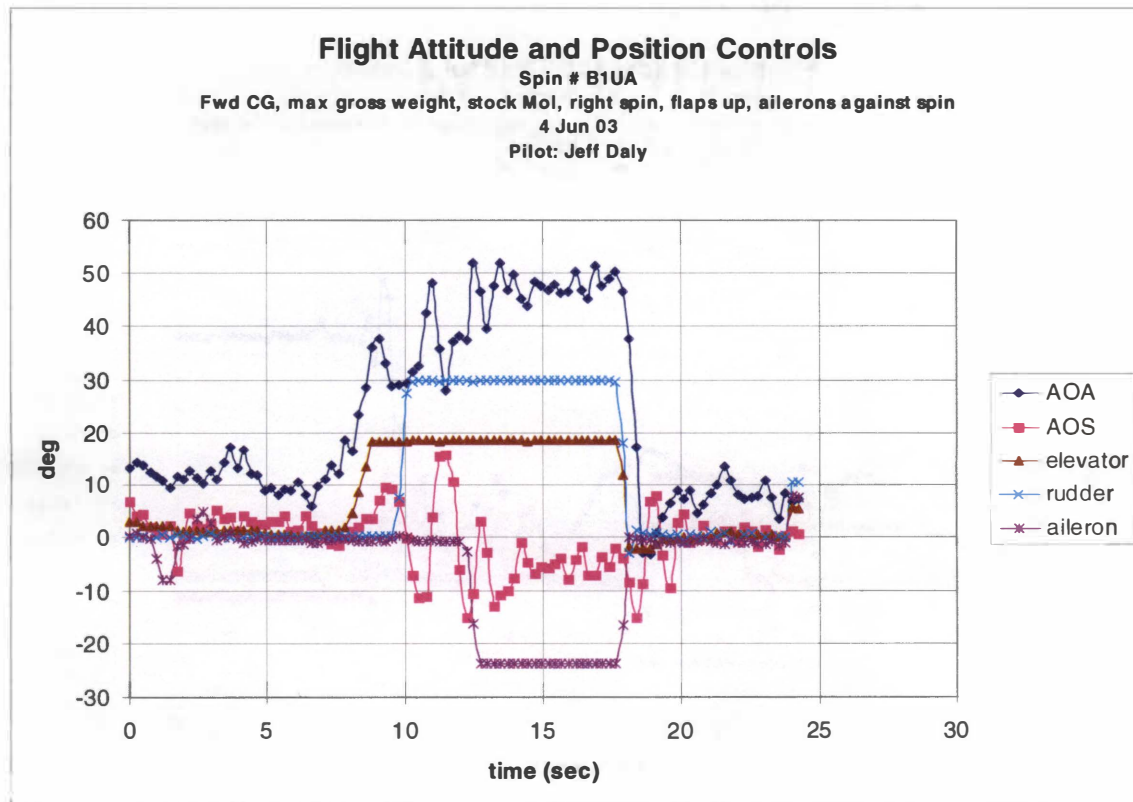
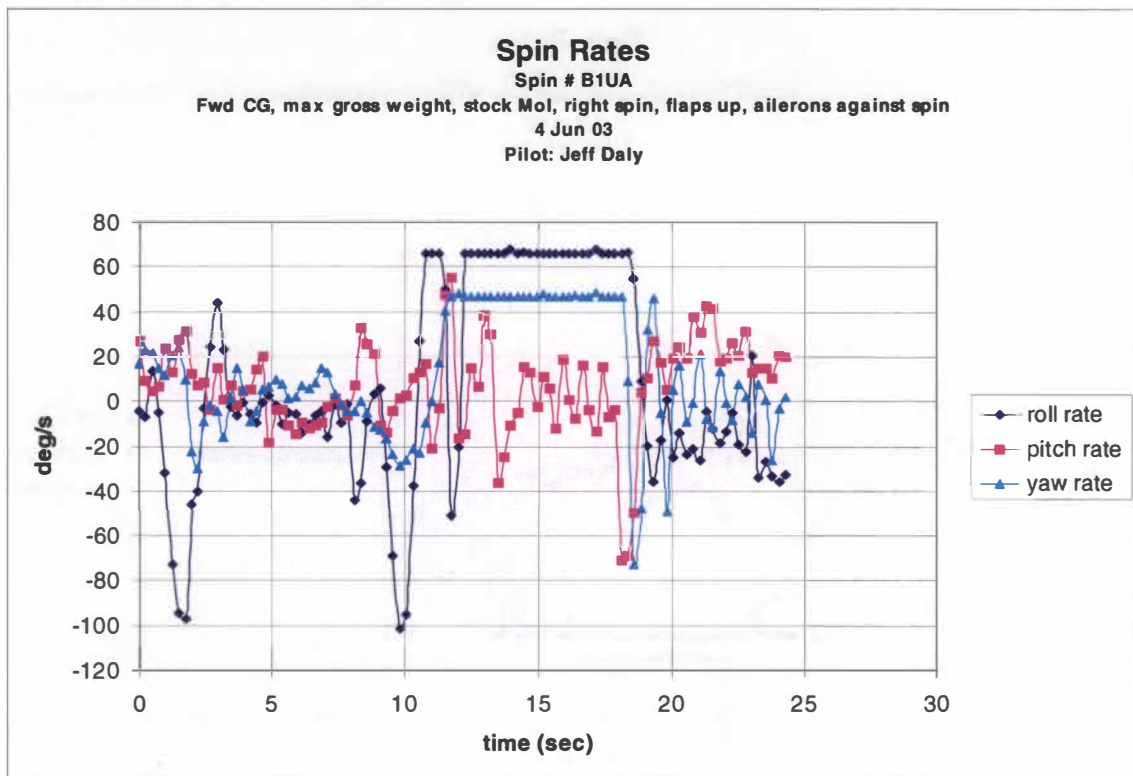


Figure F-35. Spin # B1UA.

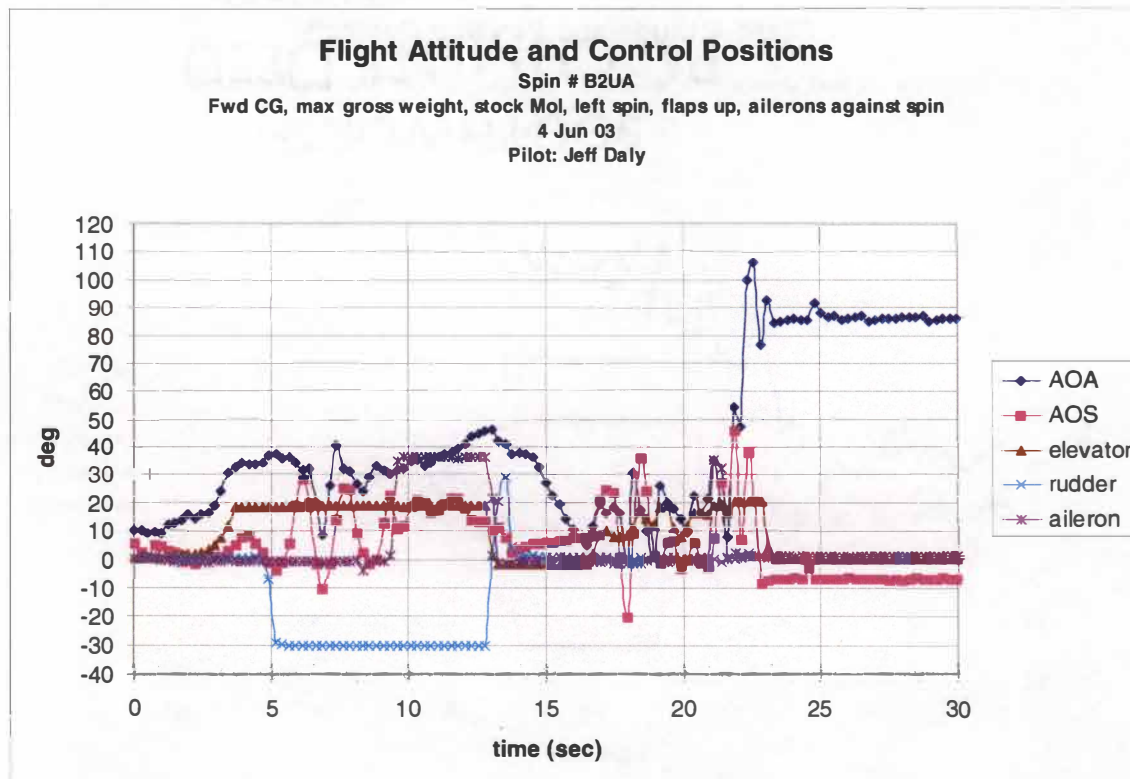
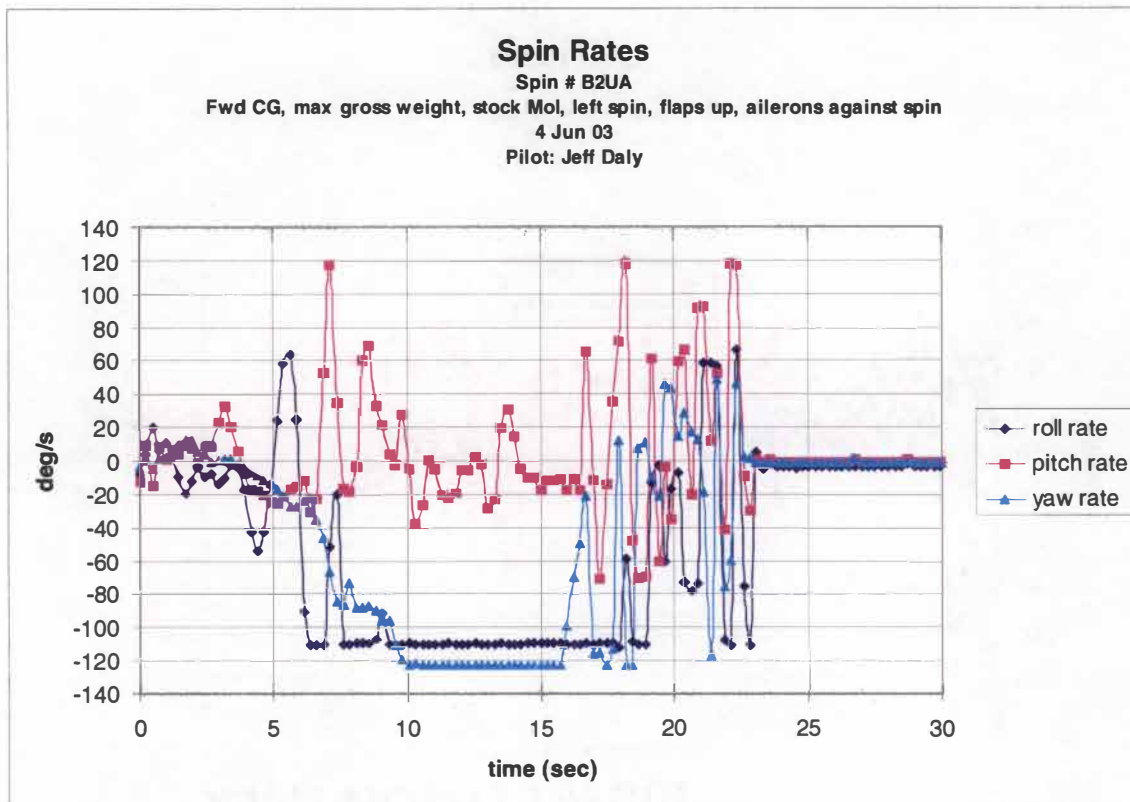









Figure F-36. Spin # B2UA.

APPENDIX G: Model Spin Parameters from Flight Tests

Table G-1. Flight Data. Forward Center of Gravity. Left Spins.

Inertia Configuration	Reduced IYMP = -109×10^{-4}				Stock IYMP = -48×10^{-4}				Increased IYMP = 8×10^{-4}			
Flap Position	up		down		up		down		up		down	
Aileron Position	neutral	against	neutral	against	neutral	against	neutral	against	neutral	against	neutral	against
Spin Number	A1U	-	A3D	-	B1U	B2UA	B3D	-	C1U	-	C3D	-
Stone Spin Block		-		-				-		-		-
α_{AVG} (deg)	25	-	16	-	24	45	17	-	23	-	-	-
β_{AVG} (deg)	-	-	-	-	15	12	10	-	-	-	-	-
p_{AVG} (deg/s) ¹⁴	-39	-	-38	-	-32	-45	-27	-	-38	-	-	-
q_{AVG} (deg/s)	11	-	12	-	12	-4	4	-	13	-	-	-
r_{AVG} (deg/s)	-43	-	-32	-	-35	-50	-15	-	-37	-	-	-
Ω (deg/s) ¹⁵	94	-	100	-	94	143	85	-	95	-	122	-
Spin Chute Required?	No	-	No	-	No	Yes	No	-	No	-	No	-
Pro-spin turns	2 ½	-	3	-	2 ½	4	1 ½	-	2 ½	-	2 ½	-
Turns for recovery	0	-	¼	-	0	4	¼	-	¼	-	½	-
Spin Mode ¹⁶	steep	-	steep	-	steep	mod flat	steep	-	steep	-	steep	-
Spin Recovery Description ¹⁷	fast		fast		fast	very slow	fast		fast		fast	








¹⁴ p, q, and r data were converted to full-scale. They were not used to calculate Ω because of insufficient gyro range.

¹⁵ Ω converted to full-scale, and was measured from the video data.

¹⁶ Criteria in Table 2-1.

¹⁷ Criteria in Table 2-2.

Table G-2. Flight Data. Forward Center of Gravity. Right Spins.

Inertia Configuration	Reduced IYMP = -109×10^{-4}				Stock IYMP = -48×10^{-4}				Increased IYMP = 8×10^{-4}			
Flap Position	up		down		up		down		up		down	
Aileron Position	neutral	against	neutral	against	neutral	against	neutral	against	neutral	against	neutral	against
Spin Number	A2U	-	A4D	-	B2U	B1UA	B4D	-	C2U	-	C4D	-
Stone Spin Block		-		-				-		-		-
α_{AVG} (deg)	37.5	-	33	-	38.1	48	31	-	41	-	29	-
β_{AVG} (deg)	-	-	-	-	-2	-6	-4	-	-	-	-	-
p_{AVG} (deg/s) ¹⁸	33	-	32	-	33	27	33	-	35	-	29	-
q_{AVG} (deg/s)	17	-	19	-	11	0	13	-	14	-	11	-
r_{AVG} (deg/s)	21	-	20	-	23	19	22	-	22	-	20	-
Ω (deg/s) ¹⁹	87	-	94	-	92	72	108	-	102	-	94	-
Spin Chute Required?	No	-	No	-	No	No	No	-	No	-	No	-
Pro-spin turns	2 ½	-	2	-	2	3	2	-	3	-	3 ½	-
Turns for recovery	¼	-	¼	-	¼	¼	¼	-	1	-	1 ½	-
Spin Mode ²⁰	mod steep	-	mod steep	-	mod steep	mod flat	mod steep	-	mod steep	-	Steep	-
Spin Recovery Description ²¹	fast		fast		fast	fast	fast		fast		slow	







¹⁸ p, q, and r data were converted to full-scale. They were not used to calculate Ω because of insufficient gyro range.

¹⁹ Ω converted to full-scale, and was measured from the video data.

²⁰ Criteria in Table 2-1.

²¹ Criteria in Table 2-2.

Table G-3. Flight Data. Mid Center of Gravity. Left Spins.

Inertia Configuration	Reduced IYMP = -114×10^{-4}				Stock IYMP = -52×10^{-4}				Increased IYMP = 2×10^{-4}			
Flap Position	up		down		up		down		up		down	
Aileron Position	neutral	against	neutral	against	neutral	against	neutral	against	neutral	against	neutral	against
Spin Number	D1U	-	D3D	-	E1U	-	E3D	-	F1U	-	F3D	-
Stone Spin Block		-		-		-		-		-		-
α_{AVG} (deg)	25	-	17	-	25	-	18	-	24	-	18	-
β_{AVG} (deg)	-	-	-	-	-	-	-	-	-	-	-	-
P_{AVG} (deg/s) ²²	-27	-	-35	-	-33	-	-36	-	-24	-	-35	-
q_{AVG} (deg/s)	9	-	13	-	9	-	8	-	11	-	9	-
r_{AVG} (deg/s)	-31	-	-29	-	-33	-	-31	-	-24	-	-29	-
Ω (deg/s) ²³	97	-	98	-	89	-	106	-	90	-	108	-
Spin Chute Required?	No	-	No	-	No	-	No	-	No	-	No	-
Pro-spin turns	2	-	2	-	2	-	1 ½	-	2 ½	-	2 ¼	-
Turns for recovery	½	-	¼	-	¼	-	½	-	½	-	¼	-
Spin Mode ²⁴	steep	-	steep	-	steep	-	steep	-	steep	-	steep	-
Spin Recovery Description ²⁵	fast		fast		fast		fast		fast		fast	







²² p, q, and r data were converted to full-scale. They were not used to calculate Ω because of insufficient gyro range.

²³ Ω converted to full-scale, and was measured from the video data.

²⁴ Criteria in Table 2-1.

²⁵ Criteria in Table 2-2.

Table G-4. Flight Data. Mid Center of Gravity. Right Spins.

Inertia Configuration	Reduced IYMP = -109×10^{-4}				Stock IYMP = -48×10^{-4}				Increased IYMP = 8×10^{-4}			
Flap Position	up		down		up		down		up		down	
Aileron Position	neutral	against	neutral	against	neutral	against	neutral	against	neutral	against	neutral	against
Spin Number	D2U	-	D4D	-	E2U	-	E4D	-	F2U	-	F4D	-
Stone Spin Block		-		-		-		-		-		-
α_{AVG} (deg)	38	-	34	-	41	-	35	-	43	-	33	-
β_{AVG} (deg)	-	-	-	-	-	-	-	-	-	-	-	-
p_{AVG} (deg/s) ²⁶	29	-	34	-	34	-	32	-	34	-	34	-
q_{AVG} (deg/s)	11	-	17	-	15	-	17	-	18	-	14	-
r_{AVG} (deg/s)	21	-	21	-	21	-	21	-	22	-	21	-
Ω (deg/s) ²⁷	75	-	91	-	113	-	103	-	117	-	104	-
Spin Chute Required?	No	-	No	-	No	-	No	-	No	-	No	-
Pro-spin turns	2	-	2	-	2	-	2	-	2 ¼	-	2	-
Turns for recovery	1	-	1	-	1 ¾	-	¾	-	¾	-	¼	-
Spin Mode ²⁸	mod steep	-	mod steep	-	mod steep	-	mod steep	-	mod steep	-	mod steep	-
Spin Recovery Description ²⁹	fast		fast		slow		fast		fast		fast	









²⁶ p, q, and r data were converted to full-scale. They were not used to calculate Ω because of insufficient gyro range.

²⁷ Ω converted to full-scale, and was measured from the video data.

²⁸ Criteria in Table 2-1.

²⁹ Criteria in Table 2-2.

Table G-5. Flight Data. Aft Center of Gravity. Left Spins.

Inertia Configuration	Reduced IYMP = -1.18×10^{-4}				Stock IYMP = -56×10^{-4}				Increased IYMP = -4×10^{-4}			
Flap Position	up		down		up		down		up		down	
Aileron Position	neutral	against	neutral	against	neutral	against	neutral	against	neutral	against	neutral	against
Spin Number	G1U	K1U	G3D	-	H1U	-	H3D	-	J1U	J5A	J3D	-
Stone Spin Block				-		-		-				-
α_{AVG} (deg)	33	47	-	-	30	-	23	-	29	49	-	-
β_{AVG} (deg)	9	11	-	-	9	-	12	-	5	10	-	-
p_{AVG} (deg/s) ³⁰	-33	-34	-	-	-29	-	-34	-	-34	-34	-	-
q_{AVG} (deg/s)	12	-2	-	-	11	-	6	-	15	1	-	-
r_{AVG} (deg/s)	-34	-49	-	-	-37	-	-30	-	-40	-50	-	-
Ω (deg/s) ³¹	94	128	-	-	98	-	92	-	106	141	-	-
Spin Chute Required?	No	No	-	-	No	-	No	-	No	Yes	-	-
Pro-spin turns	2	3	-	-	1 ½	-	2 ½	-	2 ½	3	-	-
Turns for recovery	½	3	-	-	¾	-	½	-	½	∞	-	-
Spin Mode ³²	mod steep	mod flat	-	-	steep	-	steep	-	steep	mod flat	-	-
Spin Recovery Description ³³	fast	slow			fast		fast		fast	no recovery		








³⁰ p, q, and r data were converted to full-scale. They were not used to calculate Ω because of insufficient gyro range.

³¹ Ω converted to full-scale, and was measured from the video data.

³² Criteria in Table 2-1.

³³ Criteria in Table 2-2.

Table G-6. Flight Data. Aft Center of Gravity. Right Spins.

Inertia Configuration	Reduced IYMP = -118×10^{-4}				Stock IYMP = -56×10^{-4}				Increased IYMP = -4×10^{-4}			
Flap Position	up		down		up		down		up		down	
Aileron Position	neutral	against	neutral	against	neutral	against	neutral	against	neutral	against	neutral	against
Spin Number	G2U	K2U	G4D	-	H2U	-	H4D	-	J2U	-	J4D	-
Stone Spin Block				-		-		-		-		-
α_{AVG} (deg)	41	43	-	-	43	-	34	-	44	-	-	-
β_{AVG} (deg)	3	-4	-	-	4	-	-3	-	3	-	-	-
p_{AVG} (deg/s) ³⁴	36	33	-	-	38	-	30	-	36	-	-	-
q_{AVG} (deg/s)	11	5	-	-	14	-	11	-	9	-	-	-
r_{AVG} (deg/s)	20	21	-	-	22	-	20	-	22	-	-	-
Ω (deg/s) ³⁵	81	60	-	-	85	-	85	-	97	-	-	-
Spin Chute Required?	No	No	-	-	No	-	No	-	No	-	-	-
Pro-spin turns	2	2	-	-	2	-	2	-	2 ½	-	-	-
Turns for recovery	¼	¼	-	-	¾	-	¼	-	¾	-	-	-
Spin Mode ³⁶	mod steep	mod steep	-	-	mod steep	-	mod steep	-	mod steep	-	-	-
Spin Recovery Description ³⁷	fast	fast			fast		fast		fast			

³⁴ p, q, and r data were converted to full-scale. They were not used to calculate Ω because of insufficient gyro range.

³⁵ Ω converted to full-scale, and was measured from the video data.

³⁶ Criteria in Table 2-1.

³⁷ Criteria in Table 2-2.

APPENDIX H: Level Flight Data

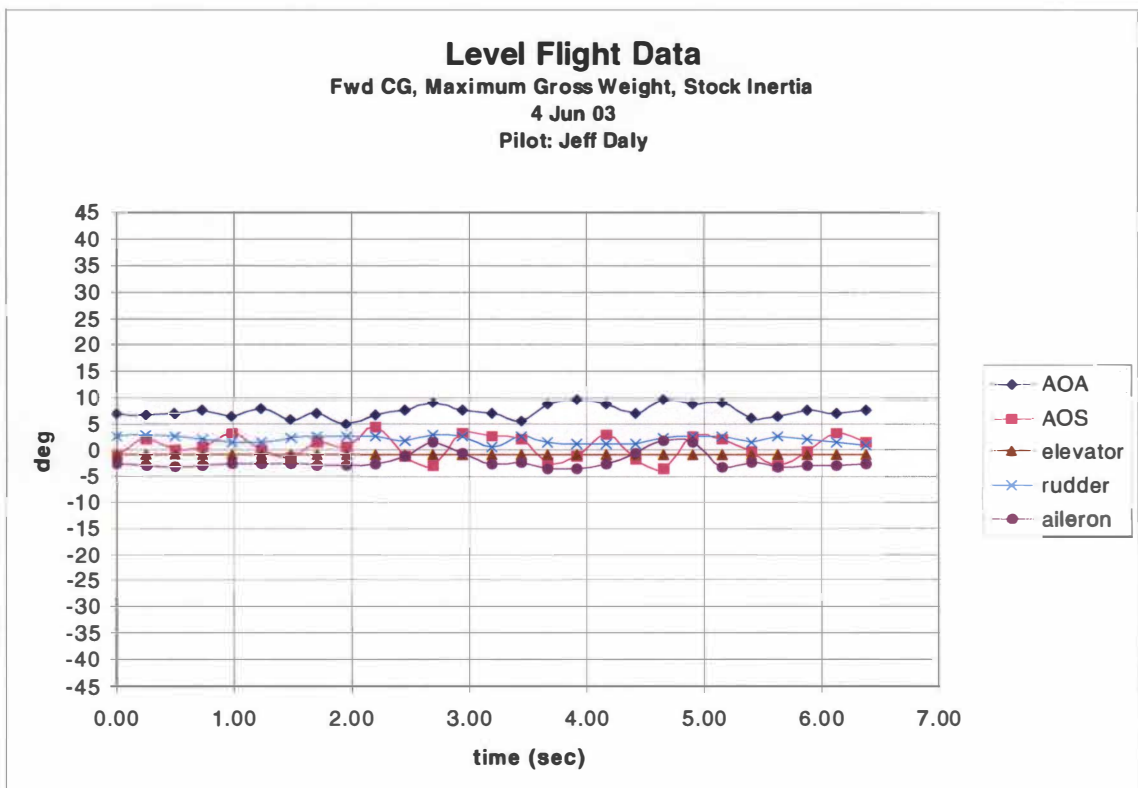
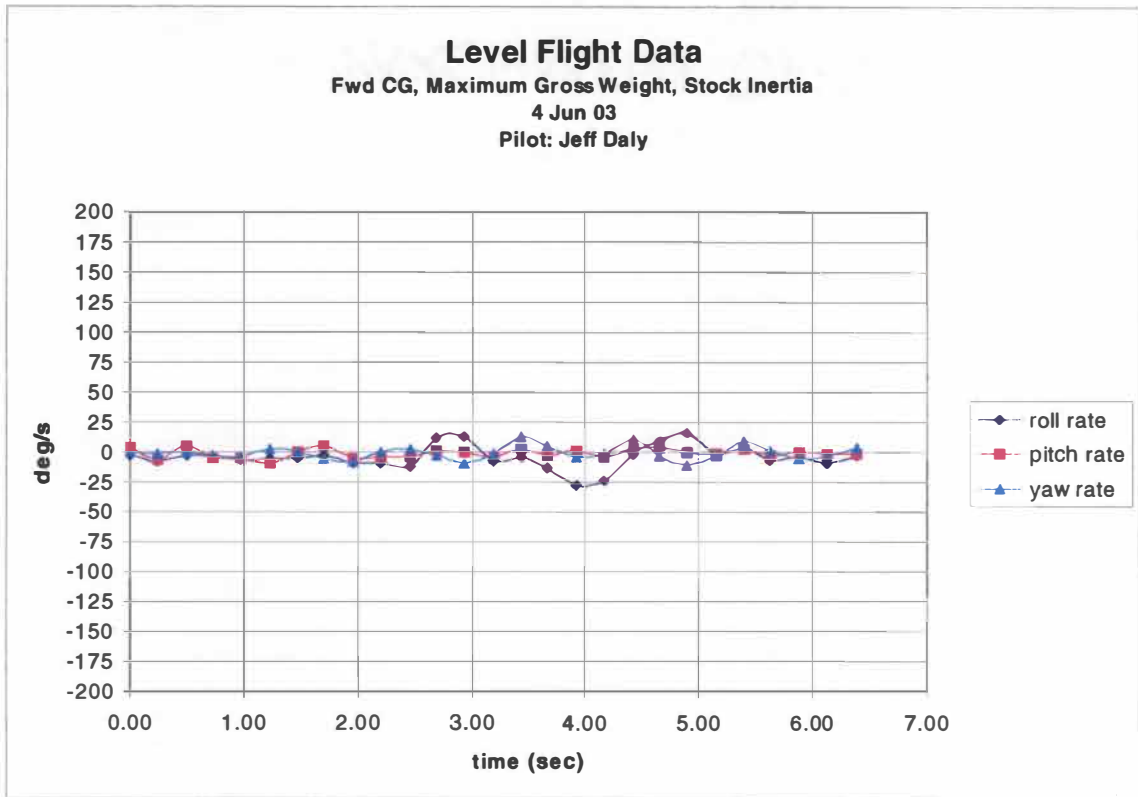


Figure H-1. Level Flight Data.

VITA

Jeffrey Duane Daly was born on 23 October 1966, in St. Boniface, Manitoba, Canada. Growing up in an Air Force family, he attended schools in many locations in Canada and the United States, including Summerside P.E.I., Greenwood Nova Scotia, Ottawa Ontario, Toronto Ontario, Winnipeg Manitoba, and Patuxant River Maryland. In June 1984, he graduated from Three Oaks High School in Summerside, Prince Edward Island. In 1989, he graduated from the University of Western Ontario with a Bachelor's Degree in Mechanical Engineering. Prior to graduating, he enrolled in the Registered Officer's Training Plan of the Canadian Forces in 1987. After completion of occupational training as an Aerospace Engineering Officer in 1990, Lieutenant Daly was posted to 414 Electronic Warfare Squadron in North Bay, Ontario as an Aircraft Maintenance Officer for the Lockheed T-33 Silverstar and the Canadair Challenger aircraft. Two years later, Captain Daly was moved to Shearwater, Nova Scotia with his Squadron, changing names to 434 Combat Support Squadron. After serving there for two years, he underwent French second language training for one year. In 1995, he was moved back to North Bay, Ontario for two years where he became a Staff Officer in Fighter Group Canadian Regional NORAD Headquarters. Capt Daly then moved to Ottawa, Ontario in 1997 where he was employed for two years as an Electronic Warfare Specialist and as the Project Manager for the T-33 Avionics Update Project. In 1999, he assumed the technical responsibilities for the entire T-33 fleet in the Canadian Forces, as the T-33 Aircraft Engineering Officer. The Canadian Forces subsequently selected him in 2001 for post graduate training at UTSI where he completed a Master of Science degree in Aerospace Engineering in August 2003. During his studies, Capt Daly was promoted to the rank of Major in 2002.

3872 2089 62
04/14/04 MAB 